A photochemical investigation of two sunscreen absorbers in a polar and a non-polar medium

by

Rivash Panday

Submitted in fulfilment of the academic
requirements for the degree of
Master of Science in the
School of Pure and Applied Chemistry
University of Natal
Durban

April 2002

This thesis is dedicated to

my sister Reshmi

and

her husband Pravesh Panday

Abstract

Protection against the harmful effects of ultraviolet radiation is of increasing importance due to the depletion of stratospheric ozone, which shields the earth from harmful UVC rays (in the range 200-280 nm) and some UVB rays (in the range 280-290 nm). In addition, as the skin is repeatedly exposed to solar radiation, the possibility exists that the incidence of skin cancer is enhanced. This has led to the increased use of commercial sunscreens, which apart from their benefits, also have undesirable effects such as photodegradation and skin penetration. We therefore studied the photodegradation of two sunscreen absorbers that are used in most sunscreen formulations.

The combination of the UVB filter, 2-ethylhexyl-*p*-methoxycinnamate (EHMC), and the UVA filter, avobenzone (AVO), are commonly used in sunscreen products. These two filters are known to exhibit differing photostabilities in different media. The aim of this project was to investigate their photochemical behaviour in a polar and a non-polar solvent and to identify the UV-induced breakdown products. Methanol was chosen as the polar medium and cyclohexane as the non-polar medium. The sunscreen filters were irradiated either singly or in combination in the two solvents with wavelengths greater than 300 nm. The irradiated samples were analysed by UV-spectrophotometry, high performance liquid chromatography (HPLC) and gas chromatography (GC). The effects of direct irradiation with UVB and UVA light, quenchers and photosensitisers were also examined.

EHMC is supplied commercially as the *trans*-isomer and upon irradiation photoisomerises, in both methanol and cyclohexane, to its *cis*-isomer. AVO is photostable in methanol but photodegrades in cyclohexane. This behaviour is also evident when mixtures of the two filters are irradiated. The loss in absorbance of both EHMC and AVO was monitored by UV-spectrophotometric analysis. Since EHMC does not absorb UV light at the wavelength of maximum absorbance of AVO, a method to quantify the amount of EHMC and AVO present in the mixture was devised.

In order to identify the degradation products, HPLC and GC techniques were implemented. The photoproducts formed in the polar methanolic medium were separated and quantified by HPLC analysis. Gas chromatography with flame ionisation detection (GC-FID) was used to separate the photoproducts formed in the non-polar cyclohexane medium. Gas chromatography with mass-spectral detection (GC-MS) was used to identify the photoproducts formed upon irradiation of AVO and to show that UVA irradiation of AVO photosensitises the isomerisation of EHMC.

The rate of a photochemical reaction depends upon a number of factors including the number of photons absorbed by sunscreen absorbers. Chemical actinometry was used to determine the number of photons absorbed by EHMC, AVO and the mixture of the two in methanol and cyclohexane. The number of photons absorbed by AVO in cyclohexane was used to determine the quantum yield for the photodegradation of AVO. We also determined the rate constants for EHMC photoisomerisation and AVO photodegradation. Finally, we investigated the effect of sunlight on commercial sunscreens containing EHMC and AVO.

Preface

This thesis presents work performed by the author in the School of Pure and Applied Chemistry, University of Natal, King George V Avenue, Durban, 4001, from February 2000 to December 2001 under the supervision of Professor B.S. Martincigh.

This thesis is the original work of the author and has not been submitted in part, or in whole, to any other university. Where use has been made of the work of others, it has been duly acknowledged in the text.

Acknowledgements

I would like to thank my supervisor Professor B.S. Martincigh for giving me the opportunity to study in a field of growing interest and also for sensitising my awareness to detail during my write-up and all aspects of life. I would also like to thank Professor S.B. Jonnalagadda from the University of Durban-Westville for giving me the inspiration and encouragement to pursue a career in the field of chemistry.

I would like to thank Professor A.A. Spark for his assistance and expertise in gas chromatographic analysis, Ali Salim for his assistance in HPLC analysis, Peter Cheplogoi and Neil Koorbanally for interpretation of NMR data and Bret Parel for GC-MS analysis. Most thanks must go to Martin Onani who never refused to share his knowledge of chemistry and life in general.

The computing help of Mr K. Singh is greatly appreciated. Thanks also goes to Mr G. Moodley, Mrs J. Govender, Mr L. Murugas and Mr R. Suchipersadh for assistance.

I am extremely grateful to my colleagues, Jonathan Chetty, Nishlan Govender and Avashnee Sewlall, for providing social upliftment at home and abroad.

I would like to express my gratitude to my sister Reshmi Panday and her husband Pravesh for providing an environment that was conducive to studying during my undergraduate and postgraduate stay at university, not forgetting my parents for their overwhelming support.

Finally, I would like to thank the National Research Foundation and the University of Natal for financial support.

Table of Contents

CHAPTER 1

Introduction

South Africa has a climate that encourages outdoor activities; thus the incidence of skin cancer in the fair-skinned population is amongst the highest in the world. With the increasing awareness of skin cancer a number of sunscreen formulations are available on the market to protect the skin from the harmful effects of solar radiation.

It is now recognized that suncare products should provide a high and broad-spectrum protection in the ultraviolet range incident on the surface of the earth. To achieve this broad-spectrum protection formulations contain a combination of filter substances. Two of the most commonly used sunscreen absorbers are 2-ethylhexyl-*p*-methoxycinnamate (EHMC) and 4-*tert*-butyl-4′-methoxydibenzoylmethane known as avobenzone (AVO). However, it has been shown that these combination sunscreen products are not always photostable [1], and in particular those containing EHMC and AVO [1,2]. Furthermore, the photostability can be altered by the polarity of the solvent [3]. This prompted us to investigate the photostability of EHMC and AVO upon irradiation with ultraviolet light in both a polar medium (methanol) and a non-polar medium (cyclohexane).

The effects of ultraviolet (UV) light on human skin, the role of topical sunscreens in providing a protective layer to the UV chromophores found in the skin, and previous studies conducted on the two sunscreen components of interest here, namely, EHMC and AVO are discussed in this introduction.

1.1 Effect of UV light on human skin

Ultraviolet radiation only constitutes about 15% of the total solar energy reaching the earth's surface but is the most energetic and therefore most likely to induce biological damage [4]. The UV region of the electromagnetic spectrum can be divided into three regions, namely, the ultraviolet C (UVC) which is the region between 100-280 nm,

ultraviolet B (UVB) that corresponds to the region between 280-315 nm and ultraviolet A (UVA) corresponding to the region between 315-400 nm.

UVC is completely absorbed by the stratospheric ozone and oxygen layers and consequently does not reach the earth's surface. Considering the fact that DNA absorbs in the UVC and UVB regions, it is these wavelengths that are most destructive to living organisms but at sea level only UVB radiation having lower energy than 290 nm is incident on the earth [4]. UVB is therefore most significant in the induction of skin cancer [4].

Part of the UVB region penetrates the ozone layer and is responsible for most of the photobiological events induced by exposure to the sun. UVB is responsible for erythema (superficial inflammation of the skin in patches), DNA damage and skin cancer. Beneficial effects of UVB irradiation are that it offers some protection and initiation of the vitamin D cascade, which is important to calcium metabolism [5].

UVA rays, which were initially thought to be harmless, are now known to cause wrinkling, photoaging of the skin, dermatological photosensitization, some erythema and also contribute to melanoma induction. They were also shown to induce single strand breaks in DNA [4].

UVA rays induce an immediate erythema which diminishes within 2 hours and a delayed erythema response which reaches a peak at 6 hours. These rays induce an immediate pigment darkening reaction and new melanin pigment formation. UVA exposure can also damage blood vessels. With regard to photoaging, hairless mice were irradiated with UVA light for several weeks by Shaath *et al.* [5] and they developed a significant degree of elastosis, thus UVA radiation is capable of inducing profound photodamage to dermal connective tissue in mice.

Tanning of the skin protects us against UV-radiation. Eggset *et al.* [6] showed the percentage transmission of untanned and tanned epidermis with UVB or PUVA (psoralen with a combination of UVA radiation). Untanned epidermis transmitted 13-43% of UVB radiation while tanned epidermis transmitted 8-12% of UVB radiation and the percentage transmission was slightly lower for PUVA tanned epidermis.

UVB and PUVA induce increased melanin content and thickening of the epidermis. Melanin is efficient in UVA protection whereas thickening in skin protects against UVB rays [6].

Studies carried out on hairless mice were used to show that wavelengths in the UVB region are responsible for the induction of skin cancer and high doses of UVA were also shown to cause skin cancer [5]. Exposure to UV radiation not only results in the appearance of skin cancer but also interferes with the immune defense mechanism that protects against the development of skin cancer [7].

There are three major types of skin cancer: basal cell carcinoma, squamous cell carcinoma and malignant melanoma. Basal cell carcinoma occurs mainly on the face and other exposed areas, and is diagnosed by raised, translucent nodules that may crust, ulcerate and sometimes bleed. Squamous cell carcinoma appears on exposed areas of the body and is diagnosed by raised pink opaque nodules that ulcerate or form sores in the middle. The most dangerous form of skin cancer is malignant melanoma that is often diagnosed as small brown or black, or multi-coloured patches that crust and bleed. The spread of cancer cells beyond their original site is called metastasis [8].

Human skin has its own defense mechanisms to survive UV-radiation. Keratinization protects the stratum corneum. Eumelanin pigmentation provides melanosomes that absorb and scatter UV-radiation. The carotenoid pigments act as singlet oxygen quenchers. Urocanic acid absorbs UV-radiation and undergoes *cis-trans* isomerisation [5].

Human skin colour is a composite of red (oxyhemoglobin), blue (reduced hemoglobin), yellow (carotenoids and flavins) and brown (melanin). The human race is divided on their basic skin colour of white, brown and black as a result of the variations in the amount and distribution of melanin in epidermal cells.

UV-light is absorbed by the skin and targets the deoxyribonucleic acid (DNA) molecule. The DNA molecule is a double stranded molecule consisting of two helical antiparallel polynucleotide chains coiled around a common axis. Each of the two

strands is made up of a repeating sugar-phosphate backbone to which four nucleic acid bases, namely, adenine, guanine, thymine and cytosine are joined (see Figures 1.1 and 1.2).

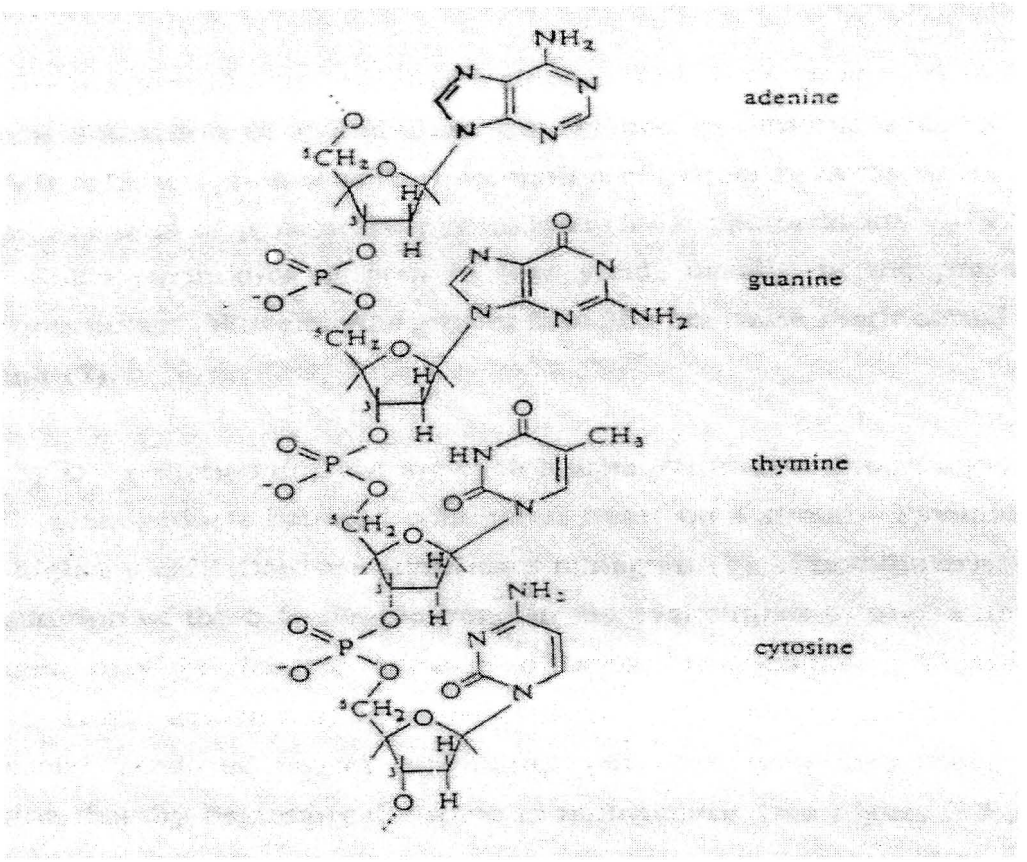

Figure 1.1: A section of a single strand of DNA showing the attachment of the purine and pyrimidine bases to the sugar-phosphate backbone [9].

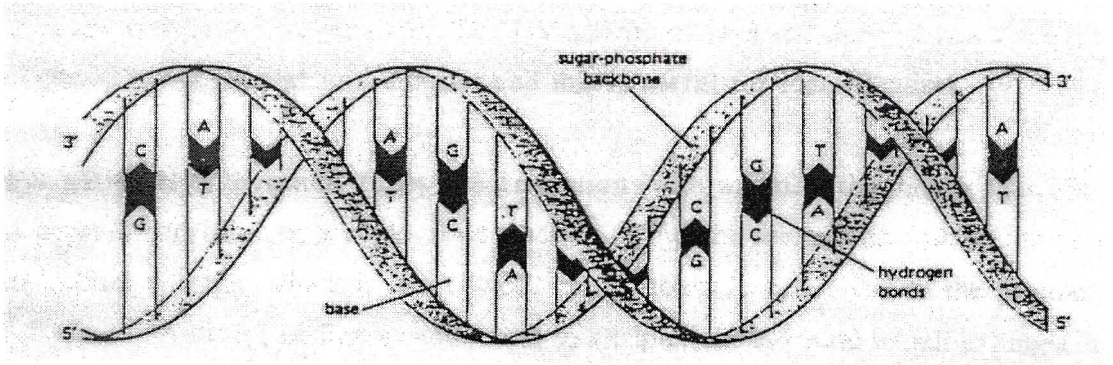

Figure 1.2: A schematic representation of double-stranded DNA showing the interstrand hydrogen bonds [10].

Genetic information is carried in the base sequence of the chain. The DNA molecule also serves as a template for replication as well as transcription into ribonucleic acid (RNA) for protein synthesis. Mutations to the genetic coding could lead to incorrect transfer of information ultimately leading to cancerous cells [11].

Mutations of DNA can be caused through chemical, physical and viral sources [11]. Chemical mutations occur when a reaction with DNA yields products that interfere with gene expression or intercalate into the helix. Physical damage is caused due to the DNA molecule absorbing different wavelengths of UV radiation from the sun. Viral damage is caused when viruses enter the host cell and interact with its nucleus thus forming new DNA and altering the expression of cellular DNA.

The nucleic acid bases in DNA contain chromophores that absorb UV radiation. The absorption of UV radiation leads to lesions in DNA [12] and the two principal UVB induced lesions are the cyclobutane pyrimidine dimers and the pyrimidine-(6-4)-pyrimidone photoproduct formed between contiguous bases on a strand. Both these lesions are mutagenic. Photodimerisation occurs by [2+2] cycloaddition of the 5,6-double bond of pyrimidine bases adjacent in the DNA strand (see Figure 1.3). Only the *cis-syn* isomer of the thymine dimer may be formed due to steric restrictions. Thymine dimer predominates with small amounts of cytosine-cytosine and cytosine-thymine adducts also being formed. Dimer formation causes uncoiling and bending in the DNA molecule. Dimers are therefore thought to be the precursors to skin cancer.

The incidence of skin cancer on South Africans is on the increase. Stastistics show that one in every four South Africans at some stage in their lives will suffer from some form of cancer. Considering the climate we live in skin cancer would definitely be one of the prominent forms of cancer. Individuals who are most at risk of developing skin cancer are those that spend most parts of the day out in the sun. The risk of skin cancer is even higher if you are fair-skinned, have many moles or skin spots and have had skin cancer before or it runs in the family. In order for individuals to protect themselves from UV-induced skin cancer, the use of sunscreens is advocated.

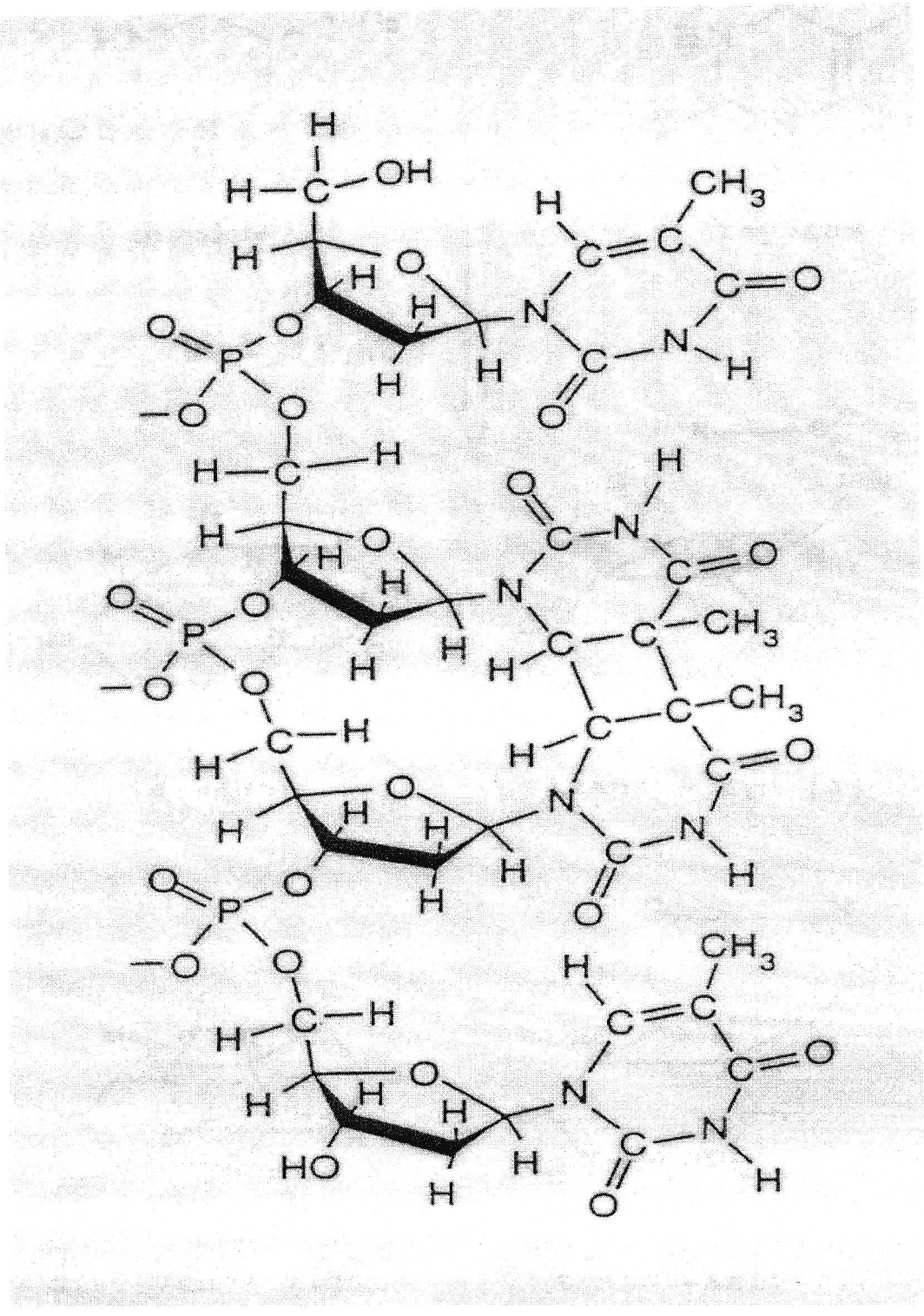

Figure 1.3: Diagram showing a portion of a DNA strand involving the thymine dimer [13].

1.2 The use of sunscreens

A number of sunscreen products have been developed in order to reduce the harmful reactions induced by exposure to UVB and UVA radiation. The role of these topical sunscreens is to provide a protective layer of exogenous UV chromophores on the skin surface to absorb or block UV-radiation before it penetrates into the viable layers of the skin.

Sunscreen formulations are made up of physical blockers like TiO_2 and ZnO, which scatter and reflect UV-light, and chemical absorbers that absorb harmful UV-light [3]. These chemical absorbers can be classified into seven broad categories, *viz.*, benzophenones, anthranilates, dibenzoyl methanes, *p*-aminobenzoic acid derivatives, salicylates, cinnamates and camphor derivatives, as shown in Figure 1.4.

This thesis concentrates on two chemical absorbers, namely, the dibenzoylmethane derivative, 4-*tert*-butyl-4′-methoxydibenzoylmethane (AVO), and the cinnamate derivative, 2-ethylhexyl-*p*-methoxycinnamate (EHMC). These compounds contain aromatic rings conjugated with carbonyl and methoxy groups thus allowing electron delocalisation on absorption of a photon of UV light, and thereby prevent harmful UV radiation from reaching the skin.

The manner in which these chemical absorbers work is that by absorbing a photon of light, the molecule goes from the singlet ground state (S_0), where the paired electrons of opposite spin occupy the lowest vibrational energy level, to the first excited singlet state (S_1), where one of the electrons is promoted to a higher energy level but still maintains it's spin configuration [4]. The molecule now possesses excess electronic, vibrational and rotational energy. The molecule can return to the ground state by dissipating this excess energy via several pathways (see Figure 1.5). It can emit the energy thermally through a series of vibrational transitions. This is called nonradiative decay or vibrational relaxation. The molecule can return to the ground state by emitting a photon. This process is called fluorescence. The molecule can also undergo internal conversion (ic), which is a nonradiative process occurring

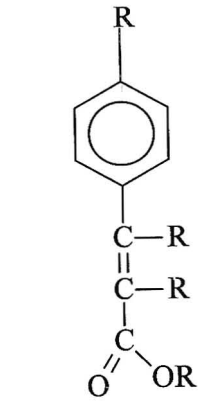

Cinnamate Derivatives

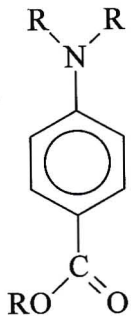

Para-aminobenzoate Derivatives

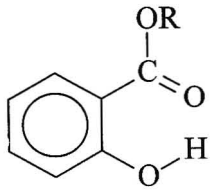

Salicylate Derivatives

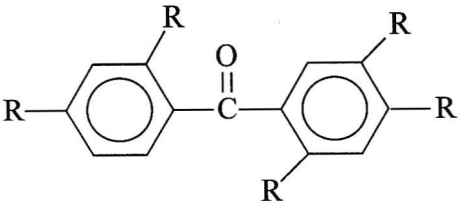

Benzophenone Derivatives

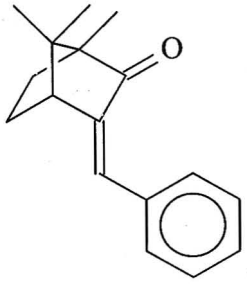

Camphor Derivatives

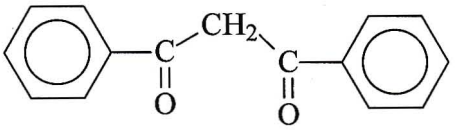

Dibenzoyl Methane Derivatives

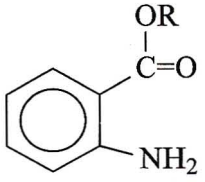

Anthranilate Derivatives

Figure 1.4: The seven major groups of chemical absorbers currently used in the preparation of sunscreen formulations.

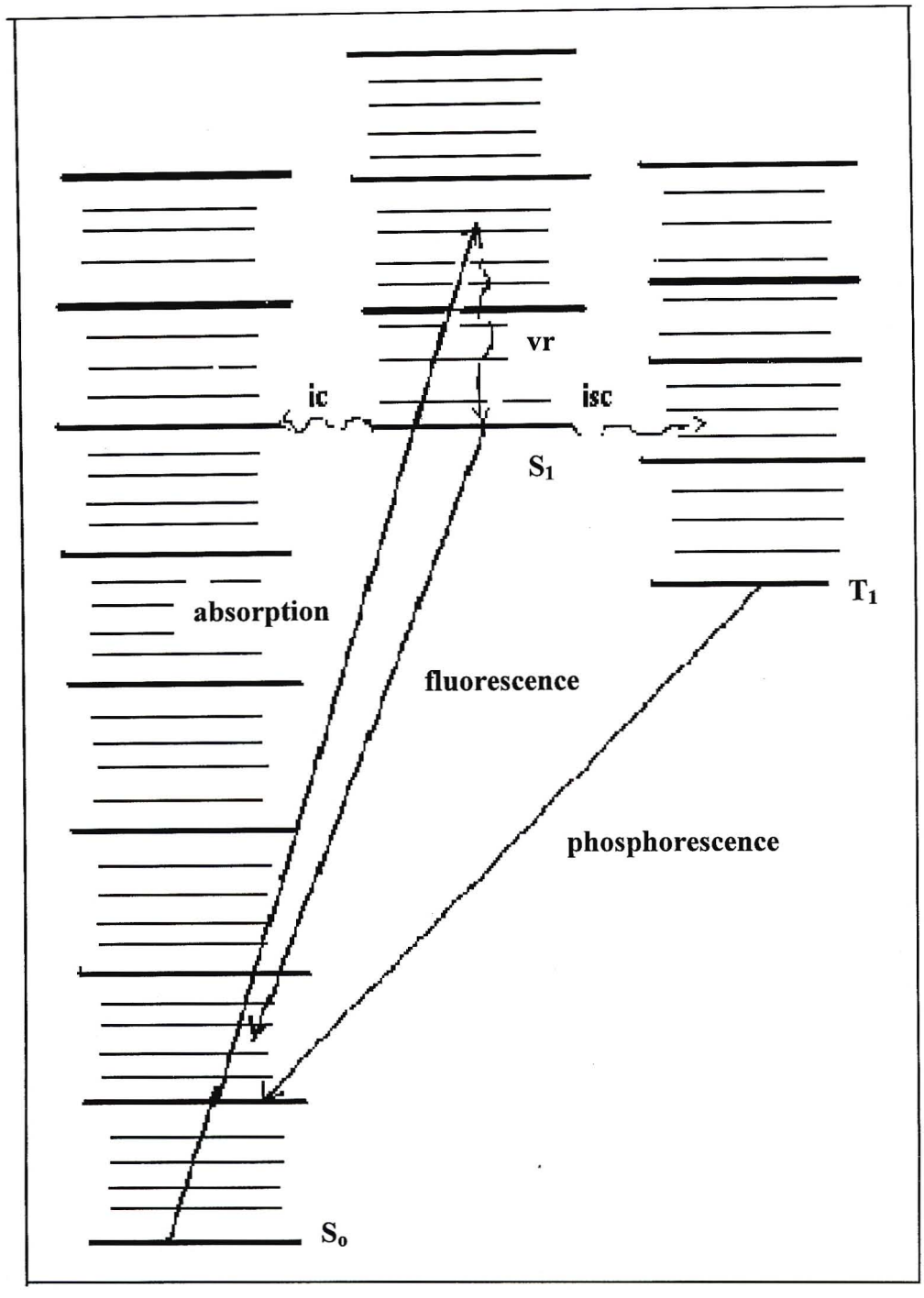

Figure 1.5: Jablonski diagram illustrating the release of energy from a molecule in its excited state [4] (ic – internal conversion, isc – intersystem crossing, vr – vibrational relaxation).

between degenerate vibrational-rotational levels of different electronic states if the electronic states have the same spin. The molecule can convert to a lower energy excited state called the triplet state (T_1) by intersystem crossing (isc), in which the electrons are not spin paired. Emission of a photon can occur from this state to the ground state and this process is referred to as phosphorescence. While the molecule is in an excited state, especially in T_1, since it exists in this state for a longer time, it can react with other molecules and produce photoproducts. The molecule can also undergo photolysis where one or more covalent bonds are ruptured when the energy of the absorbed photon exceeds the bond energy.

When energy transfer results in the deactivation of the excited species the process is referred to as quenching. Oxygen is regarded as a triplet quencher since it has a triplet ground state [4]. The singlet oxygen ($^1O_2$) produced is very reactive towards certain organic molecules and is regarded to be cytotoxic. It was shown that the once commonly used sunscreen absorber *p*-aminobenzoic acid (PABA) [14] and other sunscreens photochemically produced $^1O_2$ [26].

A compound able to transfer its triplet energy to a donor molecule is referred to as a photosensitiser and the process is referred to as photosensitisation. PABA was shown to photosensitise the formation of thymine dimer in pUC_{19} plasmid DNA [15]. Schwack and Rudolph [16] postulated that acetophenones could photosensitise the degradation of AVO.

Other types of reactions could involve steric rearrangements. The absorption of a UV-photon by *trans*-EHMC results in the formation of the *cis*-isomer without interactions with other molecules. Irreversible photodegradation of the chemical absorber on absorption of a photon has also been observed. Therefore, sunscreen absorbers have the potential to cause damage or to photodegrade and not be as effective as expected depending on how they lose their excitation energy.

The evaluation of a sunscreen's efficiency on humans is based on the determination of the minimum erythema dose (MED). At present there are several protocols for evaluation of the photoprotective efficiency of sunscreens against UVB in humans. The operating conditions differ from one protocol to another and the results differ in

the value of the sun protection factor (SPF) [17]. However, these protocols do not elucidate the pathway of energy dissipation.

SPF simply means that if you usually start to burn in 5 minutes, a sunscreen with SPF 15 protects your skin 15 times as long or for a period of 75 minutes. To achieve a high SPF it is necessary to have a formulation that shows significant UV absorbance in the 290-340 nm range. If the sunscreen exhibits a significant shift in absorbance from the region 290-340 nm to one outside this range the SPF will be reduced significantly. Sunscreens tend to react with their vehicle components and also tend to photodegrade on exposure to UV light. These factors tend to reduce SPF [18].

It has been reported by Agrapidis-Paloympis *et al.* [3] that the sunscreen's effectiveness could be influenced by the solvent in which it is dissolved. For various sunscreen absorbers studied in different solvents, changes in their wavelengths of maximum absorbance (λ_{max}) and their molar absorption coefficients are observed. Polar solvents shift the λ_{max} of polar sunscreens to shorter wavelengths (hypsochromic shift) and that of less polar sunscreens to longer wavelengths (bathochromic shift).

1.3 Previous studies of 2-ethylhexyl-*p*-methoxycinnamate and avobenzone

EHMC and AVO are the two most common chemical absorbers used in sunscreen formulations. In most sunscreen formulations a UVB absorber and a UVA absorber are present. EHMC is regarded as a UVB absorber, since it absorbs maximally in the UVB region, and AVO is regarded as a UVA absorber since it absorbs maximally in the UVA region. Sayre *et al.* [19] showed that excitation of AVO with UVA radiation caused photodegradation of EHMC. EHMC was converted to some other compound not specified. We therefore investigated the photostability and possible product formation on irradiating EHMC and AVO in methanol and cyclohexane with UV-light.

EHMC is the most commonly used sunscreen agent in sunscreen formulations [20]. It belongs to the cinnamate class of sunscreen absorbers. The raw material is supplied as almost 100% *trans*-isomer. Tarras-Wahlberg *et al.* [21] showed that EHMC

decomposed slightly after exposure to UVB radiation and then more rapidly upon UVA radiation. They showed by mass-spectral analysis that this degradation was due to a *trans-cis* photoisomerisation reaction (see Figure 1.6) and the UV-spectrum changes slightly before photoequilibrium is established.

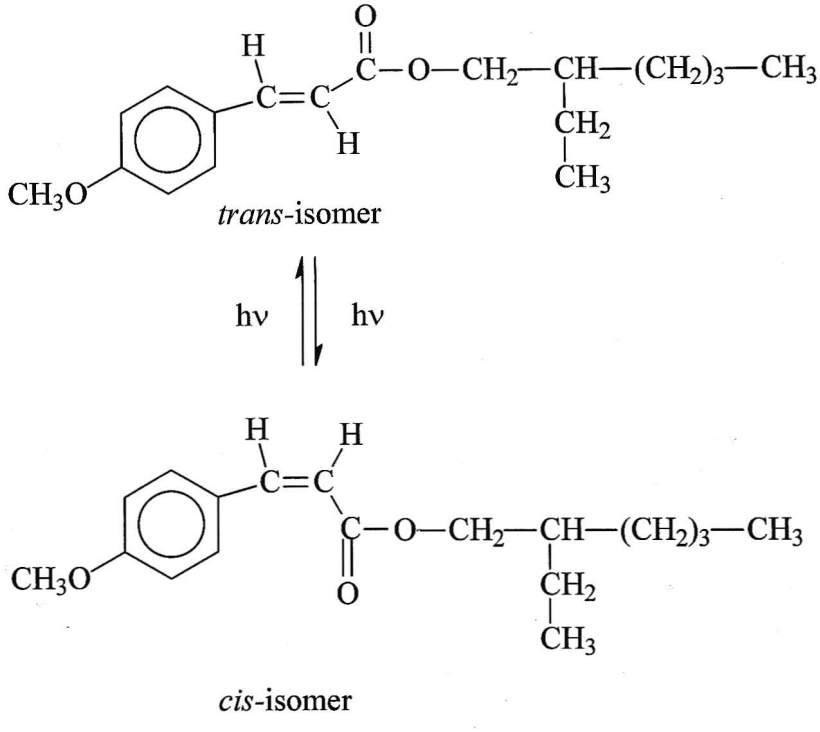

Figure 1.6: *Trans-cis* photoisomerisation of EHMC.

This photoisomerisation reaction arises because of the presence of the methoxy group in the *para* position, which facilitates electron delocalisation resulting in the temporary loss of the carbon-carbon double bond. This excited state molecule can return to the ground state in either the *cis* or *trans* form. This electron rearrangement is illustrated in Figure 1.7.

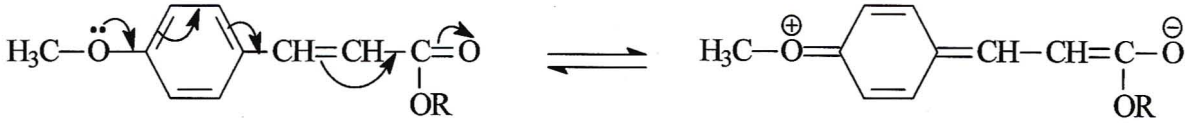

Figure 1.7: Electron delocalisation in EHMC.

Broadbent [22] and Kowlaser [23] showed that this isomerisation reaction leads to a loss in absorbing ability as the *cis*-isomer is a less efficient UVB absorber. The loss in absorbing ability is attributed to the *cis*-isomer having a lower molar absorption coefficient than that of the *trans*-isomer. Kowlaser [23] showed that on irradiation of 98% *trans*-EHMC the photostationary equilibrium of the isomerisation reaction lies towards to the formation of the *cis*-isomer. On exposing a sunscreen formulation consisting of 8-10% *trans*-EHMC to sunlight, she noticed that the photostationary equilibrium lies closer to the *trans*-isomer. Kowlaser [23] also showed the molar absorption coefficient (ε) of *cis*-EHMC at 304 nm to be 1.835 x 10^4 dm^3 mol^{-1} cm^{-1} which is lower than that of the *trans*-isomer (2.33 x 10^4 dm^3 mol^{-1} cm^{-1} at 311 nm [5]). The loss in absorbing ability is also attributed to *trans*-EHMC undergoing a self-dimerisation reaction by a [2+2] cycloaddition reaction [24]. Eleven isomers of these dimers were proposed seven of which are *meso* and four are racemic in character (see Figure 1.8) [23]. Kowlaser [23] showed the formation of an adduct between *trans*-EHMC and thymidine-5′-monophosphate, and consequently EHMC has the potential to form mutagenic products in DNA should it penetrate into the nucleus of the cell.

Singlet oxygen ($^1O_2$) has been shown to cause oxidative damage to biological systems by reacting with nucleic acids, proteins and lipids [25]. $^1O_2$ may therefore be responsible for some of the dermatological reactions and toxic effects observed with the use of sunscreens. Allen *et al.* [26] therefore investigated the production of $^1O_2$ upon irradiating solutions of EHMC. They used furfuryl alcohol (FFA) as a trap for $^1O_2$ and showed that FFA was consumed when EHMC was irradiated. They therefore showed that EHMC upon irradiation produces $^1O_2$.

Taylor *et al.* [27] used the Ames *Salmonella Typhimurium* test to show that EHMC acts an initiator of tumors in mice. Work done by Butt and Christensen [28] showed the dark toxicity and possible toxicity of EHMC to mouse cells after UV irradiation. They found that EHMC exposed to light was more toxic than the unexposed filter and attributed this toxicity to the existence of breakdown products.

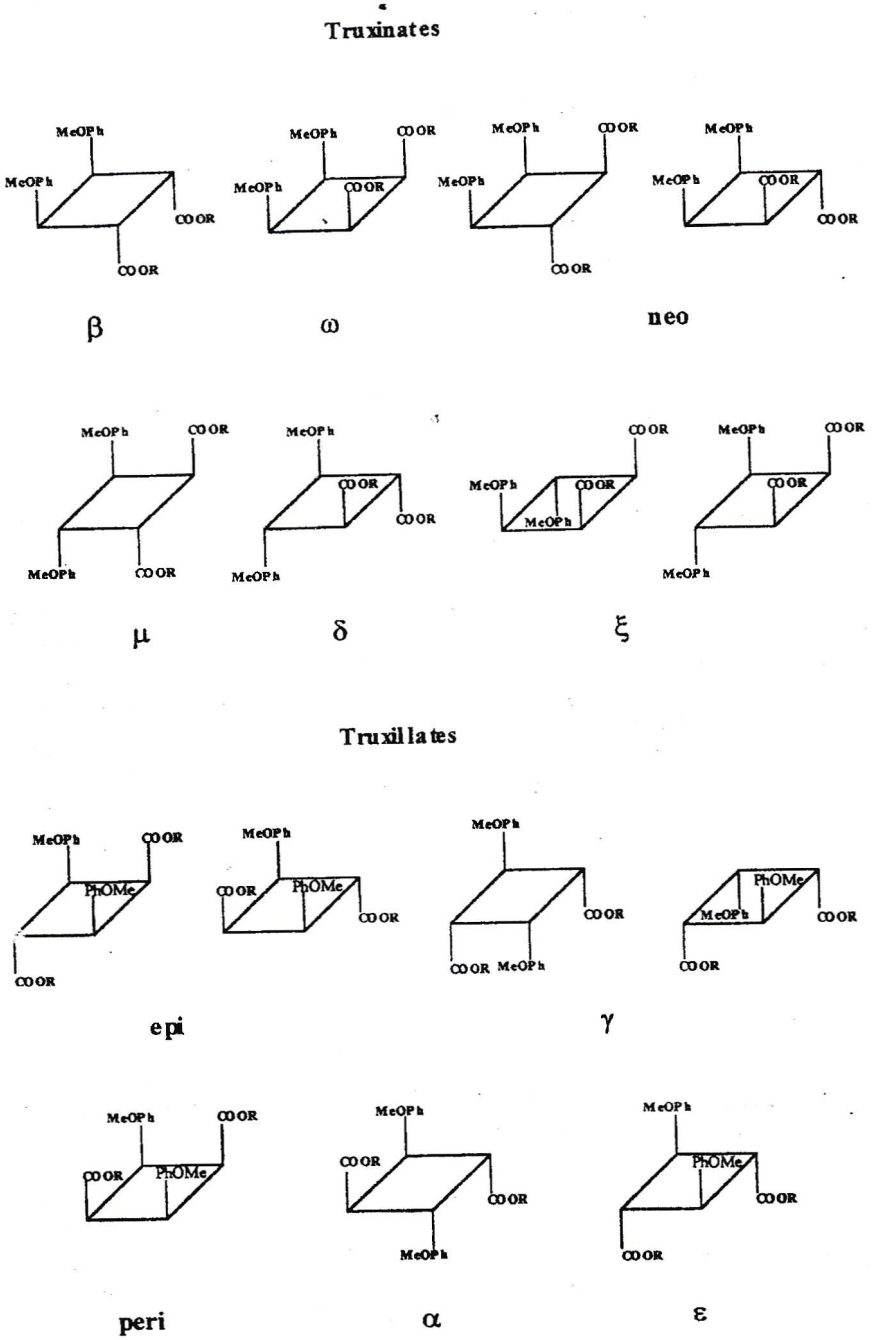

Figure 1.8: Structures of the eleven possible isomeric forms of the EHMC dimer [23].

The UVA portion of the solar spectrum is now known to cause harmful effects on human skin such as photoaging and photocarcinogenesis. Photoprotection against UVA sunlight by sunscreens has thus assumed increasing importance. The most frequently used UVA absorber is avobenzone (see Figure 1.9), which belongs to the dibenzoylmethane class of sunscreens.

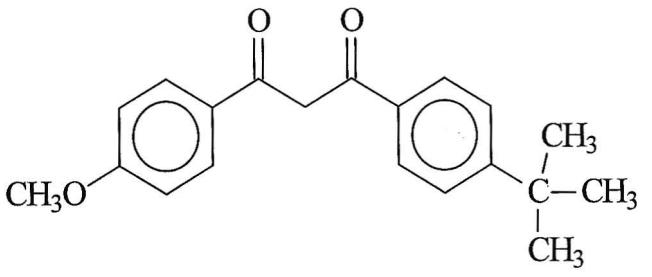

Figure 1.9: Chemical structure of avobenzone.

AVO has a typical absorption near 355 nm with a molar absorption coefficient of 35 000 dm^3 mol^{-1} cm^{-1} in acetonitrile [29]. AVO exists in three tautomeric forms (see Figure 1.10): two *cis* enols and a β-diketone. The enol form predominates in solution [29]. Dubois *et al.* [29] showed by means of ^1H and ^{13}C nuclear magnetic resonance spectroscopy (NMR) that irradiation of AVO in acetonitrile with a xenon lamp increases the percentage of β-diketone. Due to this isomerisation reaction there is definite loss in absorbing ability of AVO thus reducing its protective efficiency.

Andrae *et al.* [30] showed that continuous irradiation of AVO in acetonitrile leads to a new absorption band at 270 nm (the diketo form of AVO) with the loss of the enol form (357 nm). They used high performance liquid chromatography (HPLC) to separate the two forms of AVO. They also looked at the photoprotection of human lymphoid cells with and without AVO. About 40% of lymphoid cells were killed in the absence of the sunscreen, but in the presence of AVO only 5% of cells were killed.

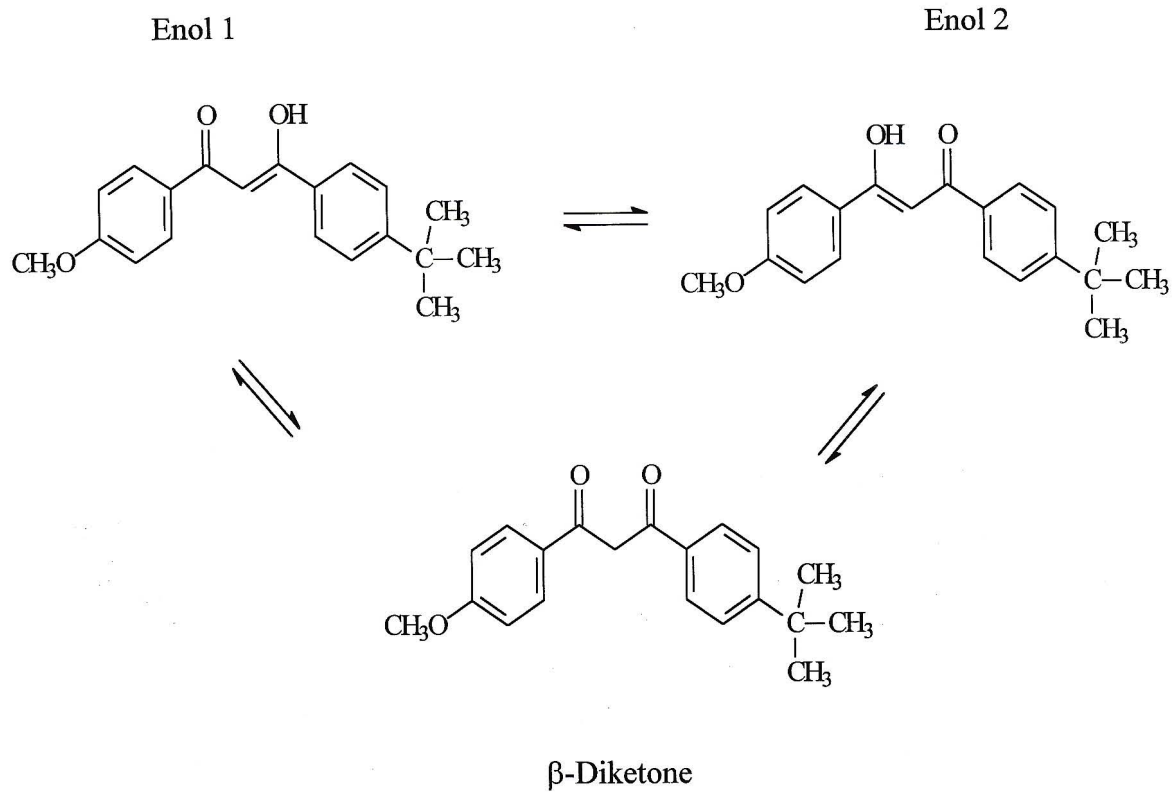

Figure 1.10: The three tautomeric forms of AVO [29].

Schwack and Rudolph [16] showed that by using a solar simulator attached to a UVA filter as an irradiation source, AVO was found to photodegrade in a non-polar solvent but showed photostability in a polar solvent. A number of photoproducts were identified and their formation involved primary α-bond cleavages of carbonyl groups, followed by hydrogen abstraction and radical recombination. They postulated that product formation is from the excited triplet state and proceeds through the excitation of AVO in its 1,3-diketo form. Photoproducts originate from two radical precursors, either from a benzoyl radical or from a phenacyl radical. The photoproducts formed were classified into seven groups, namely, benzaldehydes, benzoic acids, phenylglyoxals, acetophenones, benzils, dibenzoyl methanes and dibenzoyl ethanes. They showed that photoproduct formation could possibly occur from the triplet state of AVO, by looking at the triplet quenching effect of O_2. Roscher *et al.* [31] irradiated AVO in cyclohexane for 100 hours and they also obtained several similar

photoproducts. Tarras-Wahlberg *et al.* [21] suggested from mass-spectral analysis that for AVO to undergo photodegradation it first undergoes photoisomerisation from the diketo form to the *cis*-enol form and the photoproducts that do form have strong absorption in the UVB region.

Damiani *et al.* [32], like Schwack and Rudolph [16], showed that AVO breaks down into two carbon-centred free radicals upon irradiation. They then looked at the damage caused by the radicals on DNA. DNA was damaged when irradiated in the presence of AVO. They also showed that the damage caused by AVO is suppressed by using indolinonic nitroxides as antioxidants.

Chatelain and Gabard [2] investigated the photostabilisation of formulations containing AVO and EHMC using *bis*-ethylhexyloxyphenol methoxyphenyl triazine (Tinosorb S). They looked at sunscreens containing AVO and a combination of EHMC and AVO and showed that the SPF of sunscreens containing only AVO (2.5% or 5%) ranged between 2.5 and 4 while the addition of EHMC or Tinosorb or both boosted the SPF values to 20-50. Upon irradiation of sunscreens containing AVO, or a combination of EHMC and AVO, both sunscreen agents experienced photodegradation but photodegradation was greatly reduced on addition of Tinosorb S.

Sayre and Dowdy [33] devised an apparatus and an analytical technique to assess the photostability of sunscreen products exposed to a solar-like radiation source. Their results showed that sunscreen products containing avobenzone experience photodegradation from UV-exposure. They also showed that EHMC, which is normally regarded as a photostable UVB sunscreen, is not as effective in products containing AVO. The authors ascribed this photoinstability to either AVO or the formulations causing a photosensitised degradation of EHMC but did not show any experimental evidence for this assertion.

1.4 Outline of this project

Our objective was to study the photochemical behaviour of *trans*-EHMC and AVO in polar and non-polar environments as it has been shown that the polarity of the

environment affects the photochemical behaviour of sunscreen absorbers [3]. We used methanol as the polar environment and cyclohexane as the non-polar environment. Initially, UV-spectroscopy was used to monitor the photostability of AVO and EHMC individually and in a mixture in the two solvents. A calculation technique was devised to quantify the amount of absorbing species remaining after a particular irradiation time. In addition, as the photodegradation of the sunscreen agents is proportional to the number of UV photons absorbed, chemical actinometry was used to determine the number of photons absorbed by the respective sunscreen agents.

The nature of the photoproducts formed was monitored by chromatographic techniques. HPLC was used to separate the sunscreen agents from their photoproducts for solutions in methanol while gas chromatography (GC) techniques were used for irradiated solutions of cyclohexane. Gas chromatography with mass spectral detection (GC-MS) was used to determine the photoproducts of AVO in cyclohexane. To assess the nature of the excited state involved in the degradation process we looked at O_2 and *cis*-piperylene as triplet quenchers and benzophenone as a photosensitiser. We also looked at AVO as a possible photosensitiser for the isomerisation reaction of *trans*-EHMC to its *cis*-isomer.

Using the intensity of light absorbed by AVO in cyclohexane, which was measured by chemical actinometry, we were able to determine the quantum yield for the photodegradation of AVO. The rate constants for the photoisomerisation of EHMC and photodegradation of AVO were determined. We went on to further investigate the photochemical behaviour of EHMC and AVO in commercial sunscreen formulations on direct exposure to sunlight. Ambre Solaire (A.S.) and Lubriderm (Lubri) were chosen as they contained EHMC and AVO as the main chemical absorbers.

CHAPTER 2

Experimental

In this chapter we describe the experimental techniques used to investigate the photochemical reactions of EHMC and AVO in methanol and cyclohexane. We also describe the chromatographic techniques used in photoproduct analysis and chemical actinometry used to determine the number of photons absorbed by EHMC and AVO upon irradiation. Finally, we checked the effect of sunlight on EHMC and AVO in commercial sunscreen formulations.

2.1 Materials

The materials used for the experimental work, together with the manufacturer's name and grades of reagents used, are described in Appendix A.

2.2 Equipment

The equipment used for spectroscopic and photoproduct analyses is listed in Appendix B.

2.3 Fourier transform infrared analysis of EHMC and AVO

Infrared (IR) spectroscopy is the most widely used tool in the identification of organic compounds. Spectra of gaseous, liquid and solid samples can be measured using this technique. Functional group information can be gathered easily from an IR spectrum and a vast amount of reference data is available in the literature for direct comparison. IR spectroscopy can be used for quantitative as well as qualitative analysis. We used IR spectroscopy to check the isomeric form of the sunscreen agents supplied.

IR spectra were traditionally displayed as % transmission and not absorbance and the ability to manipulate data was poor. With dispersive instruments scanning an IR spectrum was a lengthy process if it was done at high resolution [34]. The

development of Fourier transform spectroscopy has reduced many of the above problems by providing a good signal to noise ratio, increased scanning rate, simultaneous measurements of all frequencies and intensities, and digitising information making data manipulation easier.

Nuclei of atoms bonded by covalent bonds undergo vibrations or oscillations. When these molecules absorb IR radiation, the absorbed energy causes an increase in the amplitude of the vibrations of the bonded atoms. The molecule is therefore in an excited vibrational state. The wavelength of absorption by a given type of bond depends upon the type of vibration of that bond. Therefore, different types of bond (C-H, C-C, OH, etc.) absorb IR radiation at different wavelengths [35].

An IR spectrophotometer is used to measure absorption of IR radiation (refer to Figure 2.1). At one end of the instrument is a light source, which emits a wide range of IR radiation. The light source is split by the beamsplitter into two beams and one beam is reflected onto the stationary mirror and the other to the moving mirror. When the distance of the mirrors from the beamsplitter are the same, constructive interference occurs thus producing an interferogram which when Fourier transformed produces the final infrared spectrum [23].

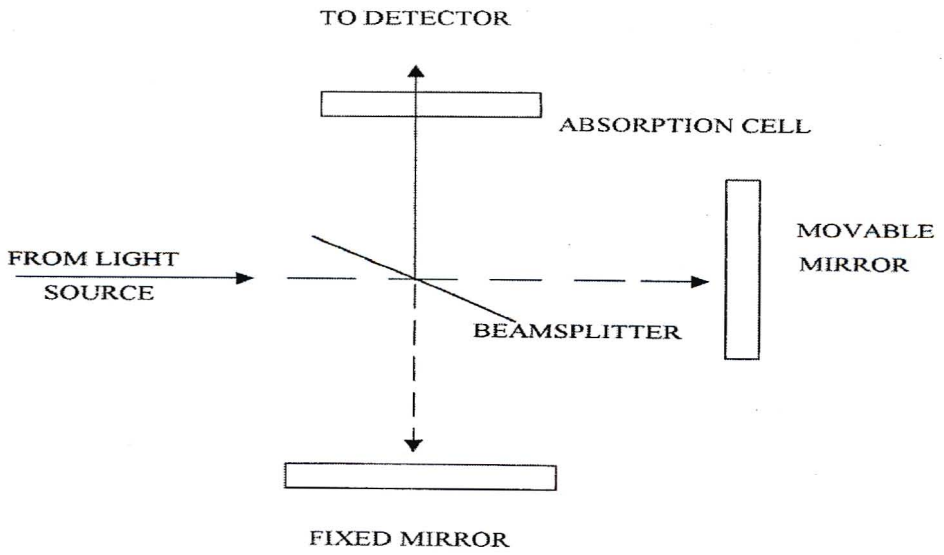

Figure 2.1: Diagram illustrating the operation of an FTIR-spectrometer [23].

Fourier transform infrared (FTIR) analysis was carried out on a Nicolet Impact 400D spectrometer attached to a Hewlett Packard 7440 Colour Pro Plotter. In this study, the infrared spectra of *trans*-EHMC and AVO were determined. EHMC is a liquid while AVO is a solid thus the sample preparation was different for these two filters.

In the case of AVO, KBr was dispensed into a mortar with a small amount of AVO and ground up with a pestle. The ground powder was then layered between two dies in the die holder and developed under pressure using a 15 ton manual hydraulic press to produce a disc. In the case of EHMC, the disc was prepared as above except that EHMC was not added to the KBr prior to disc preparation. EHMC, which was dissolved in a minimum amount of butanone, was added dropwise onto the transparent KBr disc. The solvent was allowed to evaporate and the remaining oily film was spread evenly on the disc. Both discs were placed in a sample holder and the samples were ready for analysis. Resolution was set at 2 cm^{-1} and the wavelength range was from 400-4000 cm^{-1}. Background correction was done by recording a spectrum of the background and utilising the software to subtract it from the sample spectrum. The sample holder containing the KBr disc was then placed in the sample compartment and the spectrum recorded. The results obtained are discussed in Section 3.1.

2.4 NMR analysis of EHMC and AVO

Nuclear magnetic resonance (NMR) spectroscopy is another form of absorbance spectroscopy and was used to check the predominant isomeric form in solution of the sunscreen agents supplied. A sample can absorb electromagnetic radiation in the radio-frequency (rf) region at frequencies governed by the characteristics of the sample. Absorption is a function of the states of the nuclei in the molecule. A plot of the frequencies of the absorbance peaks versus peak intensities constitutes an NMR spectrum [36].

All nuclei carry a charge. In some nuclei this charge spins on the nuclear axis and this circulation of nuclear charge generates a magnetic dipole along the axis thus on interaction with an externally applied magnetic field the magnetic nuclei, e.g. ^{1}H, ^{13}C, either become aligned with the magnetic field or oppose it. When a sample is placed

in this magnetic field and irradiated with the correct radio-frequency, interaction between the radio-frequency and the nuclei occurs.

An NMR spectrometer consists of a magnet, rf transmitter and a suitable rf detector. When a sample containing molecules having magnetic properties is placed between the poles of a magnet and subjected to the rf field of the oscillator, absorption of rf energy occurs and an rf signal is picked up by the detector (refer to Figure 2.2) [37]. A Varian Gemini 300 MHz NMR spectrometer was used in this work. EHMC and AVO were dissolved in both deuterated methanol and deuterated cyclohexane and ^{1}H NMR spectra of each were recorded. An interpretation of these spectra is given in Section 3.2.

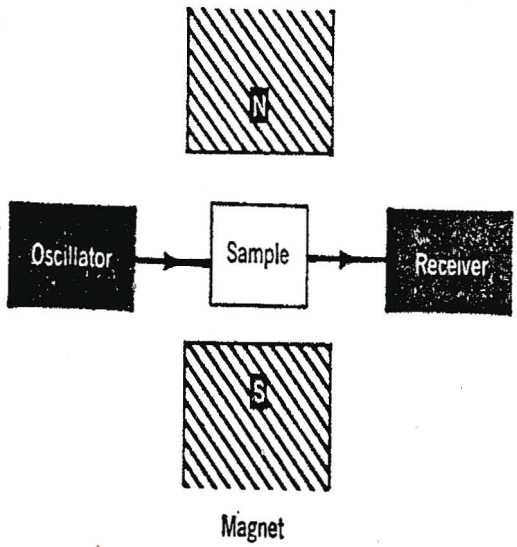

Figure 2.2: Diagram illustrating the operation of a NMR spectrometer [37].

2.5 UV-irradiation source

All irradiation experiments were carried out with the use of an Osram HBO 500 W/2 high pressure mercury lamp (see Figure 2.3) as the irradiation source and a Schrieber power-supply. The HBO lamp contains a specific quantity of mercury in a pressurised atmosphere of an inert gas. This light source emits radiation in the region of the medium-wave ultraviolet to the infrared (see Figure 2.4). This made it possible to irradiate solutions in both the UVB and UVA regions.

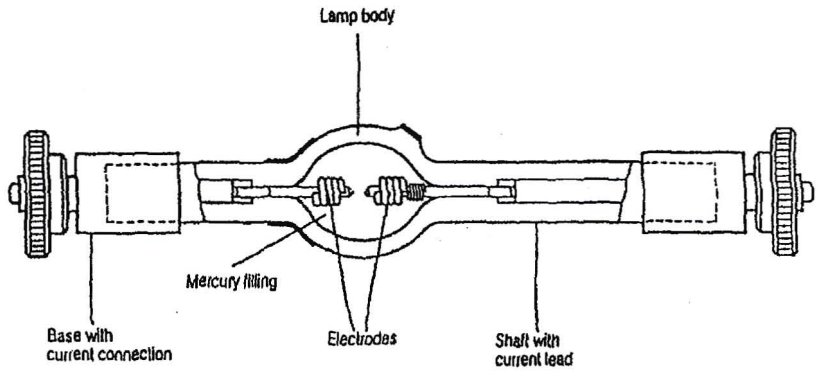

Figure 2.3: The Osram 500 W/2 high pressure mercury lamp.

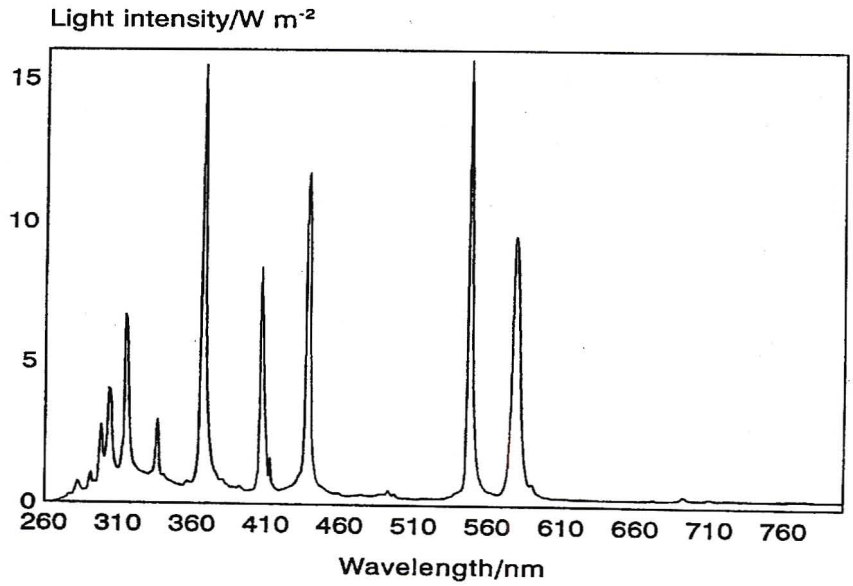

Figure 2.4: Output of the Osram HBO 500 W/2 high pressure mercury lamp.

The lamp was housed in an insulated box made of mild steel and connected to the power supply. Ventilation was crucial to cool the lamp from the great amount of heat produced during usage. This was achieved by an extractor connected to the lamp housing and leading to the outside of the building, air-conditioning of the irradiation room and a fan placed in front of the lamp. An aperture in the box in front of the lamp allowed radiation to reach the irradiation cell. An external bracket was fixed to the aperture of the box, which housed the shutter gate, filter holder, and irradiation cell holder (see Figure 2.5). Two filter holders were constructed, one for the Pyrex filter which was square in shape, and the other for the 313 nm and the 365 nm filters which were circular in shape.

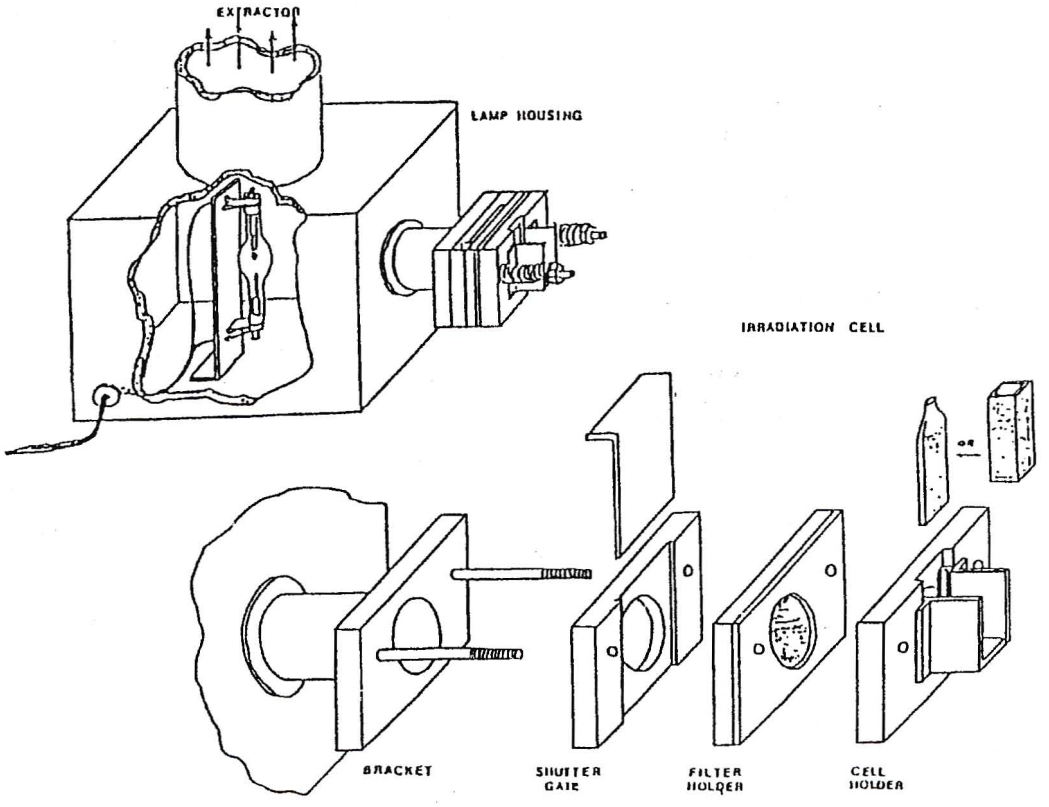

Figure 2.5: Lamp housing and optical train of the Osram HBO 500 W/2 high pressure mercury lamp.

When the power-supply was turned on the lamp was given a warm-up period of 15 minutes. The lifetime of the lamp was approximately 400 hours. The light intensity was checked with a Blak-Ray J-221 longwave UV intensity meter.

Four filters were used in this work in order to irradiate the samples with selected wavelengths. These were a 10 mm thick Pyrex filter which allows for the transmittance of light greater than 300 nm, 313 nm and 365 nm narrow bandpass interference filters purchased from Andover Corporation, which allow for the transmittance of a narrow band of wavelengths centred on those wavelengths, and a 254 nm narrow bandpass interference filter from Acton Corporation. The transmission spectra of these filters are shown in Figures 2.6 to 2.9.

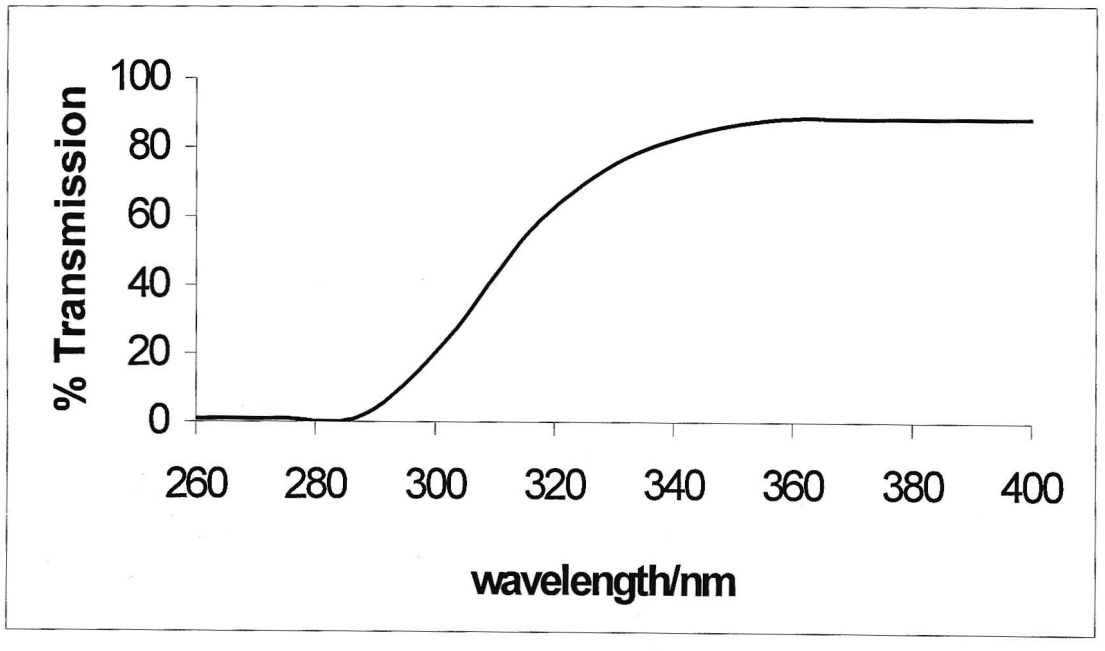

Figure 2.6: Transmission spectrum of the 10 mm thick Pyrex filter.

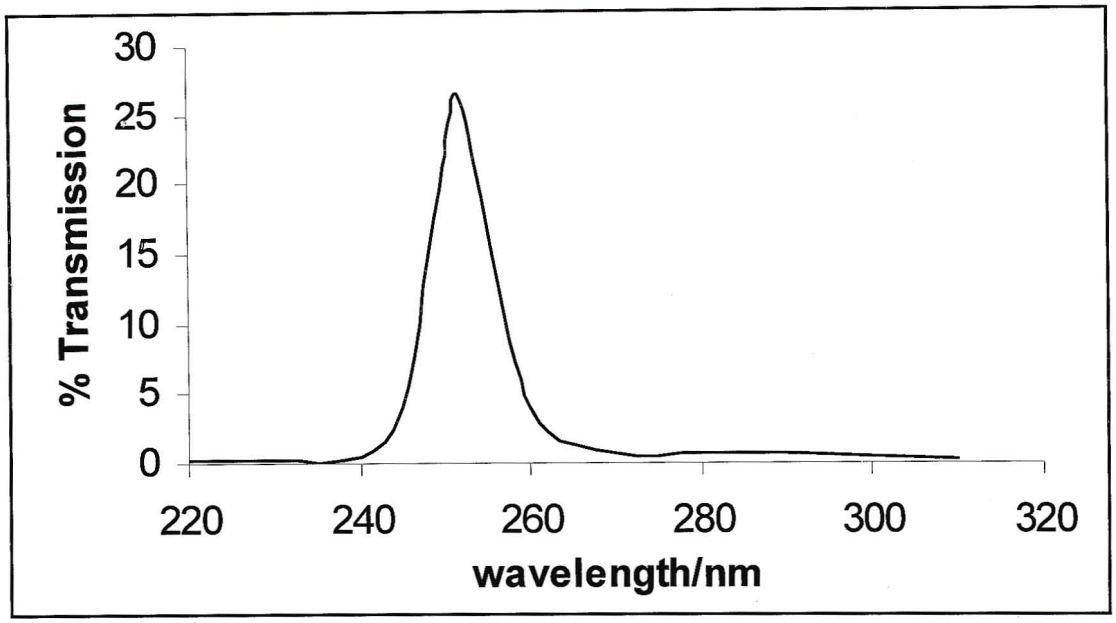

Figure 2.7: Transmission spectrum of the 254 nm narrow bandpass interference filter.

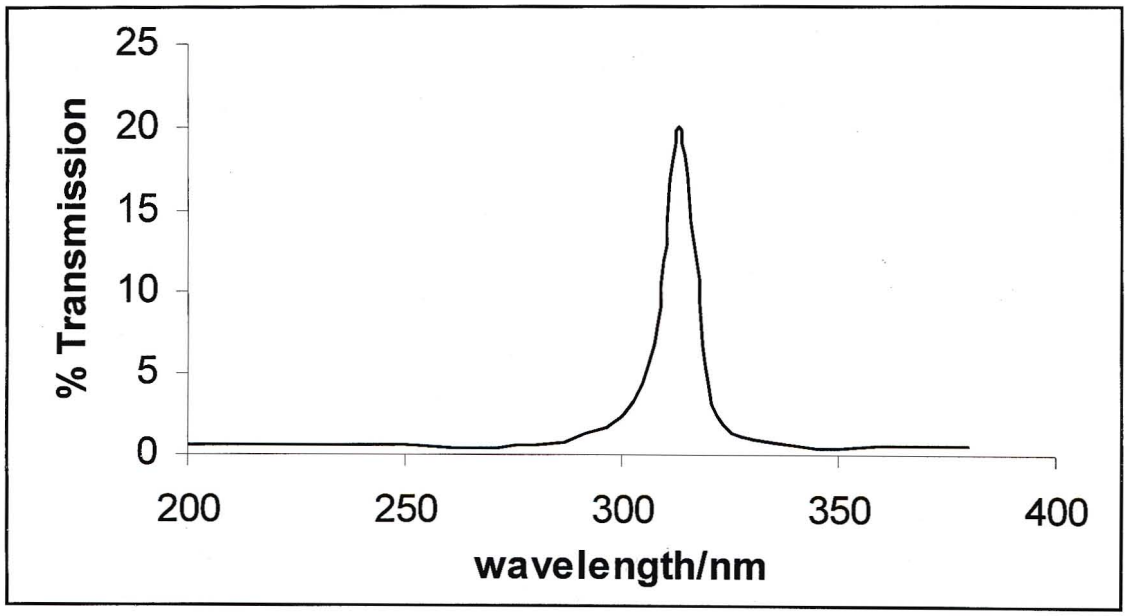

Figure 2.8: Transmission spectrum of the 313 nm narrow bandpass interference filter.

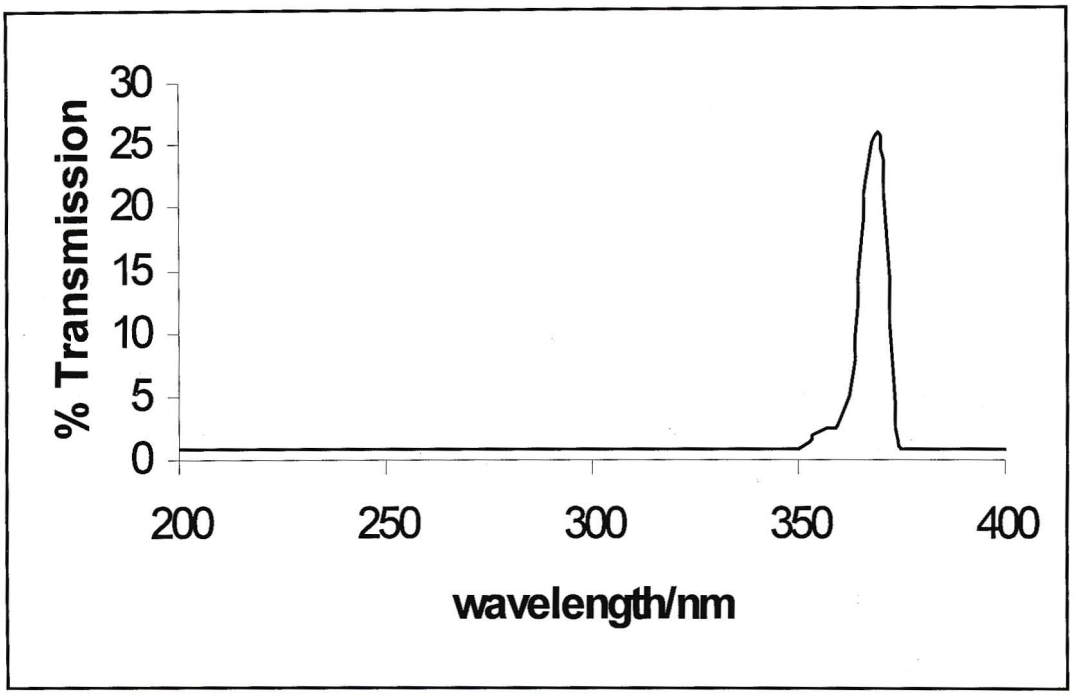

Figure 2.9: Transmission spectrum of the 365 nm narrow bandpass interference filter.

2.6 UV-spectral analyses of EHMC, AVO and mixtures thereof in both methanol and cyclohexane

Most sunscreens are classified as either UVB or UVA absorbers depending upon the region of the UV-spectrum in which they absorb. All sunscreens have their own unique UV absorption spectrum thus UV spectroscopy is a technique used in determining the presence of a particular sunscreen. This analytical technique can also be used to determine the photostability of sunscreens by monitoring the absorbance at their wavelength of maximum absorbance on exposure to light.

All UV-visible analyses were carried out with the use of a Varian DMS 300 UV/VIS spectrophotometer that consists of an energy source (a deuterium lamp used as the UV source whereas a tungsten lamp is used as the visible source), a sample and reference cell, a dispersing devise (prism/grating) and a detector. The double beam spectrophotometer allows one to record absorbance as well as transmittance data as a function of wavelength. The lamp was given 30 minutes to reach full intensity prior to samples being analysed. Matched 1 cm pathlength quartz cuvettes were used to analyse the samples.

2.6.1 UV-spectra prior to irradiation

EHMC and AVO are soluble in both methanol and cyclohexane. Stock solutions of approximately 1 x 10^{-3} M of both sunscreen agents were prepared and were serially diluted to appropriate concentrations that complied with the Beer Lambert law. The wavelength of maximum absorbance (λ_{max}) of both filters was determined by recording a spectrum over the wavelength range of 200-400 nm. Since the combination of these two filters is common in most sunscreen formulations, a mixture of the two was made up in both methanol and cyclohexane. UV-spectra of the mixtures were also recorded. The slit width was set at 2 nm and the scan rate at 100 nm/min. The resulting UV spectra are presented and disscussed in Section 3.3.1.

2.6.2 UV quantitation of EHMC and AVO

As EHMC and AVO photodegrade in one or both of the solvents used in this study, a method of quantifying the amount of sunscreen absorber remaining after irradiation was required.

From the UV-spectra of the sunscreen absorbers it is evident that EHMC does not absorb at the wavelength of maximum absorbance of AVO (λ_{maxA}). Hence at the λ_{maxA}:

$$A_{\lambda \text{ max } A} = \varepsilon^{A} c_{A} l \tag{2.1}$$

where $A_{\lambda maxA}$ is the absorbance of AVO at its λ_{max}, ε^{A} is the molar absorption coefficient of AVO at its λ_{max}, c_A is the concentration of AVO and l is the path length.

The concentration of AVO in a mixture can consequently be determined from a previously constructed calibration curve of $A_{\lambda maxA}$ against c_A.

Since absorbance is additive at the absorbance maximum of EHMC (λ_{maxE}) we have :

$$A_{\lambda \text{ max } E} = \varepsilon^{E} c_{E} l + \varepsilon^{A} c_{A} l \tag{2.2}$$

where $A_{\lambda maxE}$ is the absorbance of the mixture at the wavelength of maximum absorbance of EHMC, ε^{E} and ε^{A} are the molar absorption coefficients of EHMC and AVO respectively, c_E and c_A are the concentrations in mol dm^{-3} of EHMC and AVO respectively and l is the path length. Since *cis*-EHMC was not isolated its molar absorption coefficient could not be determined therefore the molar absorption coefficient of *trans*-EHMC was used in the above equation.

The molar absorption coefficients (ε) of both EHMC and AVO at the λ_{maxE} can be determined from the slope of the curve of absorbance of each compound at λ_{maxE} against their respective concentrations. The concentration of EHMC (c_E) in a mixture can then be determined, as c_A is known from the measurements made at the λ_{maxA}.

2.6.2.1 Spectroscopic method used to quantify EHMC and AVO in methanol

The wavelengths of maximum absorbance of EHMC and AVO in methanol are 308 nm and 356 nm respectively. As described earlier a calibration curve must be obtained to determine the concentration of AVO at 356 nm in methanol. The molar absorption coefficients of both EHMC and AVO at 308 nm then need to be determined. From equation 2.2, the concentration of EHMC in mixtures of the two sunscreen absorbers can be determined.

A 1 x 10^{-3} M AVO stock solution was diluted with methanol in a 25 ml volumetric flask to give a concentration of AVO that had an absorbance approximately equal to one. This solution was then serially diluted to give different concentrations of AVO and their absorbance readings were taken at 308 nm and 356 nm by programming the spectrophotometer to read multiwavelength absorbance. Duplicate absorbance measurements of freshly prepared AVO samples were also taken. The concentrations of AVO taken together with the initial and duplicate absorbance values at 356 nm and 308 nm are shown in Table 2.1. A graph of the initial and duplicate absorbance values at 356 nm *versus* the concentration of AVO was then plotted (see Figure 2.10). The slope of this curve is equivalent to the molar absorption coefficient of AVO at 356 nm ($\varepsilon^{A}_{356\ nm}$) in methanol. Agrapidis-Paloympis *et al.* [3] showed the molar absorption coefficient of AVO in methanol to be in the region of 3.3 x 10^4 dm^3 mol^{-1} cm^{-1} and we obtained a value of 3.86 x 10^4 dm^3 mol^{-1} cm^{-1}. The value we obtained is in fair accordance with the literature value implying that Figure 2.10 is a good calibration curve which shows linearity for concentrations of AVO in the region of 0.5 x 10^{-5} M to 2.6 x 10^{-5} M. From this graph the concentration of AVO (c_A) in any AVO-containing solution whose absorbance at 356 nm is known, can be determined.

We then needed to determine the molar absorption coefficient of AVO at 308 nm ($\varepsilon^{A}_{308\ nm}$). From absorbance values measured at 308 nm of solutions of known concentrations of AVO (refer to Table 2.1) we plotted a graph of the absorbance of the initial and the duplicate measurements at 308 nm *versus* the concentration of AVO (refer to Figure 2.11). The slope of this graph is equivalent to the $\varepsilon^{A}_{308\ nm}$. The value obtained was 0.884 x 10^4 dm^3 mol^{-1} cm^{-1}. Due to the low absorbance of AVO at 308 nm the degree of error is much greater. This explains the poor linearity of the graph with R^2 equivalent to 0.9511.

Table 2.1: Initial and duplicate absorbance readings measured at 356 nm and 308 nm of different concentrations of AVO dissolved in methanol.

[AVO]/10^{-5} M	$A_{356\ nm}$	Duplicate $A_{356\ nm}$	$A_{308\ nm}$	Duplicate $A_{308\ nm}$
2.6	0.971	0.994	0.210	0.230
2.34	0.861	0.883	0.201	0.200
1.76	0.653	0.683	0.146	0.155
1.58	0.609	0.626	0.139	0.140
1.26	0.509	0.522	0.118	0.121
0.88	0.375	0.383	0.092	0.089
0.71	0.314	0.315	0.082	0.075
0.56	0.259	0.260	0.068	0.064
0.45	0.216	0.215	0.058	0.055

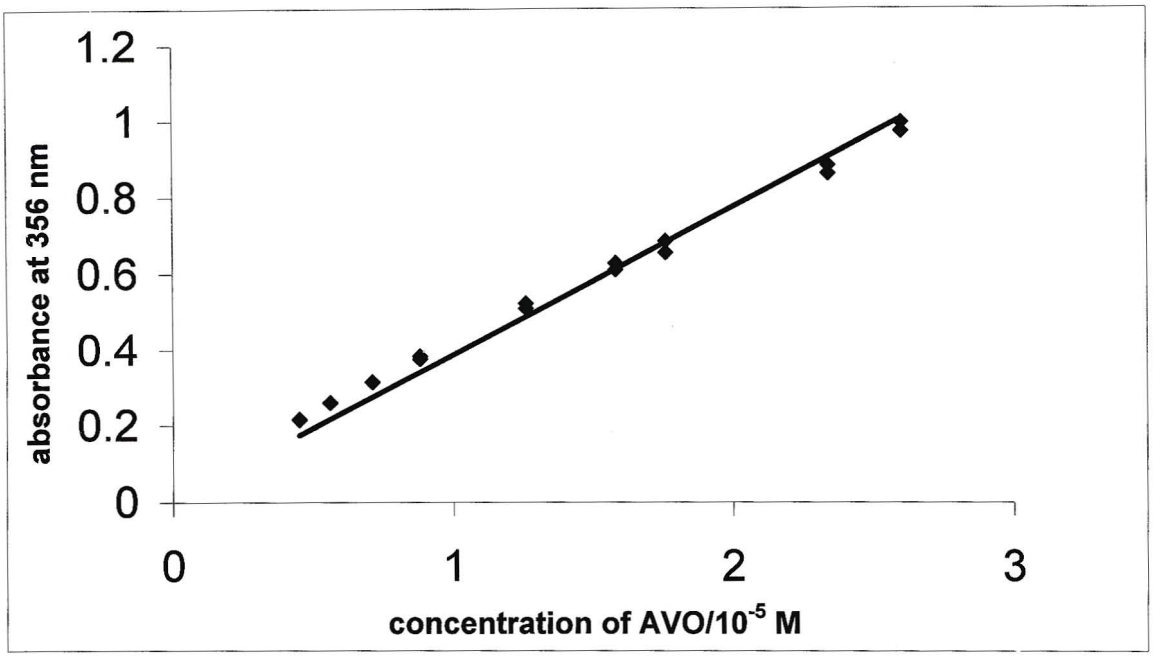

Figure 2.10: Calibration curve illustrating the absorbance of AVO at 356 nm *versus* the concentration of AVO. The slope, equivalent to $\varepsilon^{A}_{356\ nm}$, = 3.86 x 10^4 dm^3 mol^{-1} cm^{-1} and R^2 = 0.983.

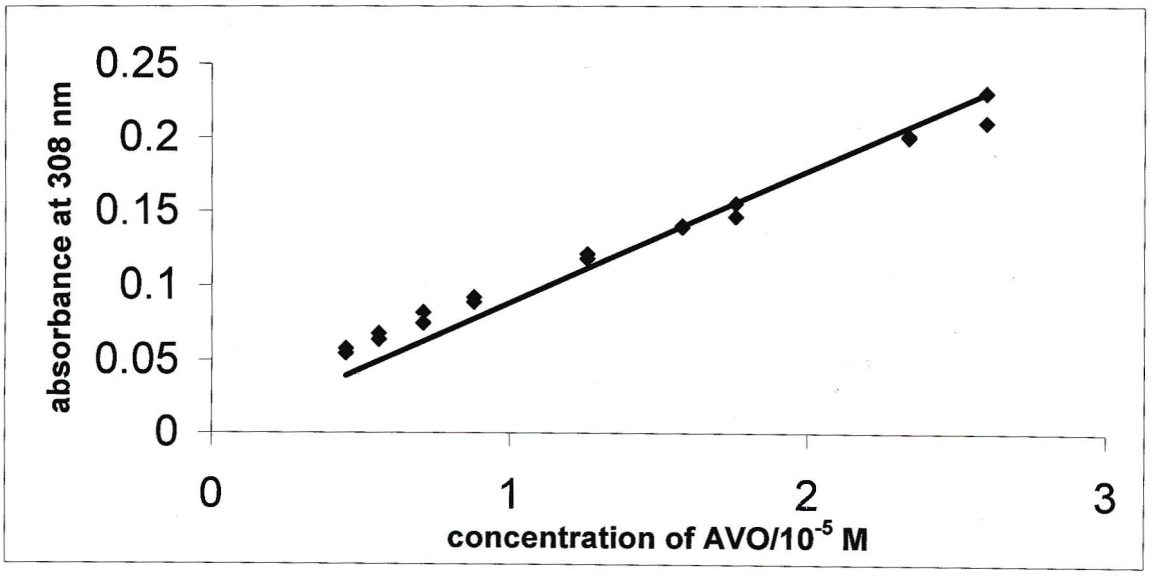

Figure 2.11: Calibration curve illustrating the absorbance of AVO at 308 nm *versus* the concentration of AVO. The slope, equivalent to $\varepsilon^{A}_{308\ nm}$, = 0.884 x 10^4 dm^3 mol^{-1} cm^{-1} and R^2 = 0.9511.

A 1 x 10^{-3} M EHMC stock solution was prepared. This solution was diluted with methanol in a 25 ml volumetric flask to give a concentration of EHMC that had an absorbance approximately equal to one. This solution was then serially diluted to give different concentrations of EHMC and absorbance measurements were taken at 308 nm. Duplicate measurements of fresh solutions were also taken. The initial and duplicate absorbance readings at 308 nm of different concentrations of EHMC are shown Table 2.2. A graph using the initial and duplicate absorbance measurements at 308 nm *versus* the concentration of EHMC was plotted (see Figure 2.12). This graph shows linearity for concentrations of EHMC in the region of 0.6 x 10^{-5} M to 3.0 x 10^{-5} M. The slope of the curve is equivalent to the molar absorption coefficient of EHMC at 308 nm ($\varepsilon^{E}_{308\ nm}$), and the value obtained was 2.65 x 10^{4} dm^{3} mol^{-1} cm^{-1}. Agrapidis-Paloympis [3] quotes ε for *trans*-EHMC at a wavelength of 311 nm to be 2.33 x 10^{4} dm^{3} mol^{-1} cm^{-1} thus the value we obtained is in fair accordance with the literature value.

Table 2.2: Initial and duplicate absorbance values measured at 308 nm for different concentrations of EHMC dissolved in methanol.

[EHMC]/10^{-5} M	$A_{308\ nm}$	Duplicate $A_{308\ nm}$
3.04	0.756	0.789
2.43	0.614	0.650
1.94	0.515	0.529
1.56	0.427	0.430
1.25	0.350	0.335
1.00	0.280	0.273
0.80	0.245	0.234
0.64	0.211	0.194

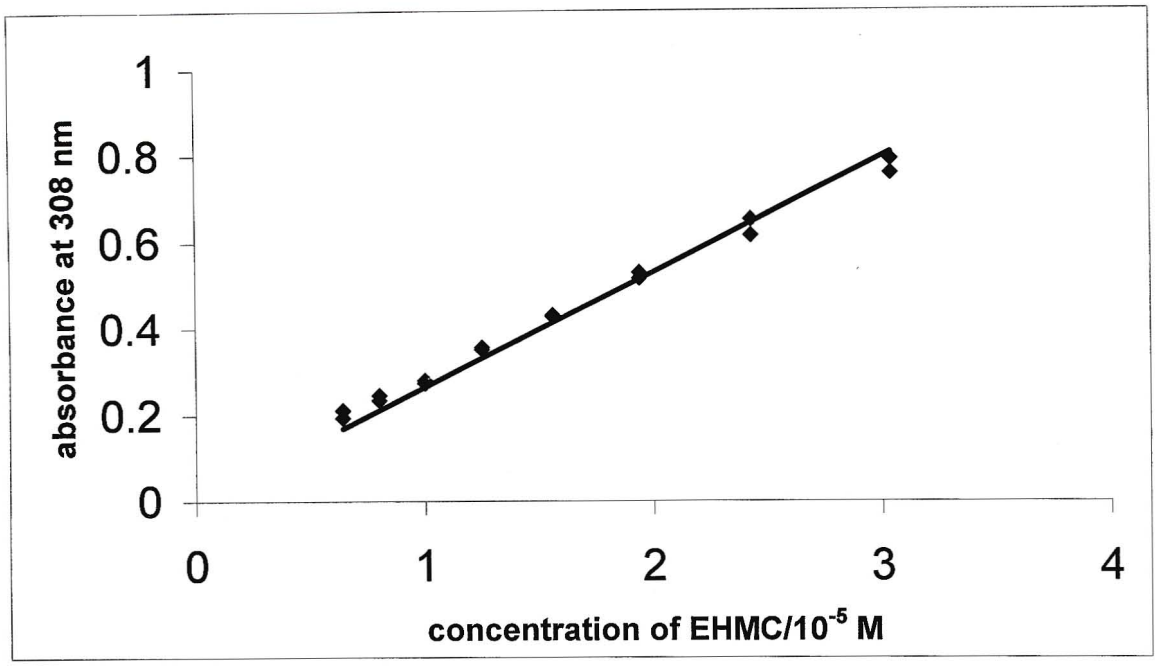

Figure 2.12: Calibration curve illustrating the absorbance of EHMC at 308 nm *versus* the concentration of EHMC. The slope, equivalent to $\varepsilon^{E}_{308\ nm}$, = 2.65 x 10^4 dm^3 mol^{-1} cm^{-1} and R^2 = 0.9834.

In the mixtures of EHMC and AVO dissolved in methanol the concentration of AVO (c_A) can be determined from the calibration curve shown in Figure 2.10 upon measuring the absorbance of the mixture at 356 nm. The molar absorption coefficient of EHMC and AVO in methanol at 308 nm was found to be 2.65 x 10^4 dm^3 mol^{-1} cm^{-1} and 0.884 x 10^4 dm^3 mol^{-1} cm^{-1} respectively. Thus by measuring the absorbance at 308 nm, the following equations can then be used to determine the concentration of EHMC in the mixture:

$$A_{308\ nm} = \varepsilon^{E}_{308\ nm} c_E l + \varepsilon^{A}_{308\ nm} c_A l$$

$$c_E = \frac{A_{308\ nm} - \varepsilon^A_{308\ nm} c_A l}{\varepsilon^E_{308\ nm} l}$$

$$= \frac{A_{308nm} - 0.884 \times 10^4 \times c_A}{2.65 \times 10^4}$$

where $A_{308\ nm}$ is the absorbance reading of the mixture taken at 308 nm, ε^E and ε^A are the molar absorption coefficients of EHMC and AVO at 308 nm respectively, c^E and c^A are the concentration of EHMC and AVO respectively and l is the path length of the cuvette which is equivalent to 1 cm.

A mixture of EHMC and AVO was made up in a 25 ml volumetric flask such that their absorbances were approximately equal to one. This solution was then serially diluted and the absorbances of the solutions were measured at 308 nm and 356 nm. The concentration of AVO was determined from the calibration curve at 356 nm (refer to Figure 2.10) and the concentration of EHMC was determined using the equations above. Since the concentrations of EHMC and AVO in the solutions were known from the dilutions performed, we could compare the calculated and expected results (refer to Table 2.3). From the results obtained we can say that the calculation method developed shows satisfactory agreement with the expected results since the margin of error is within reasonable limits.

2.6.2.2 Spectroscopic method used to quantitate EHMC and AVO in cyclohexane

The wavelengths of maximum absorbance for EHMC and AVO dissolved in cyclohexane are 290 nm and 350 nm respectively. Since EHMC does not absorb at the wavelength of maximum absorbance of AVO a calculation method can be developed to determine the concentrations of EHMC and AVO remaining in a mixture upon irradiation.

Table 2.3: Absorbance readings measured at 308 nm and 356 nm for mixtures of AVO and EHMC dissolved in methanol and a comparison of the expected and calculated concentration values. The % error in the calculated sunscreen absorber concentration is also given.

$A_{308\ nm}$	$A_{356\ nm}$	Expected results		Calculated results		% Error	
		[EHMC]/ 10^{-5} M	[AVO]/ 10^{-5} M	[EHMC]/ 10^{-5} M	[AVO]/ 10^{-5} M	EHMC/ %	AVO/ %
0.868	0.676	3.0	2.0	2.7	1.8	10	10
0.814	0.652	2.8	1.8	2.5	1.7	11	5.6
0.771	0.528	2.6	1.6	2.4	1.5	7.7	6.3
0.736	0.548	2.4	1.4	2.3	1.5	4.2	7.1
0.881	0.414	3.2	1.2	3.0	1.1	6.3	8.3
0.902	0.371	3.4	1.0	3.1	1.0	8.8	0
0.806	0.292	3.0	0.8	2.8	0.8	6.7	0
0.785	0.258	3.0	0.6	2.7	0.7	10	17
0.958	0.791	3.0	2.2	2.9	2.1	3.3	4.5

We first need to develop a calibration curve to determine the concentration of AVO at 350 nm in cyclohexane. We then need to determine the molar absorption coefficients of both EHMC and AVO at 290 nm. From equation 2.2, we can then determine the concentration of EHMC in mixtures.

A 1 x 10^{-3} M AVO stock solution was diluted with cyclohexane in a 25 ml volumetric flask to give a concentration of AVO that had an absorbance approximately equal to one. This solution was then serially diluted to give different concentrations of AVO and their absorbance readings were taken at 290 nm and 350 nm by programming the spectrophotometer to read multiwavelength absorbance. Duplicate absorbance measurements of freshly prepared AVO samples were also taken. The concentrations of AVO together with the initial and duplicate absorbance values at 350 nm and 290 nm are shown in Table 2.4. A graph using the initial and duplicate absorbance values at 350 nm was plotted against the concentration of AVO (see Figure 2.13). The slope of this curve is equivalent to the molar absorption coefficient of AVO at 350 nm ($\varepsilon^{A}_{350\,nm}$) in cyclohexane. Agrapidis-Paloympis *et al.* [3] showed the molar absorption coefficient of AVO in non-polar solvents to be in the region of 3 x 10^4 dm^3 mol^{-1} cm^{-1} and we obtained a value of 3.38 x 10^4 dm^3 mol^{-1} cm^{-1}. The value we obtained is in fair accordance with the literature value implying that Figure 2.13 is a good calibration curve which shows linearity for concentrations of AVO in the region of 0.5 x 10^{-5} M to 2.8 x 10^{-5} M. From this graph the concentration of AVO (c_A) in any solution whose absorbance at 350 nm is known, can be determined. We then needed to determine the molar absorption coefficient of AVO at 290 nm ($\varepsilon^{A}_{290\,nm}$). From absorbance values measured at 290 nm for solutions of known concentrations of AVO (refer to Table 2.4) we plotted a graph taking the absorbance of the initial and the duplicate measurements at 290 nm against the concentration of AVO (refer to Figure 2.14). The slope of this graph is equivalent to $\varepsilon^{A}_{290\,nm}$ and the value obtained was 0.995 x 10^4 dm^3 mol^{-1} cm^{-1}. Due to the low absorbance of AVO at 290 nm the degree of error is much greater which explains the poor linearity of the graph (R^2 = 0.9475).

Table 2.4: Initial and duplicate absorbance values at 350 nm and 290 nm for different concentrations of AVO dissolved in cyclohexane.

[AVO]/10^{-5} M	$A_{350\ nm}$	Duplicate $A_{350\ nm}$	$A_{290\ nm}$	Duplicate $A_{290\ nm}$
2.67	0.912	0.910	0.232	0.238
2.14	0.723	0.729	0.203	0.189
1.71	0.572	0.587	0.173	0.167
1.37	0.460	0.471	0.142	0.138
1.09	0.366	0.375	0.114	0.117
0.88	0.292	0.287	0.099	0.096
0.70	0.230	0.228	0.090	0.089
0.56	0.172	0.176	0.061	0.072
0.45	0.131	0.132	0.045	0.055

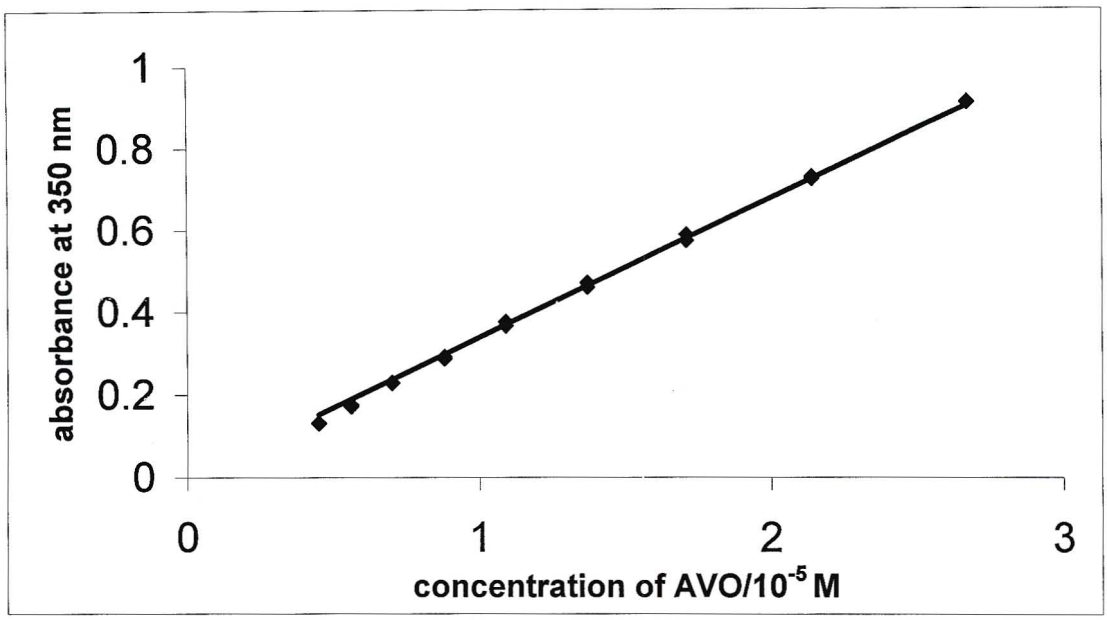

Figure 2.13: Calibration curve illustrating the absorbance of AVO in cyclohexane at 350 nm *versus* the concentration of AVO. The slope, equivalent to $\varepsilon^{A}_{290\,nm}$, = 3.38 x 10^4 dm^3 mol^{-1} cm^{-1} and R^2 = 0.9982.

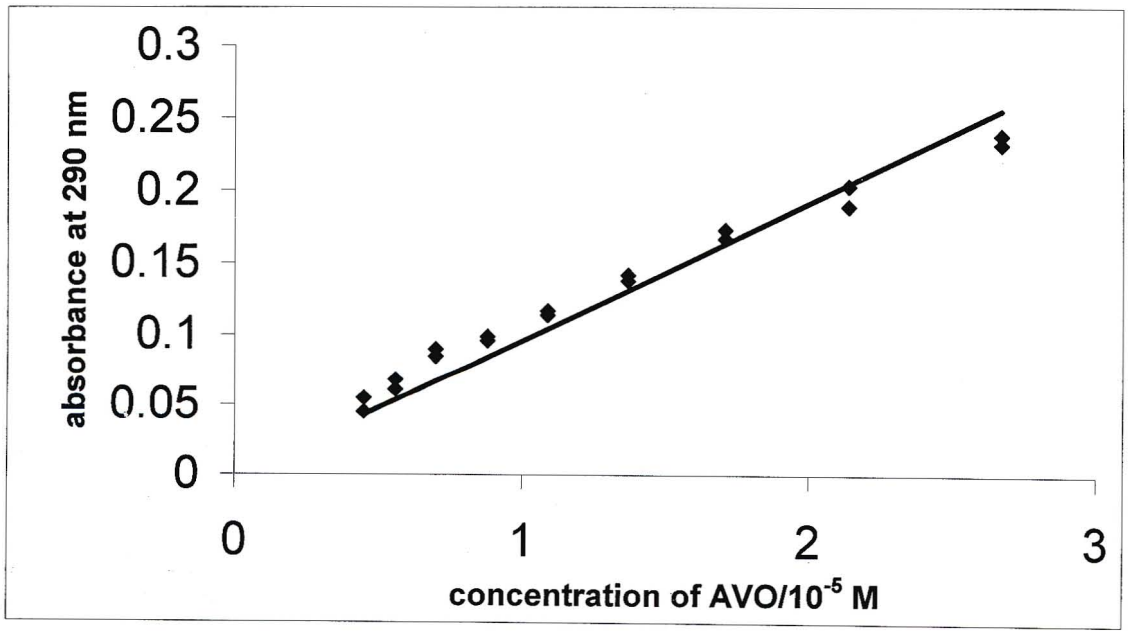

Figure 2.14: Calibration curve representing the absorbance of AVO in cyclohexane at 290 nm *versus* the concentration of AVO. The slope, equivalent to $\varepsilon^{A}_{290\,nm}$, = 0.995 x 10^4 dm^3 mol^{-1} cm^{-1} and R^2 = 0.9475.

A 1 x 10^{-3} M EHMC stock solution was prepared. This solution was diluted with cyclohexane in a 25 ml volumetric flask to give a concentration of EHMC that had an absorbance approximately equal to one. This solution was serially diluted to give different concentrations of EHMC and their absorbance readings at 290 nm were taken. Duplicate measurements of fresh solutions were also taken. The initial and duplicate absorbance readings at 290 nm of different concentrations of EHMC are shown Table 2.5. A graph of the initial and duplicate absorbance measurements at 290 nm was plotted against the concentration of EHMC (see Figure 2.15). This graph is linear for concentrations of EHMC in the region of 0.8 x 10^{-5} M to 4.8 x 10^{-5} M. The slope of the curve is equivalent to the molar absorption coefficient of EHMC at 290 nm (ε^{E}_{308nm}), and the value obtained was 2.53 x 10^{4} dm^{3} mol^{-1} cm^{-1}. Agrapidis-Paloympis *et al.* [3] showed the molar absorption coefficient of EHMC in non-polar solvents to be in the region of 2 x 10^{4} dm^{3} mol^{-1} cm^{-1}. The value we obtained is in fair accordance with the literature value.

Table 2.5: Initial and duplicate absorbance values at 290 nm for different concentrations of EHMC dissolved in cyclohexane.

[EHMC]/10^{-5} M	$A_{290\ nm}$	Duplicate $A_{290\ nm}$
3.75	0.941	0.936
3.00	0.757	0.755
2.40	0.608	0.607
1.92	0.495	0.498
1.54	0.385	0.403
1.23	0.318	0.311
0.98	0.253	0.241
0.79	0.200	0.191

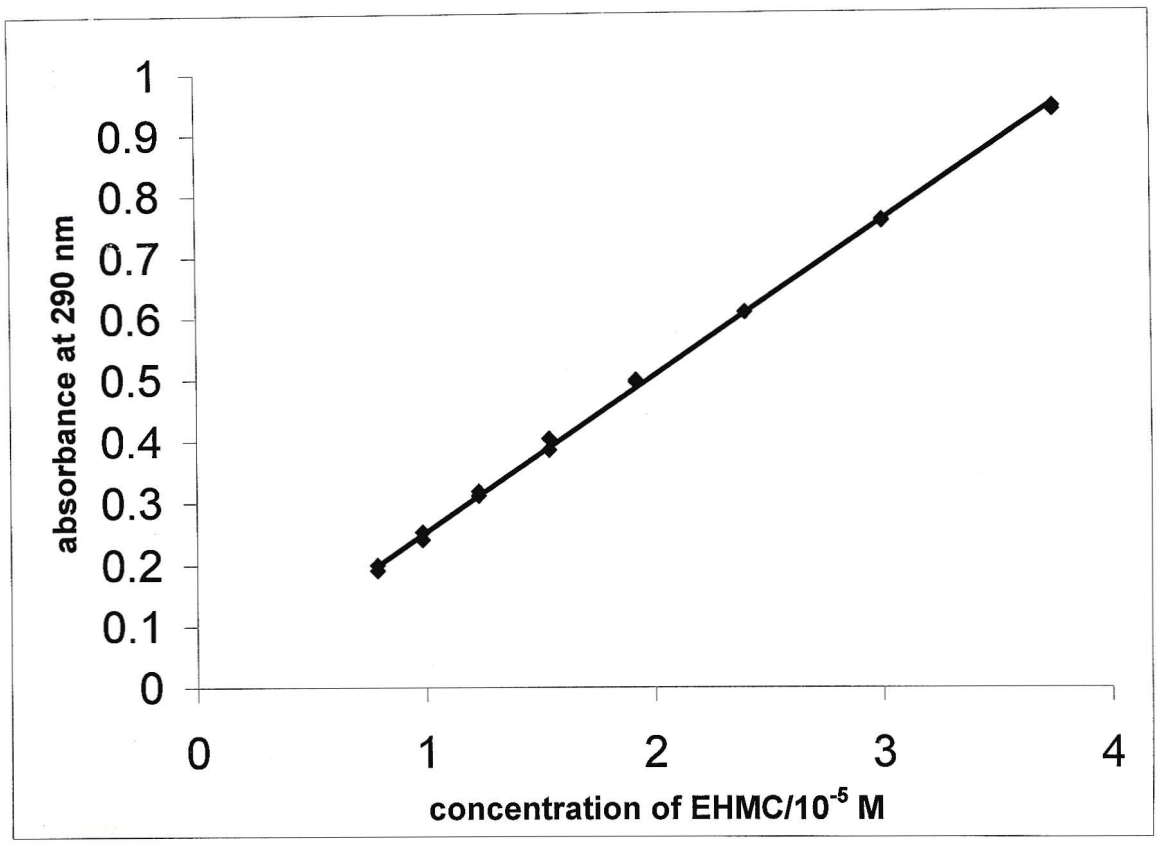

Figure 2.15: Calibration curve representing the absorbance of EHMC in cyclohexane *versus* the concentration of EHMC. The slope of the curve, equivalent to ε^{E}_{290nm}, = 2.53 x 10^4 dm^3 mol^{-1} cm^{-1} and R^2 = 0.9991.

If the absorbance at 350 nm of a mixture of EHMC and AVO dissolved in cyclohexane is known, it can be used to determine the concentration of AVO from the calibration curve depicted in Figure 2.13, since EHMC does not absorb at this wavelength. The molar absorption coefficient of EHMC and AVO in cyclohexane at 290 nm was found to be 2.53 x 10^4 dm^3 mol^{-1} cm^{-1} and 0.995 x 10^4 dm^3 mol^{-1} cm^{-1} respectively. Thus by measuring the absorbance at 290 nm, the following equations can then be used to determine the concentration of EHMC in the mixture:

$$A_{290\ nm} = \varepsilon^{E}_{290\ nm} c_E l + \varepsilon^{A}_{290\ nm} c_A l$$

$$c_E = \frac{A_{290\ nm} - \varepsilon^{A}_{290\ nm} c_A l}{\varepsilon^{E}_{290\ nm} l}$$

$$= \frac{A_{290\ nm} - 0.995 \times 10^4 \times c_A}{2.53 \times 10^4}$$

where $A_{290\ nm}$ is the absorbance of the mixture of AVO and EHMC dissolved in cyclohexane at 290 nm, ε^E is the molar absorption coefficient of EHMC at 290 nm, ε^A is the molar absorption coefficient of AVO at 290 nm and l is the cuvette pathlength which is taken as 1 cm.

A mixture of EHMC and AVO was made up in a 25 ml volumetric flask such that their absorbances were approximately equal to one. This solution was then serially diluted to give different concentrations and their absorbance values were measured at 290 nm and 350 nm. The concentration of AVO was determined from the calibration curve at 350 nm (refer to Figure 2.13) and the concentration of EHMC was determined using the equations derived above. Since the concentrations of EHMC and AVO mixed were known, we could compare the calculated and expected results (refer to Table 2.6). From the results obtained we can say that the calculation method developed shows satisfactory agreement with the expected results.

2.6.3 UV spectra of irradiated samples of EHMC, AVO and a mixture of the two in methanol and cyclohexane

On having devised a method to determine the concentrations of both EHMC and AVO in mixtures dissolved either in methanol or cyclohexane, we were able to quantify the two sunscreen absorbers after various irradiation periods and check their photostabilities. Irradiation of the sunscreen absorbers was carried out with the use of an Osram HBO 500 W/2 high pressure mercury lamp. A 10 mm Pyrex filter that transmitted light of wavelengths greater than 300 nm was attached to the lamp. Solutions having unknown concentrations of EHMC dissolved in methanol and

Table 2.6: Absorbance readings measured at 290 nm and 350 nm for mixtures of AVO and EHMC dissolved in cyclohexane and a comparison of the expected and the calculated concentration values. The % error in the calculated sunscreen absorber concentrations is also given.

$A_{290\ nm}$	$A_{350\ nm}$	Expected Values		Calculated Values		% Error	
		[AVO]/ 10^{-5} M	[EHMC]/ 10^{-5} M	[AVO]/ 10^{-5} M	[EHMC]/ 10^{-5} M	AVO/ %	EHMC/ %
0.999	1.140	2.8	2.8	2.9	2.8	3.6	0
0.816	0.935	2.2	2.2	2.5	2.2	14	0
0.669	0.755	1.8	1.8	1.9	1.9	5.6	5.3
0.564	0.619	1.4	1.4	1.7	1.6	21	14
0.468	0.501	1.1	1.1	1.4	1.3	27	18
0.388	0.410	0.9	0.9	1.2	1.1	33	22
0.354	0.338	0.7	0.7	0.9	1.0	29	43

cyclohexane were irradiated at 1 minute intervals up to a total period of 5 minutes and the concentration of EHMC remaining after each irradiation interval was determined by measuring the absorbances of the solutions and making use of the calibration curves developed (see Figures 2.12 and 2.15). Unknown concentrations of AVO in methanol and cyclohexane were irradiated at 30 minute intervals for a total period of 120 minutes and the concentration of AVO remaining after each irradiation interval was determined from its calibration curve (see Figure 2.10 and 2.13). A mixture of AVO and EHMC in methanol was irradiated at 1 minute intervals up to 5 minutes since AVO does not degrade in polar solvents, whereas the mixture of the filters dissolved in cyclohexane was irradiated at 30 minute intervals for a total period of 120 minutes. The concentrations of EHMC and AVO in the mixtures after each irradiation interval were determined by making use of the calculation method developed in Section 2.6.2. The results obtained are shown and discussed in Sections 3.3.2 and 3.3.3.

2.6.4 Photostability upon irradiation with either UVA or UVB radiation

Instead of using a 10 mm Pyrex filter which transmits light of wavelengths greater than 300 nm, i.e. transmits both UVB and UVA, we wanted to check the effect of irradiating AVO and EHMC individually and also in a mixture with either UVB or UVA light. A 313 nm narrow bandpass filter was used to transmit UVB light while a 365 nm filter was used to transmit UVA light.

The sunscreen absorbers were made up in their respective solvents and placed in a 1 cm pathlength quartz cuvette. Samples were irradiated with the 313 nm filter for various time intervals and absorbance measurements were taken. The same solution was continuously irradiated for specific time intervals.

The following solutions were irradiated and monitored in the manner described above:

- 3.8×10^{-5} M EHMC in methanol was irradiated at 1 minute intervals for a total period of 5 minutes.
- 3.7×10^{-5} M EHMC in cyclohexane was irradiated at 1 minute intervals for a total period of 5 minutes.

- 2.7×10^{-5} M AVO in methanol was irradiated at 30 minute intervals for a total period of 120 minutes.
- 3.2×10^{-5} M AVO in cyclohexane was irradiated at 30 minute intervals for a total period of 120 minutes.
- A mixture of AVO and EHMC was prepared such that they both had absorbances approximately equal to one. The mixture in methanol was irradiated at 1 minute intervals for a total period of 5 minutes while that in cyclohexane was irradiated at 30 minute intervals for a total period of 120 minutes.

The procedure used to check the effect of irradiating the sunscreen absorber solutions with the 365 nm filter was the same as that of the 313 nm filter. The following solutions were analysed:

- 3.2×10^{-5} M EHMC in methanol, irradiated at 1 minute intervals for a total period of 5 minutes.
- 3.7×10^{-5} M EHMC in cyclohexane, irradiated at 1 minute intervals for a total period of 5 minutes.
- 1.9×10^{-5} M AVO in methanol, irradiated at 30 minute intervals for a total period of 120 minutes.
- 3.2×10^{-5} M AVO in cyclohexane, irradiated at 30 minute intervals for a total period of 120 minutes.
- A mixture of the two sunscreen absorbers was prepared in a similar manner to that of the mixture prepared when using the 313 nm filter. This mixture in both solvents was irradiated at 30 minute intervals for a total period of 120 minutes.

The concentrations of EHMC and AVO remaining upon irradiation with the 313 nm and the 365 nm filters were determined using the calculation method developed. The results obtained are discussed in Section 3.3.4.

2.6.5 The effect of quenchers on photostability

When the transfer of electronic energy causes deactivation of an excited state we call this process quenching. This is one way of determining whether a photochemical reaction of a sunscreen occurred from the singlet or triplet excited state. Oxygen can act as a quencher of triplet states. However, as the results obtained with oxygen can never be regarded as conclusive we also looked at *cis*-piperylene as a triplet-state quencher. The work of Chatelain and Gabard [2] shows that Tinosorb S photostabilises AVO and mixtures of AVO and EHMC. One possibility for this photostabilisation is that it is acting as a triplet-state quencher. However, as the triplet-state energy of Tinosorb S is not known this possibility was not investigated.

Oxygen exists in its triplet ground state [4]. It can act as a triplet quencher by taking up the energy of molecules that are in their excited triplet-state to form excited singlet oxygen Thus molecules that are quenched will go back to their ground state and product formation will have been prevented if this is derived from the triplet state.

The oxygen was reduced from solutions of AVO, EHMC and a mixture of the two, in cyclohexane and methanol, by purging the solutions with N_2 for a period of 10 minutes. These purged solutions are referred to being absent of oxygen. The solutions were then irradiated for the same time intervals as described in Section 2.6.3 and the UV-spectra of the irradiated solutions were recorded and are shown in Section 3.3.5. The results obtained were compared to those observed when O_2 was present and are presented in Section 3.3.5. If the loss in absorbance observed when O_2 is present is prevented this would mean that the products formed are from the triplet excited state.

The triplet energies of AVO and *cis*-piperylene are 249 kJ mol^{-1} and 247 kJ mol^{-1} respectively [38]. Since *cis*-piperylene has a lower triplet energy than that of AVO we thought that it would act as a quencher to irradiated samples of AVO. As the triplet energy of EHMC at 238 kJ mol^{-1} [39] is lower than that of *cis*-piperylene, *cis*-piperylene would have no quenching effects here.

Cis-piperylene has a wavelength of maximum absorbance of 222 nm in both methanol and cyclohexane (see Figure 2.16). This is ideal since upon irradiating with the 10 mm thick Pyrex filter there would be no effect on *cis*-piperylene. We prepared 1.0 x 10^{-3} M stock solutions each of EHMC, AVO and *cis*-piperylene in both methanol and cyclohexane. These solutions were not purged for the removal of oxygen.

The individual sunscreen absorber solutions were made up by mixing 1 ml of the absorber solution with 1 ml of *cis*-piperylene in a 20 ml volumetric flask which was made up to the mark with the respective solvent. The solution was then serially diluted such that the absorbance of the sunscreen absorbers was approximately equal to one. This solution was then placed in a 1 cm pathlength cuvette and irradiated for the following time intervals:

- AVO mixed with *cis*-piperylene in cyclohexane was irradiated at 30 minute intervals for a total period of 120 minutes. We did not look at the quenching effect of *cis*-piperylene on irradiated solutions of AVO dissolved in methanol since AVO shows photostability in this solvent.
- EHMC mixed with *cis*-piperylene in methanol and cyclohexane was irradiated at 1 minute intervals for a total period of 5 minutes.

In the preparation of a mixture of the sunscreen absorbers, 0.5 ml of EHMC and 0.5 ml of AVO was mixed with 1 ml of *cis*-piperylene in a 20 ml volumetric flask which was made up to the mark with the respective solvents. The solution was then serially diluted such that the absorbance of the sunscreen absorbers was approximately equal to one. This solution was then placed in a 1 cm pathlength cuvette and irradiated for the following time intervals:

- The mixture in cyclohexane was irradiated at 30 minute intervals for a total period of 120 minutes.
- The mixture in methanol was irradiated at 1 minute intervals for a total period of 5 minutes.

All the irradiated samples were then analysed with the UV-spectrophotometer and the UV-spectra recorded and compared to those in the absence of the quencher. The results can be seen in Section 3.3.5.

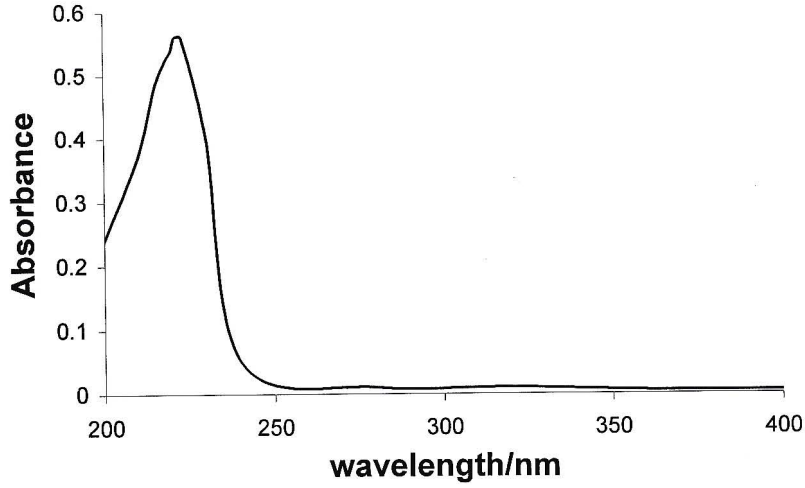

Figure 2.16: UV-spectrum of *cis*-piperylene dissolved in methanol.

2.6.6 The effect of photosensitisers on photostability

In order to determine whether photoproduct formation is from the singlet or triplet state of the sunscreen agents used we made use of photosensitisers. We used benzophenone as a photosensitiser since it has a triplet energy (289 kJ mol^{-1}) higher than that of either AVO (249 kJ mol^{-1}) or EHMC (238 kJ mol^{-1}) [39]. We did not investigate the effect of acetophenone (postulated as a possible photosensitiser by Schwack and Rudilph [16]) since it absorbs UV-radiation in the same region as EHMC.

A 1 x 10^{-3} M stock solution of each of benzophenone, EHMC and AVO was made up in both methanol and cyclohexane without the removal of O_2. Benzophenone absorbs maximally close to 250 nm in both solvents which can be seen from the UV-spectra in Figures 2.17 and 2.18. From the UV-spectra of EHMC and AVO in both solvents (shown in Section 3.3.6) it can be said that EHMC and AVO absorb minimally at 254 nm. Therefore we used a 254 nm filter for irradiation experiments to ensure that essentially only benzophenone would be excited.

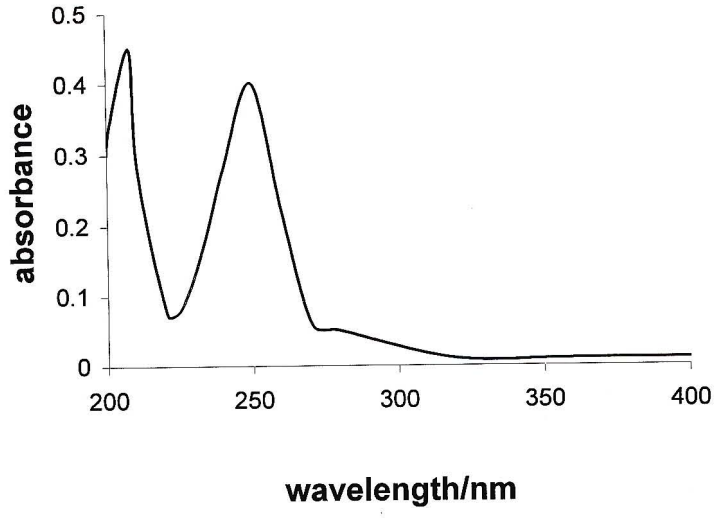

Figure 2.17: UV-spectrum of benzophenone in methanol.

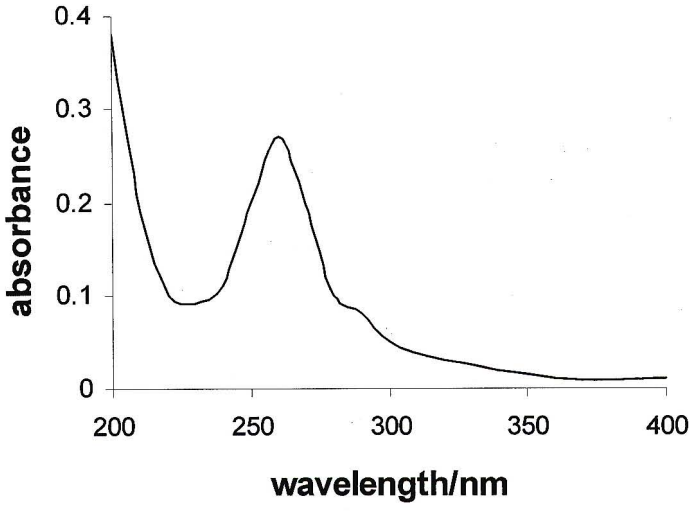

Figure 2.18: UV-spectrum of benzophenone in cyclohexane.

The individual sunscreen absorber solutions were made up by mixing 1 ml of the absorber solution with 1 ml of benzophenone in a 20 ml volumetric flask which was made up to the mark with the respective solvent. The solution was then serially diluted such that the absorbance of the sunscreen absorbers was approximately equal to one. This solution was then placed in a 1 cm pathlength cuvette and irradiated for the following time intervals:

- AVO mixed with benzophenone in cyclohexane was irradiated at 30 minute intervals for a total period of 120 minutes. We did not look at the photosensitising effect of benzophenone on irradiated solutions of AVO dissolved in methanol since AVO shows photostability in this solvent.
- EHMC mixed with benzophenone in methanol and cyclohexane was irradiated at 1 minute intervals for a total period of 5 minutes.

In the preparation of a mixture of sunscreen absorbers, 0.5 ml of EHMC and 0.5 ml of AVO were mixed with 1 ml of benzophenone in a 20 ml volumetric flask which was made up to the mark with the respective solvents. The solution was then serially diluted such that the absorbance of the sunscreen absorbers was approximately equal to one. This solution was then placed in a 1 cm pathlength cuvette and irradiated for the following time intervals:

- The mixture in cyclohexane was irradiated at 30 minute intervals for a total period of 120 minutes.
- The mixture in methanol was irradiated at 1 minute intervals for a total period of 5 minutes.

All the irradiated samples were then analysed with the UV-spectrophotometer and the UV-spectra recorded and compared to those in the absence of the photosensitiser. The results can be seen in Section 3.3.6.

As AVO has a triplet energy higher than that of EHMC, it is therefore possible that AVO could photosensitise the isomerisation of *trans*-EHMC. From the UV-spectra in Section 3.3.4 (refer to Figures 3.23 and 3.24) we noticed the possibility of this effect occurring upon irradiating a mixture of EHMC and AVO in cyclohexane with the 365 nm filter but this effect did not occur in a methanolic solution. We therefore irradiated a 3.7×10^{-3} M solution of EHMC and a mixture of EHMC and AVO in cyclohexane with the 365 nm filter (so that only AVO would be excited) and then compared UV-spectra to check for any photosensiting effects of AVO by monitoring the loss in absorbance of EHMC. The results obtained can be seen in Section 3.3.6.

2.7 Photoproduct analysis

In this work chromatographic techniques were used to analyse for the formation of photoproducts in irradiated samples of EHMC and AVO dissolved in either methanol or cyclohexane. Chromatography is a physical method of separation in which the components to be separated are distributed between two phases one of which is a stationary phase while the other is a mobile phase. M.S. Tswett, a Russian botanist, is credited with the discovery of chromatography. He used a column of powdered calcium carbonate to separate green leaf pigments into a series of coloured bands by allowing a solvent to flow through the column bed [40].

A distinction between the principle chromatographic methods can be made in terms of the properties of the mobile phase. In gas chromatography the mobile phase is an inert gas and in liquid chromatography the mobile phase is a liquid of low viscosity.

2.7.1 High performance liquid chromatography

In classical liquid chromatography an adsorbent, for instance alumina or silica, is packed into a column and the mobile phase flows through the column by means of gravity. A mixture to be separated is introduced at the top of the column and is washed through the column by the eluting liquid. If a component of the mixture is adsorbed weakly onto the surface of the solid stationary phase it will travel down the column faster than other solutes. Thus separation of solutes is possible if there are differences in their adsorption by the solid. This method is called adsorption chromatography or liquid solid chromatography [41].

As high performance liquid chromatography (HPLC) has developed, the particle size of the stationary phase used has become progressively smaller. Porous silica particles with spherical or irregular shape and diameters of 10, 5 and 3 μm are used. The different separation mechanisms can be realized by bonding different chemical groups to the surface of the silica particle to produce what are called bonded phases.

In our case EHMC and AVO are large non-polar organic molecules therefore we require reverse phase separation where we have a non-polar stationary phase and a polar mobile phase. We therefore chose a Nucleosil 100 column, which has a C_{18} alkyl group attached to the surface of the silica particle, and 85% (v/v) MeOH/H_2O was used as the mobile phase. This type of bonded phase is called ODS (octadecyl silane).

When packed into a column, the small size of these particles leads to considerable resistance to solvent flow, so that the mobile phase has to be pumped through the column under high pressure. Columns of 10-25 cm long and 4.6 mm internal diameter are usually used. Columns are usually made of stainless steel, although glass or plastics are also used. There is growing interest in the use of columns that have diameters of 2 mm or less (microbore columns).

There are two modes of elution in HPLC. The first is isocratic elution, where the composition of the mobile phase is constant. The second is gradient elution, where the composition of the mobile phase can be made to change in a predetermined way during the separation. Gradient elution is used when two solutes cannot be resolved and eluted in a reasonable time using a single solvent or solvent mixture.

From Figure 2.19 it can be seen that an analytical HPLC system consists of a solvent reservoir (containing the mobile phase), solvent delivery system (pump), injector, column, detector, data processor and a printer.

Separation and photoproduct analysis of the sunscreen absorbers dissolved in methanol was carried out by the use of HPLC. This technique involved the selection of a suitable column, determination of a suitable mobile phase to resolve the sunscreen filters and their photoproducts, and then, using the software provided, to analyse the extent of the photochemical reaction. Therefore, a description of the equipment used, determination of a suitable mobile phase and analysis of the photoproducts are presented below.

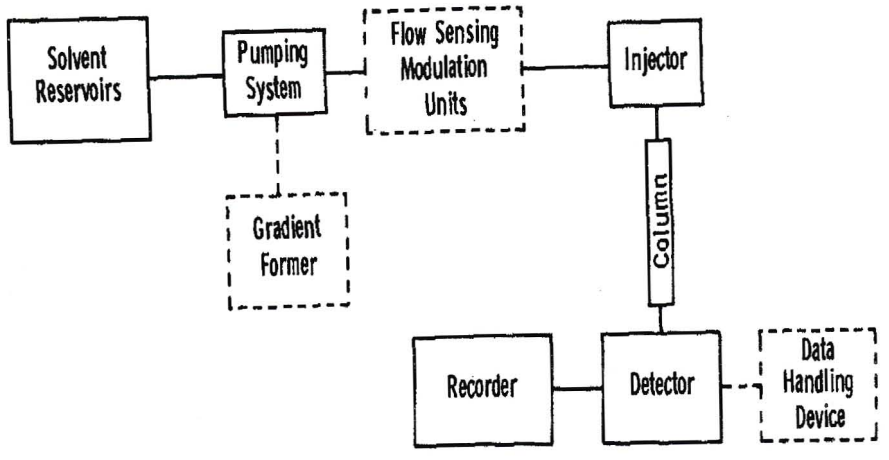

Figure 2.19: Block diagram illustrating an analytical high performance liquid chromatograph system [40].

2.7.1.1 HPLC equipment and operation

An analytical HPLC was used for the optimisation of the separation of the two filters and the photoproducts of *trans*-EHMC, peak identification and quantification experiments.

This system consists of a Waters 600 multisolvent delivery system with 225 µl pumpheads, a U6K injector, a Waters 996 photodiode array detector, a De` Mark Pentium II computer and a Hewlett Packard Deskjet 950C colour printer. The Waters Millenium software was used to acquire data, develop a processing method, review results and print reports.

The Waters 600 system has programmable features to facilitate the use of gradient and isocratic modes of elution. The flow and sparge rates for the different modes could also be easily programmed. Sparging was carried out using He to remove dissolved air from the mobile phase. A Waters Guard-Pak µ-Bondapak C_{18} precolumn insert was included between the solvent delivery system and the column to remove contaminants and particulate matter. The photodiode array detector (PDA) monitors UV absorbance in the wavelength range from 190 to 600 nm.

The column used for the separation of the two filters and the photoproducts of *trans*-EHMC, was a Nucleosil 100 C_{18} reversed phase column. This column has an internal diameter of 4.6 mm, length of 250 mm and 5 μm particle size. Kowlaser [23] used a semi-preparative Spherisorb 5 ODS 2 reverse phase column for the separation of the photoproducts of *trans*-EHMC but we found shorter retention times with the use of the Nucleosil 100 reversed phase column.

Before using the column it was conditioned, in order to remove impurities that could have been retained from previous analyses, by running the following gradient: water (H_2O) for 30 minutes at 1.0 ml/min, H_2O to methanol (MeOH) over 5 minutes at 1.0 ml/min, MeOH for 30 minutes at 1.0 ml/min; MeOH to acetonitrile (ACN) over 5 minutes at 1.0 ml/min, ACN for 30 minutes at 1.0 ml/min; ACN to tetrahydrofuran (THF) over 5 minutes at 1.0 ml/min, THF for 30 minutes at 1.0 ml/min. The procedure was then reversed.

All solvents used were of HPLC grade which were filtered through Millipore 0.45 μm HV organic aqueous filters. Water used for HPLC analysis was obtained from a Millipore Milli-Q water purification system. A Hamilton airtight 100 μl syringe was used to make all injections. The PDA detector was allowed a 1 hour warm-up period so that the deuterium-lamp could reach full intensity.

2.7.1.2 Isocratic mode of separation

For the separation of the two filters and *cis*-EHMC a mobile phase of 85% (v/v) MeOH/H_2O produced optimum resolution with short retention times. The flow rate was 1.0 ml/min and the injection volume was 80 μl. Blank injections with methanol were made prior to injection of samples to ensure that carryover of sample from previous injections did not occur. The column backpressure limit was set at 3500 psi. When the column backpressure increased beyond this pressure limit the pre-column insert was replaced to maintain normal pressure conditions and bleeding of the pump was also carried out for the removal of air-bubbles. The detection wavelength for monitoring the isomers of EHMC and AVO was set at 335 nm.

2.7.1.3 HPLC analysis of methanol solutions

The use of 85% (v/v) MeOH/H_2O was used for complete resolution of the two filters and *cis*-EHMC was also resolved with this isocratic mobile phase. In order to quantify the sunscreens remaining upon irradiation we first needed to develop calibration curves of the sunscreen concentrations *versus* their peak areas from HPLC analysis. A solution containing 1 x 10^{-3} M EHMC and 1 x 10^{-3} M AVO in methanol was prepared in a 100 ml volumetric flask. The mixture was serially diluted and 80 µl of each of the diluted solutions was injected into the HPLC. The concentrations of AVO and EHMC taken together with their peak areas are shown in Tables 2.7 and 2.8 respectively. The Millennium software was used to process this data and calibration curves of EHMC and AVO were developed (see Figures 2.20 and 2.21). The R^2 values for the calibration curves of AVO and EHMC are 0.9997 and 0.9994 respectively. This implies that there is good linearity for the concentrations of AVO in the region of 0.5 x 10^{-5} M to 30 x 10^{-5} M and concentrations of EHMC in the region of 0.5 x 10^{-5} M to 33 x 10^{-5} M. These calibration curves were used to quantify the amount of EHMC and AVO remaining upon irradiation.

Table 2.7: The peak areas of different concentrations of AVO injected into the HPLC and eluted with a mobile phase of 85% (v/v) MeOH/H_2O on a Nucleosil 100 C_{18} column. The detection wavelength was 335 nm and the injection volume was 80 µl.

[AVO]/10^{-5} M	Peak Area/10^7
28.55	2.744
14.28	1.330
7.140	0.650
3.570	0.317
1.790	0.129
0.893	0.054
0.357	0.036

Table 2.8: The peak areas of different concentrations of EHMC injected into the HPLC and eluted with a mobile phase of 85% (v/v) $MeOH/H_2O$ on a Nucleosil 100 C_{18} column. The detection wavelength was 335 nm and the injection volume was 80 µl.

[EHMC]/10^{-5} M	Peak Area/10^6
32.87	11.64
17.03	5.964
8.515	3.269
4.258	1.781
2.219	0.952
1.070	0.512
0.426	0.250

A solution of 4.4 x 10^{-4} M EHMC in methanol was irradiated at 1 minute intervals up to a total of 5 minutes. The mixture of 2.5 x 10^{-5} M of EHMC and 2.7 x 10^{-5} M AVO in methanol was irradiated at 1 minute intervals up to 5 minutes and thereafter at 15 minute intervals up to 60 minutes. The irradiations were carried out with an Osram HBO 500 W/2 high pressure mercury lamp in combination with a 10 mm thick Pyrex filter that allowed light of wavelengths greater than 300 nm to pass through.

A mobile phase of 85% (v/v) $MeOH/H_2O$ was used for the separation of the photoproducts. The quantitation of *trans*-EHMC was done from the calibration curve of concentration of EHMC *versus* peak area (see Figure 2.21). The concentration of *cis*-EHMC was calculated by difference from the initial concentration of *trans*-EHMC and that remaining after irradiation. The results are shown and discussed in Section 3.4.1.

Solutions of AVO in methanol showed photostability upon irradiation therefore there was no need to analyse the irradiated AVO solution, using HPLC, for photoproducts of AVO.

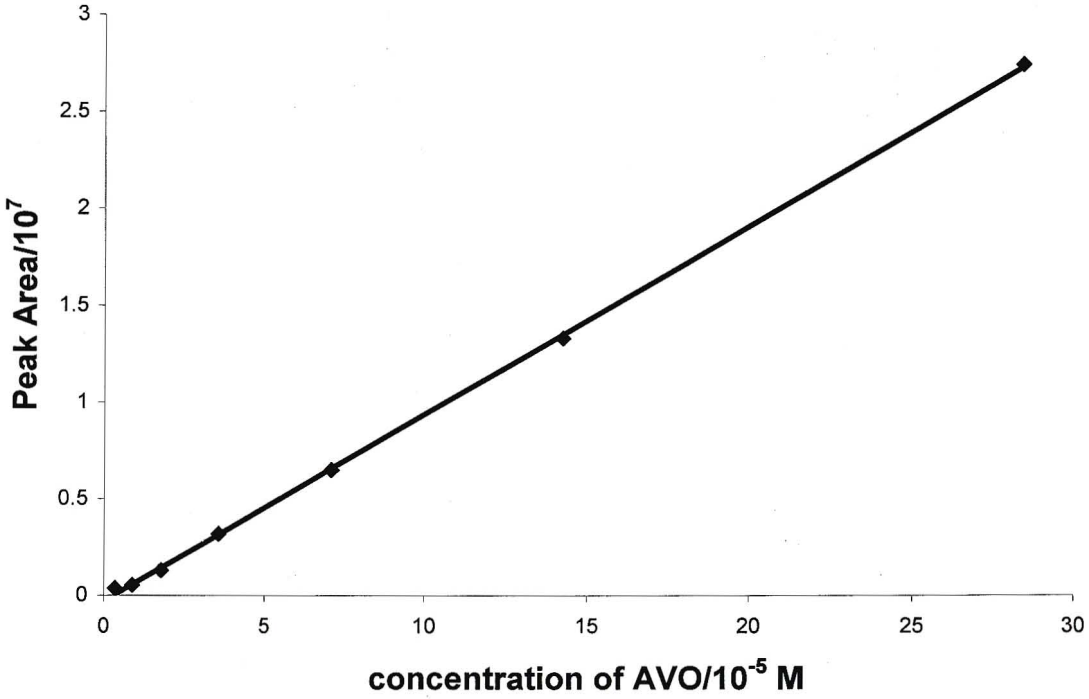

Figure 2.20: Calibration curve of different concentrations of AVO *versus* their peak areas upon HPLC analysis on a Nucleosil 100 C_{18} column, using 85% (v/v) MeOH/H_2O as the mobile phase at a flow rate of 1 ml/min. The detection wavelength was 335 nm and the injection volume was 80 µl. The slope of the curve is 0.965 and $R^2 = 0.9997$.

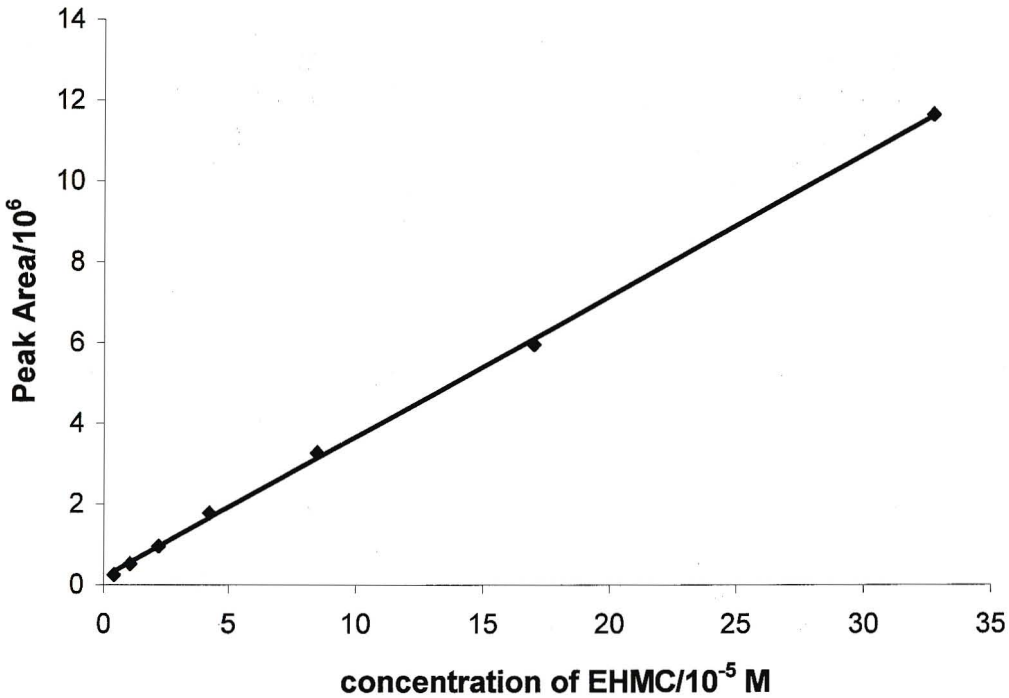

Figure 2.21: Calibration curve showing different concentrations of EHMC versus their respective peak areas upon HPLC analysis on a Nucleosil 100 C_{18} column, using 85% (v/v) MeOH/H_2O as the mobile phase at a flow rate of 1 ml/min. The detection wavelength was 335 nm and the injection volume was 80 µl. The slope of the curve is 0.3477 and $R^2 = 0.9994$.

2.7.2 Gas chromatography (GC)

The principle behind gas chromatography is similar to that applied to HPLC except that the distinctive feature of gas chromatography is the use of a gas as the mobile phase. The sample mixture containing components to be separated is introduced into the gas stream just before it encounters the stationary phase. These components are separated on the basis of their distribution between the two phases and are detected as they emerge in the gas at the other end of the column [42].

Figure 2.22 illustrates the instrumentation of gas chromatography. Carrier gas (mobile phase) from a tank of compressed gas passes to a flow regulater in order to maintain constant flow of gas. The gas then passes to the beginning of the column. At the inlet to the column there is a sample injector where the sample to be analysed is injected. The carrier gas then elutes the components of the mixture through the column. As the components are eluted they are detected by the detector which uses some physical or chemical property of the vapours by which they can be detected [43].

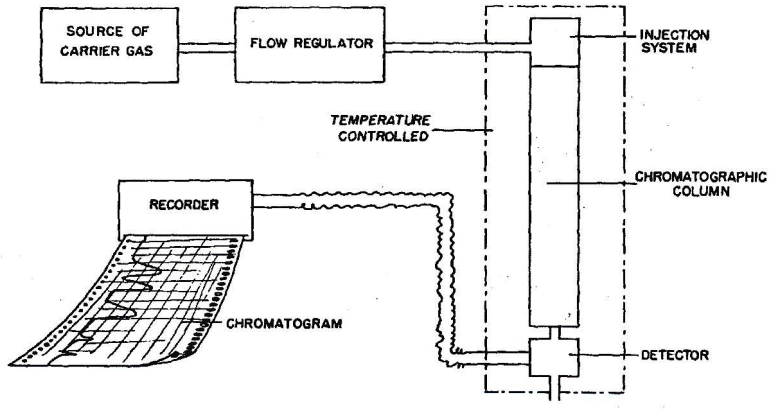

Figure 2.22: Diagram of apparatus for analytical gas chromatography [43].

In most cases helium, argon, nitrogen or hydrogen are used as carrier gases. In our case we used nitrogen as the carrier gas and the pressure and rate of flow of this gas was controlled by flow controls.

Separation of a mixture depends on its components having different distribution equilibria. These distribution equilibria are controlled by the components vapour pressures and their adsorption by the stationary phase.

There are two types of columns: packed and capillary. Packed columns are tubes 1 m to 10 m long, and between 2 mm and 9 mm in internal diameter [42]. These columns are packed with coarse or granular powder with particles between 0.1 mm and 0.6 mm diameter [43]. These packings fall into one of two categories. It can be uncoated solid where the technique of analysis is referred to as gas solid chromatography (gsc) or alternatively the packing can be an inert solid coated with a thin film of a non-volatile liquid. This technique is referred to as gas liquid chromatography (glc). Kieselguhr, ground fibrebrick, glass beads, etc., are used as solid supports [43].

A capillary column consists of a long fine tube of fused silica of which the inner surface is coated with stationary liquid. The type of liquid chosen should be able to dissolve all the components of the mixture and must also be completely involatile relative to any of them. Stationary liquids must have boiling points which are high in comparison with the boiling points of the components of the mixture [43]. The types of high boiling point liquids used are silicone oils, high boiling esters such as phthalates, high boiling paraffins, and liquid polymers. For the separation of EHMC, AVO and their photoproducts we made use of a capillary column.

Injection is usually achieved by means of a syringe inserted through a self-sealing silicone-rubber septum. In the case of capillary columns, injection of a large volume of sample would cause an overload. This is overcome by the use of a stream splitter. On injection the sample is vaporised and mixed with the carrier gas and a fraction of this is delivered to the column and the remainder is vented into the atmosphere. In our case dilute solutions of EHMC and AVO where made up in cyclohexane. We made splitless injections, where the stream splitter was turned off and all the sample was injected onto the column. The oven temperature was programmed to start close to the boiling point of AVO so that all the cyclohexane vaporised and eluted from the column immediately. We therefore needed to optimize the temperature programming conditions to resolve the sunscreen agents and their photoproducts.

Detection is based on a physical property of the effluent gas stream. The physical property chosen must be one which changes significantly when the carrier gas contains a component eluting from the column [42]. There are a number of detectors used but in this work we made use of a flame ionisation detector (FID) (see Figure 2.23).

This detector has a high sensitivity and selectivity for carbon-compounds thus making it ideal for EHMC and AVO analysis. The way this detector operates is by mixing H_2 with the effluent from the gas chromatograph column and then burning the mixed gases in air. Two electrodes, maintained at constant potential difference, are in or near the flame and the DC current flowing between them is monitored. The current is proportional to the amount of carbon in the form of volatile organic compounds, which enters the flame in the column effluent. A graphical record is made in the form of a chromatogram. This detector is perfect for analysing EHMC and AVO since standards of the two can be injected to determine their presence but for photoproduct analysis we needed to make use of GC-MS.

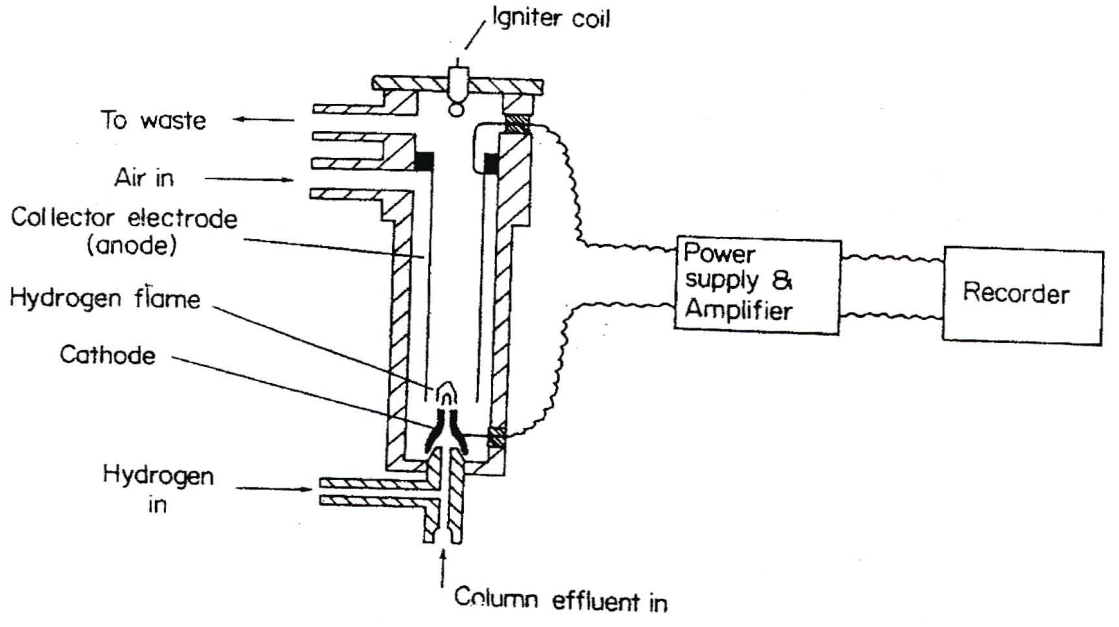

Figure 2.23: A flame ionisation detector [42].

Reversed phase HPLC could not be used to separate the filters and their photoproducts in cyclohexane since EHMC and AVO are both non-polar and so is cyclohexane. Since cyclohexane has a boiling point of about 80°C gas chromatography was an ideal technique to use to resolve the filters and their photoproducts. Gas chromatography with flame ionisation detection (GC-FID) was used to check if any photoproducts formed. Gas chromatography with mass spectral detection (GC-MS) was used to identify the photoproducts formed.

2.7.2.1 GC-FID equipment and operation

GC with a flame ionization detector (GC-FID) was used to check whether EHMC and AVO dissolved in cyclohexane formed any products upon irradiation. This technique was used by Natalie Ingouville [44] to show the isomerisation of *trans*-EHMC.

A Perkin Elmer Autosystem Gas Chromatograph was used together with a FID detector. The column was a Supelco 25 m x 250 μm x 0.25 μm PET-S fused silica capillary column. The nitrogen carrier gas flow rate was 0.5 ml/min. The FID used an air/hydrogen flame with flow rates of approximately 300 ml/min and 30 ml/min respectively. The injector was used in a splitless mode.

2.7.2.2 GC-FID analysis of cyclohexane solutions

EHMC and AVO are fairly large molecules therefore it was necessary to have a high detector temperature and a temperature programme set to the highest possible temperature which could be withstood by the column.

The following conditions were used:
Detector temperature: 320°C
Temperature programme: 200°C held for 1 minute then increased to 300°C at 10°C/min and held at 300°C for 5 minutes.

Dibutyl phthalate (DBP) was used as an internal standard. Analysis of the unirradiated solutions of the sunscreen agents containing DBP showed this internal

standard to elute at 2.5 minutes, EHMC at 4.9 minutes and AVO at 8.3 minutes. Since the response of the FID could not be assumed to be constant on a day-to-day basis the relative response factor (RRF) of the detector was calculated to accommodate for variation in detector response.

The RRF was calculated by determining the exact amount of DBP and sunscreen agent used and taking into account their peak areas from the chromatograms obtained:

$$RRF = \frac{m_{DBP}}{m_{sunscreen}} \times \frac{A_{sunscreen}}{A_{DBP}}$$

where m_{DBP} is the total mass of DBP, $m_{sunscreen}$ is the total mass of the sunscreen agent used, $A_{sunscreen}$ is the peak area of either AVO or EHMC and A_{DBP} is the peak area of DBP.

The mass of sunscreen agents remaining after irradiation was obtained by rearranging the above equation since the RRF was known:

$$m_{sunscreen} = \frac{m_{DBP}}{RRF} \times \frac{A_{sunscreen}}{A_{DBP}}$$

The detector response is dependent on the molecular mass of the sample and since *cis*- and *trans*-EHMC have the same molecular mass the RRF was taken to be the same for both isomers. The RRF determined can therefore be used to calculate the mass of *cis*-EHMC formed upon irradiation if the peak area for *cis*-EHMC is known.

With the use of a 10 µl Gilson micropipette, 5 µl of unirradiated 1 x 10^{-3} M AVO solution was mixed with 5 µl of DBP in an Ependorff tube. A 1 µl aliquot of this solution was then injected into the GC. This 1 x 10^{-3} M solution of AVO was then irradiated with the Osram HBO 500 W/2 high pressure mercury lamp and 10 mm thick Pyrex filter at 1 hr intervals in a 1 mm pathlength quartz cuvette and was subsequently analysed as described above. A solution containing a mixture of 1 x 10^{-3} M AVO and 1 x 10^{-3} M EHMC was prepared and this solution was then irradiated at 1 hour intervals up to 3 hours whereas a solution containing 1 x 10^{-3} M EHMC was subjected to irradiation at 1 minute intervals. DBP was added after the samples were

irradiated and just before the samples were injected into the GC. These samples were also analysed using the GC conditions described above and the results obtained are shown and discussed in Section 3.4.2.

2.7.2.3 GC-MS equipment and operation

From GC-FID analysis we determined that the loss in absorbance of *trans*-EHMC in cyclohexane was due to it isomerising to its *cis*-isomer. The loss in absorbance of AVO in cyclohexane was due to it photodegrading to several photoproducts. We therefore needed to determine the identity of these photoproducts. We also checked whether AVO photosensitises the isomerisation of EHMC in cyclohexane. Thus, unirradiated and irradiated samples were subjected to GC-MS analysis. We also used GC-MS to determine the formation of UVB absorbing photoproducts upon irradiation of a mixture of EHMC and AVO dissolved in cyclohexane.

For the analysis of a solution of AVO dissolved in cyclohexane and irradiated for 8 hours, an Agilent 6890 series gas chromatograph with an Agilent 5973 series mass selective detector (electron impact) controlled by a Pentium III 600 computer, was used. The column used was a HP-5 methyl silicon 25 m x 250 μm x 0.25 μm capillary column. All injections were done with an Agilent P/N: 23-265/42/HP syringe with the injector in the splitless mode. A 1 μl aliquot of irradiated sample was injected. Helium was used as the mobile phase at a flow rate of 0.5 ml/min.

The following conditions were used on this system:

Detector temperature:	280°C
Temperature programme:	50°C, held for 1 minute then raised to 300°C at 20°C/min, the final temperature held for 10 minutes.

For the analysis of a mixture of EHMC and AVO dissolved in cyclohexane and irradiated for 8 hours, a Perkin Elmer Turbomass gas chromatograph with a mass selective detector (electron impact) controlled by a Dell Pentium III computer, was used. The software was equipped with NIST and NBS libraries. The column used was a BP-5 methyl silicon 30 m x 320 μm x 0.25 μm capillary column. A 1 μl

sample was injected. Helium was used as the mobile phase at a flow rate of 1.8 ml/min.

The following conditions were used on this system:

Detector temperature: 250°C

Temperature programme: 50°C, held for 1 minute then raised to 300°C at 20°C/min, the final temperature held for 10 minutes.

2.7.2.4 GC-MS analysis of cyclohexane solutions

A 1 x 10^{-3} M solution of AVO in cyclohexane was irradiated with the Osram HBO 500 W/2 high pressure mercury lamp in conjunction with a 10 mm thick Pyrex filter in a 1 mm pathlength quartz cuvette for 8 hrs. A 1 µl aliquot of this solution was injected into the GC-MS. The GC-MS software was equipped with the National Institute of Standards and Technology (NIST) 98 library, containing the electron impact mass spectra of different compounds, and compared the mass spectrum of any given chromatographic peak from the total ion chromatogram with the spectra in the library. The software then listed the compounds in the library which best matched the mass spectrum of that peak.

We looked at the effect of irradiating EHMC and AVO using a 313 nm and a 365 nm filter. From the UV spectra we noticed that on irradiating EHMC in cyclohexane with the use of a 365 nm filter, it showed no degradation but irradiating a mixture of AVO and EHMC in cyclohexane using the same filter we noticed that EHMC undergoes degradation. We therefore suspected that AVO acts as a photosensitiser.

To check the photosensitising effect of AVO, we first irradiated a 1 x 10^{-3} M EHMC solution in cyclohexane, using the Osram 500 W/2 high pressure mercury lamp with the 365 nm filter for 1 hour. We then irradiated a mixture of EHMC and AVO for the same duration. The samples were then analysed by GC-MS. The results are displayed in Section 3.4.4.

2.8 Chemical actinometry

In order to measure the number of photons absorbed by a sunscreen agent we need to know the irradiance incident on the front surface of the absorbing substance and also the fraction of light absorbed. This can be done by the use of a chemical actinometer (where the rate of the chemical reaction is proportional to the rate of photon absorption). In chemical actinometry we measure the extent of photochemical reaction for a reaction in which the quantum yield is accurately known. The most widely used solution-phase chemical actinometer for photochemical research today is the potassium ferrioxalate, $K_3Fe(C_2O_4)_3$, system developed by Parker and Hatchard [45,46].

Solutions of $K_3Fe(C_2O_4)_3$ are sensitive to a wide wavelength range from 250-577 nm, and upon irradiation iron in its ferric state undergoes reduction to the ferrous state and oxidation of oxalate ion occurs [47]:

$$2[Fe(C_2O_4)_3]^{3-} \rightarrow 2Fe(C_2O_4) + 3(C_2O_4)^{2-} + 2CO_2 .$$

The ferrous ion (Fe^{2+}) and oxalate ion formed do not absorb the incident light but when ferrous ion is complexed with 1,10-phenanthroline in the presence of acetate buffer, it becomes highly absorbing. The red coloured complex formed absorbs strongly at 510 nm thus enabling the concentration of ferrous ions produced to be measured by absorbance measurements. The quantum yield for the production of ferrous ion has been determined as 1.24 at 324 nm over the temperature range 5-80°C [12].

2.8.1 Determination of the molar absorption coefficient of the iron-phenanthroline complex at 510 nm

In order to determine the number of Fe^{2+} ions produced we need to determine the molar absorption coefficient of the iron(II)-1,10-phenanthroline complex at 510 nm. The Hatchard and Parker method was used to prepare the calibration curve for the

determination of the molar absorption coefficient of the Fe^{2+} complex [46]. To do this the following had to be prepared:

(a) 0.1 M $FeSO_4$ in 0.05 M H_2SO_4 was prepared from $(NH_4)_2SO_4FeSO_4.6H_2O$ and standardised by titration against a standard potassium dichromate solution using n-phenanthranilic acid as indicator [46]. Serial dilution of the 0.1 M $FeSO_4$ stock solution with 0.05 M H_2SO_4 gave the required 4 x 10^{-4} M $FeSO_4$ solution.

(b) 0.1% (by mass) n-phenanthranilic acid was dissolved in 0.005 M NaOH by slight heating and stirring and used as an indicator in standardising the $FeSO_4$ solution.

(c) 0.1% (by mass) 1,10-phenanthroline was dissolved in water by slight heating and stirring.

(d) Acetate buffer solution was prepared by mixing 600 ml of 1 M sodium acetate, 360 ml of 0.5 M H_2SO_4 and 40 ml of Millipore water.

A series of acidic $FeSO_4$ solutions containing buffer and 0.1% 1,10-phenanthroline were prepared from the 4 x 10^{-4} M $FeSO_4$ stock solution according to the method of Calvert and Pitts [47], and allowed to stand for 1 hr. The absorbance at 510 nm was measured (refer to Table 2.9) and the calibration curve of absorbance *versus* concentration of Fe^{2+} was then plotted (see Figure 2.24). The R^2 value obtained was 0.9987 implying that for the concentrations of the iron-phenanthroline complex in the region of 0.8 x 10^{-5} M to 7.6 x 10^{-5} M there is good linearity. The gradient of this curve gives the molar absorption coefficient (ε) to be 1.11 x 10^4 dm^3 mol^{-1} cm^{-1} which is exactly the same as obtained by Calvert and Pitts [47] and Aliwell [12]. This molar absorption coefficient is used in actinometric calculations.

2.8.2 Preparation of potassium ferrioxalate

The Parker method for the preparation of potassium ferrioxalate was used in this work [45]. Since potassium ferrioxalate decomposes in the presence of light the procedure was carried out in the dark (i.e. under a red photographic lamp). A volume of 750 ml of 1.5 M potassium oxalate solution was added to 250 ml of a 1.5 M ferric chloride solution with vigorous mixing and the resulting solution of $K_3Fe(C_2O_4)_3$ was evaporated to 250 ml and the green potassium ferrioxalate crystals precipitated.

Recrystallisation in hot water was repeated three times to yield 26 g of pure compound.

Table 2.9: Absorbance data obtained by varying the concentrations of Fe^{2+} then complexing it with 1,10-phenanthroline and measuring the absorbance at 510 nm.

V_{FeSO_4}/ ml[a]	$[Fe^{2+}]$/ 10^{-5} M	$V_{H_2SO_4}$/ml[b]	$V_{1,10\text{-}phenanthroline}$/ ml[c]	V_{buffer}/ml[d]	A_{510nm}
0	0	10	2	5	0
0.5	0.76	9.5	2	5	0.073
1.0	1.52	9.0	2	5	0.168
1.5	2.25	8.5	2	5	0.250
2.0	3.04	8.0	2	5	0.333
2.5	3.80	7.5	2	5	0.423
3.0	4.56	7.0	2	5	0.494
3.5	5.32	6.5	2	5	0.588
4.0	6.08	6.0	2	5	0.698
4.5	6.84	5.5	2	5	0.757
5.0	7.60	5.0	2	5	0.836

[a] $[FeSO_4] = 4 \times 10^{-4}$ M

[b] $[H_2SO_4] = 0.05$ M

[c] 0.1% 1,10 phenanthroline

[d] Acetate buffer prepared by mixing 600 ml of 1 M sodium acetate, 360 ml of 0.5 M H_2SO_4 and 40 ml Millipore water.

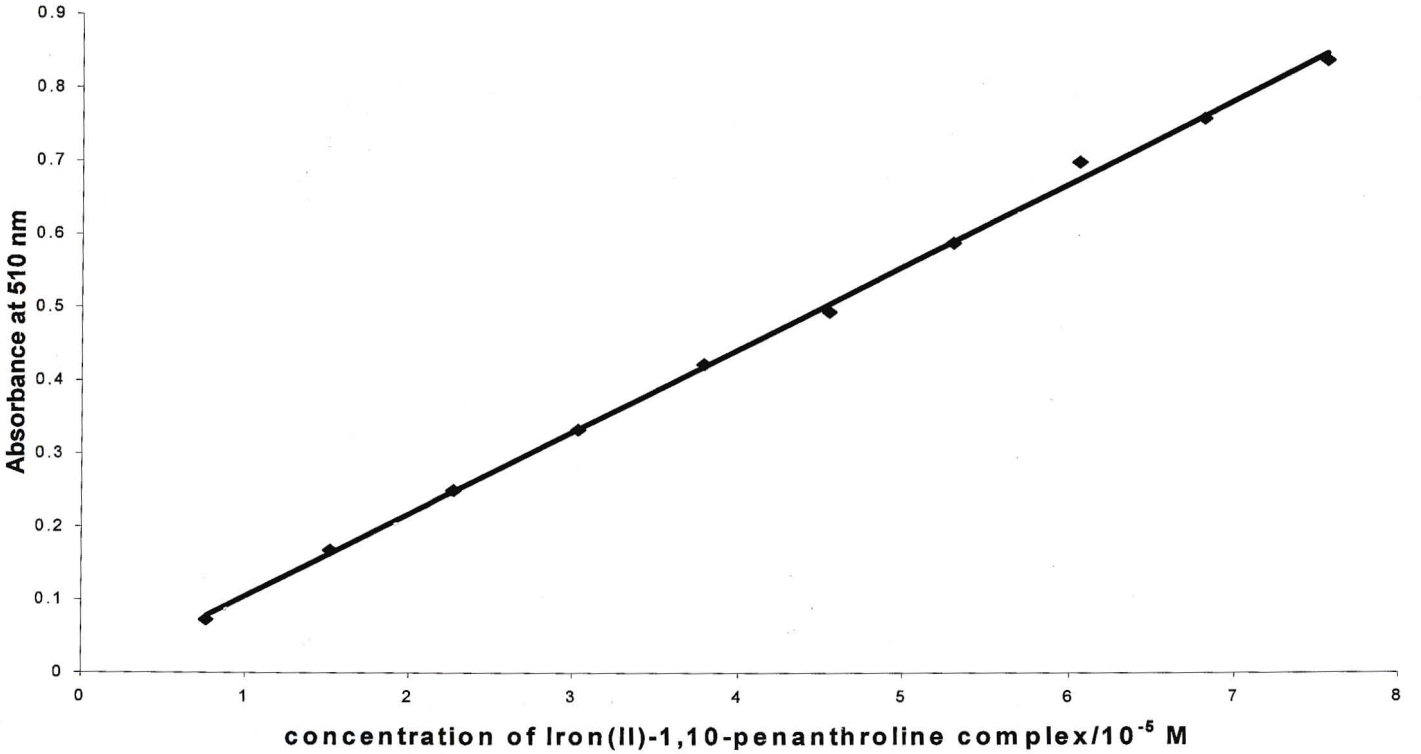

Figure 2.24: Calibration curve of absorbance at 510 nm versus the concentration of the iron(II)-1,10-phenanthroline complex. The slope of this curve gives the molar absorption coefficient of the iron(II)-1,10-phenanthroline complex to be 1.11 x 10^4 dm^3 mol^{-1} cm^{-1}. R^2 = 0.9987.

A 0.02 M potassium ferrioxalate solution was prepared by dissolving 4.91 g of potassium ferrioxalate in 400 ml of Milli-Q water, adding 50 ml of 0.5 M H_2SO_4 and diluting to 500 ml.

2.8.3 Procedure for actinometry

To determine the number of photons absorbed by EHMC, AVO and a mixture of EHMC and AVO in methanol and cyclohexane, a subtraction method was employed. The actinometer solution was placed behind the optical train in the presence and absence of the substrate and the solution was irradiated using an Osram HBO 500 W/2 high pressure mercury lamp in combination with a 10 mm thick Pyrex filter. The EHMC solution was irradiated for 45 s since it reaches its photostationary state quite rapidly, while AVO in cyclohexane was irradiated for 600 s since it takes much longer to photodegrade. The difference between the light absorbed by the actinometer solution in the absence of the sunscreen solution and in the presence is the amount of light absorbed by the substrate. Preparation and handling of the actinometer solutions were carried out in the dark.

A 1 mm pathlength quartz cuvette was filled with the sunscreen absorber solution and placed in the optical train. A volume of 3.5 ml of 0.02 M potassium ferrioxalate was filled in a 1 cm pathlength quartz cuvette and placed directly behind the 1 mm pathlength quartz cuvette. The shutter was opened for a 45 s duration and in the case of AVO, in the presence and absence of EHMC in cyclohexane, it was opened for 600 s. The absorbance of the sunscreen absorber solution before and after irradiation was measured with a LKB Ultrospec II E single beam spectrophotometer at their wavelength of maximum absorbance (λ_{max}). The λ_{max} of EHMC and AVO in methanol is 308 nm and 356 nm respectively, whereas λ_{max} for EHMC and AVO in cyclohexane is 290 nm and 350 nm respectively. To determine the concentration of EHMC in the mixture the calculation method described in Section 2.6.2 was employed. A 0.5 ml aliquot of the irradiated actinometer solution was then placed in a 10 ml volumetric flask containing 1 ml of acetate buffer and 0.5 ml of 1,10-phenanthroline which was then made up to the mark using Millipore water. The solution was allowed to stand for 1 hour. The absorbance of this solution at 510 nm

was determined against an identical unirradiated solution. This procedure was repeated for a second irradiation with the sunscreen absorber solution replaced by water. The above procedure was repeated three times.

Using the absorbance measurements taken, we can determine the number of Fe^{2+} ions formed during irradiation using the following equation:

$$nFe^{2+} = \frac{6.022 \times 10^{23} \times V1 \times V3 \times A}{V2 \times l \times \varepsilon} \tag{2.3}$$

where V1 is the volume of actinometer solution irradiated (3.5 x 10^{-3} dm^3), V2 is the volume of aliquot taken for analysis (0.5 x 10^{-3} dm^3), V3 is the volume to which V2 is diluted (10 x 10^{-3} dm^3), l is the pathlength of the quartz cell (1 cm), ε is the molar absorption coefficient of the iron-phenanthroline complex at 510 nm (1.11 x 10^4 dm^3 mol^{-1} cm^{-1}) and A is the measured absorbance at 510 nm.

To determine the irradiance of light absorbed by a solution we use the following equation:

$$I_o = \frac{nFe^{2+}}{\Phi Fe^{2+} \times t} \tag{2.4}$$

where ΦFe^{2+} is the quantum yield for the production of Fe^{2+} and t is the time of actinometry irradiation. The value for ΦFe^{2+} used was 1.24, the value at 324 nm [46], since this value is more or less constant over the wavelength range of 300 to 400 nm over which the sunscreen absorbers absorb. Since a subtraction method was employed in the determination of the light intensity absorbed by the sunscreen solutions, the intensity calculated would be incorrect by some constant factor by using this value of ΦFe^{2+}.

Thus to determine the intensity of light absorbed by the substrate (I_a), we take the difference between the light transmitted through the photolysis solution containing no absorbing substrate and that containing the substrate.

2.9 Irradiation and analysis of commercial sunscreen formulations containing EHMC and AVO

To assess possible photoproduct formation in commercial sunscreen formulations, Lubriderm (0.8% AVO and 4% EHMC) and Ambre Solaire (2.5% AVO, 2.5% EHMC, 5% Benzophenone 3 and 4% TiO_2) were exposed to sunlight.

The two sunscreen formulations, of known mass, were placed on microscope slides and left out in the sun for 6 hours on the 8 June 2001. We then washed off the residue on the slides in 50 ml beakers with methanol and cyclohexane. The solutions were transferred to volumetric flasks and made up to 100 ml with their respective solvents. An aliquot of these samples was then centrifuged at 2500 rpm for fifteen minutes, and the supernatant was filtered to remove insoluble particles, as per sample preparation outlined by Shaath [5]. For the methanolic sunscreen solution, a volume of 80 µl of the centrifuged samples were subjected to HPLC analysis using 85% (v/v) MeOH/H_2O as the mobile phase and the cyclohexane solutions were analysed using the GC-FID conditions described in Section 2.7.2.2 Formulations unexposed to sunlight were compared to those that were exposed to 6 hours of sunlight.

The Ambre Solaire formulation was used to determine the extent of photoisomerisation of *trans*-EHMC over different time periods. Six slides containing accurately known masses of Ambre Solaire were placed out in the sun. These slides were removed at 1 hour intervals from 9:00 to 15:00 hours on 8 June 2001. The solutions were made up as described above. A volume of 80 µl of the centrifuged samples was subjected to HPLC analysis using 85% (v/v) MeOH/H_2O as the mobile phase.

The UVB irradiance values from 9:00 to 15:00 for 8 June 2001 were obtained from the School of Pure and Applied Physics at the University of Natal, Durban. They

used a Yankee Environmental Systems (YES UVB-1) ultraviolet pyranometer to monitor UVB irradiance. This instrument measures the integrated UVB irradiance (in W m^{-2}) over the wavelength range 280-320 nm at ten minute intervals throughout the day. All the readings were summed and multiplied by 600 to obtain the incident UVB irradiance (in J m^{-2}). The results obtained are discussed in Section 3.7.

CHAPTER 3

Results and Discussion

In this chapter we discuss the results obtained on using various analytical techniques together with chemical actinometry to determine the photochemical behaviour of EHMC and AVO in methanol and cyclohexane. Finally, we discuss the results obtained on checking the effect of sunlight on EHMC and AVO in commercial sunscreen formulations.

3.1 FTIR analysis of EHMC and AVO

FTIR is a technique used to identify functional groups of a compound thus enabling one to determine the isomeric form of the commercially supplied sunscreen agents.

3.1.1 FTIR of *trans*-EHMC

The FTIR-spectrum obtained for *trans*-EHMC is shown in Figure 3.1. The ethylhexyl side chain can be observed in the region of 2900 cm^{-1}. The bands occurring at 2949 and 2872 cm^{-1} result from asymmetrical and symmetrical stretching modes of CH (methyl) group. The bands at 2932 and 2863 cm^{-1} are characteristic of the methylene groups of the ethylhexyl side chain. The band at 1716 cm^{-1} is due to the stretching vibration of the C=O group. The C=C stretching band is at 1633 cm^{-1}. The aromatic ring stretch appears at 1607 cm^{-1}. The Ph-O stretch appears at 1253 cm^{-1}. The peak at 1013 cm^{-1} could be due to the deformation of hydrogen on the double bonded carbon, shifted by conjugation. The deformation of the *para*-substituted aromatic hydrogen is shown at 819 cm^{-1}. This FTIR-spectrum complied well with the FTIR-spectra of *trans*-EHMC recorded by both Broadbent [22] and Kowlaser [23]. Thus it can be concluded that EHMC is provided in the *trans*-form.

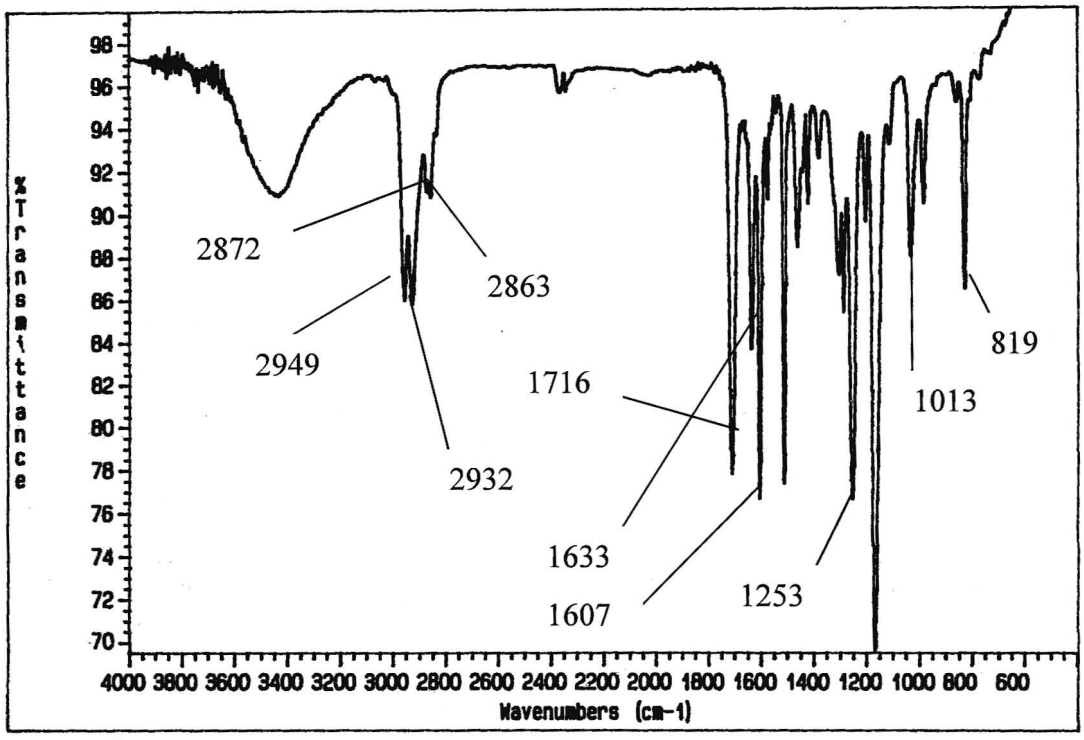

Figure 3.1: Fourier transform infrared spectrum of *trans*-EHMC from 500 to 4000 cm^{-1} recorded as a thin film on a KBr disc.

3.1.2 FTIR of AVO

The FTIR-spectrum of AVO can be seen in Figure 3.2. The region between 2960 and 2835 cm^{-1} is due to the C-H stretching vibrations. The absorption at 1500 cm^{-1} is due to the aromatic ring and the C-H out of plane bending is below 900 cm^{-1}. The absorption at 1600 cm^{-1} is due to the carbonyl carbon. The absorbance at 1170 cm^{-1} is due to the methyl groups. There is no absorption between the 3200 and 3600 cm^{-1} implying that OH stretching vibrations are absent. It can therefore be concluded that AVO is supplied in the diketo form.

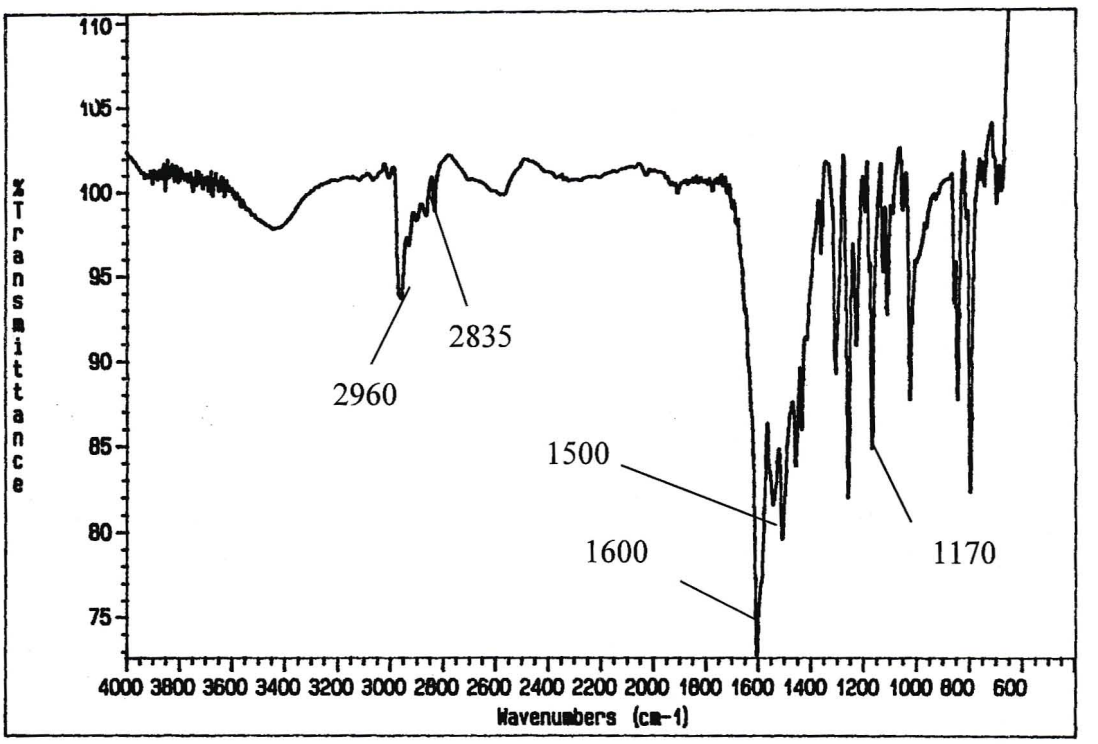

Figure 3.2: Fourier transform infrared spectrum of AVO recorded as a KBr disc.

3.2 NMR analysis of EHMC and AVO

Since both EHMC and AVO are reported to undergo isomerisation reactions we needed to determine the form in which they both are present in solution. ^{1}H NMR analyses of both EHMC and AVO were carried out and the results obtained are discussed below.

3.2.1 ^{1}H NMR of *trans*-EHMC

The ^{1}H NMR of *trans*-EHMC dissolved in deuterated methanol (see Figure 3.3) shows that the 2-ethylhexyl group hydrogens appear as a multiplet in the 0.9 to 1.7 ppm region. The three methoxy protons resonate as a singlet at 3.85 ppm. The two hydrogens belonging to the $-O-CH_2-$ group resonate as a doublet at 4.1 ppm. The peak at 4.9 ppm is due to the solvent. The *trans*-ethylenic hydrogens appear at 6.3 and 7.6 ppm. The four aromatic hydrogens resonate as doublets at 6.9 and 7.5 ppm.

We therefore confirmed that the *trans*-isomer is present in methanolic solutions by comparison with the ^{1}H NMR spectrum recorded by both Broadbent [22] and Kowlaser [23].

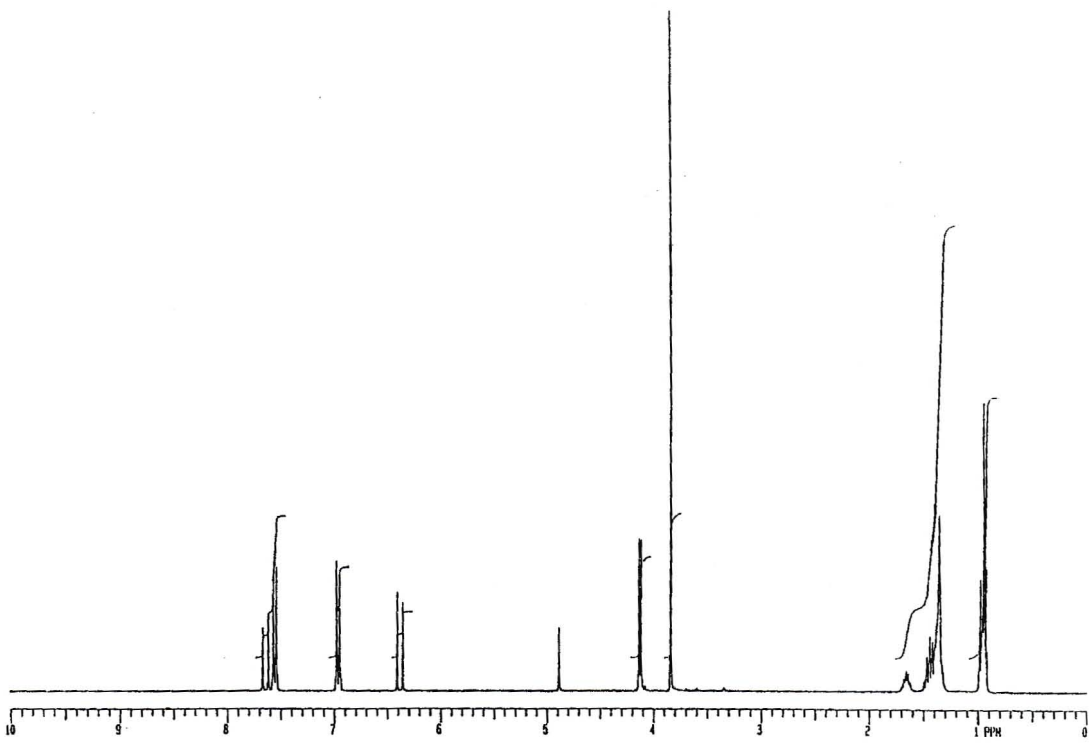

Figure 3.3: Proton NMR of EHMC in deuterated methanol.

The ^{1}H NMR of *trans*-EHMC dissolved in deuterated cyclohexane (see Figure 3.4) shows that the 2-ethylhexyl group hydrogens appear as a multiplet in the 0.9 to 1.8 ppm region. The solvent peak is at 1.36 ppm. The three methoxy protons resonate as a singlet at 3.7 ppm. The two hydrogens belonging to the –O-CH_2- group resonate as a doublet at 4.06 ppm. The *trans*-ethylenic hydrogens appear at 6.2 and 7.6 ppm. The four aromatic hydrogens resonate as doublets at 6.8 and 7.4 ppm. This confirms that *trans*-isomer is present in cyclohexane solutions.

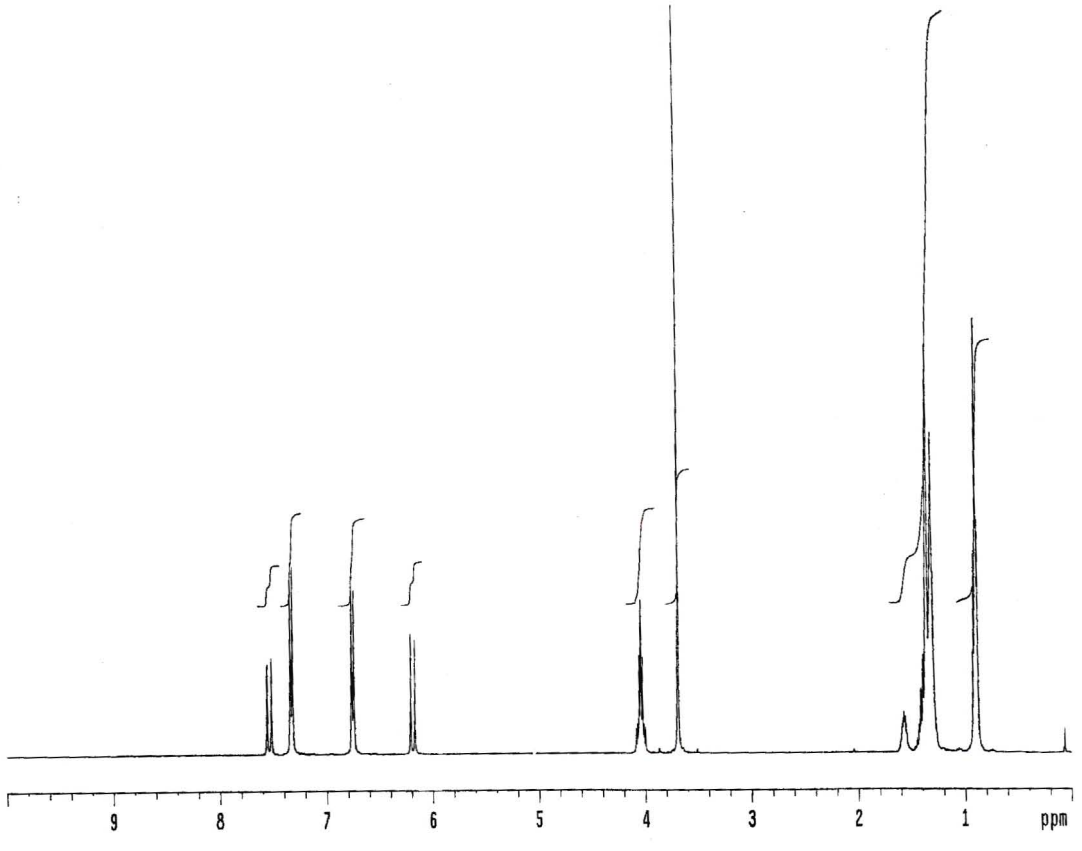

Figure 3.4: Proton NMR of EHMC in deuterated cyclohexane.

3.2.2 ^{1}H NMR of AVO

The ^{1}H NMR of AVO dissolved in deuterated methanol (see Figure 3.5) shows that the nine methyl protons resonate at 1.4 ppm. The peak at 3.4 ppm is an impurity. The three methoxy protons resonate as a singlet at 3.9 ppm. The peak at 4.9 ppm is due to the solvent. The proton resonance at 7.06 ppm is attributed to the proton between the carbonyl and enol groups. The reason for the downfield shift of the methylene group results from the deshielding effects of the carbonyl and the enol groups. The aromatic protons appear at 8.1 ppm, 7.6 ppm and 7.1 ppm. The enol proton would not appear in a deuterated methanol proton spectrum due to deuterium exchange. The presence of the vinylic proton conclusively shows that in methanolic solutions AVO appears in the enol form.

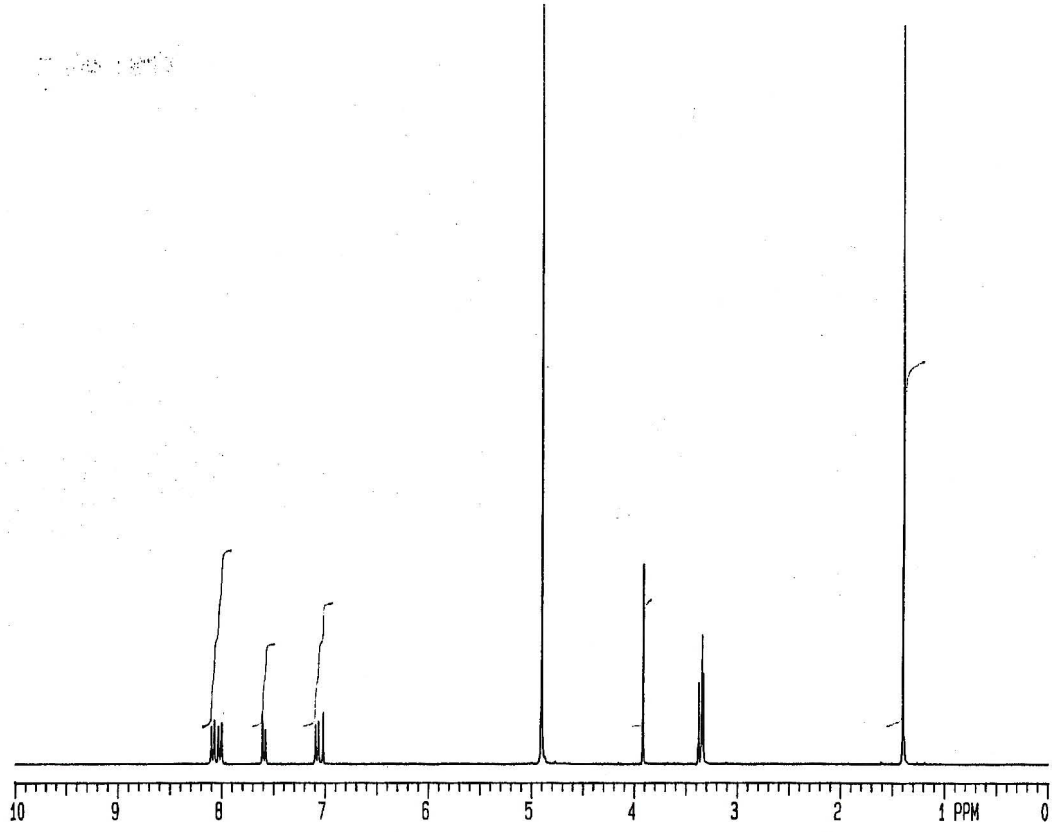

Figure 3.5: Proton NMR of AVO in deuterated methanol.

The ^{1}H NMR of AVO dissolved in deuterated cyclohexane (see Figure 3.6) shows that the nine methyl protons resonate at 1.32 ppm. The peak at 1.36 is due to the solvent. The three methoxy protons resonate as a singlet at 3.74 ppm. The proton resonance at 6.65 ppm is attributed to the proton between the carbonyl and enol groups. The aromatic protons appear at 7.9 ppm, 7.4 ppm and 6.8 ppm. This shows that in cyclohexane solutions AVO appears in the enol form. Both Dubois *et al.* [29] and Andrae *et al.* [30] showed by ^{1}H NMR that AVO when dissolved in deuterated acetonitrile exists in the enol form. Hence from the presence of vinylic proton it appears that in solution AVO exists in the enol form.

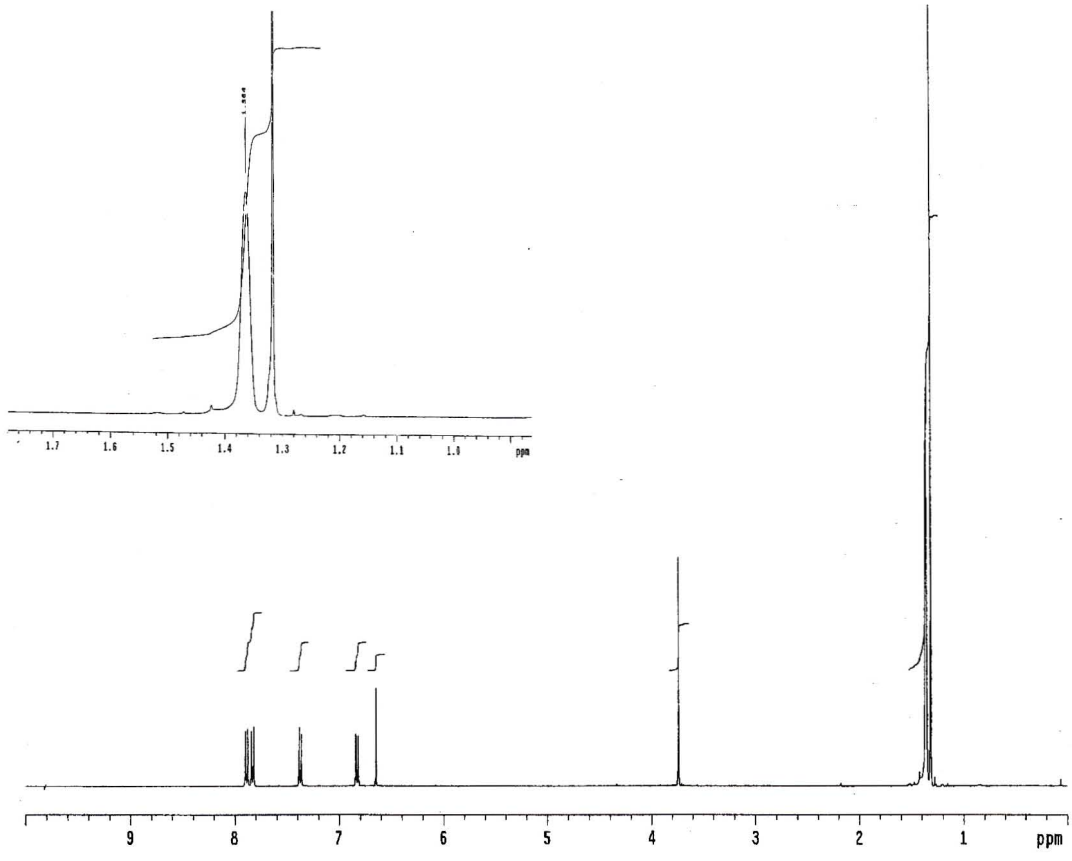

Figure 3.6: Proton NMR of AVO in deuterated cyclohexane.

3.3 UV-spectral analyses of EHMC, AVO and mixtures thereof in both methanol and cyclohexane

In this section we discuss the results of the UV-spectral technique used in analysing the photochemical behaviour of EHMC, AVO and a mixture of the two in methanol and cyclohexane. We also discuss the results obtained on checking the effect of irradiating EHMC and AVO with either UVA or UVB radiation and the effect of O_2, quenchers and photosensitisers.

A spectroscopic method described in Section 2.6.2 has been developed to determine the amounts of EHMC and AVO in a mixture. Since we know that these sunscreen agents photodegrade upon irradiation in specific solvents the method developed is quite useful in determining the amount of sunscreen agents remaining.

3.3.1 UV-spectra prior to irradiation

EHMC and AVO in methanol gave λ_{max} values of 308 nm and 356 nm respectively (refer to Figure 3.7) whereas in cyclohexane their λ_{max} values were 290 nm and 350 nm respectively (refer to Figure 3.8). Thus it can be seen that by changing the polarity of the solvent in which the filters are dissolved, the filters undergo shifts in their λ_{max} values. In addition to shifts in λ_{max} values both increases and decreases in the molar absorption coefficients of sunscreen chemicals were also observed in different solvents [3] and the results obtained in our work are in keeping with this phenomenon. The molar absorption coefficients of EHMC and AVO in methanol and cyclohexane were determined from the slopes of the calibration curves shown in Section 2.6.2.

The molar absorption coefficient of AVO in methanol at 356 nm and cyclohexane at 350 nm was found to be 3.86×10^4 dm^3 mol^{-1} cm^{-1} and 3.38×10^4 dm^3 mol^{-1} cm^{-1} respectively. The molar absorption coefficient of EHMC in methanol at 308 nm and in cyclohexane at 290 nm was found to be 2.65×10^4 dm^3 mol^{-1} cm^{-1} and 2.53×10^4 dm^3 mol^{-1} cm^{-1} respectively. These results show that both EHMC and AVO suffer a loss in their molar absorption coefficients on going from a polar to a non-polar environment.

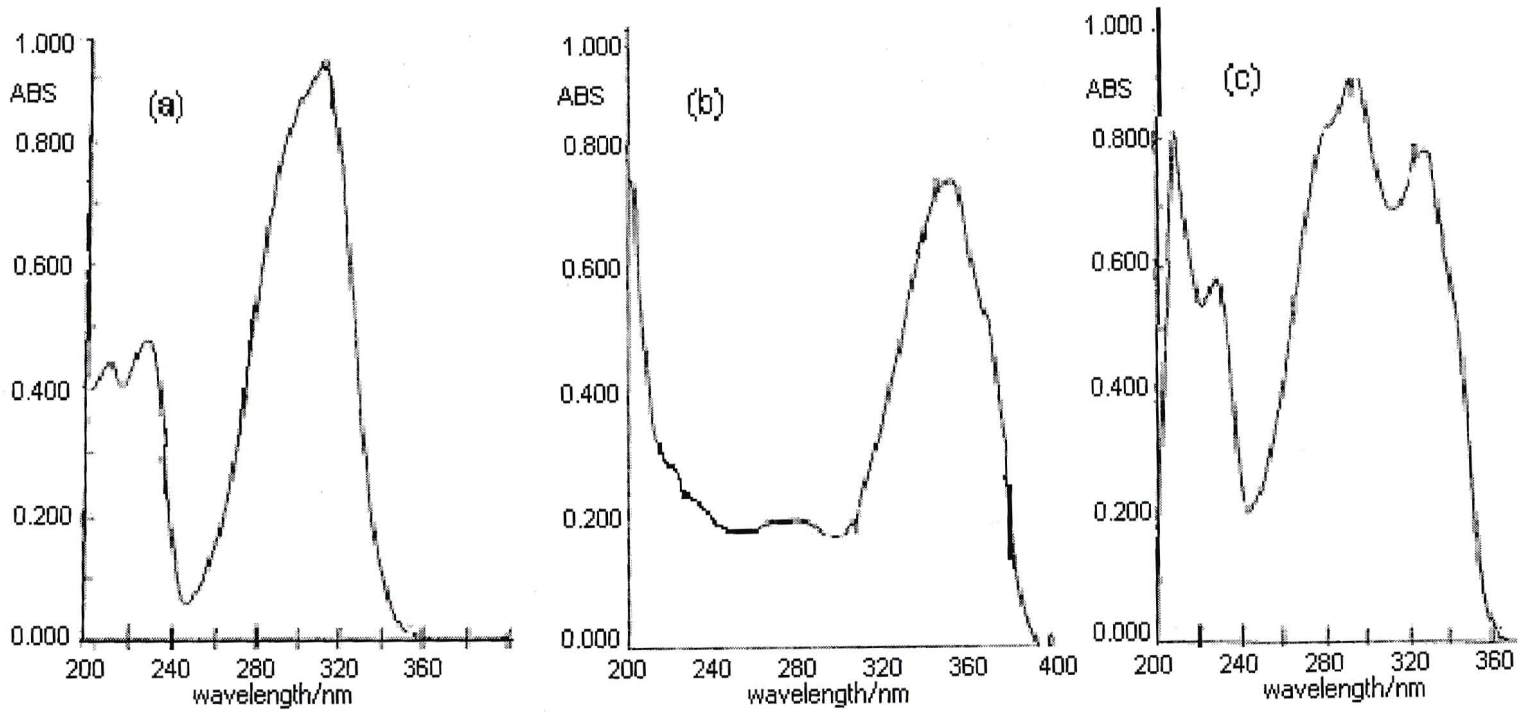

Figure 3.7: UV-spectra of EHMC and AVO in methanol: (a) EHMC (λ_{max} = 308 nm), (b) AVO (λ_{max} = 356 nm) and (c) a mixture of AVO and EHMC.

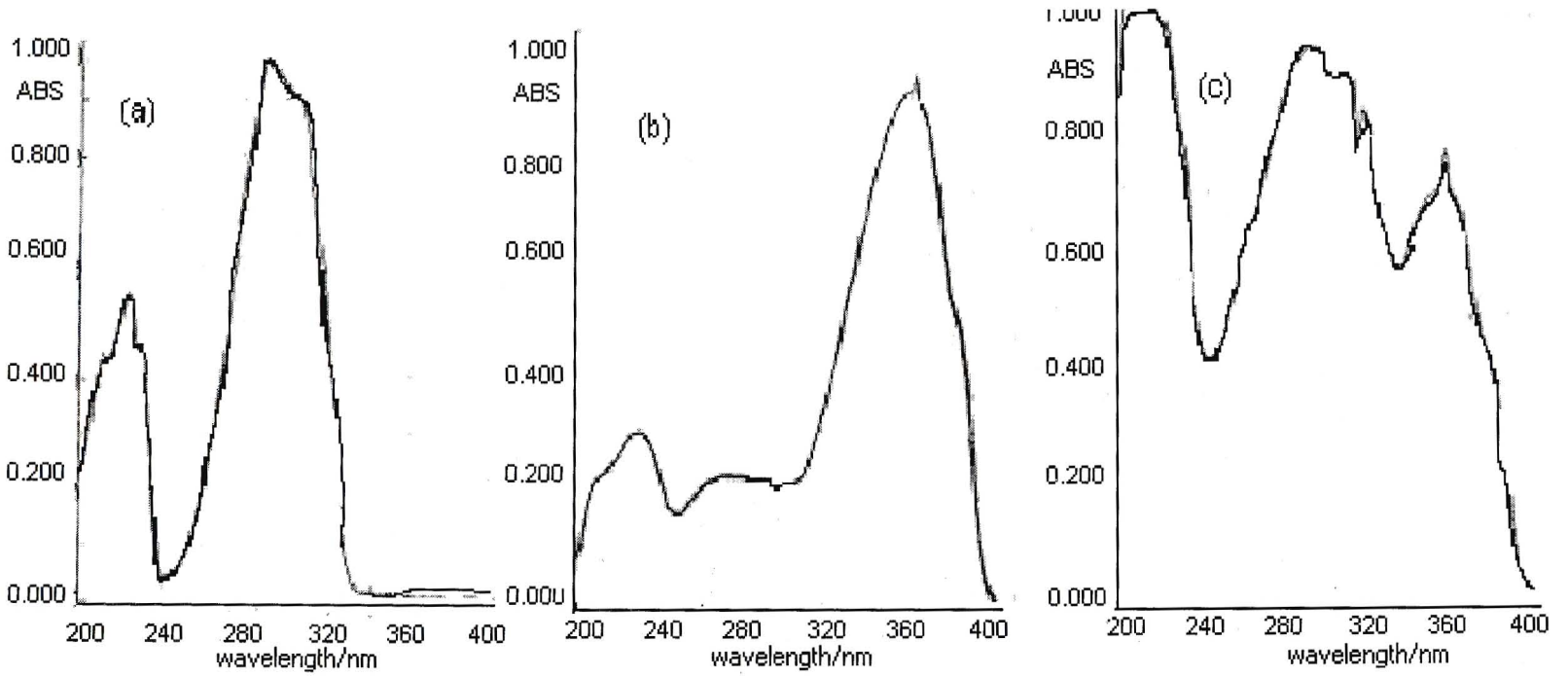

Figure 3.8: UV-spectra of EHMC and AVO in cyclohexane: (a) EHMC (λ_{max} = 290 nm), (b) AVO (λ_{max} = 350 nm), and (c) a mixture of EHMC and AVO.

3.3.2 Irradiation experiments carried out on the filters dissolved in methanol

When a solution of 4 x 10^{-5} M EHMC dissolved in methanol was irradiated with light of wavelengths greater than 300 nm UV-spectra of the irradiated solution were recorded at one minute intervals (see Figure 3.9a) and these showed a definite loss in absorbance with increasing irradiation time. From the absorbance values measured at 308 nm we were able to determine the concentration of EHMC by making use of the calibration curve shown in Figure 2.12. The results obtained can be seen in Table 3.1. From the graph of the concentration of EHMC remaining versus the irradiation time (see Figure 3.10) it is evident that a photostationary equilibrium is attained within the first 5 minutes.

When a solution of 3 x 10^{-5} M AVO dissolved in methanol was irradiated with light of wavelengths greater than 300 nm the UV-spectra of the irradiated solution were recorded at 30 minute intervals and AVO showed no significant loss in absorbance (see Figure 3.9b).

From the UV-spectra recorded of irradiated samples of mixtures of EHMC and AVO in methanol (see Figure 3.9c) we realised that only EHMC undergoes a photochemical reaction. We therefore only irradiated the mixture containing 3.1 x 10^{-5} M EHMC and 1.9 x 10^{-5} M AVO at 1 minute intervals. Absorbance readings were then taken at 308 nm and 356 nm and the calculation method devised in Section 2.6.2.1 was used to determine the concentrations of total EHMC and AVO after each irradiation interval (refer to Table 3.2). The graph of the concentration of total EHMC remaining in the mixture *versus* irradiation time was plotted (see Figure 3.11). On comparison of Figures 3.10 and 3.11 it is evident that EHMC reaches its photostationary equilibrium at almost the same rate as when mixed with AVO. From previous studies carried out by Broadbent [22] and Kowlaser [23] it is known that EHMC photoisomerises to its *cis*-isomer and if this is the case here then this implies that the rate of the isomerisation reaction is independent of the presence or absence of AVO. We have cofirmed the formation of the *cis*-isomer upon irradiation of *trans*-EHMC by chromatographic analysis as will be discussed in Section 3.4.1.

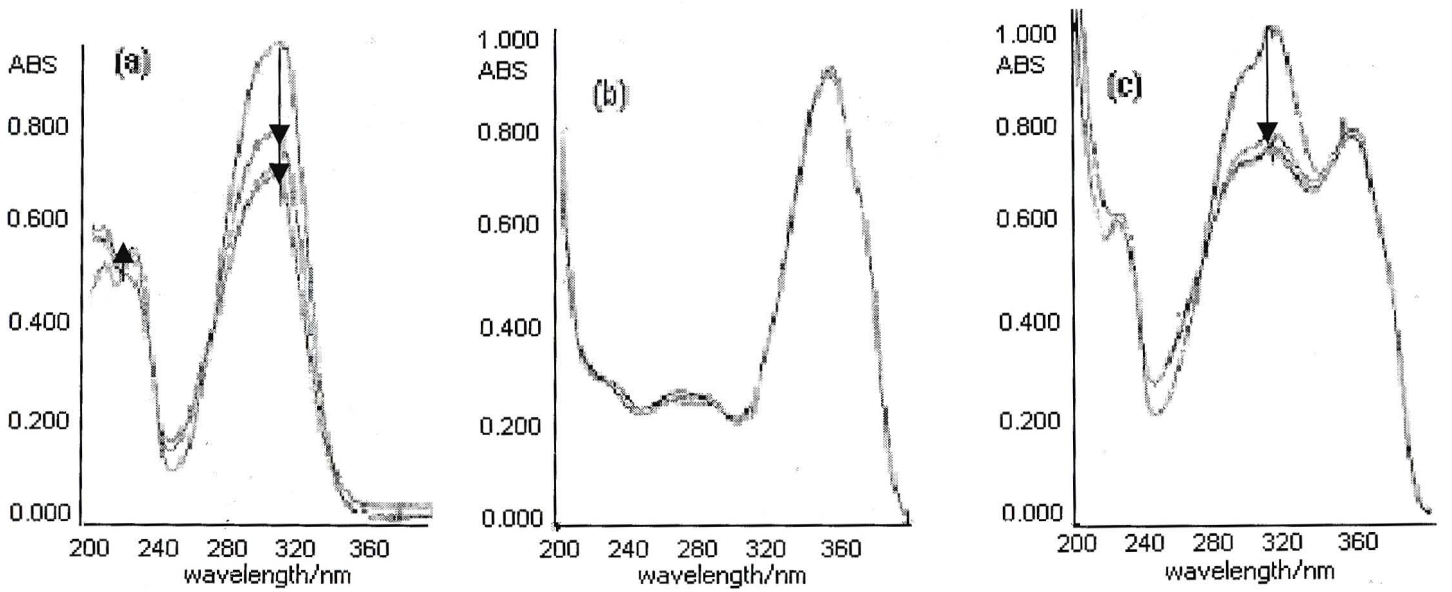

Figure 3.9: UV-spectra of the sunscreen agents irradiated in methanol: (a) 4×10^{-5} M EHMC irradiated at 1 minute intervals, (b) 3×10^{-5} M AVO irradiated at 30 minute intervals and (c) a mixture of 3.1×10^{-5} M EHMC and 1.9×10^{-5} M AVO irradiated at 30 minute intervals.

Table 3.1: Photodegradation of EHMC dissolved in methanol upon irradiation with light of wavelengths greater than 300 nm. The concentration of EHMC was determined from the plot of absorbance at 308 nm *versus* [EHMC].

Irradiation time/minutes	$A_{308\ nm}$	[EHMC]/10^{-5} M
0	1.00	4.05
1	0.800	3.2
2	0.717	2.8
3	0.703	2.6
4	0.697	2.6

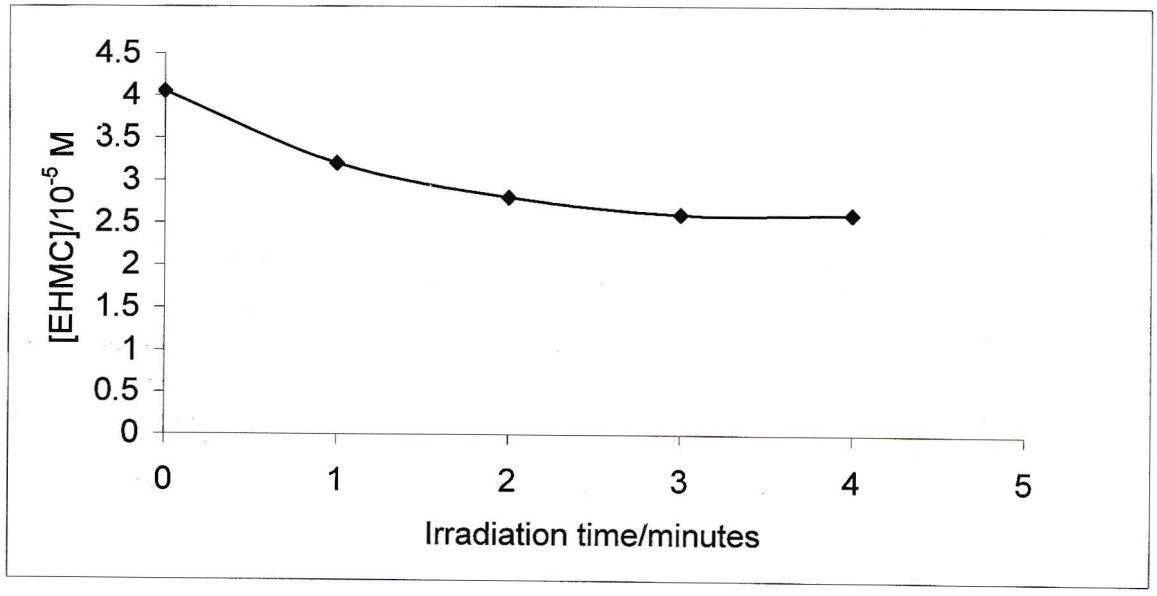

Figure 3.10: Photodegradation of a 4 x 10^{-5} M solution of EHMC dissolved in methanol upon irradiation with light of wavelengths greater than 300 nm.

Table 3.2: Photodegradation of EHMC mixed with AVO and dissolved in methanol upon irradiation with light of wavelengths greater than 300 nm. The concentrations of EHMC and AVO were determined by the calculation method developed in Section 2.6.2.1.

Irradiation time/minutes	$A_{308\ nm}$	$A_{356\ nm}$	[EHMC]/ 10^{-5} M	[AVO]/ 10^{-5} M
0	0.902	0.710	2.77	1.90
1	0.710	0.696	2.06	1.86
2	0.670	0.694	1.91	1.86
3	0.665	0.693	1.90	1.85

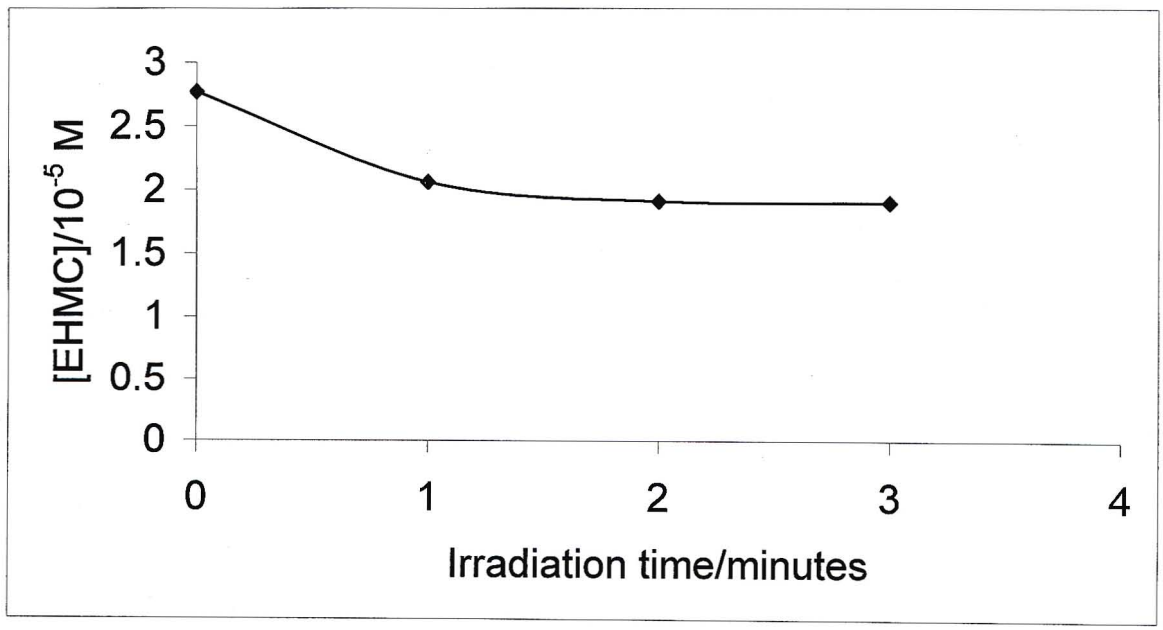

Figure 3.11: Photodegradation of 3.1 x 10^{-5} M EHMC in a mixture with 1.9 x 10^{-5} M AVO dissolved in methanol upon irradiation with light of wavelengths greater than 300 nm.

3.3.3 Irradiation experiments carried out on the filters dissolved in cyclohexane

On irradiation of the filters dissolved in cyclohexane we determined that both EHMC and AVO undergo photodegradation. A 3.4 x 10^{-5} M EHMC solution was therefore irradiated at 1 minute intervals but the degradation was inconsistent on repeated attempts (see Figure 3.12a). The concentration of EHMC remaining upon irradiation (refer to Table 3.3) was determined from Figure 2.15. A graph of concentration of EHMC remaining *versus* irradiation time was plotted (see Figure 3.13). This inconsistency in absorbance could be due to the formation of the *cis*-isomer which then re-equilibrates favoring the formation of the *trans*-isomer.

From the UV-spectra obtained upon irradiating AVO dissolved in cyclohexane at 30 minute intervals a decrease in absorbance until a photostationary state was reached is seen (see Figure 3.12b). In these experiments a solution of 2.5 x 10^{-5} M AVO dissolved in cyclohexane was irradiated at 30 minute intervals and its absorbance at 350 nm was measured (refer to Table 3.4). From these absorbance values the concentration of AVO remaining after each irradiation period was determined from the curve of absorbance of AVO at 350 nm *versus* its concentration (see Figure 2.13). A graph of concentration of AVO remaining *versus* irradiation time was plotted (see Figure 3.14).

A mixture consisting of 2.5 x 10^{-5} M AVO and 2.3 x 10^{-5} M EHMC was irradiated at half hour intervals. From the UV-spectra recorded (see Figure 3.12c) AVO showed definite photodegradation and EHMC showed depletion in absorption in the first half hour of irradiation but gave inconsistent results from then on. The absorbance values at 350 nm and 290 nm were measured (refer to Table 3.5) and the concentrations of EHMC and AVO remaining upon irradiation were calculated by using the calculation method developed in Section 2.6.2.2. A graph of concentration of AVO in the mixture *versus* irradiation time was plotted (see Figure 3.15). On comparing Figures 3.14 and 3.15 it can be seen that the rate of photodegradation of AVO is enhanced in the presence of EHMC. A graph of concentration of EHMC against irradiation time was plotted (see Figure 3.16) and this showed an increase in EHMC concentration upon irradiation. This is not possible and the only explanation would be that one of the photoproducts of AVO absorbs at 290 nm. Thus, if this is the case then the

calculation method for the determination of the concentration of EHMC upon irradiation of a mixture of EHMC and AVO dissolved in cyclohexane does not hold and the concentrations of EHMC plotted here are incorrect.

Table 3.3: Photodegradation of EHMC dissolved in cyclohexane upon irradiation with light of wavelengths greater than 300 nm. The concentration of EHMC was determined from Figure 2.15.

Irradiation time/minutes	**$A_{290\ nm}$**	**[EHMC]/10^{-5} M**
0	0.830	3.3
1	0.625	2.5
2	0.660	2.6
3	0.700	2.8
4	0.685	2.7

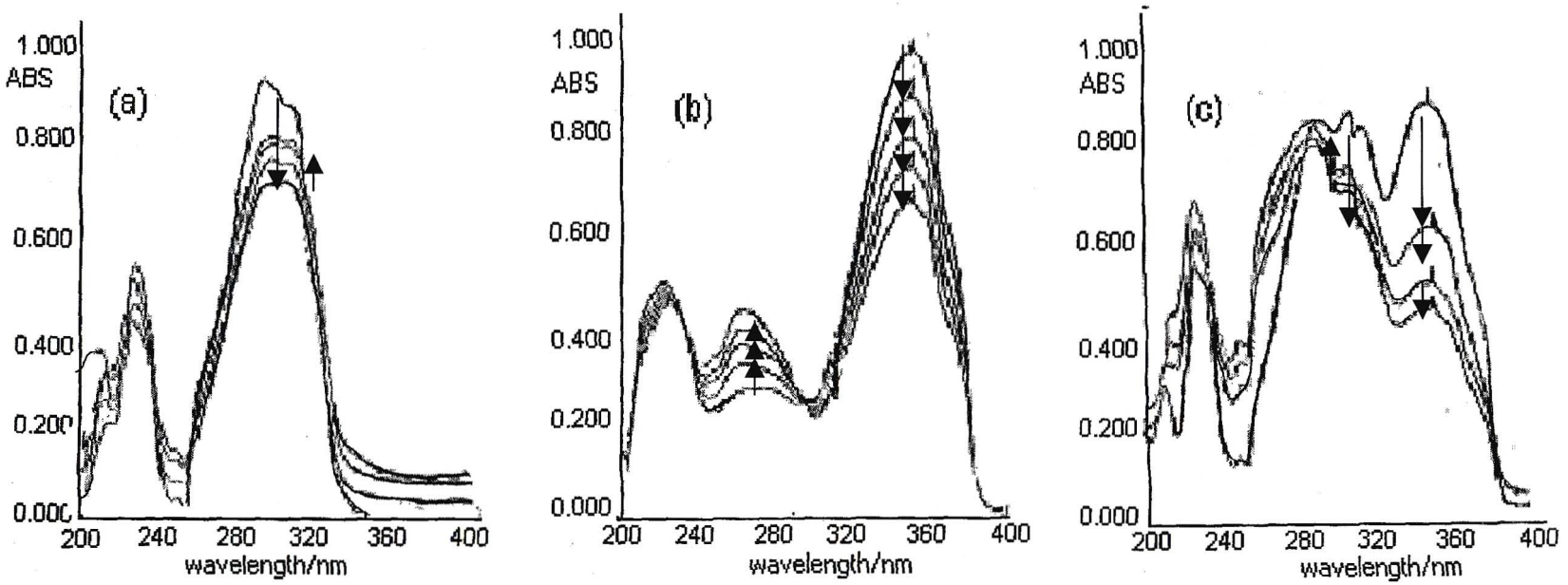

Figure 3.12: UV-spectra of the sunscreen agents irradiated in cyclohexane: (a) 3.4 x 10^{-5} M EHMC irradiated at 1 minute intervals, (b) 2.5 x 10^{-5} M AVO irradiated at 30 minute intervals and (c) a mixture of 2.3 x 10^{-5} M EHMC and 2.5 x 10^{-5} M AVO irradiated at 30 minute intervals.

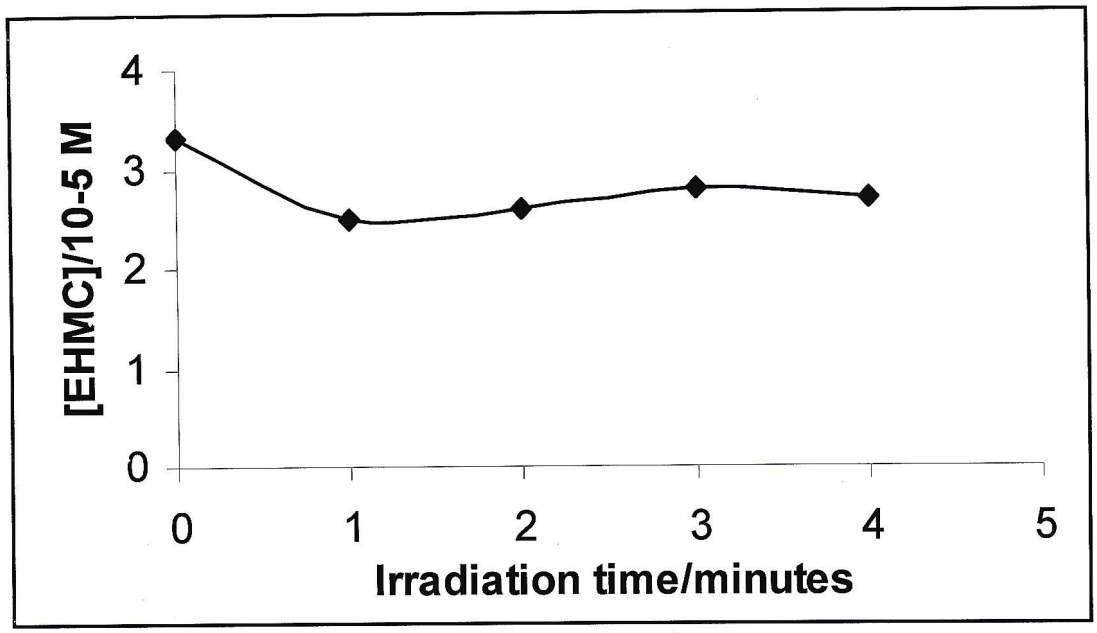

Figure 3.13: Photodegradation of a 3.4 x 10^{-5} M solution of EHMC dissolved in cyclohexane upon irradiation with light of wavelengths greater than 300 nm.

Table 3.4: Photodegradation of AVO dissolved in cyclohexane upon irradiation with light of wavelengths greater than 300 nm. The concentration of AVO was determined from Figure 2.13.

Irradiation time/minutes	**$A_{350\ nm}$**	**[AVO]/10^{-5} M**
0	0.889	2.5
30	0.818	2.3
60	0.742	2.1
90	0.683	1.8
120	0.618	1.7

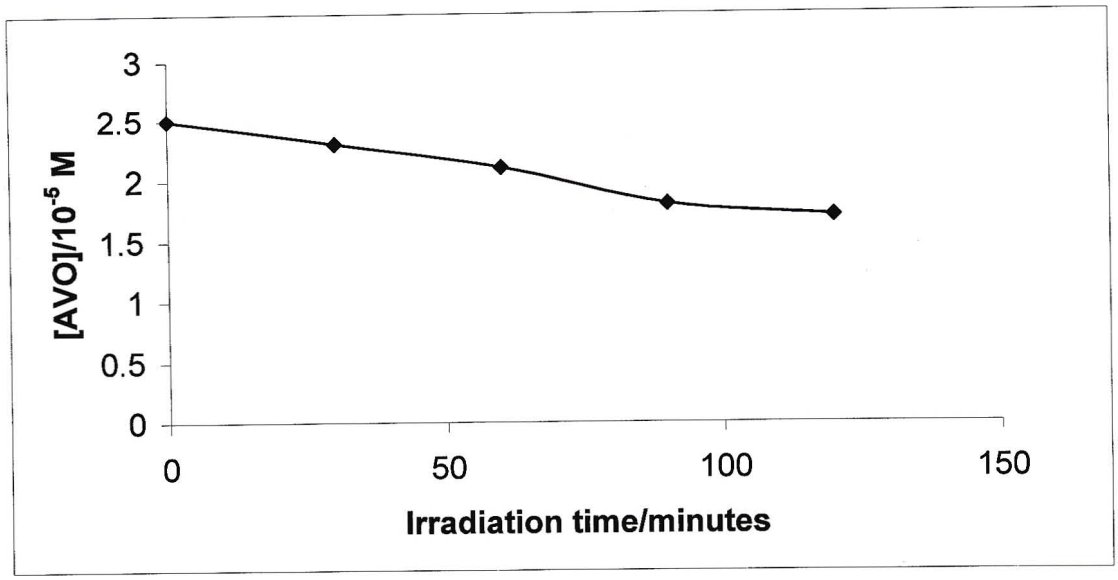

Figure 3.14: Photodegradation of a 2.5 x 10^{-5} M solution of AVO dissolved in cyclohexane upon irradiation with light of wavelengths greater than 300 nm.

Table 3.5: Photodegradation of a mixture of 2.5 x 10^{-5} M AVO and 2.3 x 10^{-5} M EHMC upon irradiation with light of wavelengths greater than 300 nm. The concentrations of EHMC and AVO were determined by the calculation method developed in Section 2.6.2.2

Irradiation time/minutes	**$A_{290\ nm}$**	**$A_{350\ nm}$**	**[EHMC]/ 10^{-5} M**	**[AVO]/ 10^{-5} M**
0	0.821	0.845	2.25	2.55
30	0.776	0.617	2.38	1.75
60	0.787	0.488	2.58	1.35
90	0.793	0.450	2.69	1.15
120	0.817	0.448	2.79	1.14

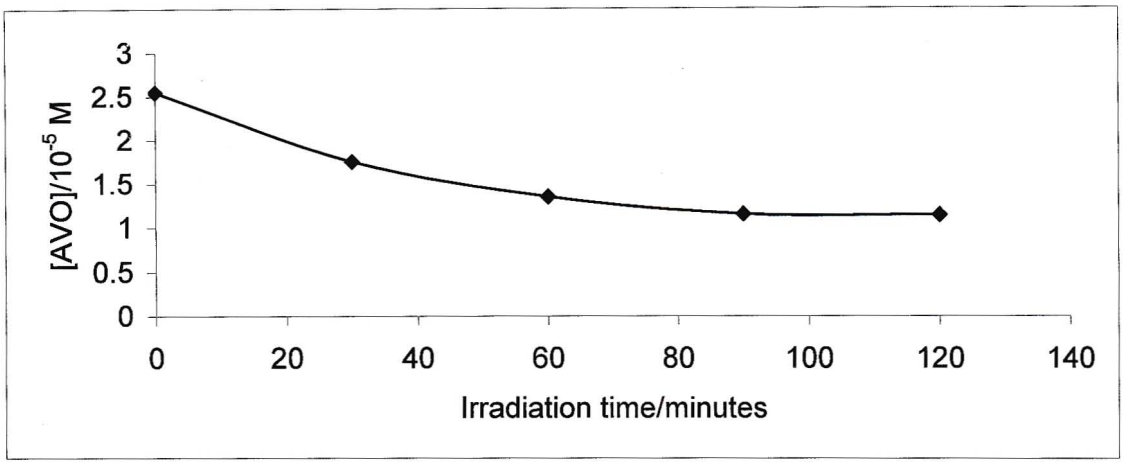

Figure 3.15: Photodegradation of a 2.5 x 10^{-5} M AVO in a mixture with 2.3 x 10^{-5} M EHMC dissolved in cyclohexane upon irradiation with light of wavelengths greater than 300 nm.

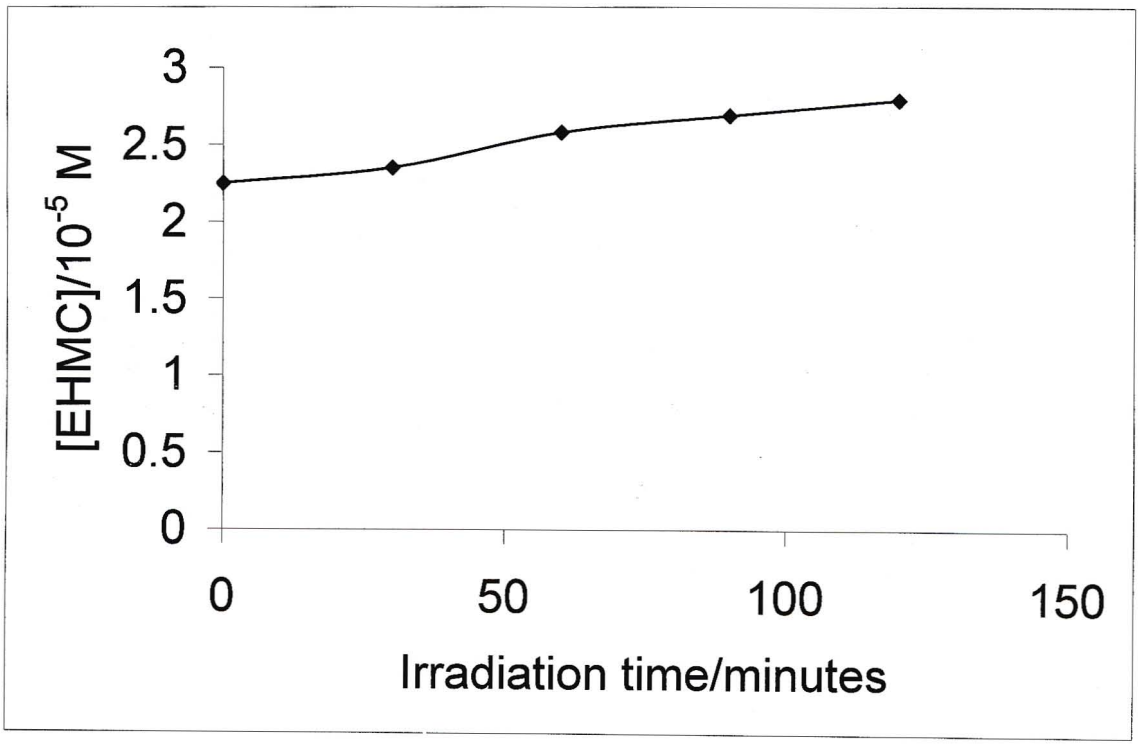

Figure 3.16: Photodegradation of 2.3 x 10^{-3} M EHMC in a mixture with 2.5 x 10^{-5} M AVO dissolved in cyclohexane upon irradiation with light of wavelengths greater than 300 nm.

3.3.4 Photostability upon irradiation with either UVA or UVB radiation

It is now recognised that in order to afford broad-spectrum protection sunscreen formulations should contain both a UVB and a UVA filter. Therefore EHMC and AVO are often used in combination as EHMC absorbs in the UVB region whereas AVO absorbs in the UVA region. So far in this work the irradiation source used was an Osram 500 W/2 high pressure mercury lamp in combination with a 10 mm Pyrex filter that transmitted light of wavelengths greater than 300 nm. This was done in an attempt to mimic the solar radiation impinging on the earth's surface. In order to separate the effects of UVB and UVA radiation we now irradiated the two sunscreens and their mixture with the Osram 500 W/2 high pressure mercury lamp but in combination with either a 313 nm narrow bandpass filter to transmit UVB light or a 365 nm narrow bandpass filter to transmit UVA light.

The UV-spectra on irradiating EHMC, AVO and a mixture of the two in methanol with the 313 nm filter (see Figure 3.17) were obtained. On comparison of the UV-spectra obtained on using the Pyrex filter the following observations could be made:

- The concentration of EHMC remaining after each irradiation period was determined from the calibration curve of absorbance at 308 nm against the concentration of EHMC (see Figure 2.12) and the values obtained are listed in Table 3.6. These concentrations were compared with those obtained when the 10 mm Pyrex filter was used (see Table 3.1). From Figure 3.18 we can say that EHMC reaches its photostationary equilibrium at a faster rate with the use of the 313 nm filter.

- From Figure 3.17b it is evident that AVO undergoes negligible photodegradation as was the case when irradiated with the 10 mm Pyrex filter. As was previously shown AVO is photostable in methanol but in addition its absorbance at 313 nm is low so one would not expect a marked effect.

- We then looked at irradiating a mixture of EHMC and AVO dissolved in methanol with a 313 nm filter (see Figure 3.17c). The concentration of EHMC remaining was determined by using the method developed in Section 2.6.2.1 and the concentration values obtained are shown in Table 3.7. These values together with those from Table 3.2 were used to plot a graph showing the

difference between irradiating EHMC in the presence of AVO with a 10 mm Pyrex filter and a 313 nm filter (see Figure 3.19). From this graph, and keeping in mind that the initial concentrations and number of photons absorbed are different, it is clear that the rate of photodegradation of EHMC with both filters is similar.

Table 3.6: Photodegradation of EHMC dissolved in methanol upon irradiation with a 313 nm filter. These values were compared with those obtained on irradiating EHMC with a 10 mm Pyrex filter.

Irradiation Time/minutes	**$A_{308\ nm}$**	**[EHMC]/10^{-5} M**
0	0.929	3.81
1	0.626	2.47
2	0.621	2.46
3	0.620	2.46

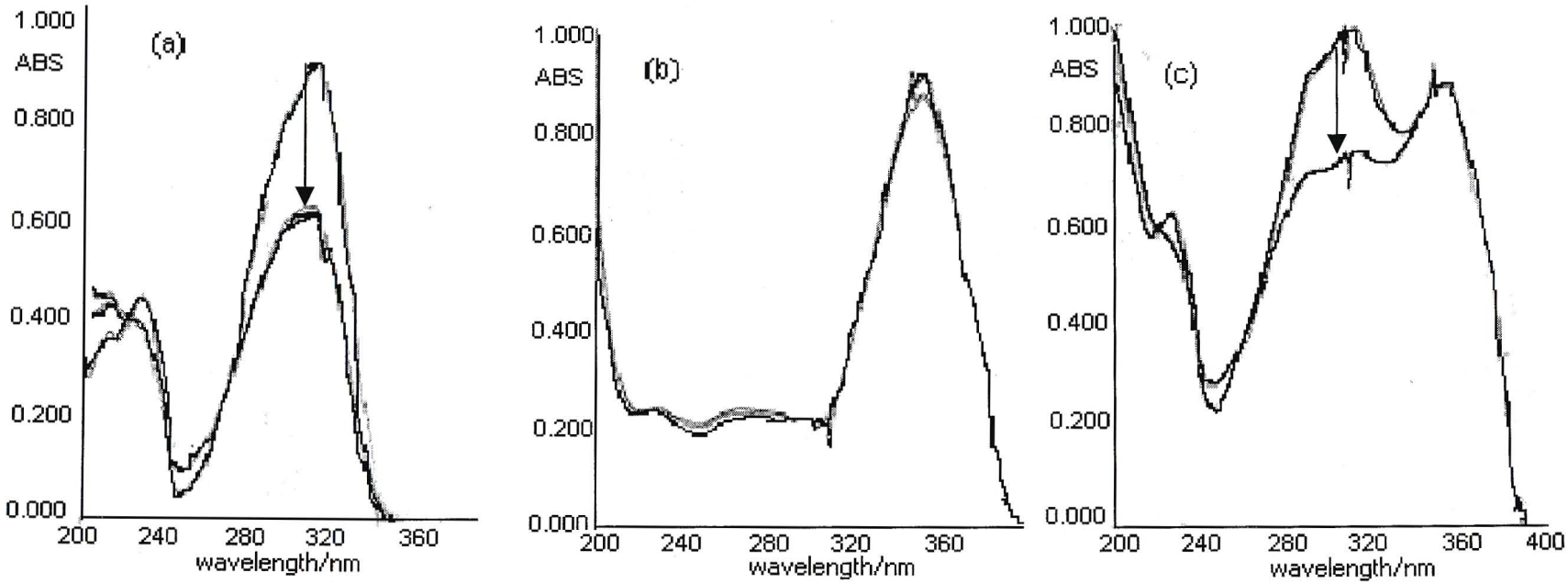

Figure 3.17: UV-spectra of sunscreen agents dissolved in methanol upon irradiating with a 313 nm filter: (a) 3.8 x 10^{-5} M EHMC irradiated at 1 minute intervals, (b) 2.7 x 10^{-5} M AVO irradiated at 30 minute intervals and (c) a mixture of EHMC and AVO that were made up such that their absorbances were approximately equal to one and was then irradiated at 30 minute intervals.

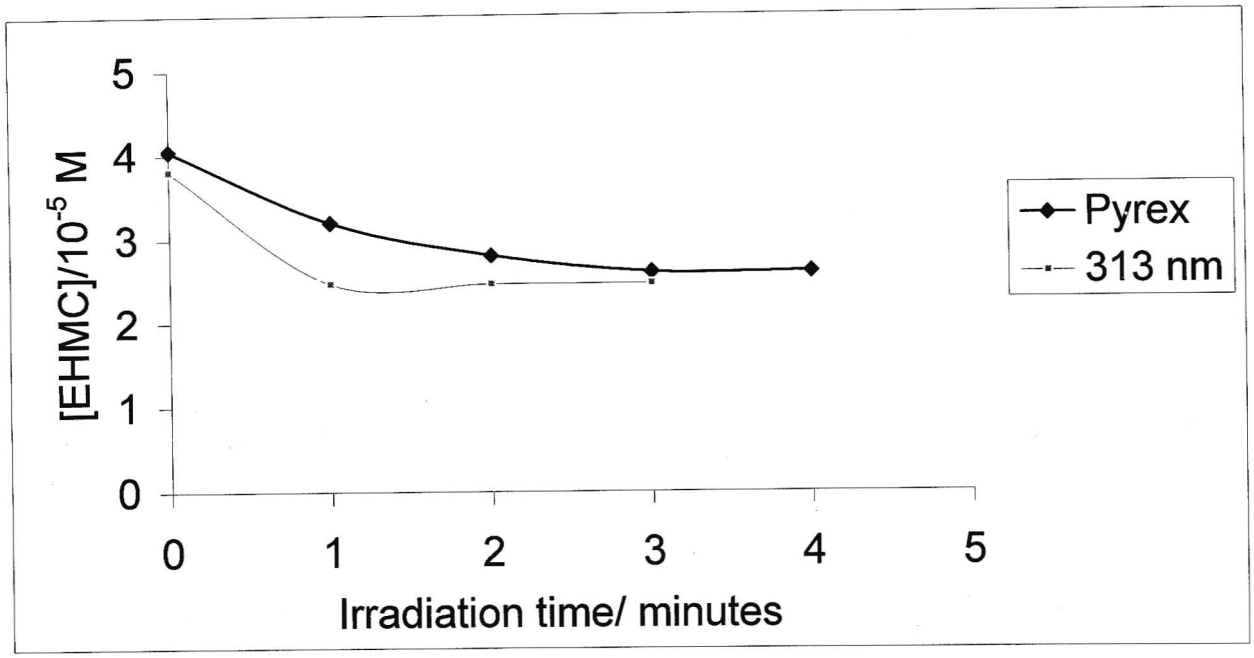

Figure 3.18: A comparison of the photodegradation observed on irradiating EHMC in methanol with either a 10 mm Pyrex filter or a 313 nm filter.

Table 3.7: Photodegradation of EHMC upon irradiating a mixture of EHMC and AVO in methanol with a 313 nm filter. The values obtained were compared with those obtained on irradiating the mixture with a 10 mm Pyrex filter.

Irradiation time/minutes	**$A_{308\ nm}$**	**$A_{356\ nm}$**	**[EHMC]/10^{-5} M**
0	0.920	0.898	3.65
1	0.742	0.896	2.76
2	0.739	0.896	2.75
3	0.739	0.897	2.75

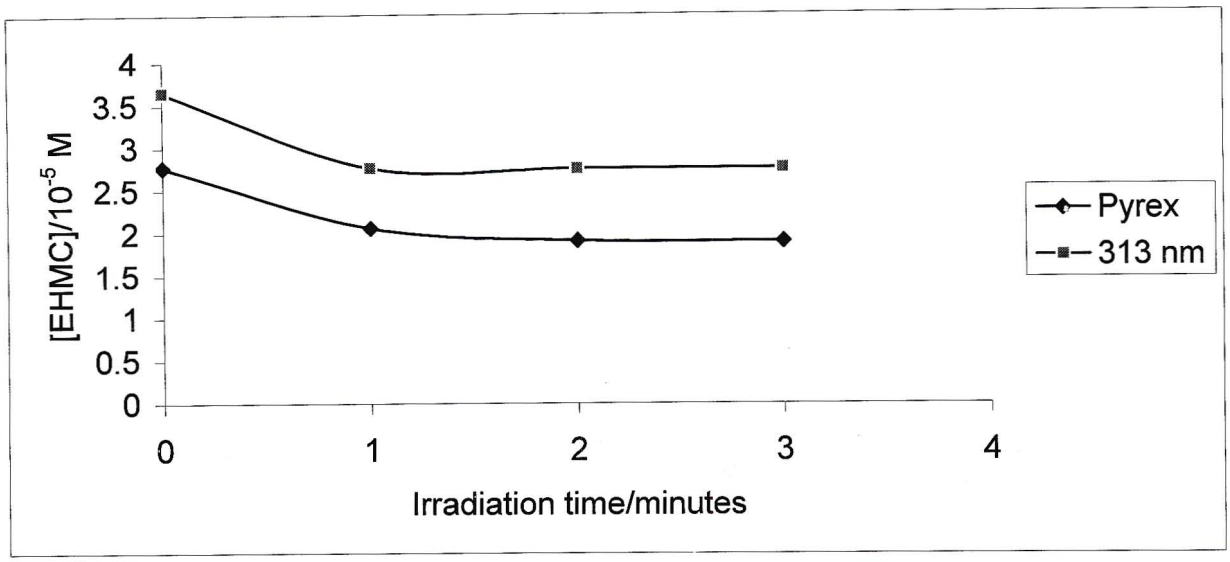

Figure 3.19: A comparison of the photodegradation observed on irradiating EHMC in the presence of AVO dissolved in methanol with either a 10 mm Pyrex or a 313 nm filter.

On comparing the UV-spectra recorded on irradiating the sunscreen agents dissolved in cyclohexane, with either the 313 nm filter or the 10 mm thick Pyrex filter, the following observations were made:

- EHMC dissolved in cyclohexane and irradiated with a Pyrex filter gave an inconsistent photodegradation, i.e. EHMC never attained a phostationary equilibrium and the concentration did not decrease monotonically (see Figure 3.12a) but with the 313 nm filter (see Figure 3.20a) a photostationary equilibrium was attained. The concentrations of EHMC, determined from Figure 2.15, are shown in Table 3.8 and these values were used to plot a graph showing the difference between irradiating EHMC with a 10 mm Pyrex filter and a 313 nm filter (see Figure 3.21).

- From Figure 3.20b we can see that upon irradiating 3.2 x 10^{-5} M AVO dissolved in cyclohexane with a 313 nm filter no significant photodegradation was observed since AVO absorbs maximally at 350 nm, whereas upon irradiating AVO with a 10 mm Pyrex filter (see Figure 3.12b) photodegradation was substantial.

- On irradiating a mixture of EHMC and AVO dissolved in cyclohexane, which was made up such that their absorbances were equal to one, we can see from Figure 3.20c that AVO

undergoes no photodegradation and the inconsistent degradation in EHMC, as experienced with the 10 mm thick Pyrex filter, is evident but not as substantial as seen in Figure 3.12c. The increase in absorbance observed at 290 nm could be due to AVO tautomerising to the enol form which has a wavelength of maximum absorbance at 270 nm. This also explains the increase in absorbance in Figure 3.20b at 270 nm. The concentration of EHMC in the mixture, determined using the method developed in Section 2.6.2.2, is shown in Table 3.9 and these values were used to plot a graph showing the difference between irradiating EHMC in the mixture with a 10 mm Pyrex filter and a 313 nm filter (see Figure 3.22).

Table 3.8: Photodegradation of EHMC dissolved in cyclohexane upon irradiation with a 313 nm filter. These values were compared with those obtained on irradiating EHMC with a 10 mm Pyrex filter.

Irradiation Time/minutes	**$A_{290\ nm}$**	**[EHMC]/10^{-5} M**
0	0.957	3.8
1	0.775	2.8
2	0.782	2.8
3	0.680	2.8

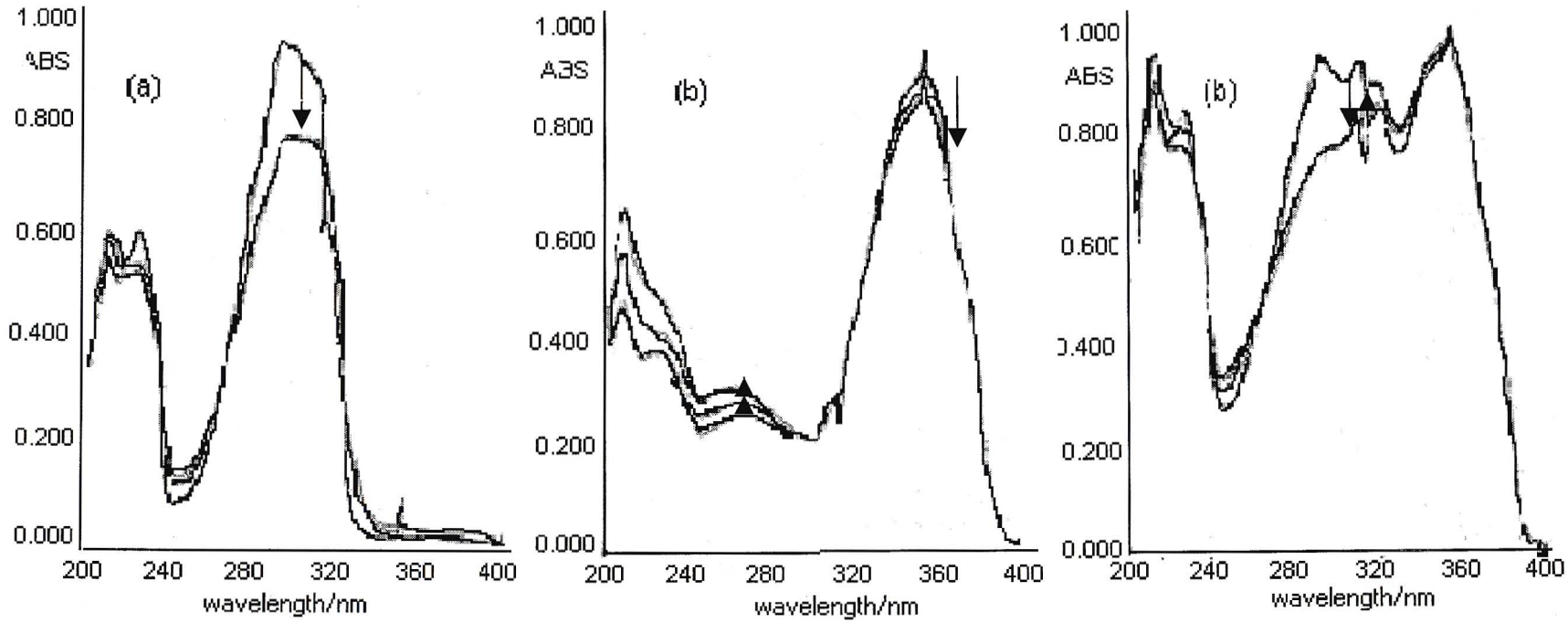

Figure 3.20: UV spectra of the sunscreen agents dissolved in cyclohexane upon irradiating with a 313 nm filter: (a) 3.7 x 10^{-5} M EHMC irradiated at 1 minute intervals, (b) 3.2 x 10^{-5} M AVO irradiated at 30 minute intervals and (c) a mixture of EHMC and AVO, made up such that their absorbances were approximately equal to one, irradiated at 30 minute intervals.

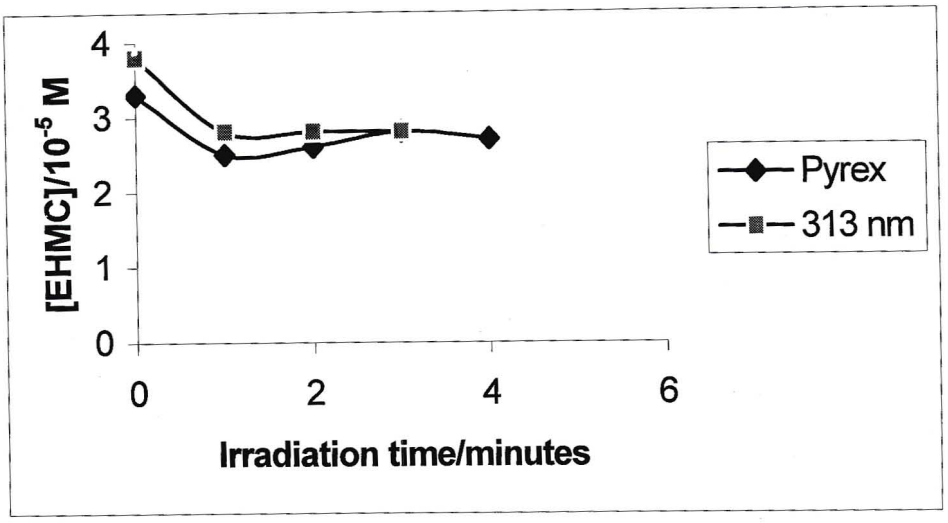

Figure 3.21: A comparison of the photodegradation observed on irradiating EHMC in cyclohexane with either a 10 mm Pyrex filter or a 313 nm filter.

Table 3.9: Photodegradation of EHMC upon irradiating a mixture of EHMC and AVO in cyclohexane with a 313 nm filter. The values obtained were compared to those obtained upon irradiating the mixture with a 10 mm Pyrex filter. The concentration of AVO was determined to be 3.0 x 10^{-5} M from Figure 2.13.

Irradiation time/minutes	**$A_{290\ nm}$**	**$A_{350\ nm}$**	**[EHMC]/10^{-5} M**
0	0.939	1.013	2.54
30	0.776	1.013	1.89
60	0.765	1.012	1.85
90	0.766	1.014	1.85

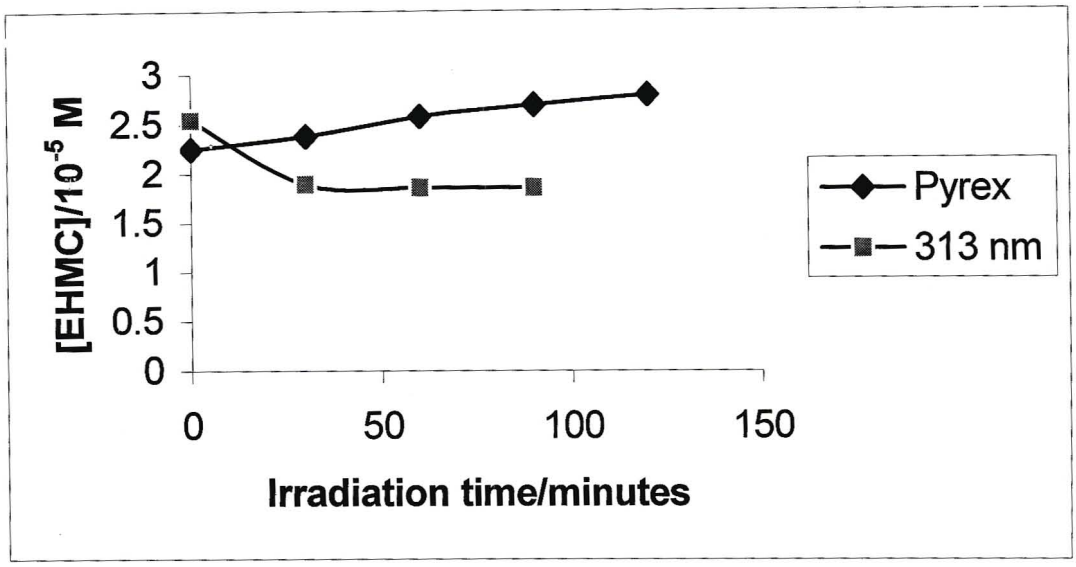

Figure 3.22: A comparison of the photodegradation observed on irradiating EHMC in the presence of AVO dissolved in cyclohexane with either a 10 mm Pyrex or a 313 nm filter.

When the UV-spectra obtained on irradiating the sunscreen agents, dissolved in methanol, with either the 365 nm filter or the 10 mm Pyrex filter were compared, the following observations could be made:

- Figure 3.23a shows 3.2 x 10^{-5} M EHMC dissolved in methanol to be photostable upon irradiation with the 365 nm filter but photounstable when irradiated with the 10 mm Pyrex filter (see Figure 3.9a). EHMC has a maximum absorbance at 308 nm in methanol and does not absorb at 365 nm which explains its photostability when irradiated with the 365 nm filter.

- A 1.9 x10^{-5} M solution of AVO is photostable in methanol irrespective of the filter used (see Figures 3.9b and 3.23b).

- On irradiating a mixture of EHMC and AVO dissolved in methanol, which was made up such that their absorbances were approximately equal to one, with the 365 nm filter EHMC degrades to a small extent which could be due to the photosensitizing effect of AVO (see Figure 3.23c). AVO as usual shows no photodegradation in methanol.

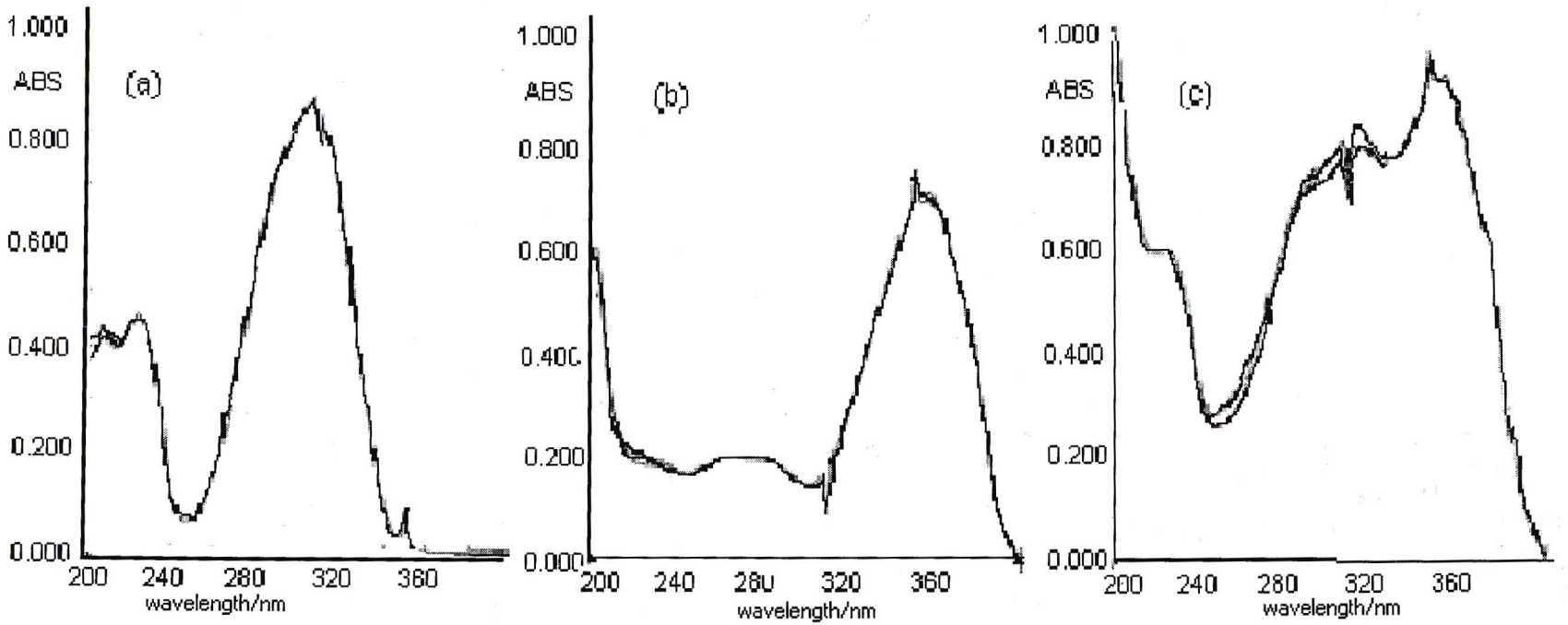

Figure 3.23: UV-spectra showing the effect of irradiating the sunscreen agents in methanol with a 365 nm filter: (a) 3.2 x 10^{-5} M EHMC irradiated at 1 minute intervals, (b) 1.9 x 10^{-5} M AVO irradiated at 30 minute intervals and (c) a mixture of EHMC and AVO, made up such that their absorbances were approximately equal to one, irradiated at 30 minute intervals.

On comparing the UV-spectra obtained on irradiating the sunscreen agents, dissolved in cyclohexane, with the 365 nm filter and the 10 mm Pyrex filter, the following observations were made:

- From Figure 3.24a it is evident that EHMC dissolved in cyclohexane and irradiated with a 365 nm filter shows no significant photodegradation but when irradiated with the 10 mm Pyrex filter (see Figure 3.12a) it undergoes definite photodegradation. This is due to EHMC absorbing maximally at 290 nm which is sufficiently close to the cutoff of the 10 mm thick Pyrex filter for EHMC to absorb significantly.

- AVO photodegrades in cyclohexane when irradiated with either the 10 mm thick Pyrex filter (see Figure 3.12b) or the 365 nm filter (see Figure 3.24b). The concentration of AVO after irradiation was determined from Figure 2.14 (see Table 3.10). From Figure 3.25 it is clear that photodegradation of AVO is enhanced when irradiated with the 365 nm filter. This is expected since AVO absorbs maximally at 350 nm in cyclohexane.

- On irradiating a mixture of EHMC and AVO dissolved in cyclohexane with the 365 nm filter it is clear that AVO undergoes definite photodegradation but so does EHMC. The concentration of AVO in the mixture of AVO and EHMC dissolved in cyclohexane was determined using Figure 2.13 (see Table 3.11). From Figure 3.26 it can be seen that the rate of photodegradation of AVO in the mixture is reduced when irradiated with the 365 nm filter. This is possibly due to AVO photosensitising the degradation of EHMC and this possibility is discussed further in Section 3.3.6. The increase in absorbance at 290 nm could be due to the absorbance of one of the photoproducts of AVO thus showing EHMC to absorb rather inconsistently. The determination of the concentration of EHMC was carried out by the method developed in Section 2.6.2.2 (see Table 3.11). From Figure 3.27 it is clear that irradiation with either the 10 mm Pyrex filter or the 365 nm filter the concentration of EHMC increases. This is not possible and can only be explained by assuming that one of the photoproducts formed absorbs at 290 nm which is investigated in Section 3.4.3.

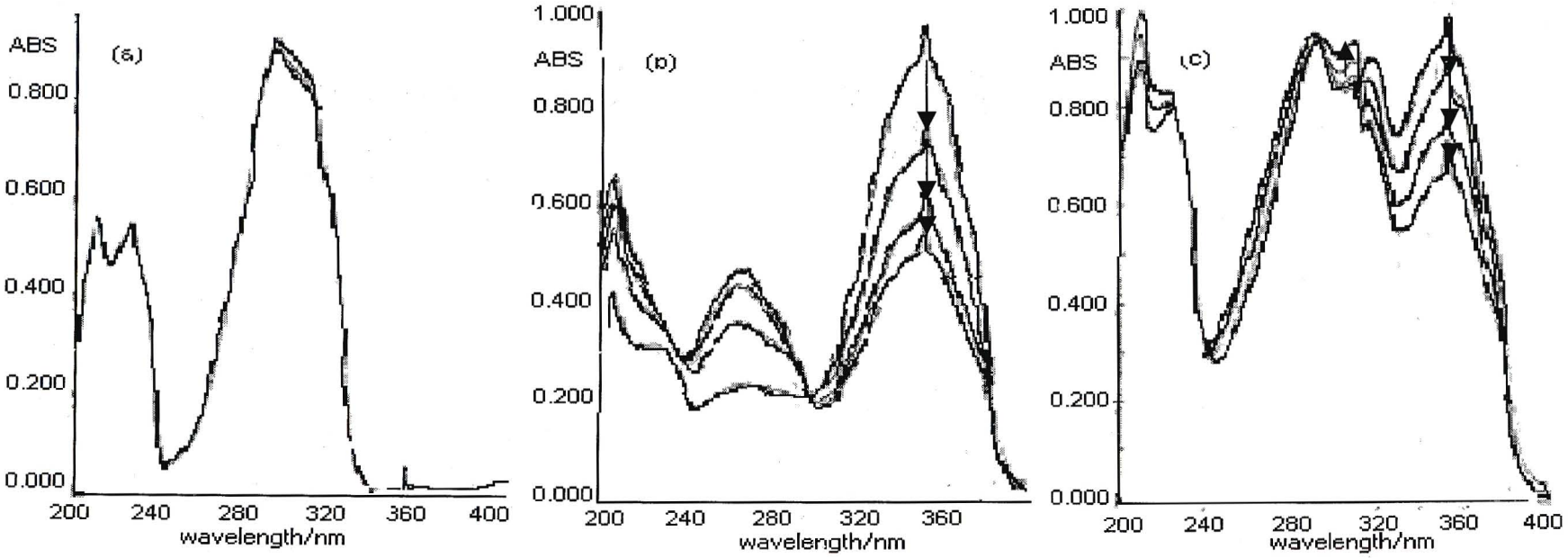

Figure 3.24: UV-spectra showing the effect of irradiating the sunscreen agents in cyclohexane with a 365 nm filter: (a) 3.7 x 10^{-5} M EHMC irradiated at 1 minute intervals, (b) 3.2 x 10^{-5} M AVO irradiated at 30 minute intervals and (c) a mixture of EHMC and AVO, made up such that their absorbances were approximately equal to one, irradiated at 30 minute intervals.

Table 3.10: The concentration of AVO dissolved in cyclohexane after irradiation for specific time periods with a 365 nm filter.

Irradiation time/minutes	$A_{350\ nm}$	$[AVO]/10^{-5}$ M
0	0.955	2.79
30	0.758	2.22
60	0.628	1.84
90	0.543	1.59

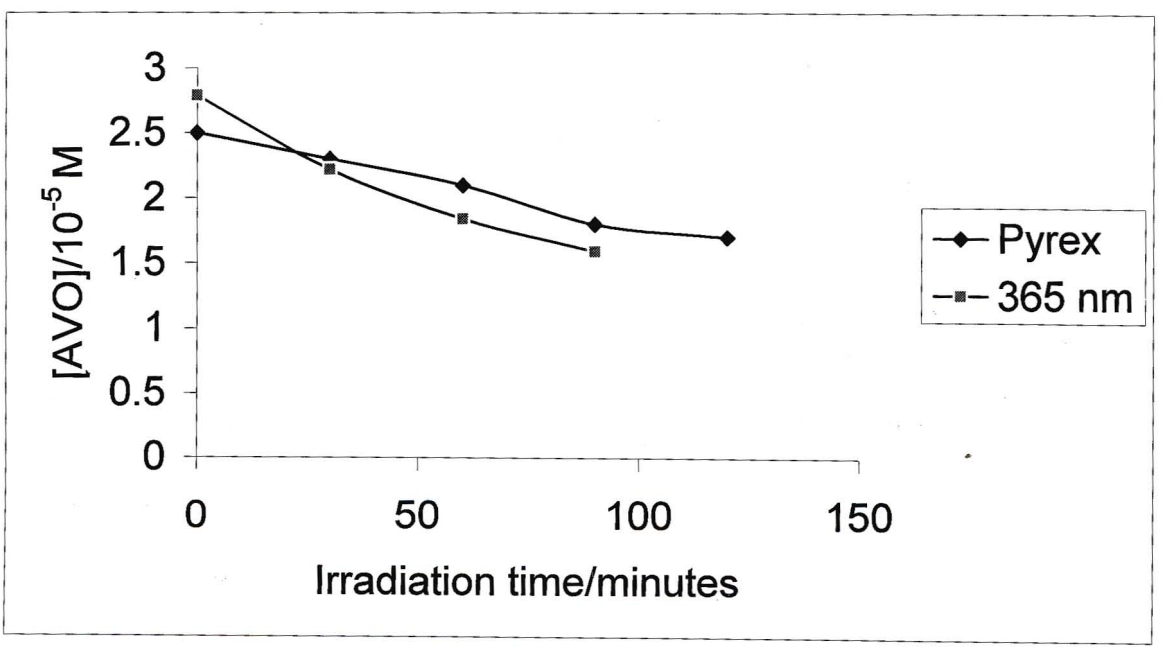

Figure 3.25: A comparison of the rate of degradation of AVO dissolved in cyclohexane when irradiated either with a 10 mm Pyrex filter or a 365 nm filter.

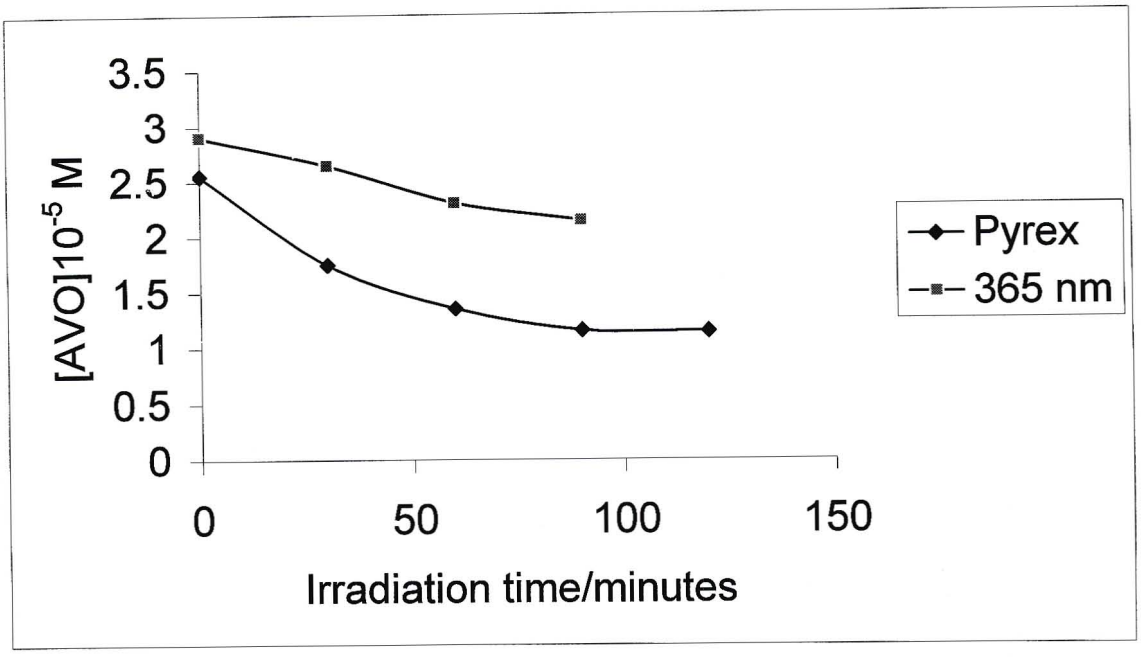

Figure 3.26: A comparison of irradiation of AVO in a mixture of AVO and EHMC in cyclohexane with a 10 mm Pyrex and a 365 nm filter.

Table 3.11: Concentration of EHMC and AVO determined upon irradiating a mixture of EHMC and AVO dissolved in cyclohexane with a 365 nm filter.

Irradiation time/minutes	**$A_{290\ nm}$**	**$A_{350\ nm}$**	**[EHMC]/10^{-5} M**	**[AVO]/10^{-5} M**
0	0.946	0.990	2.60	2.90
30	0.934	0.901	2.66	2.64
60	0.949	0.786	2.85	2.30
90	0.955	0.734	2.94	2.14

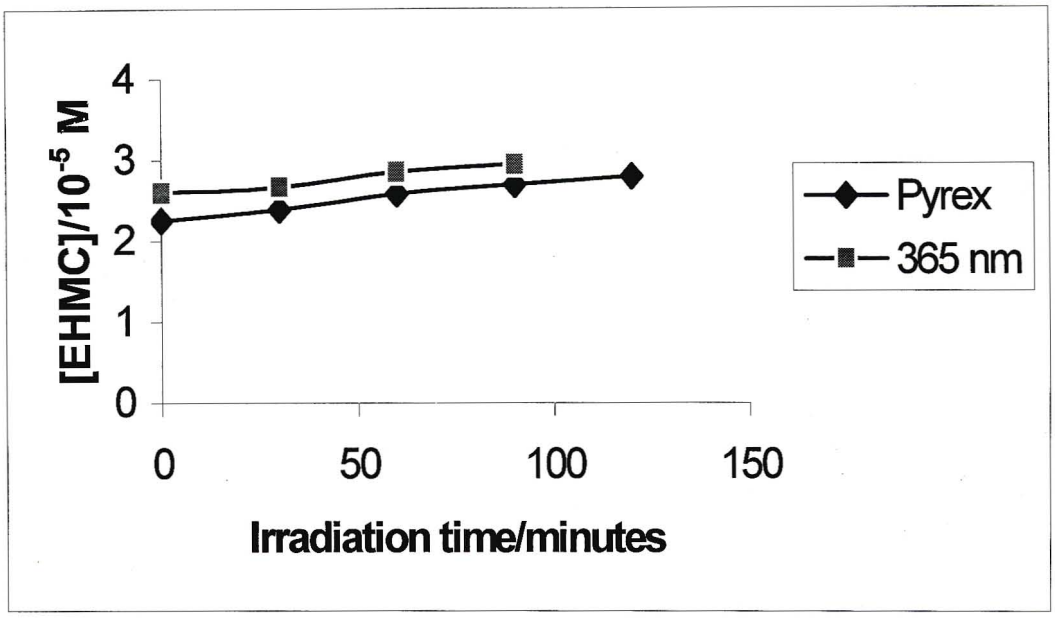

Figure 3.27: A comparison of the photodegradation observed on irradiating EHMC in the presence of AVO dissolved in cyclohexane with either a 10 mm Pyrex or a 365 nm filter.

3.3.5 The effect of quenchers on photostability

When the transfer of electronic energy causes deactivation of an excited state we call this process quenching [4]. Quenching is important in solutions where collisions are very frequent and it involves the transfer of energy between an excited molecule A^* and a quenching species, M:

$$A^* + M \longrightarrow A + M.$$

Electronic excitation in A^* is degraded to vibrational, translational or rotational energy in M. A^* has lost its excitation and is therefore deactivated. If photoproducts are derived from the excited state of a sunscreen molecule and quenching competes with other processes then a quenching species M can reduce the amount of photoproducts formed. This results in the sunscreen molecule attaining a more photostable state.

Oxygen is an efficient quencher of excited states since it causes the decay of the excited species to its ground state with no chemical reaction. Molecular oxygen in its ground state has triplet and not singlet multiplicity unlike most natural compounds. Thus it may have a photostabilising effect on reactions involving relatively long-lived excited states such as triplets. Short-lived singlet states cannot be quenched by O_2 since the concentration of O_2 is too low to make a bimolecular reaction such as quenching significant. In the quenching process the strong electrophile singlet O_2 ($^1O_2$) is generated and this may lead to detrimental reactions. Using O_2 as a triplet quencher is not a conclusive method to show that products are formed from the triplet state therefore we also used *cis*-piperylene as a triplet quencher.

We first looked at the effect of O_2 on the sunscreen agents dissolved in cyclohexane and from the UV-spectra obtained in the presence and absence of O_2 we made the following observations:

- The UV-spectra showing the effect of O_2 on sunscreen agents dissolved in cyclohexane can be seen in Figure 3.28. The concentrations of EHMC were determined from Figure 2.15 and the results are shown in Table 3.12. A graph of the concentrations of EHMC in the presence and absence of O_2 was plotted against irradiation time (see Figure 3.29). From this graph it is evident that the rate of degradation of EHMC is enhanced in the

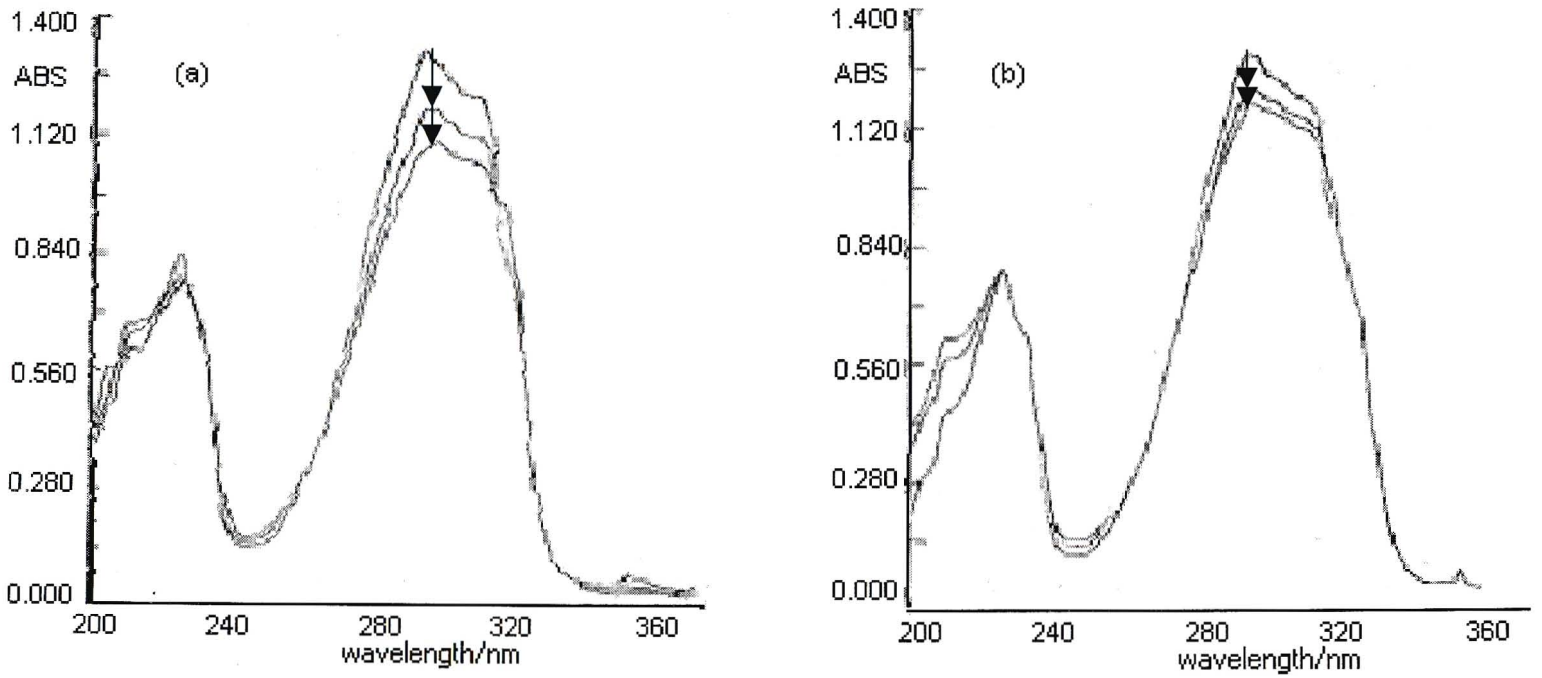

Figure 3.28: UV-spectra showing the effect of O_2 on EHMC dissolved in cyclohexane: (a) 5 x 10^{-5} M EHMC in the absence of O_2 irradiated at one minute intervals and (b) 5 x 10^{-5} M EHMC in the presence of O_2 irradiated at 1 minute intervals.

absence of O_2 implying that O_2 when present quenches excited-state EHMC. We can therefore say that upon irradiating *trans*-EHMC in cyclohexane, product formation possibly occurs from the triplet excited state.

Table 3.12: Concentrations of EHMC dissolved in cyclohexane obtained upon irradiation of light with wavelengths greater than 300 nm in the presence and absence of O_2.

Irradiation time/minutes	**$A_{290\ nm}$ (O_2 present)**	**[EHMC]/ 10^{-5} M (O_2 present)**	**$A_{290\ nm}$ (O_2 absent)**	**[EHMC]/ 10^{-5} M (O_2 absent)**
0	1.298	3.894	1.314	3.942
1	1.212	3.636	1.182	3.546
2	1.184	3.552	1.101	3.303

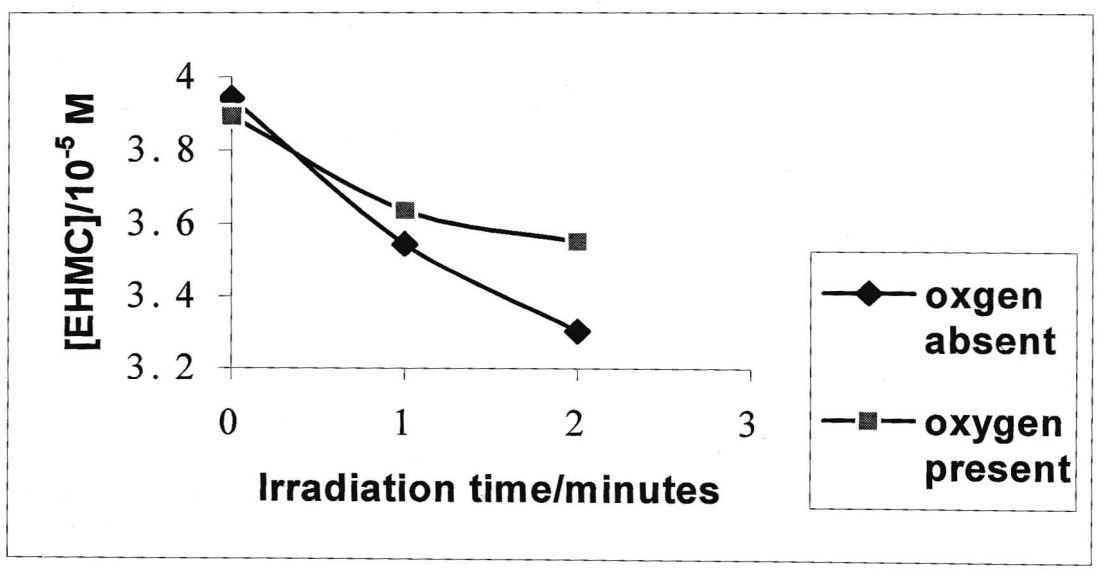

Figure 3.29: A comparison of the change in concentration of EHMC dissolved in cyclohexane when irradiated with wavelengths greater than 300 nm in the presence and absence of O_2.

- We then looked at the effect of O_2 on irradiating AVO dissolved in cyclohexane and from the UV-spectra it can be seen that the rate of loss of absorbance in the absence of O_2 is greater than in its presence (see Figure 3.30). This implies that the photoproducts are formed from the triplet state. The concentrations of AVO after irradiation in the presence and absence of O_2 were determined by using Figure 2.13 and the results are shown in Table 3.13 and plotted in Figure 3.31. From Figure 3.31 we can say that the rate of degradation of AVO when irradiated in the absence of O_2 is marginally faster than in its presence. In the absence of O_2 you can see from the UV-spectra that the absorbance in the region of 200-280 nm is increased with increased irradiation time when compared to similar spectra in the presence of O_2. This increase in absorbance, in the region 200-280 nm, could be due to benzoic acids as reported by Schwack and Rudolph [16]. An investigation of these photoproducts is described in Section 3.4.3. O_2 therefore appears to quench the excited state of AVO and thereby prevents rapid product formation.

Table 3.13: Concentrations of AVO (determined by using Figure 2.13) obtained upon irradiation in cyclohexane with wavelengths greater than 300 nm in the presence and absence of O_2.

Irradiation Time/minutes	**$A_{350\ nm}$ (O_2 present)**	**[AVO]/10^{-5} M (O_2 present)**	**$A_{350\ nm}$ (O_2 absent)**	**[AVO]/10^{-5} M (O_2 absent)**
0	1.140	2.85	1.076	2.69
30	0.759	1.95	0.647	1.70
60	0.575	1.53	0.476	1.25

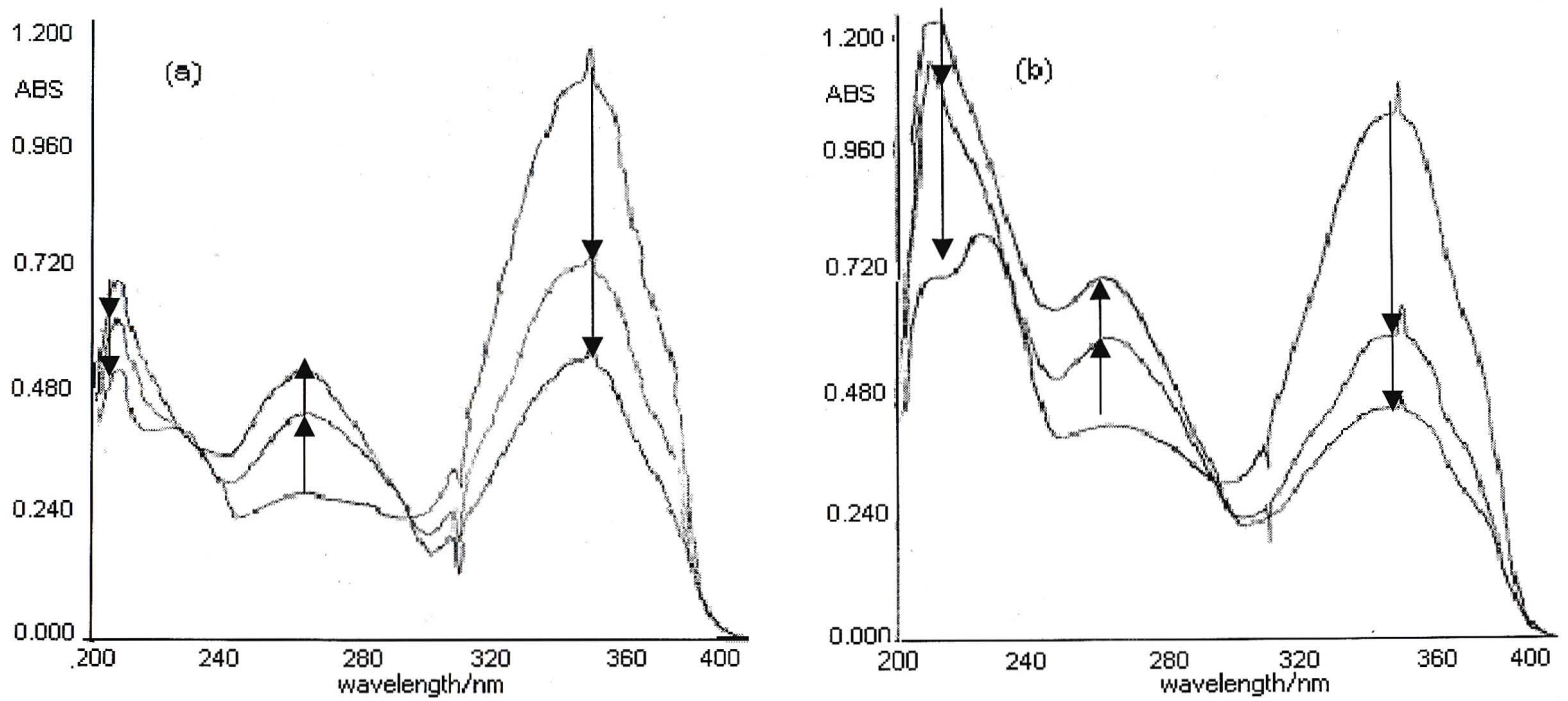

Figure 3.30: UV-spectra showing the effect of O_2 on AVO dissolved in cyclohexane: (a) 3 x 10^{-5} M AVO irradiated at 30 minute intervals in the presence of O_2, and (b) 3 x 10^{-5} M AVO irradiated at 30 minute intervals in the absence of O_2.

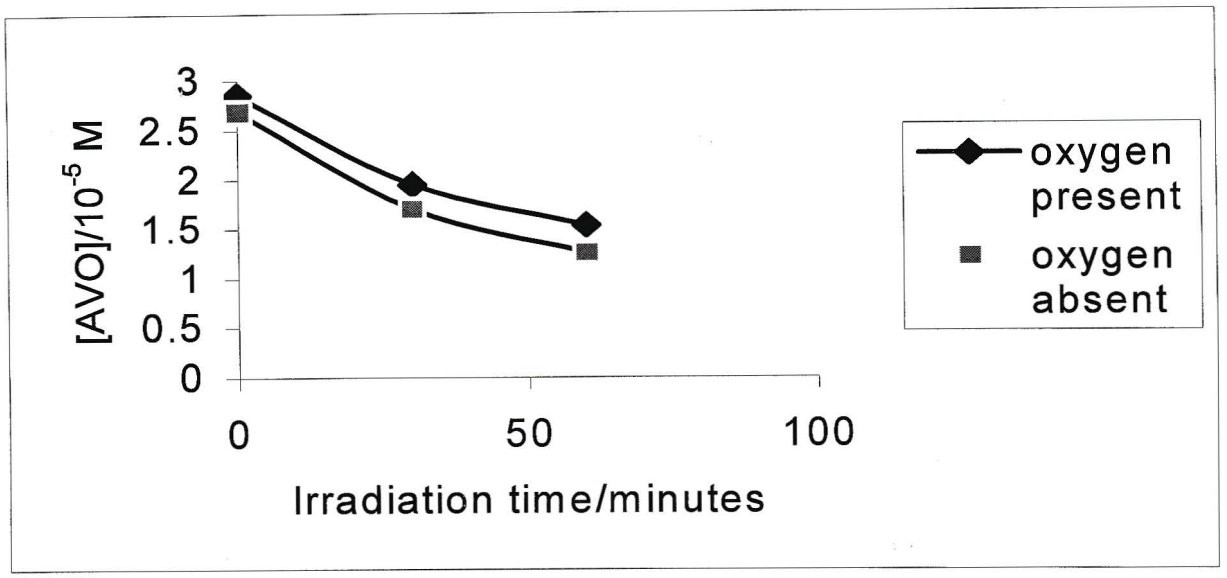

Figure 3.31: A comparison of the change in concentration of AVO dissolved in cyclohexane when irradiated with wavelengths greater than 300 nm in the presence and absence of O_2.

- In the same light we looked at the effect of O_2 on irradiating a mixture of EHMC and AVO dissolved in cyclohexane and the UV-spectra are shown in Figure 3.32. The concentrations of AVO in the mixture upon irradiation were determined from Figure 2.13 and the results are shown in Table 3.14. From Figure 3.33 we can say that the rate of degradation of AVO in the mixture is enhanced in the absence of O_2 therefore we can deduce that O_2 acts as a triplet quencher. The concentration of EHMC was determined by using the method developed in Section 2.6.2.2 and the concentration of AVO was taken from Table 3.14 (see Table 3.15). From Figure 3.34 it is clear that the concentration of EHMC increases both in the presence and absence of O_2. This could be due to the one of the photoproducts absorbing at 290 nm and this also explains the shift in the EHMC peak.

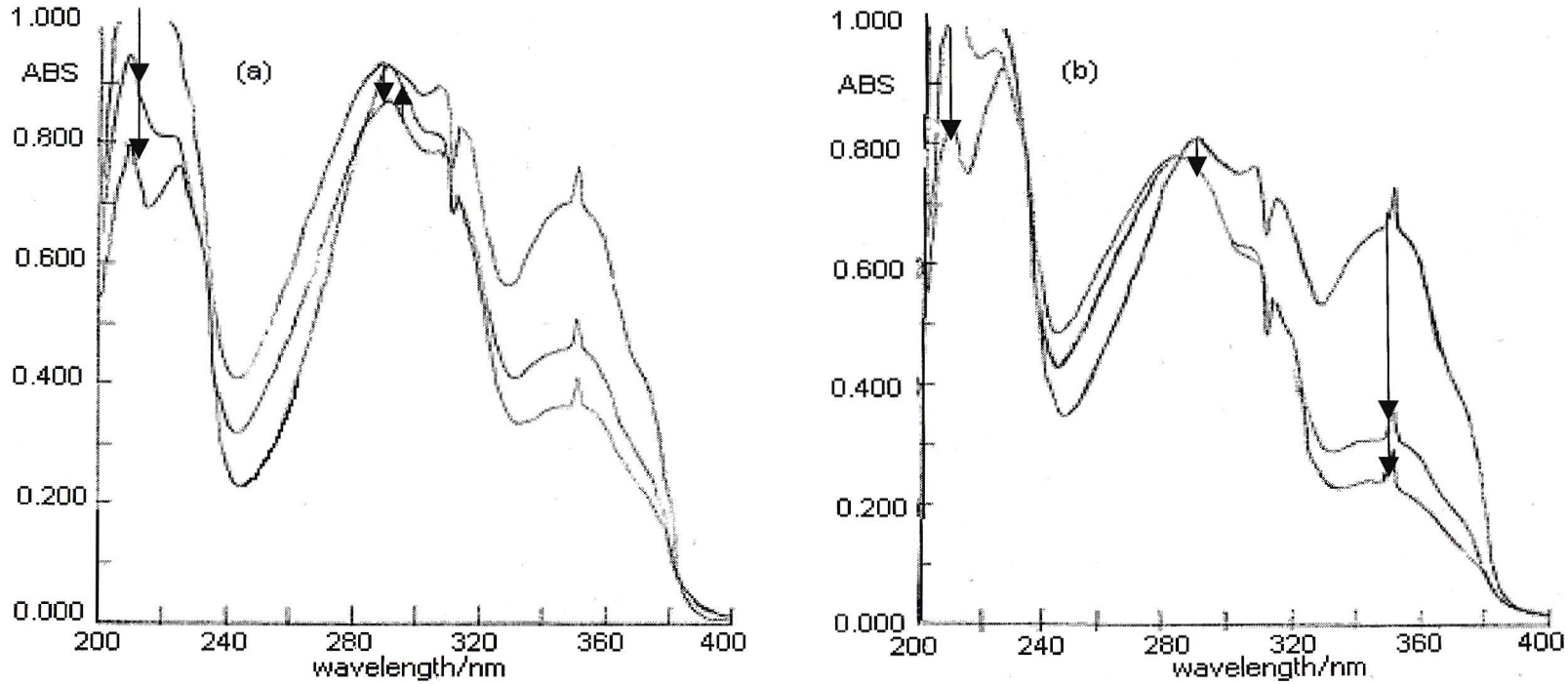

Figure 3.32: UV-spectra showing the effect of O_2 on a mixture of EHMC and AVO, that was made up such that their absorbances were approximately equal to one, in cyclohexane. (a) The mixture in the presence of O_2 upon irradiation at 30 minute intervals and (b) the mixture in the absence of O_2 upon irradiation at 30 minute intervals.

Table 3.14: Concentrations of AVO obtained upon irradiating a mixture of EHMC and AVO dissolved in cyclohexane with wavelengths greater than 300 nm in the presence and absence of O_2.

Irradiation time/minutes	$A_{350\ nm}$ (O_2 present)	[AVO]/10^{-5} M (O_2 present)	$A_{350\ nm}$ (O_2 absent)	[AVO]/10^{-5} M (O_2 absent)
0	0.759	1.95	0.728	1.90
30	0.507	1.35	0.363	0.95
60	0.408	1.10	0.290	0.70

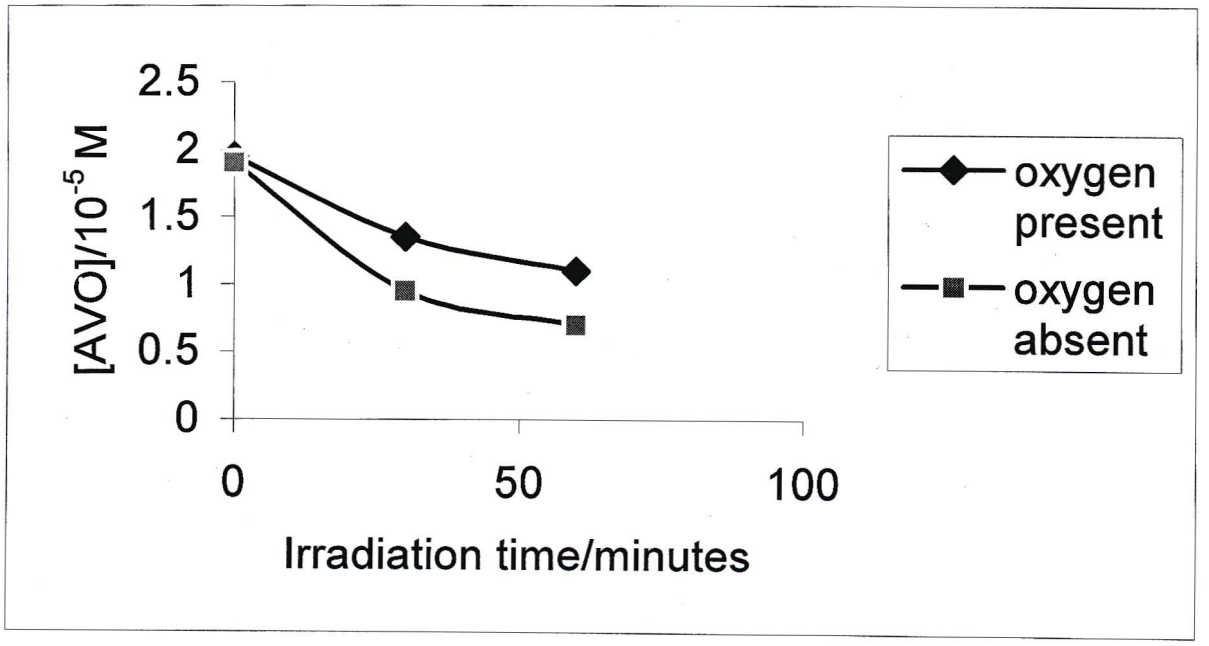

Figure 3.33: A comparison of irradiating AVO in a mixture of EHMC and AVO in cyclohexane in the presence and absence of O_2.

Table 3.15: Concentrations of EHMC obtained (using the method developed in Section 2.6.2.2 and the concentration of AVO in Table 3.14) upon irradiating a mixture of EHMC and AVO dissolved in cyclohexane with wavelengths greater than 300 nm in the presence and absence of O_2.

Irradiation time/minutes	$A_{290\ nm}$ (O_2 present)	[EHMC]/ 10^{-5} M (O_2 present)	$A_{290\ nm}$ (O_2 absent)	[EHMC]/ 10^{-5} M (O_2 absent)
0	0.931	2.92	0.728	2.48
30	0.870	2.91	0.363	2.71
60	0.935	3.27	0.290	2.82

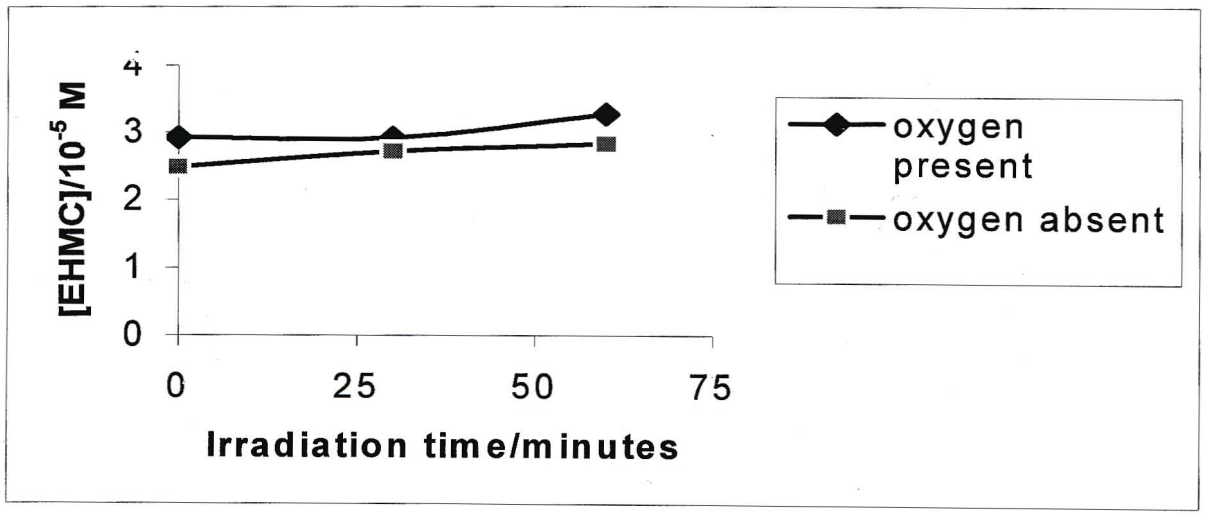

Figure 3.34: A comparison of irradiating EHMC in a mixture of EHMC and AVO dissolved in cyclohexane in the presence and absence of O_2.

When samples of the sunscreen agents dissolved in methanol were irradiated in the presence and absence O_2 we observed the following:

- From the UV-spectra (see Figure 3.35) it is evident that O_2 had no effect on EHMC dissolved in methanol. The concentration of EHMC upon irradiation was determined from the calibration curve of EHMC at 308 nm (see Figure 2.12) and the values obtained are shown in Table 3.16. From Figure 3.36 we can also deduce that the absence of O_2 has no effect on the rate of degradation of EHMC dissolved in methanol.

- The absence of O_2 has no effect on AVO dissolved in methanol either (see Figure 3.37).

Table 3.16: Concentration of EHMC obtained upon irradiation in methanol with wavelengths greater than 300 nm in the presence and absence of O_2.

Irradiation Time/minutes	**$A_{308\ nm}$ (O_2 present)**	**[EHMC]/10^{-5} M (O_2 present)**	**$A_{308\ nm}$ (O_2 absent)**	**[EHMC]/10^{-5} M (O_2 absent)**
0	1.111	4.56	1.106	4.54
1	0.775	3.18	0.770	3.16
2	0.774	3.18	0.772	3.16

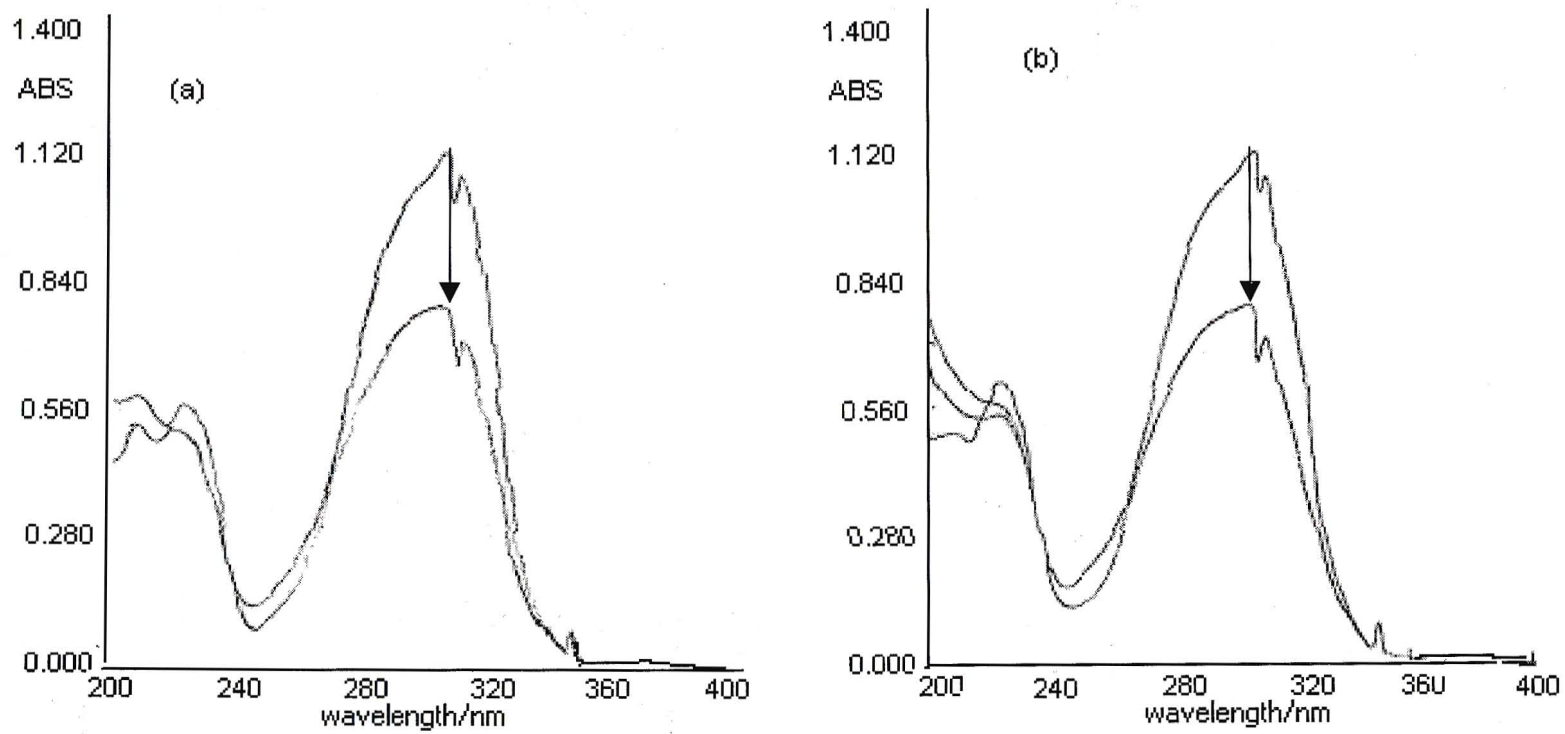

Figure 3.35: UV-spectra showing the effect of O_2 on EHMC dissolved in methanol: (a) 4.5 x 10^{-5} M EHMC in the absence of O_2 upon 1 minute irradiation and (b) 4.5 x 10^{-5} M EHMC in the presence of O_2 upon 1 minute irradiation.

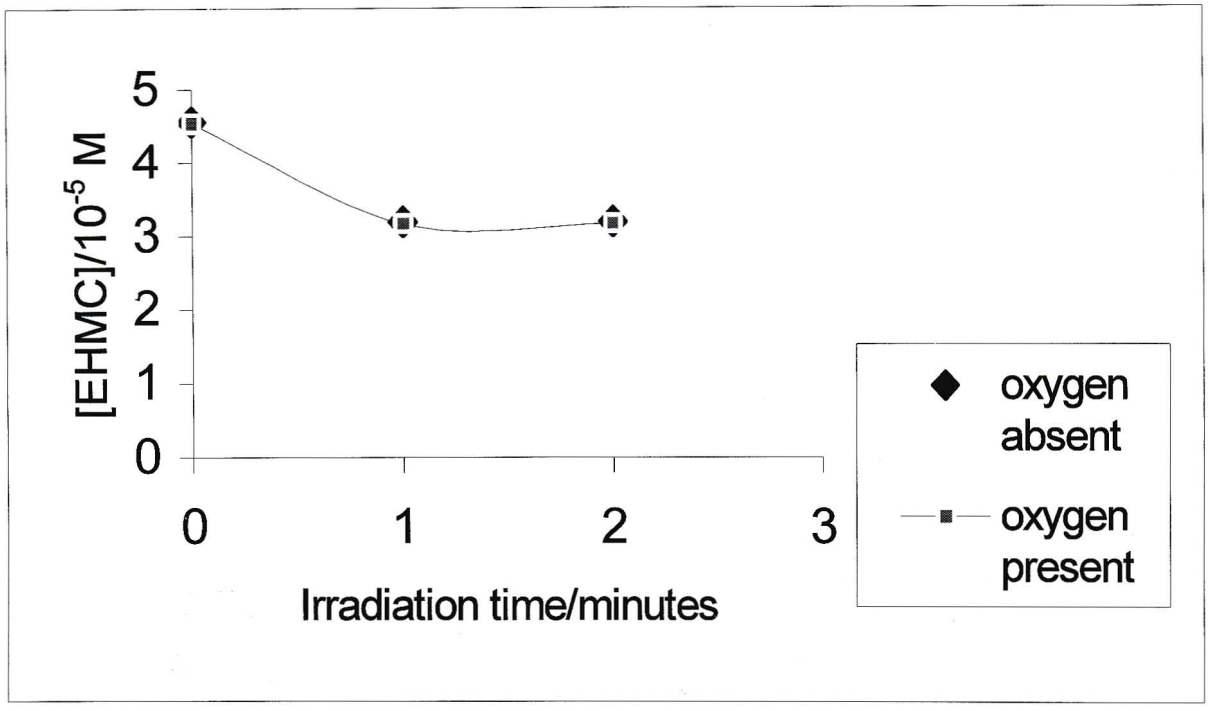

Figure 3.36: A comparison of the change in concentration of EHMC dissolved in methanol when irradiated with wavelengths greater than 300 nm in the presence and absence of O_2.

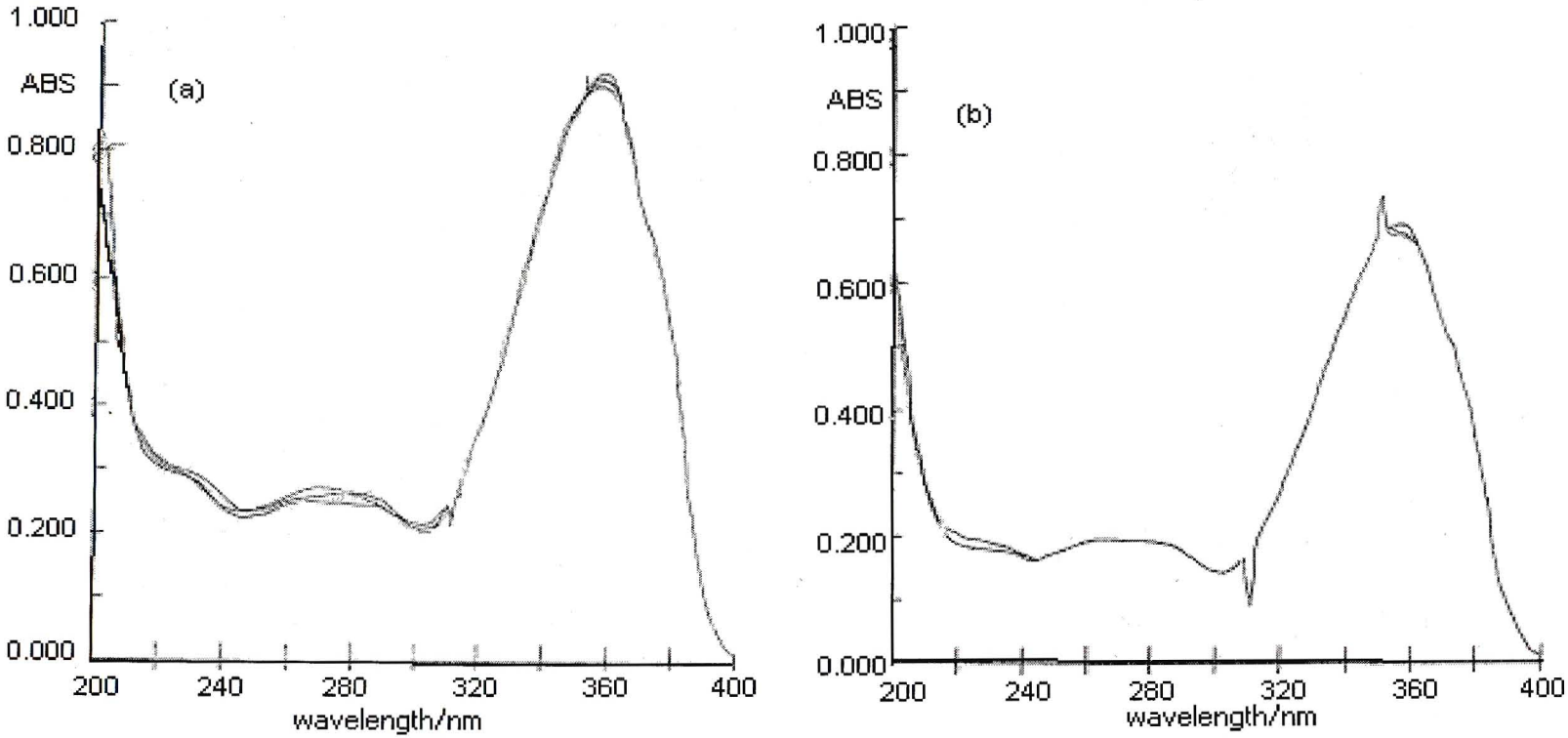

Figure 3.37: UV-spectra showing the effect of O_2 on AVO dissolved in methanol: (a) 2.0×10^{-5} M AVO in the absence of O_2 upon 30 minute irradiation and (b) 1.5×10^{-5} M AVO in the presence of O_2 upon 30 minute irradiation.

- From the UV-spectra shown in Figure 3.38 it can be seen that O_2 has no effect on a mixture of EHMC and AVO in methanol. We determined the concentration of EHMC using the method developed in Section 2.6.2.1 (see Table 3.17). From Figure 3.39 we can say that O_2 has no effect on EHMC dissolved in methanol in the presence of AVO. The concentration of AVO remained constant at 2.0×10^{-5} M.

Table 3.17: The effect of O_2 on EHMC dissolved in the presence of AVO in methanol obtained upon irradiation with wavelengths greater than 300 nm in the presence and absence of O_2. Concentrations of EHMC were determined from the method developed in Section 2.6.2.1 with the concentration of AVO determined to be 2.0×10^{-5} M.

Irradiation time/minutes	**$A_{308\ nm}$ (O_2 present)**	**[EHMC]/10^{-5} M (O_2 present)**	**$A_{308\ nm}$ (O_2 absent)**	**[EHMC]/10^{-5} M (O_2 absent)**
0	0.817	2.39	0.811	2.38
1	0.611	1.67	0.617	1.62
2	0.613	1.67	0.617	1.65

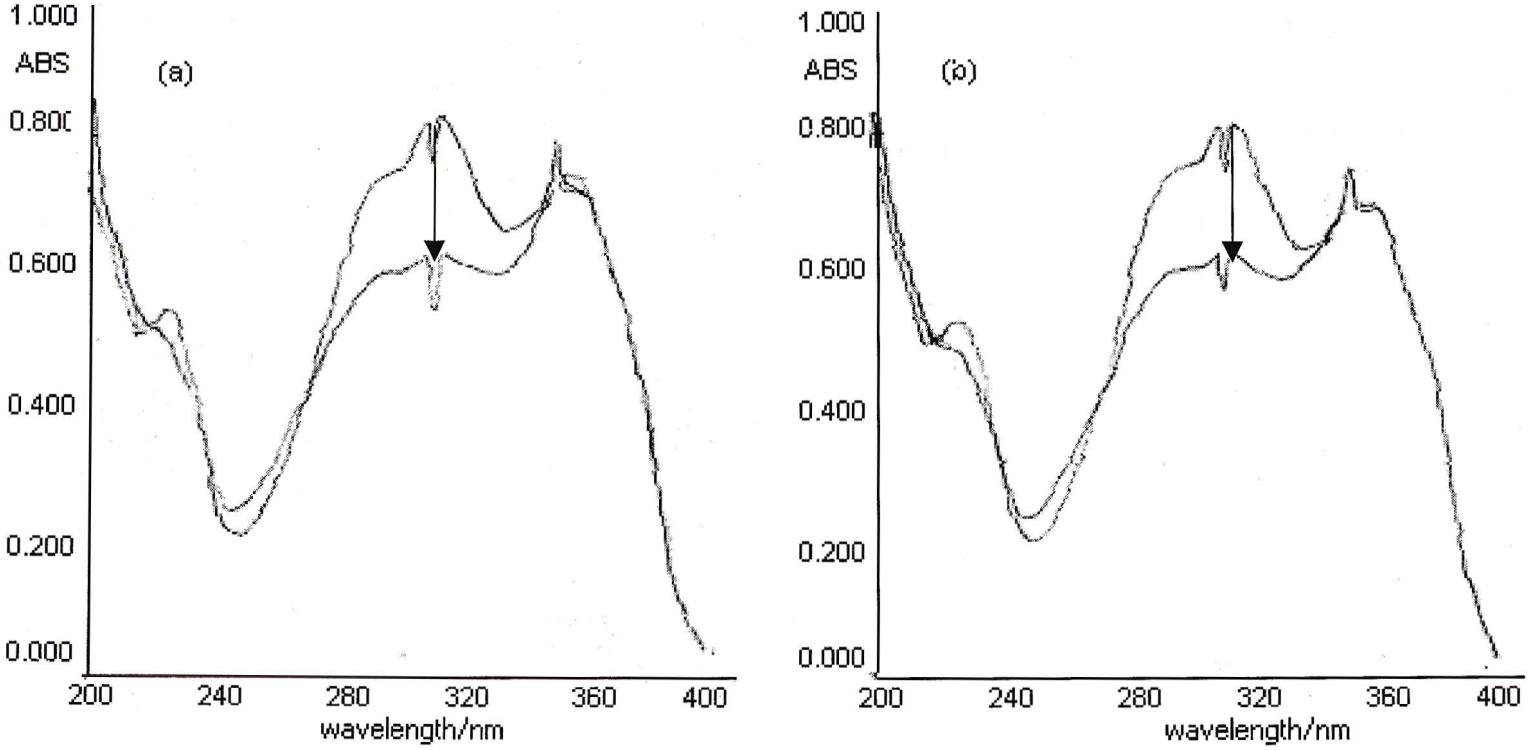

Figure 3.38: UV-spectra showing the effect of O_2 on a mixture of EHMC and AVO. Their concentrations were made up such that their absorbances were approximately equal to one. (a) The mixture in the absence of O_2 and (b) the mixture in the presence of O_2.

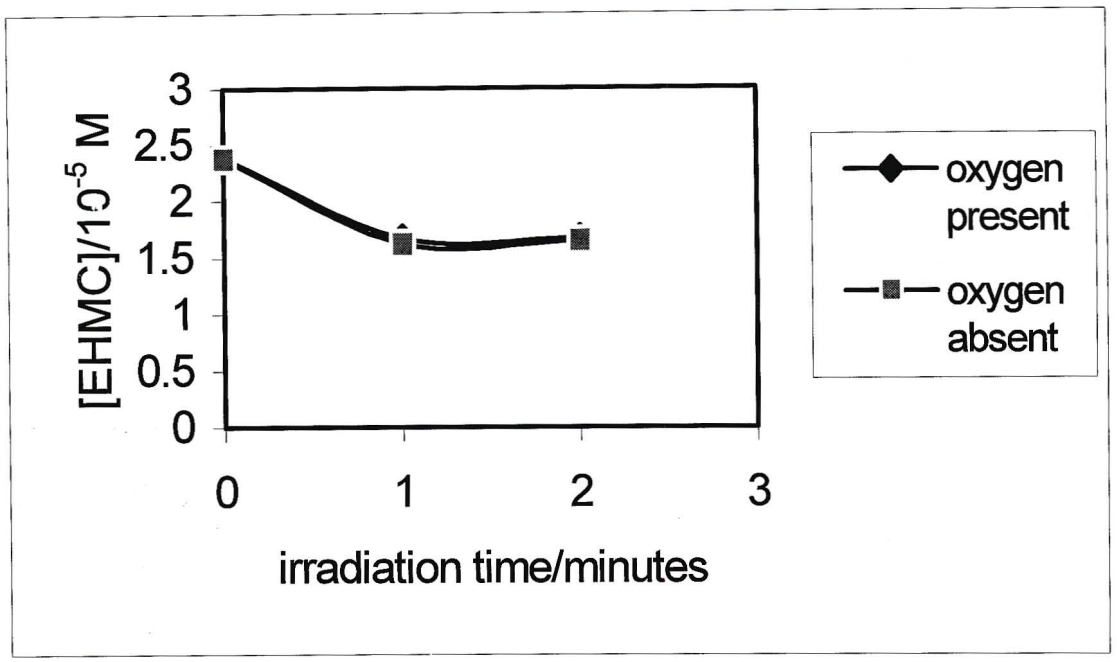

Figure 3.39: A comparison of the change in concentration of EHMC dissolved in methanol in the presence of AVO when irradiated with wavelengths greater than 300 nm in the presence and absence of O_2.

Checking the quenching effects of O_2 is not a conclusive test to determine whether photoproduct formation occurs from the triplet state since O_2 readily exists in the atmosphere and to remove it totally from solution is almost impossible. We therefore looked at the quenching effects of *cis*-piperylene, a well-known triplet-state quencher.

The wavelength of maximum absorbance of *cis*-piperylene is 222 nm in both methanol and cyclohexane and it does not absorb at wavelengths where AVO and EHMC absorb. On irradiating with the Osram HBO 500 W/2 high pressure mercury lamp in combination with the 10 mm Pyrex filter we do not expect *cis*-piperylene to absorb any radiation therefore any effects observed that are different from those when the sunscreens are irradiated alone should be due to quenching effects by *cis*-piperylene.

On checking the effect of *cis*-piperylene on irradiated sunscreen solutions in methanol the following was observed:

- The triplet energies of AVO and *cis*-piperylene are 249 kJ mol^{-1} [39] and 247 kJ mol^{-1} [38] respectively. Since *cis*-piperylene has a lower triplet energy than that of AVO we expect it to act as a quencher of any triplet state but as shown in Figure 3.40b this possible quenching effect does not lead to product formation.

- The triplet energy of EHMC is 238 kJ mol^{-1} [39] thus *cis*-piperylene would have no quenching effects. This can be seen from the UV-spectra of EHMC in methanol in the presence of *cis*-piperylene (see Figure 3.40a). The concentrations of EHMC dissolved in methanol were then determined using the method developed in Section 2.6.2.1 (see Table 3.18). From Figure 3.41 it can be said that there is no substantial quenching effect by *cis*-piperylene on EHMC dissolved in methanol.

- We then looked at the effect of *cis*-piperylene on a mixture of EHMC and AVO in methanol. From Figure 3.40c AVO showed no change as expected. The concentrations of EHMC in the mixture were then determined using the method developed in Section 2.6.2.1 (see Table 3.19). From Figure 3.42 it can be said that *cis*-piperylene has no quenching effect on a mixture of EHMC and AVO in methanol.

Table 3.18: Concentration of EHMC obtained upon irradiation in methanol with wavelengths greater than 300 nm in the presence and absence of *cis*-piperylene. The concentration of *cis*-piperylene employed was identical to the initial EHMC concentration.

Irradiation time/minutes	**$A_{308\ nm}$ (*cis*-piperylene present)**	**[EHMC]/ 10^{-5} M (*cis*-piperylene present)**	**$A_{308\ nm}$ (*cis*-piperylene absent)**	**[EHMC]/ 10^{-5} M (*cis*-piperylene absent)**
0	0.901	3.70	0.925	4.05
1	0.685	2.81	0.703	3.2
2	0.650	2.76	0.552	2.8

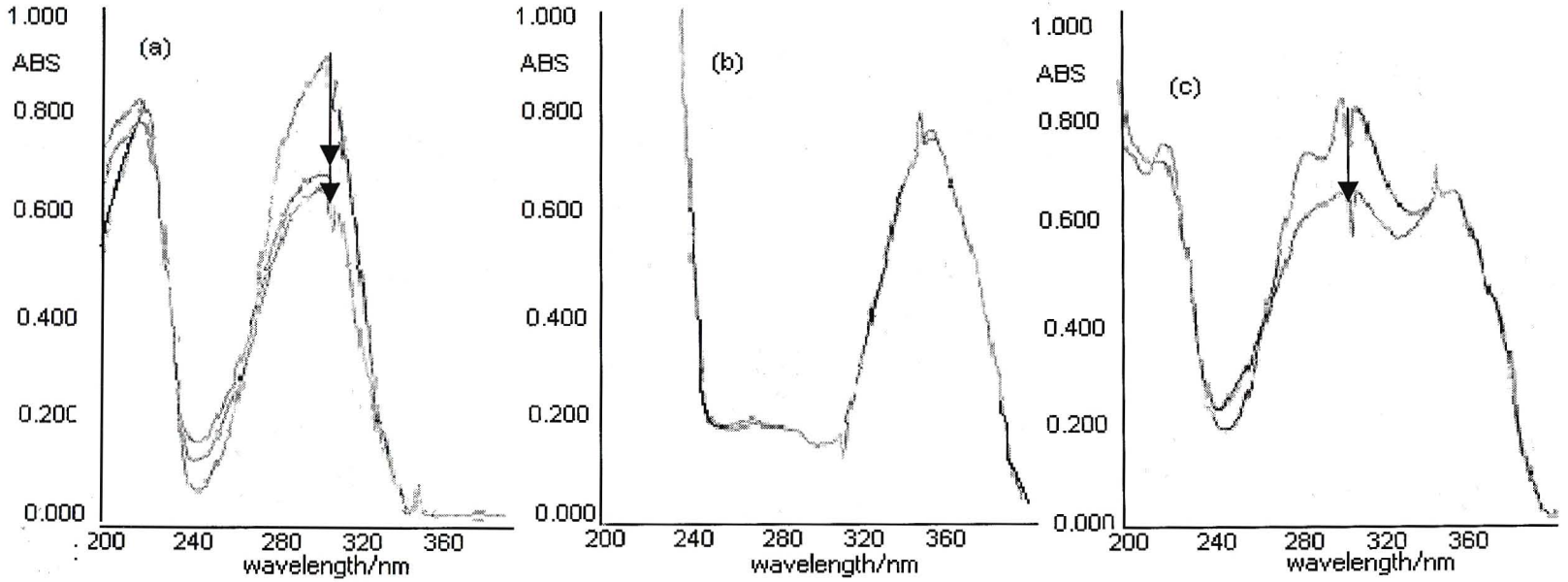

Figure 3.40: UV spectra showing the quenching effect of *cis*-piperylene (λ_{max} 222 nm) on the sunscreen agents dissolved in methanol: (a) 3.6 x 10^{-5} M EHMC in the presence of *cis*-piperylene irradiated at 1 minute intervals, (b) 1.7 x 10^{-5} M AVO in the presence of *cis*-piperylene irradiated at 30 minute intervals and (c) a mixture of AVO and EHMC in the presence of *cis*-piperylene irradiated at 1 minute intervals.

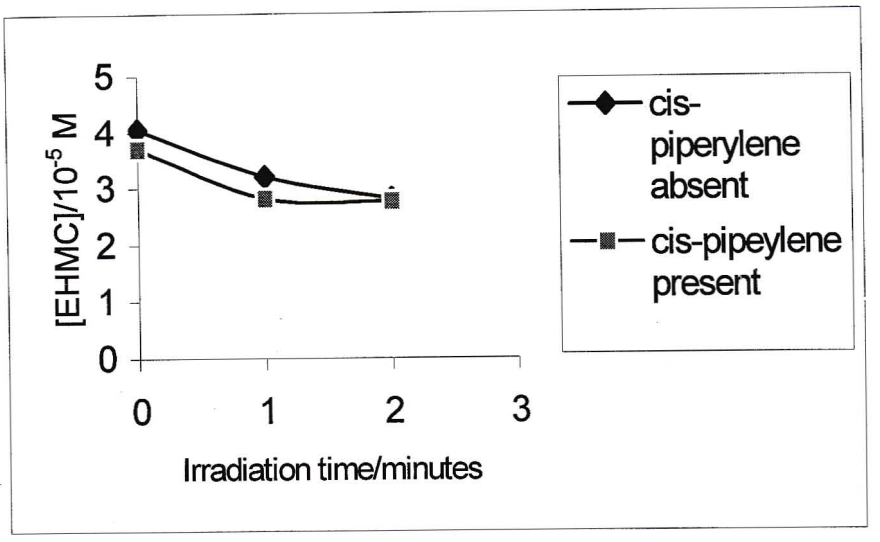

Figure 3.41: A comparison of the change in concentration of EHMC dissolved in methanol when irradiated with wavelengths greater than 300 nm in the presence and absence of *cis*-piperylene.

Table 3.19: Concentrations of EHMC determined upon irradiating a mixture of EHMC and AVO with wavelengths greater than 300 nm in the presence and absence of *cis*-piperylene. The concentration of *cis*-piperylene employed was identical to the initial EHMC concentration.

Irradiation time/minutes	**$A_{308\ nm}$ (*cis*-piperylene absent)**	**[EHMC]/10^{-5}M (*cis*-piperylene absent)**	**$A_{308\ nm}$ (*cis*-piperylene present)**	**[EHMC]/10^{-5}M (*cis*-piperylene present)**
0	0.902	2.77	0.834	2.56
1	0.710	2.06	0.634	1.84
2	0.670	1.91	0.633	1.83

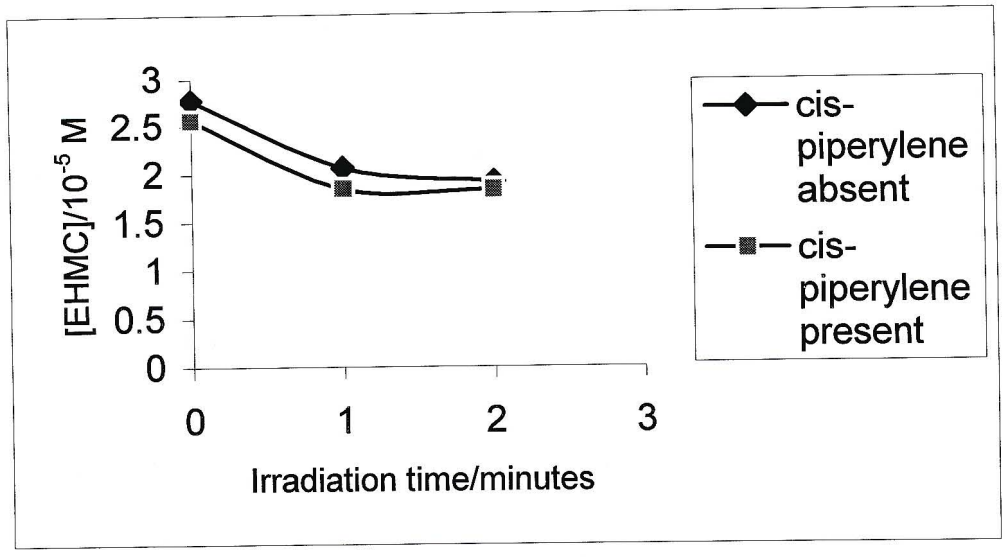

Figure 3.42: A comparison of the change in concentration of EHMC dissolved in methanol in the presence of AVO when irradiated with wavelengths greater than 300 nm in the presence and absence of *cis*-piperylene.

On checking the effect of *cis*-piperylene on irradiated sunscreen solutions in cyclohexane the following were observed:

- The effect of *cis*-piperylene on EHMC dissolved in cyclohexane can be seen in Figure 3.43a. The concentration of EHMC after irradiation is shown in Table 3.20. From Figure 3.44 it is clear that *cis*-piperylene did not have any quenching effect since *cis*-piperylene has a higher triplet energy than that of EHMC.

- The UV-spectra obtained on irradiating AVO dissolved in cyclohexane in the presence of *cis*-piperylene are shown in Figure 3.43b. The concentrations of AVO determined using Figure 2.13 are shown in Table 3.21. From Figure 3.45 it is clear that the rate of degradation of AVO is enhanced in the presence of *cis*-piperylene which is unexpected. Therefore in this case *cis*-piperylene does not quench irradiated AVO solutions.

- The UV-spectra obtained upon irradiation of a mixture of EHMC and AVO dissolved in cyclohexane in the presence of *cis*-piperylene are shown in Figure 3.43c. The concentrations of AVO determined using Figure 2.13 are shown in Table 3.22. From

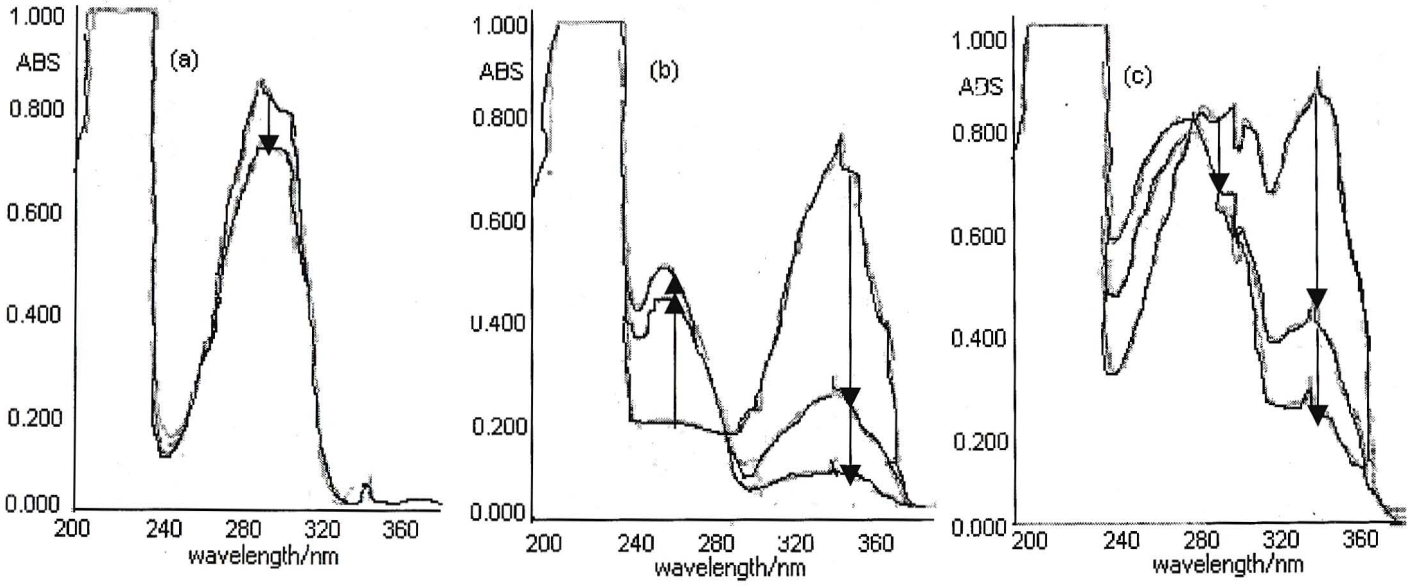

Figure 3.43: UV-spectra showing the quenching effect of *cis*-piperylene (λ_{max} 222 nm) on the sunscreen agents dissolved in cyclohexane: (a) 3 x 10^{-5} M EHMC in the presence of *cis*-piperylene upon 1 minute irradiation intervals, (b) 2 x 10^{-5} M AVO in the presence of *cis*-piperylene upon 30 minute irradiation intervals and (c) a mixture of EHMC and AVO in the presence of *cis*-piperylene upon 30 minute irradiation intervals.

Figure 3.46 it is it is evident that the rate of degradation of AVO is enhanced in the presence of *cis*-piperylene which is unexpected. Therefore in this case *cis*-piperylene does not quench AVO irradiated in solutions containing a mixture of EHMC and AVO dissolved in cyclohexane. What can be observed is that this degradation of AVO in the mixture in the presence of *cis*-piperylene is not as significant as when AVO is irradiated alone in the presence of *cis*-piperylene (compare Figures 3.45 and 3.46). The concentration of EHMC in the mixture is shown in Table 3.23. From Figure 3.47 it is clear that the concentration of EHMC is increasing but not as significant when *cis*-piperylene is present. This observed increase in concentration in EHMC could be due to the increased formation of a UVB-absorbing photoproduct of AVO in view of the enhanced degradation of AVO in the presence of *cis*-piperylene.

Table 3.20: Concentrations of EHMC dissolved in cyclohexane determined upon irradiating with wavelengths greater than 300 nm in the presence and absence of *cis*-piperylene. The concentration of *cis*-piperylene employed was identical to the initial EHMC concentration.

Irradiation time/minutes	**$A_{290\ nm}$ (*cis*-piperylene absent)**	**[EHMC]/10^{-5}M (*cis*-piperylene absent)**	**$A_{290\ nm}$ (*cis*-piperylene present)**	**[EHMC]/10^{-5}M (*cis*-piperylene present)**
0	0.830	3.3	0.872	3.6
1	0.625	2.5	0.742	3.0
2	0.660	2.6	0.740	3.0

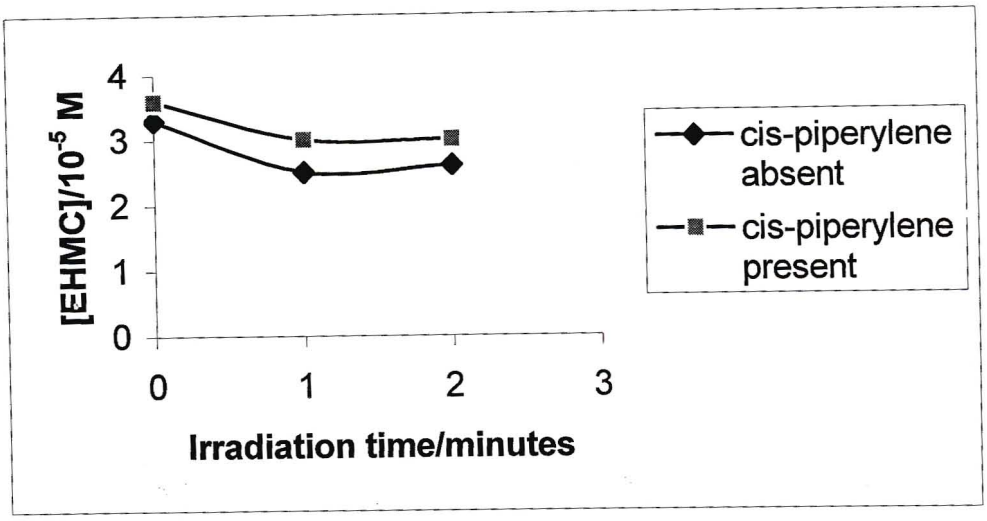

Figure 3.44: A comparison of the change in concentration of EHMC dissolved in cyclohexane when irradiated with wavelengths greater than 300 nm in the presence and absence of *cis*-piperylene.

Table 3.21: Concentrations of AVO dissolved in cyclohexane determined upon irradiating with wavelengths greater than 300 nm in the presence and absence of *cis*-piperylene. The concentration of *cis*-piperylene employed was identical to the initial EHMC concentration.

Irradiation time/minutes	**$A_{350\ nm}$ (*cis*-piperylene absent)**	**[AVO]/10^{-5} M (*cis*-piperylene) absent)**	**$A_{350\ nm}$ (*cis*-piperylene present)**	**[AVO]/10^{-5} M (*cis*-piperylene present)**
0	0.889	2.5	0.743	2.09
30	0.818	2.3	0.267	0.75
60	0.742	2.1	0.088	0.25

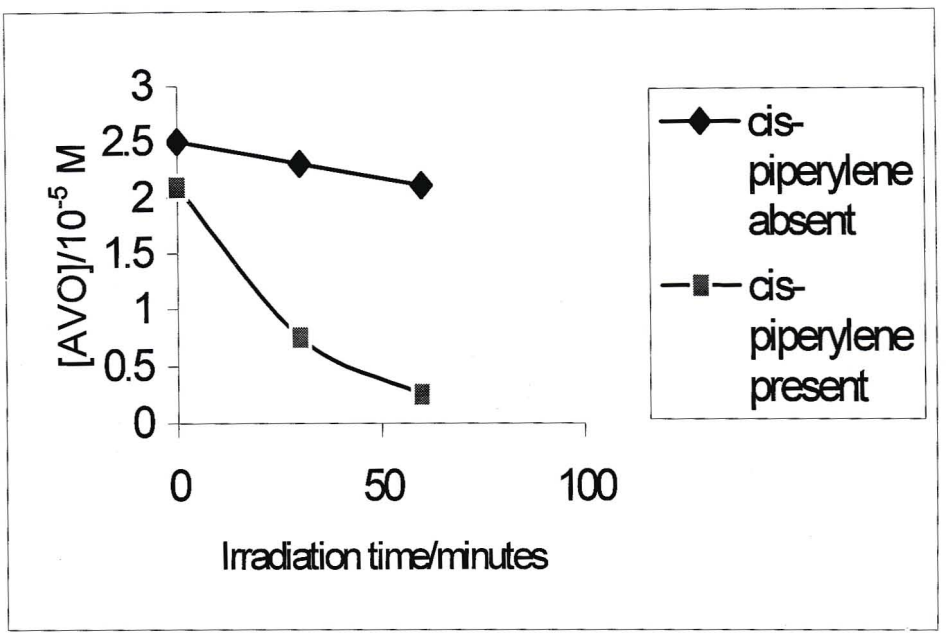

Figure 3.45: A comparison of the change in concentration of AVO dissolved in cyclohexane when irradiated with wavelengths greater than 300 nm in the presence and absence of *cis*-piperylene.

Table 3.22: Concentrations of AVO determined upon irradiation of a mixture of EHMC and AVO dissolved in cyclohexane in the presence and absence of *cis*-piperylene. The concentration of *cis*-piperylene employed was identical to the initial EHMC concentration.

Irradiation time/minutes	**$A_{350\ nm}$ (*cis*-piperylene absent)**	**[AVO]/10^{-5} M (*cis*-piperylene absent)**	**$A_{350\ nm}$ (*cis*-piperylene present)**	**[AVO]/10^{-5} M (*cis*-piperylene present)**
0	0.845	2.55	0.835	2.51
30	0.617	1.75	0.408	1.21
60	0.488	1.35	0.250	0.67

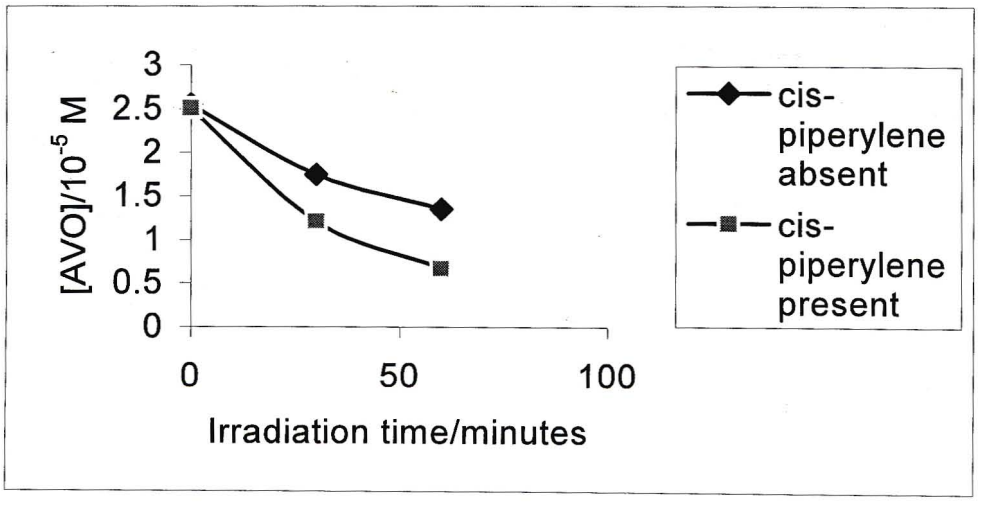

Figure 3.46: A comparison of the change in concentration of AVO dissolved in cyclohexane in the presence of EHMC when irradiated with wavelengths greater than 300 nm in the presence and absence of *cis*-piperylene.

Table 3.23: Concentrations of EHMC determined upon irradiation of a mixture of EHMC and AVO dissolved in cyclohexane in the presence and absence of *cis*-piperylene. The concentration of *cis*-piperylene employed was identical to the initial EHMC concentration.

Irradiation time/minutes	**$A_{290\ nm}$ (*cis*-piperylene absent)**	**[EHMC]/ 10^{-5} M (*cis*-piperylene absent)**	**$A_{290\ nm}$ (*cis*-piperylene present)**	**[EHMC]/ 10^{-5} M (*cis*-piperylene present)**
0	0.821	2.25	0.845	2.32
30	0.776	2.38	0.824	2.52
60	0.787	2.58	0.782	2.56

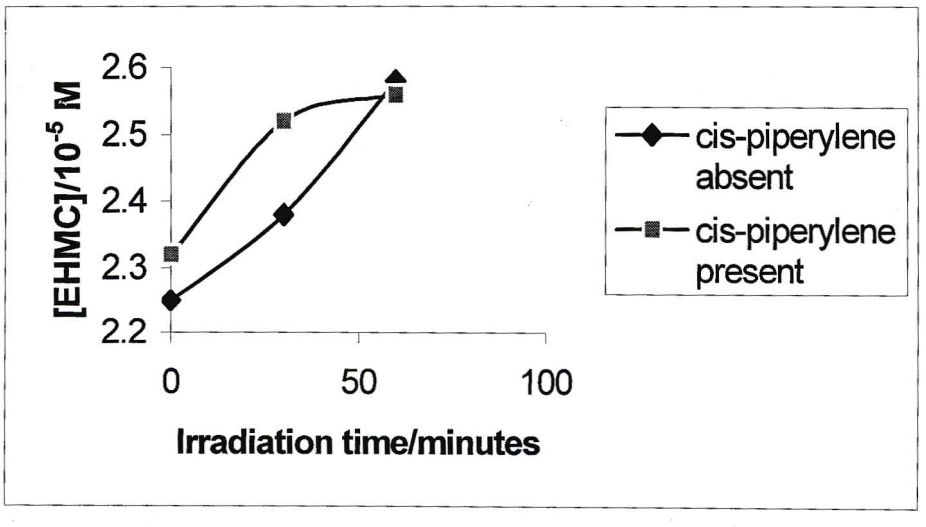

Figure 3.47: A comparison of the change in concentration of EHMC dissolved in cyclohexane in the presence of AVO when irradiated with wavelengths greater than 300 nm in the presence and absence of *cis*-piperylene.

3.3.6 The effect of photosensitisers on photostability

Triplet-triplet energy transfer is a route to produce triplet states that cannot be easily populated by direct absorption. This energy transfer mechanism is referred to as photosensitisation and the donor molecule is the photosensitiser [4]. The photosensitiser's triplet energy has to be higher than that of the acceptor molecule for any transfer to take place. We therefore looked at benzophenone as a possible photosensitiser to AVO and EHMC. We also looked at AVO being a possible photosensitiser to EHMC.

Benzophenone has a triplet energy of 289 kJ mol^{-1} and that of AVO and EHMC are 249 and 238 kJ mol^{-1}, respectively [39]. Since the triplet energy of benzophenone is higher than that of the chemical absorbers it could act as a photosensitiser [39]. Since benzophenone absorbs maximally at 250 nm by irradiating a mixture with a 254 nm narrow bandpass filter only benzophenone would be excited since AVO and EHMC both absorb minimally at 254 nm (see Figures 3.7 and 3.8). By triplet-triplet energy transfer benzophenone could then populate the triplet states of AVO and EHMC and induce their photodegradation if indeed this occurs from their triplet states.

For sunscreen agents dissolved in methanol the following results were observed:

- The UV-spectra of EHMC in the presence and absence of benzophenone are shown in Figures 3.48a and 3.48b respectively. The concentrations of EHMC remaining after irradiation are shown in Table 3.24. From Figure 3.49 we can say that benzophenone has no noticeable photosensitising effect on EHMC since the rate of degradation in the presence and absence of benzophenone is about the same.

- AVO is photostable in methanol therefore the photosensitising effect of benzophenone on AVO in methanol does not lead to photoproduct formation. The energy could therefore be dissipated by other pathways. We therefore did not investigate the photosensitising effect of benzophenone on AVO in methanol.

- From Figure 3.48c we can definitely say that benzophenone has no photosensitising effect on a mixture of EHMC and AVO in methanol since there is no substantial change in the EHMC peak at 308 nm.

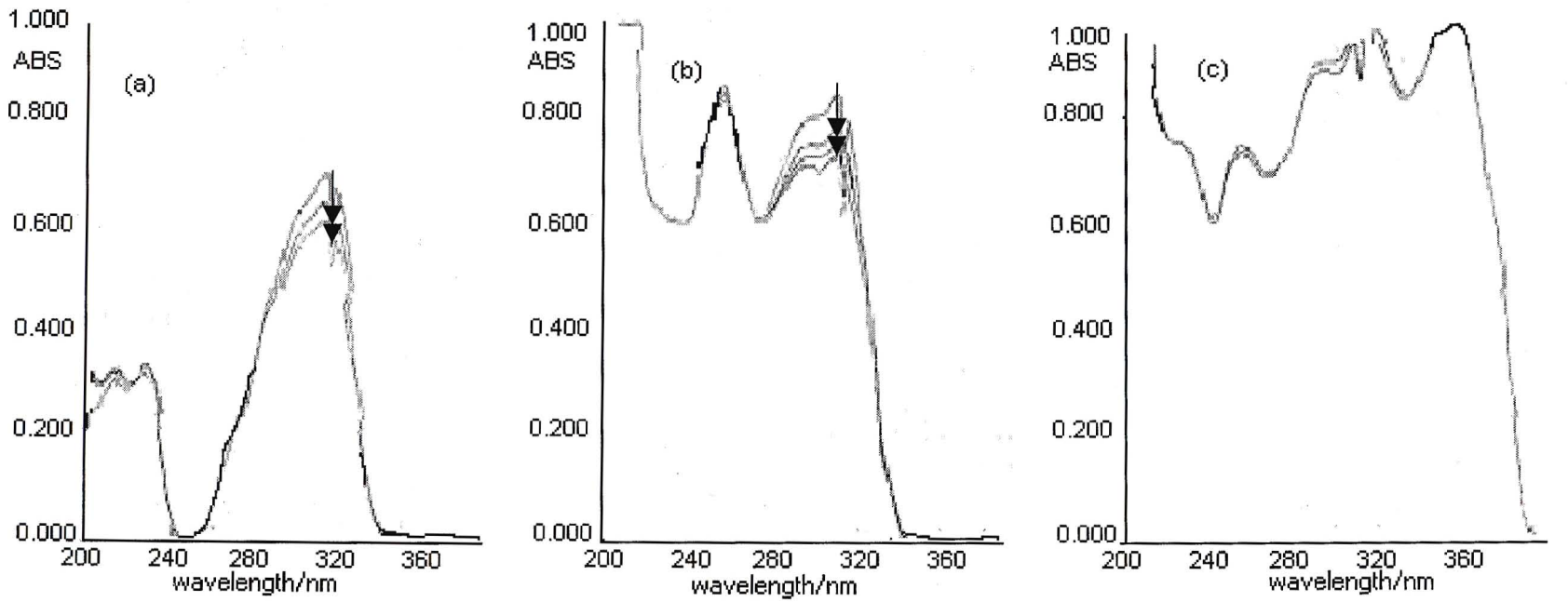

Figure 3.48: UV-spectra showing the effect of 1 x 10^{-3} M benzophenone (λ_{max} 250 nm) on the sunscreen agents in methanol when irradiated with a 254 nm filter: (a) 2.8 x 10^{-5} M EHMC and benzophenone irradiated at 1 minute intervals, (b) EHMC without benzophenone irradiated at 1 minute intervals and (c) a mixture of EHMC, AVO and benzophenone irradiated at 1 minute intervals.

Table 3.24: Concentrations of EHMC dissolved in methanol determined upon irradiation with the 254 nm narrow bandpath interference filter in the presence and absence of benzophenone.

Irradiation time/minutes	$A_{308\ nm}$ (benzophenone present)	[EHMC]/ 10^{-5} M (benzophenone present)	$A_{308\ nm}$ (benzophenone absent)	[EHMC]/ 10^{-5} M (benzophenone absent)
0	0.846	3.35	0.700	2.81
1	0.780	3.15	0.645	2.61
2	0.752	3.02	0.612	2.41
3	0.738	2.95	0.610	2.41

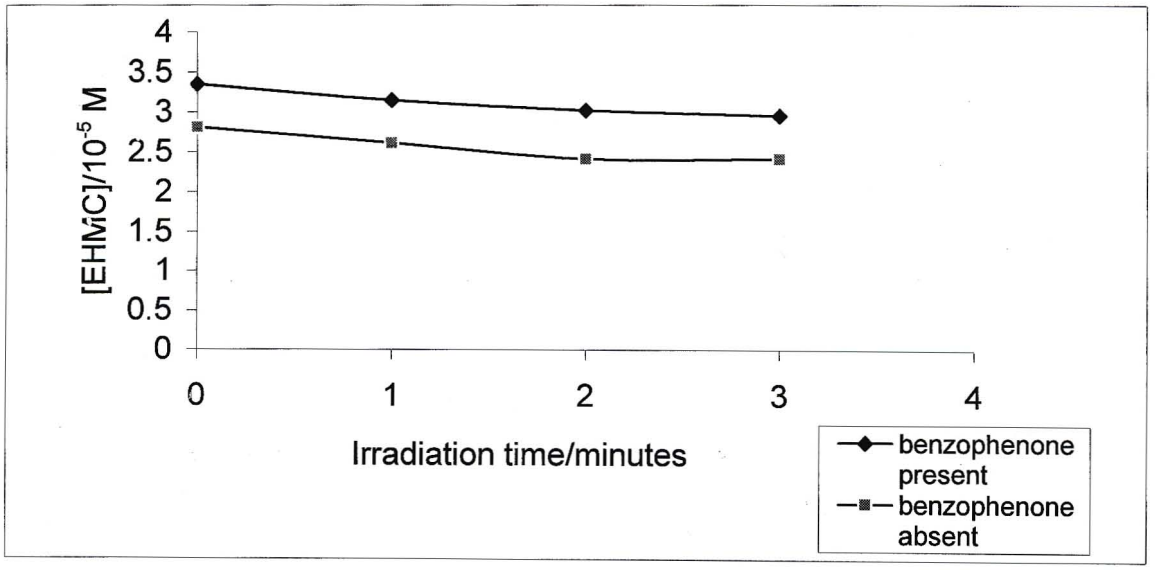

Figure 3.49: A comparison of the change in concentration of EHMC dissolved in methanol when irradiated with the 254 nm narrow bandpath interference filter in the presence and absence benzophenone.

When the sunscreen agents were dissolved in cyclohexane and irradiated in the presence of benzophenone the following effects were observed:

- The UV-spectra of EHMC dissolved in cyclohexane in the presence and absence of benzophenone are shown in Figure 3.50. The degradation of EHMC was inconsistent but from the results obtained in Table 3.25 the degradation of EHMC is enhanced in the presence of benzophenone. On comparison of Figures 3.50a and 3.50b we can say that benzophenone could have slight photosensitising effects on irradiated solutions of EHMC dissolved in cyclohexane.

- From the UV-spectra (see Figures 3.51a and 3.51b) we can certainly say that benzophenone has no photosensitising effect on irradiated solutions of AVO dissolved in cyclohexane.

- From the UV-spectrum of the mixture (see Figure 3.51c) it is evident that benzophenone has no photosensitising effect on AVO in the mixture but may have some photosensitising effect on EHMC.

Table 3.25: Concentrations of EHMC irradiated in cyclohexane with the 254 nm narrow bandpass interference filter in the presence and absence of benzophenone.

Irradiation time/ minutes	**$A_{290\ nm}$ (benzophenone present)**	**[EHMC]/ 10^{-5} M (benzophenone present)**	**$A_{290\ nm}$ (benzophenone absent)**	**[EHMC]/ 10^{-5} M (benzophenone absent)**
0	0.725	2.89	0.800	3.19
1	0.650	2.59	0.762	3.04
2	0.739	2.64	0.813	3.09

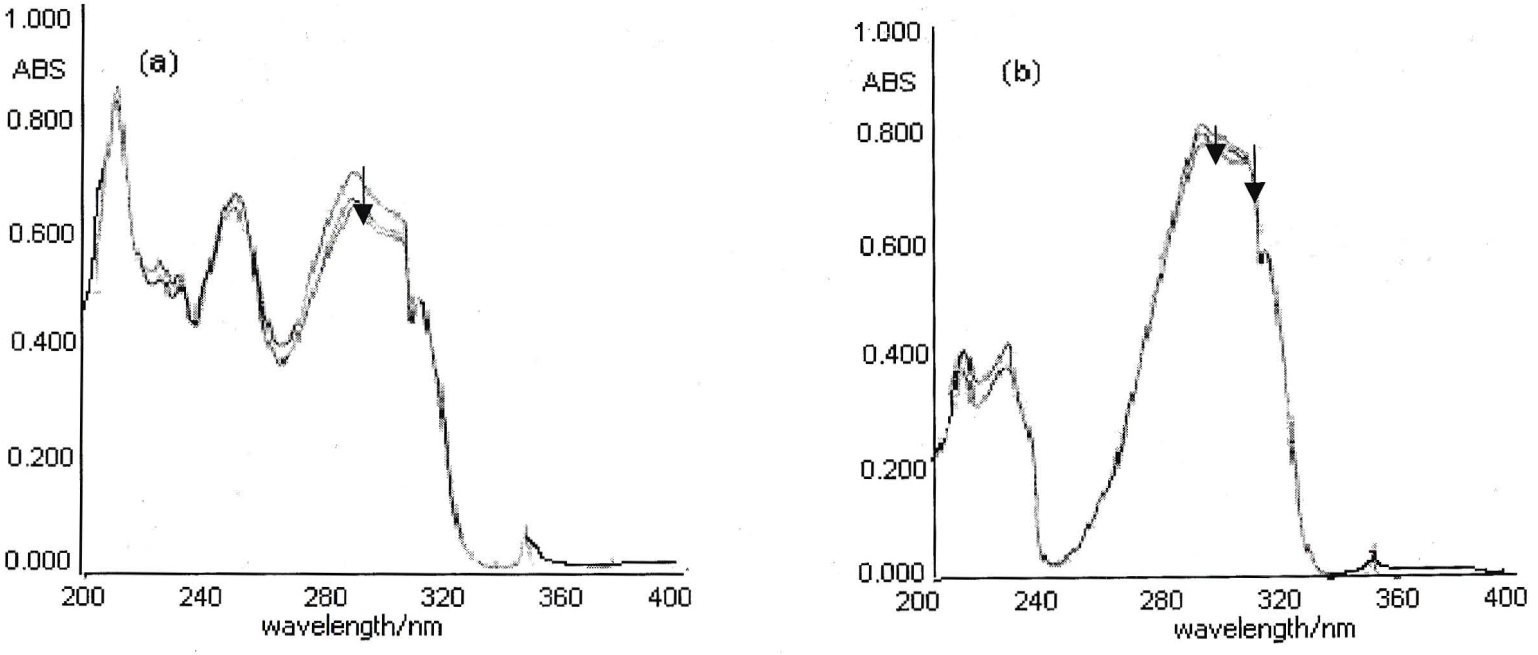

Figure 3.50: UV-spectra showing the effect of benzophenone on EHMC in cyclohexane using the 254 nm filter: (a) 2.6 x 10^{-5} M EHMC in the presence of benzophenone upon one minute irradiation and (b) 2.5 x 10^{-5} M EHMC upon one minute irradiation in the absence of benzophenone.

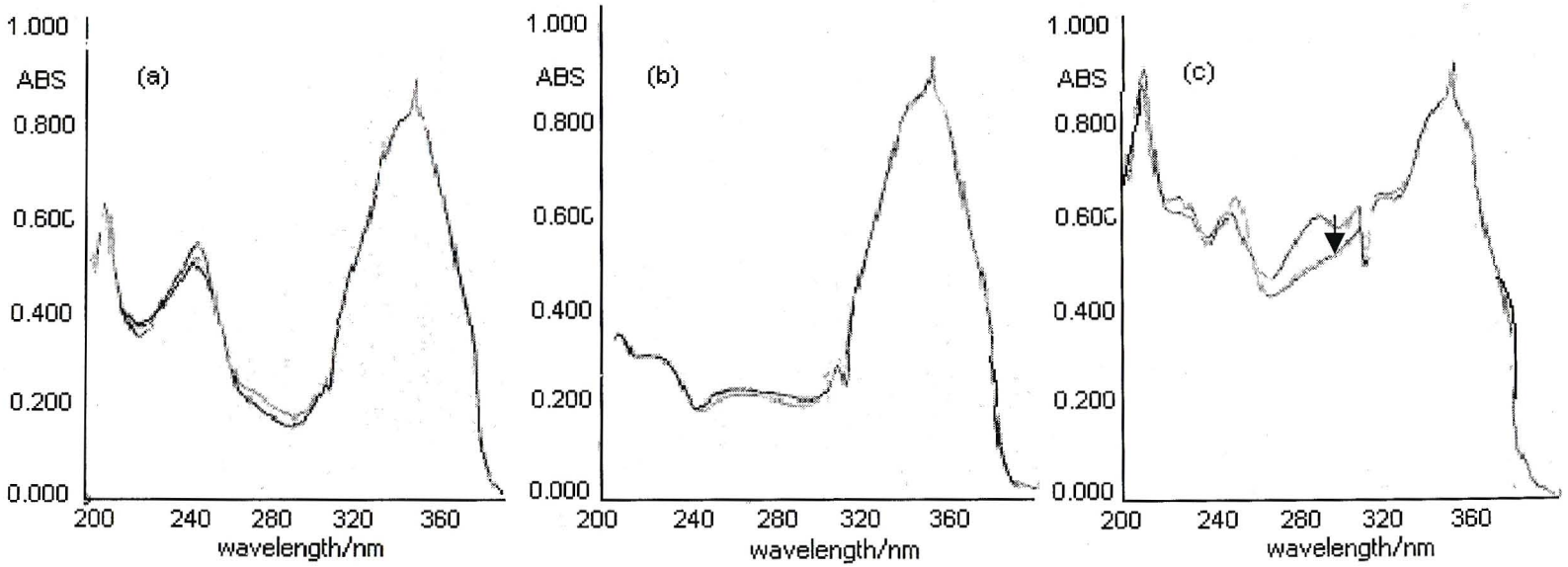

Figure 3.51: UV-spectra showing the effect of benzophenone on the sunscreen agents dissolved in cyclohexane upon 30 minute irradiation intervals with a 254 nm filter: (a) 3.0 x 10^{-5} M AVO in the presence of benzophenone, (b) 3.0 x 10^{-5} M AVO in the absence of benzophenone and (c) a mixture of 1.8 x 10^{-5} M AVO, 1.7 x 10^{-5} M EHMC and benzophenone.

Since the triplet-state energy of EHMC is much lower than that of AVO it is possible that AVO could act as a photosensitiser towards EHMC. From the UV-spectra (see Figure 3.24c) of the mixture of the two in cyclohexane irradiated with the 365 nm filter, i.e. at a wavelength were EHMC does not absorb UV-light, this possibility existed. We therefore irradiated samples of EHMC with and without AVO in cyclohexane using the 365 nm filter and used GC-MS to check for the formation of *cis*-EHMC. These results are shown in Section 3.4.4.

3.4 Photoproduct Analysis

From UV spectral analysis it was evident that EHMC undergoes photodegradation in methanol and cyclohexane while AVO photodegrades only in cyclohexane. HPLC was used to analyse the photoproducts of the sunscreen agents dissolved in methanol while GC was used in the analysis of the photoproducts when the sunscreen agents were dissolved in cyclohexane.

3.4.1 High performance liquid chromatographic analysis of methanolic solutions

High performance liquid chromatography was used for the separation of the sunscreen agents in methanol, identification of photoproducts formed and development of a method to quantify the amount of sunscreen agents remaining in solution upon irradiation. We also used the methods developed to check the applicability in commercial sunscreen formulations.

The separation of AVO and EHMC was carried out using an isocratic system of 85% (v/v) MeOH/H_2O at a flow rate of 1.0 ml/min. This isocratic system also separated the isomers of EHMC.

Initially a Spherisorb 5 ODS semi-preparative column with a 90:10% (v/v) MeOH/H_2O mobile phase as reported by Kowlaser [23] was used. With this column EHMC eluted at 26 minutes. To reduce the retention time a smaller column is required. Consequently an analytical Nucleosil 100 C_{18} reverse phase column was tried. A mobile phase of 90% (v/v) MeOH/H_2O did not completely resolve *trans*-EHMC from AVO. However, 85% (v/v) MeOH/H_2O did achieve complete resolution of the two filters and *cis*-EHMC. The formation of *cis*-EHMC was confirmed by referring to similar work done by Kowlaser [23] who showed that *trans*-EHMC (λ_{max} = 308 nm) isomerised to its *cis*-isomer which had a wavelength of maximum absorbance at 305 nm measured using the PDA detector.

The *cis*-isomer was formed by placing a solution of *trans*-EHMC into a 1 cm pathlength quartz cuvette. This solution was irradiated with the use of an Osram HBO

500 W/2 high pressure mercury lamp using the 10 mm thick Pyrex filter. A volume of 80 μl of the irradiated sample was then injected into the HPLC using the conditions described above. The *cis*-isomer eluted slightly earlier than the *trans*-isomer. This can be seen in Figures 3.52 and 3.53.

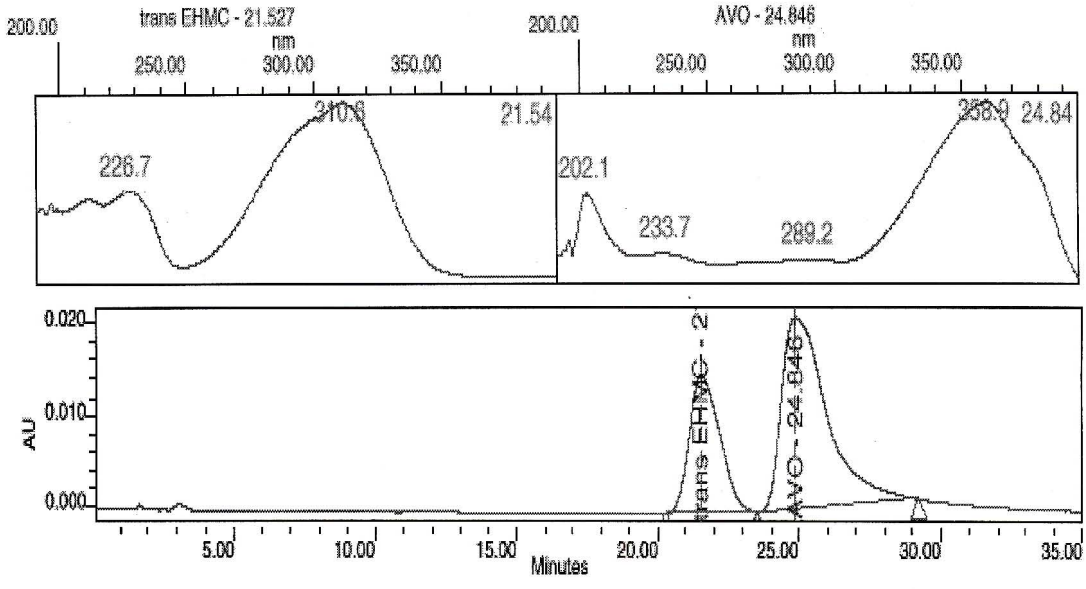

Figure 3.52: Chromatogram showing the separation of 80 μl of sample containing *trans*-EHMC and AVO, prior to irradiation, on a Nucleosil 100 C_{18} column using 85% (v/v) MeOH/H_2O as the mobile phase at a flow rate of 1 ml/min. The detection wavelength was set at 335 nm.

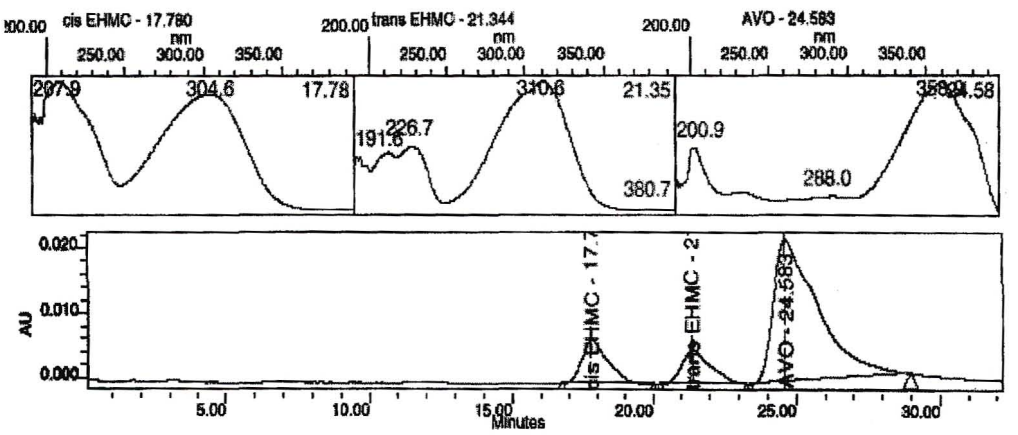

Figure 3.53: Chromatogram showing the separation of 80 µl of sample containing *trans*-EHMC and AVO and the formation of *cis*-EHMC upon irradiation, on a Nucleosil 100 C_{18} column using 85% (v/v) MeOH/H_2O as the mobile phase at a flow rate of 1 ml/min. The detection wavelength was set at 335 nm.

We needed to know the extent of the isomerisation of EHMC, upon irradiating EHMC alone and a mixture of EHMC and AVO. Calibration curves for the quantitation of *trans*-EHMC and AVO were produced (see Figures 2.21 and 2.20). From these calibration curves the concentration of *trans*-EHMC and the concentration of AVO could be determined in an unknown mixture.

The concentration of *cis*-EHMC was calculated from the difference between the initial concentration of *trans*-EHMC and the concentration of *trans*-EHMC remaining after irradiation since *cis*-EHMC is the only photoproduct of *trans*-EHMC.

The effect of increasing irradiation time on isomerisation of EHMC both in the mixture of AVO and EHMC, and in solutions of EHMC alone, was monitored. Samples were analysed at 1 minute intervals up to 5 minutes and thereafter at 15 minute intervals up to 1 hour. The results obtained are shown in Tables 3.26 and 3.27. The graphs of concentration of the isomers of EHMC remaining upon

irradiation in the individual solution and the mixture *versus* irradiation time are shown in Figures 3.54 and 3.55 respectively.

Table 3.26: Concentration of *trans*-EHMC remaining in a methanol solution after irradiation at various time intervals with an Osram HBO 500 W/2 high pressure mercury lamp in combination with a 10 mm thick Pyrex filter. The concentration of *cis*-EHMC was determined by difference from the concentration of *trans*-EHMC before and after irradiation.

Irradiation Time/minutes	***trans*-EHMC peak area/10^6**	**[*trans*-EHMC]/ 10^{-5} M**	**[*cis*-EHMC]/ 10^{-5} M**
0	15.08	44.0	0
5	5.531	1.55	42.45
15	5.356	1.53	42.47
120	5.288	1.53	42.47

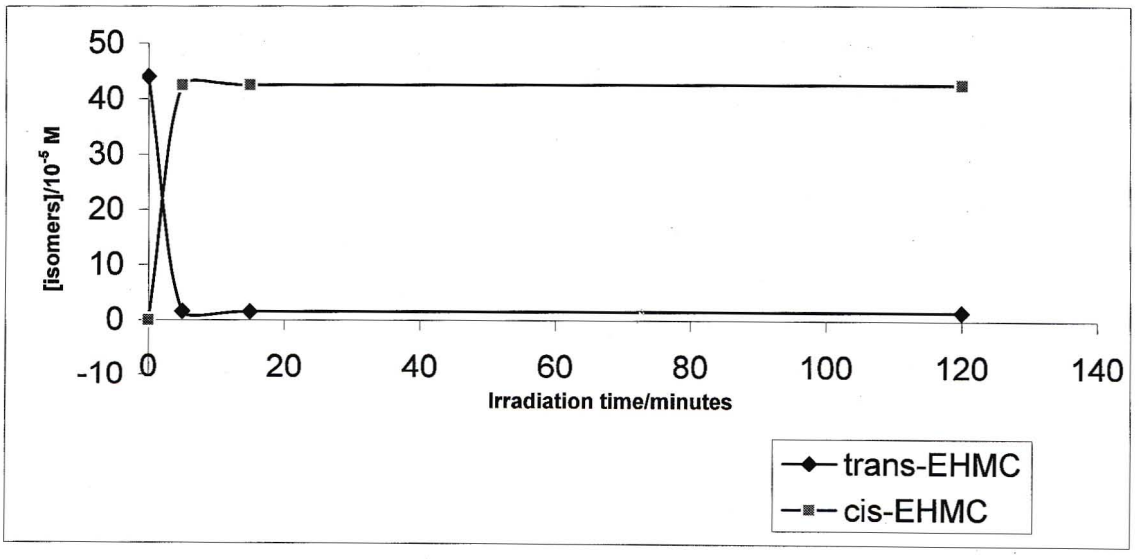

Figure 3.54: Concentration of *trans*-EHMC in methanol determined by HPLC analysis, using a Nucleosil 100 C_{18} column, 85% (v/v) MeOH/H_2O as mobile phase at a flow rate of 1 ml/min. Detection was at 335 nm. The concentration of *cis*-EHMC was determined by the difference in the concentration of *trans*-EHMC before and after irradiation.

Table 3.27: Concentration of *trans*-EHMC remaining after irradiation of a mixture of EHMC and AVO dissolved in methanol at various time intervals with an Osram HBO 500 W/2 high pressure mercury lamp in conjunction with a 10 mm thick Pyrex filter. The concentration of *cis*-EHMC was determined by difference between the concentration of *trans*-EHMC before and after irradiation. The concentration of AVO remained constant at 2.7 x 10^{-5} M at all irradiation times.

Irradiation Time/ minutes	***trans*-EHMC peak area/ 10^5**	**AVO peak area/ 10^5**	**[*trans*-EHMC]/ 10^{-5} M**	**[*cis*-EHMC]/ 10^{-5} M**
0	11.30	20.08	2.5	0
1	7.864	22.81	1.5	1.0
2	4.450	22.35	0.5	2.0
3	4.304	21.37	0.45	2.05
4	3.965	21.48	0.4	2.10
6	3.798	20.48	0.38	2.12
15	3.983	21.39	0.4	2.10
30	3.767	20.64	0.38	2.12
60	3.763	20.66	0.38	2.12

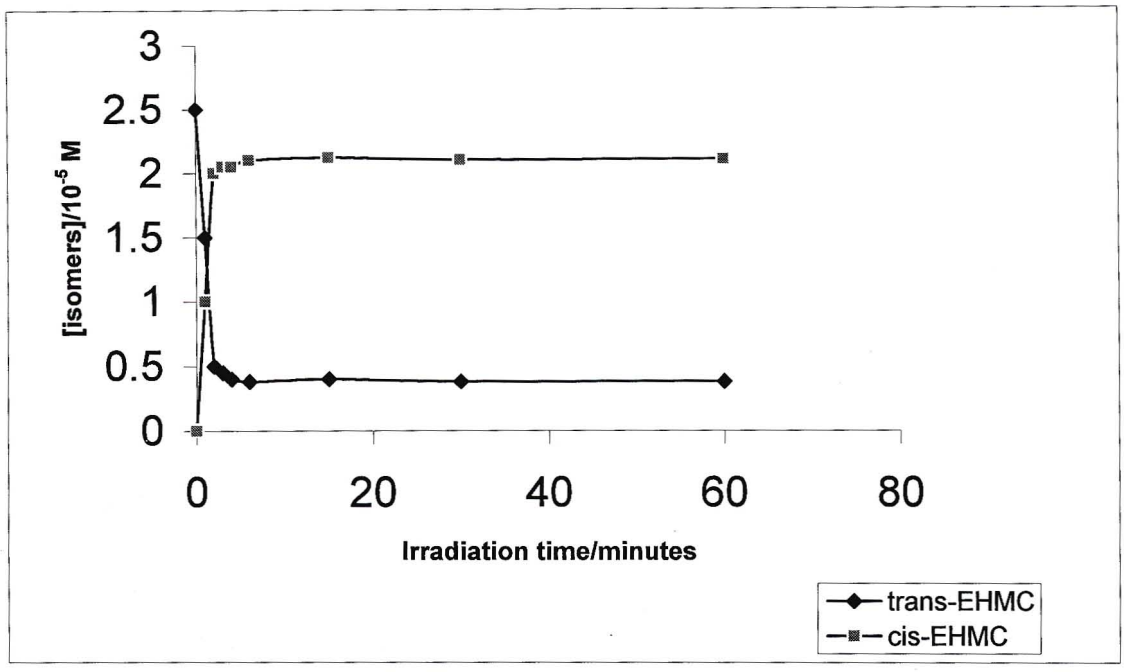

Figure 3.55: The loss of *trans*-EHMC in the presence of AVO and the formation of *cis*-EHMC. The sunscreen agents were determined by HPLC analysis, using a Nucleosil 100 C_{18} column and 85% (v/v) MeOH/H_2O mobile phase at a flow rate of 1 ml/min. Detection was at 335 nm.

3.4.2 Gas chromatographic analysis of cyclohexane solutions

On trying to analyse the photoproducts of irradiated samples of EHMC and AVO in cyclohexane by HPLC, we had difficulties separating the two sunscreen agents and their photoproducts since the non-polar solvent prevented separation. Cyclohexane has a boiling point of 80°C. It was therefore thought that gas chromatography would be a better technique to separate the isomers.

The GC-FID system described in Section 2.7.2.1 was used for the analysis of unirradiated and irradiated solutions of EHMC, AVO and a mixture of the two in cyclohexane.

In order to quantify the photoproducts and the sunscreen agents remaining we used dibutyl phthalate (DBP) as an internal standard. This internal standard eluted before EHMC, AVO and the photoproducts.

Samples of EHMC in cyclohexane were irradiated at 30 minute intervals. From the chromatogram (see Figure 3.56) it can be seen that DBP elutes at 2.5 minutes, *cis*-EHMC at 3.8 minutes and *trans*-EHMC at 4.9 minutes. DBP was used as an internal standard to determine the amount of *cis*- and *trans*-EHMC (refer to Table 3.28). From UV-spectral data of EHMC in cyclohexane we noticed inconsistency in the absorbance values upon irradiation. This inconsistency is also evident here (refer to Figure 3.57) but also confirms that *trans*-EHMC predominates when irradiated in cyclohexane solutions while *cis*-EHMC predominates when irradiated in methanolic solutions.

From UV-spectral analysis we observed that upon irradiating AVO in cyclohexane the absorbance at 350 nm decreased. We therefore investigated the reason for this depletion. GC analysis of an unirradiated and a 3-hour irradiated sample showed that AVO eluted at 8.3 minutes and the concentration of AVO dropped from 1.84×10^{-2} M to 0.87×10^{-2} M. The chromatograms can be seen in Figure 3.58. The reason for this depletion of AVO is the formation of several photoproducts as evidenced by the appearance of a number of new peaks

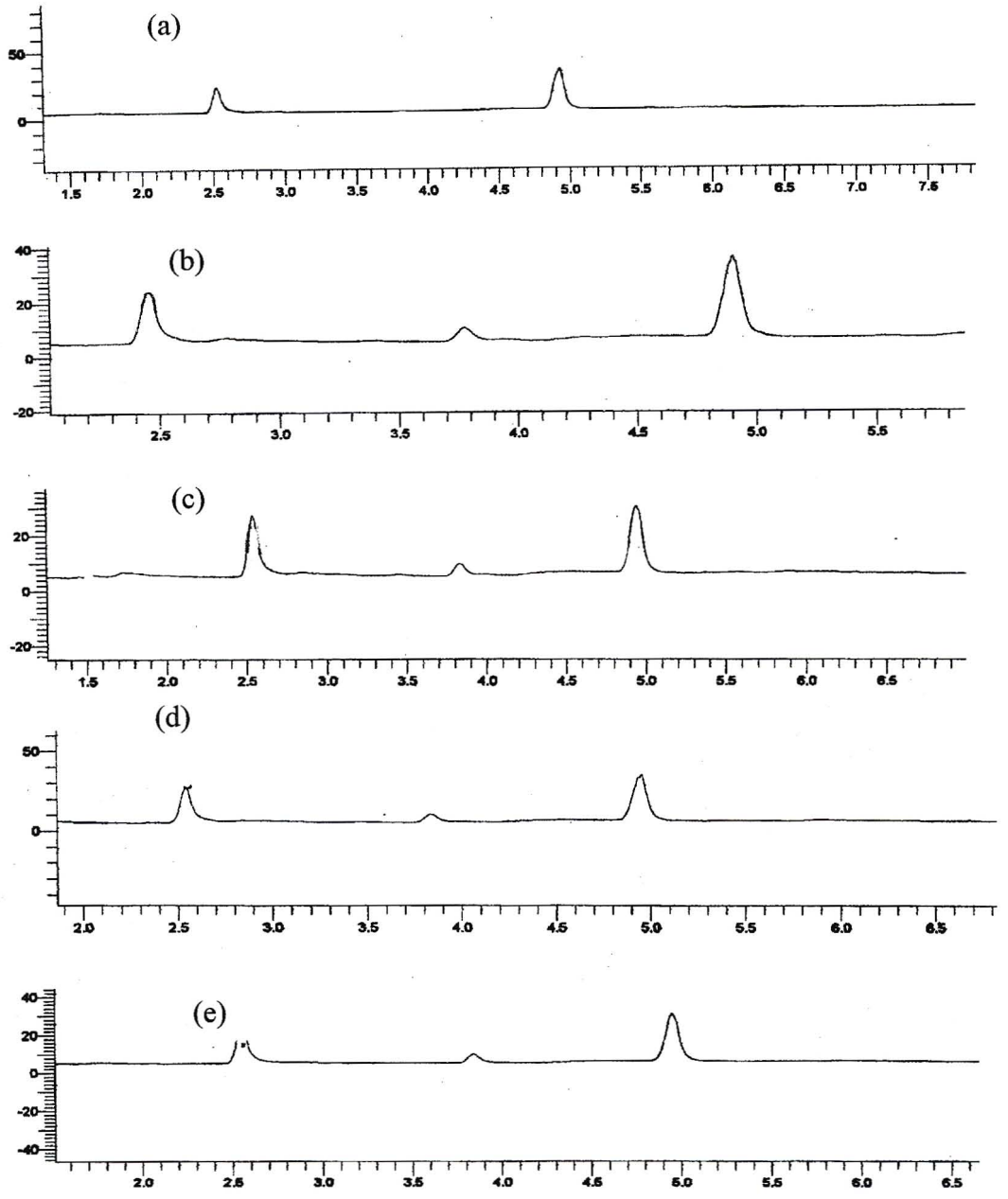

Figure 3.56: GC chromatograms of *trans*-EHMC photoisomerising to its *cis*-isomer obtained by injecting 5 µl samples on a Supelco 25 m x 250 µm PET-S fused silica capillary column. (a) *trans*-EHMC unirradiated, (b) after 30 minute irradiation, (c) after 60 minute irradiation, (d) after 90 minute irradiation and (e) after 120 minutes of irradiation. The conditions used are described in Section 2.7.2.2. N.B.: the y-axis scale for each chromatogram is different.

Table 3.28: Concentrations of *cis*-EHMC and *trans*-EHMC that were determined by using DBP as internal standard upon GC-FID analysis. The chromatograms of the irradiated samples are shown in Figure 3.56.

Irradiation Time / minutes	[*trans*-EHMC]/10^{-2} M	[*cis*-EHMC]/10^{-2} M
0	2.78	0
30	1.57	1.21
60	1.76	1.02
90	1.76	1.02
120	1.99	0.79

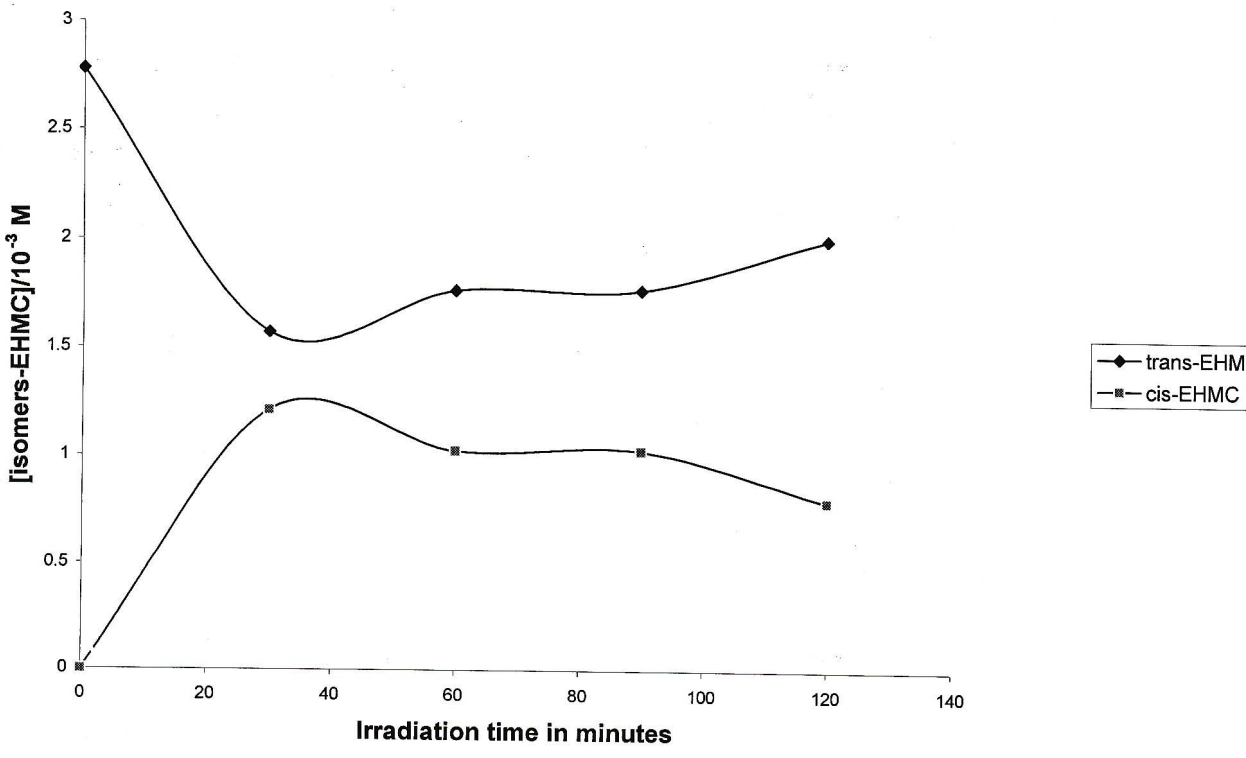

Figure 3.57: Graph showing the isomerisation of *trans*-EHMC to its *cis*-isomer. This shows that *trans*-EHMC predominates when irradiated in cyclohexane solutions.

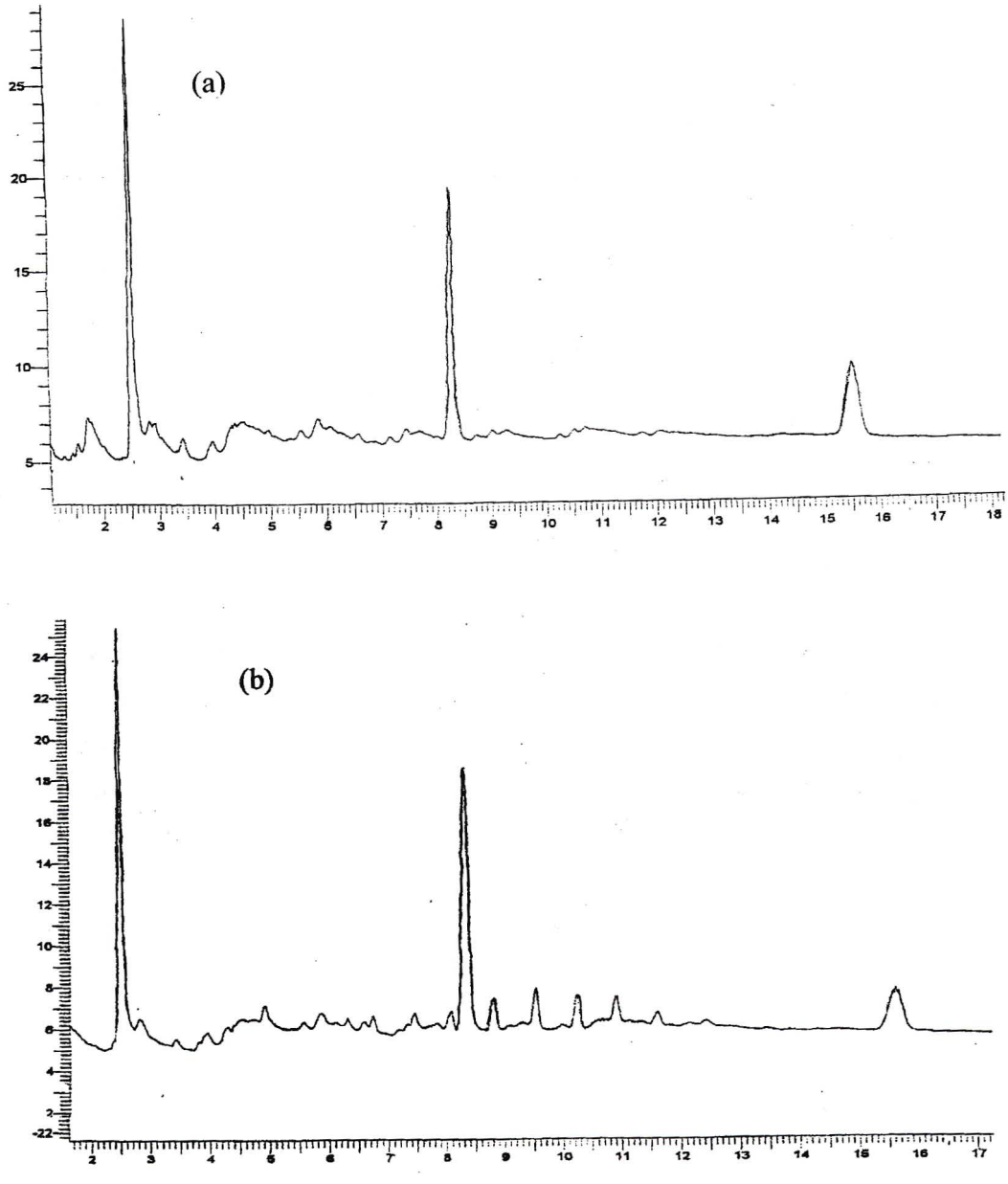

Figure 3.58: Chromatograms showing the photodegradation of AVO upon GC-FID analysis of a 5 µl sample of AVO in cyclohexane on a Supelco 25 m x 250 µm PET-S fused silica capillary column. AVO elutes at 8.3 minutes, DBP at 2.5 minutes and the peak at 15.5 minutes is an impurity from one of the solvents. The conditions used are described in Section 2.7.2.2. (a) AVO unirradiated and (b) AVO after 3 hours of irradiation. N.B.: the y-axis scale for each chromatogram is different.

in the chromatogram of the irradiated sample. It is therefore necessary to analyse the irradiated sample via GC-MS to determine the identity of the photoproducts. Consequently a GC-MS analysis of an 8-hour irradiated sample of AVO dissolved in cyclohexane was carried out. This longer irradiation period was used in order to obtain larger concentrations of photoproducts to make identification easier.

A 1 x 10^{-3} M solution of AVO in cyclohexane was irradiated in a 1 mm pathlength quartz cuvette for 8 hours and subjected to GC-MS analysis (see Section 2.7.2.3 for details). The total ion chromatogram of the 8-hour irradiated sample of AVO is shown in Figure 3.59. Electron impact (EI) mass spectra were obtained for each peak in the chromatogram. The peaks at 12.05, 13.97 and 14.60 are solvent impurities. The peak at 12.30 is caused by bleeding of the column stationary phase. In Figures 3.60 to 3.68 the EI mass spectra of all photoproducts formed are shown at the top of the Figure while the NIST library match is shown at the bottom.

The photoproducts identified from the UV degradation of AVO included tert-butylbenzene, *p*-methoxybenzoic acid and *p*-tertbutylbenzoic acid. The cyclohexyl ester of *p*-methoxybenzoic acid originates from the reaction of the solvent with radicals formed on decomposition of AVO [31]. Cyclohexane yielded cyclohexanol, cyclohexanone, bicyclohexyl and dicyclohexyl ether. The photoproducts identified correlated well with those identified by Schwack and Rudolf [16] and also Roscher *et al.* [31].

A mixture of AVO and EHMC in cyclohexane was placed into a 1 mm pathlength cuvette and irradiated up to 3 hours. This solution was then subjected to GC-FID analysis. The definite formation of *cis*-EHMC was observed but product formation from AVO was not observed (see Figure 3.69).

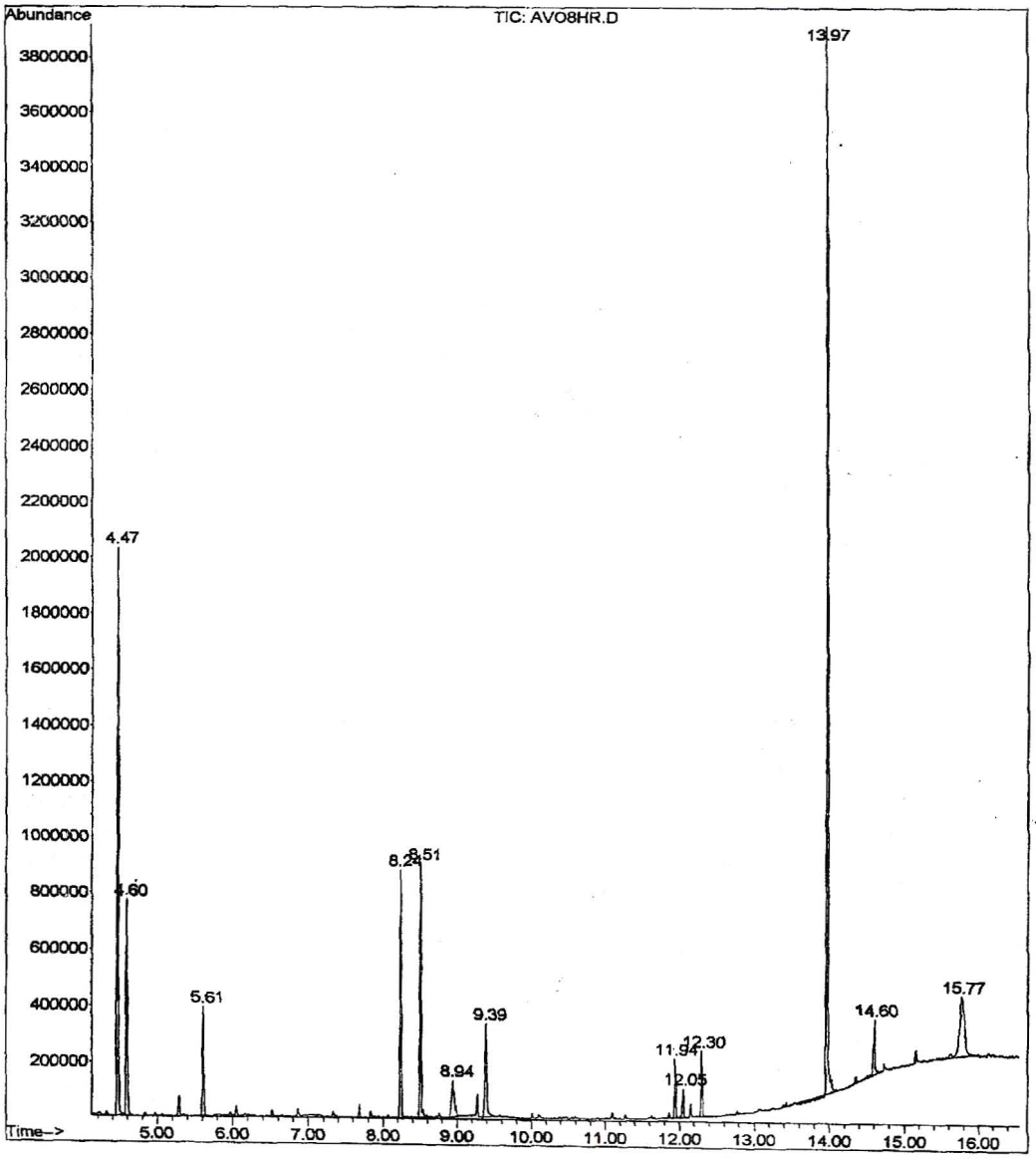

Figure 3.59: Total ion chromatogram of AVO upon 8 hours of irradiation. The column used was a HP-5 methyl silicon 25 m x 250 μm. The conditions used are described in Section 2.7.2.3.

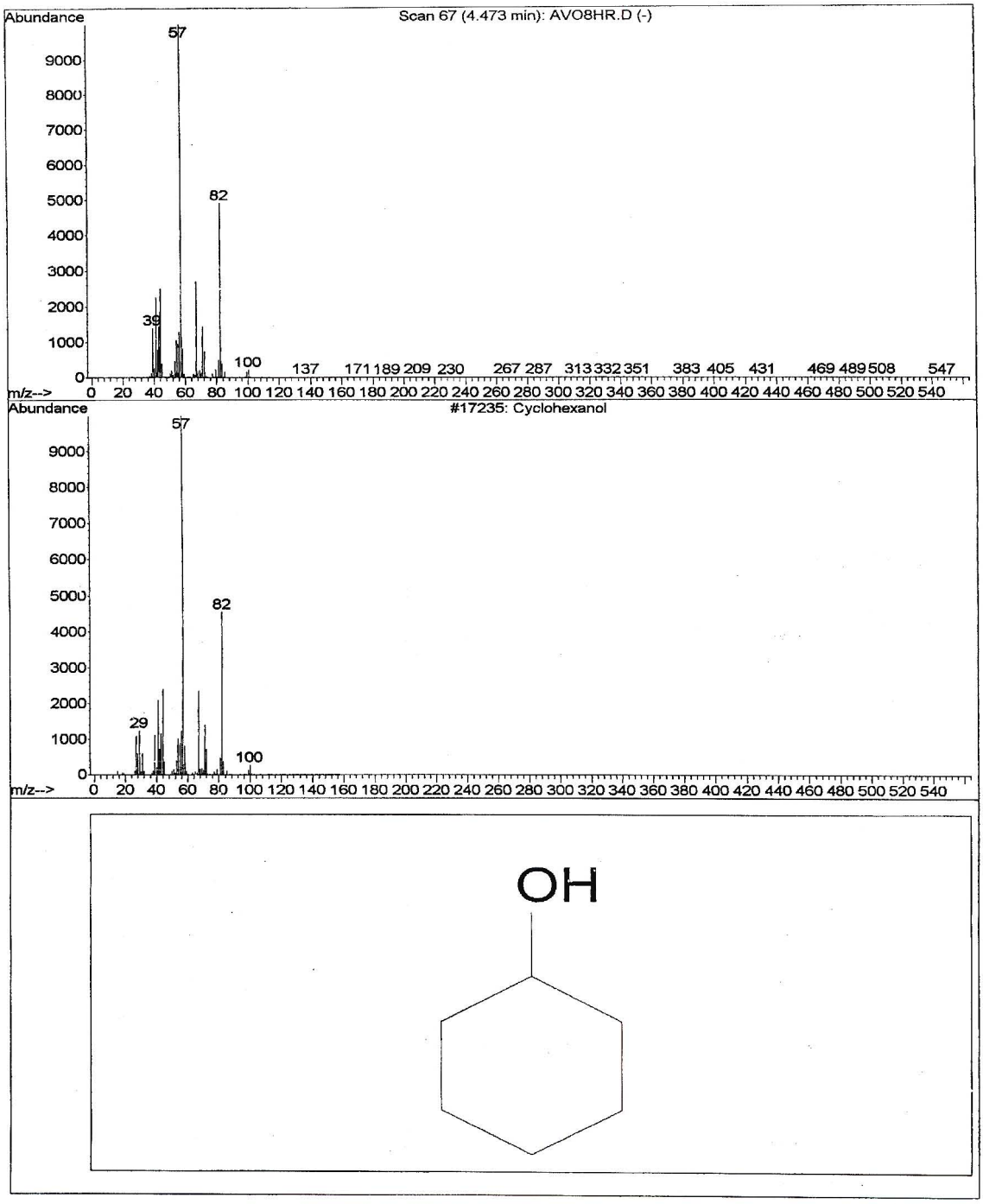

Figure 3.60: Above is the mass spectrum of cyclohexane which eluted at 4.47 minutes and below is the library match made.

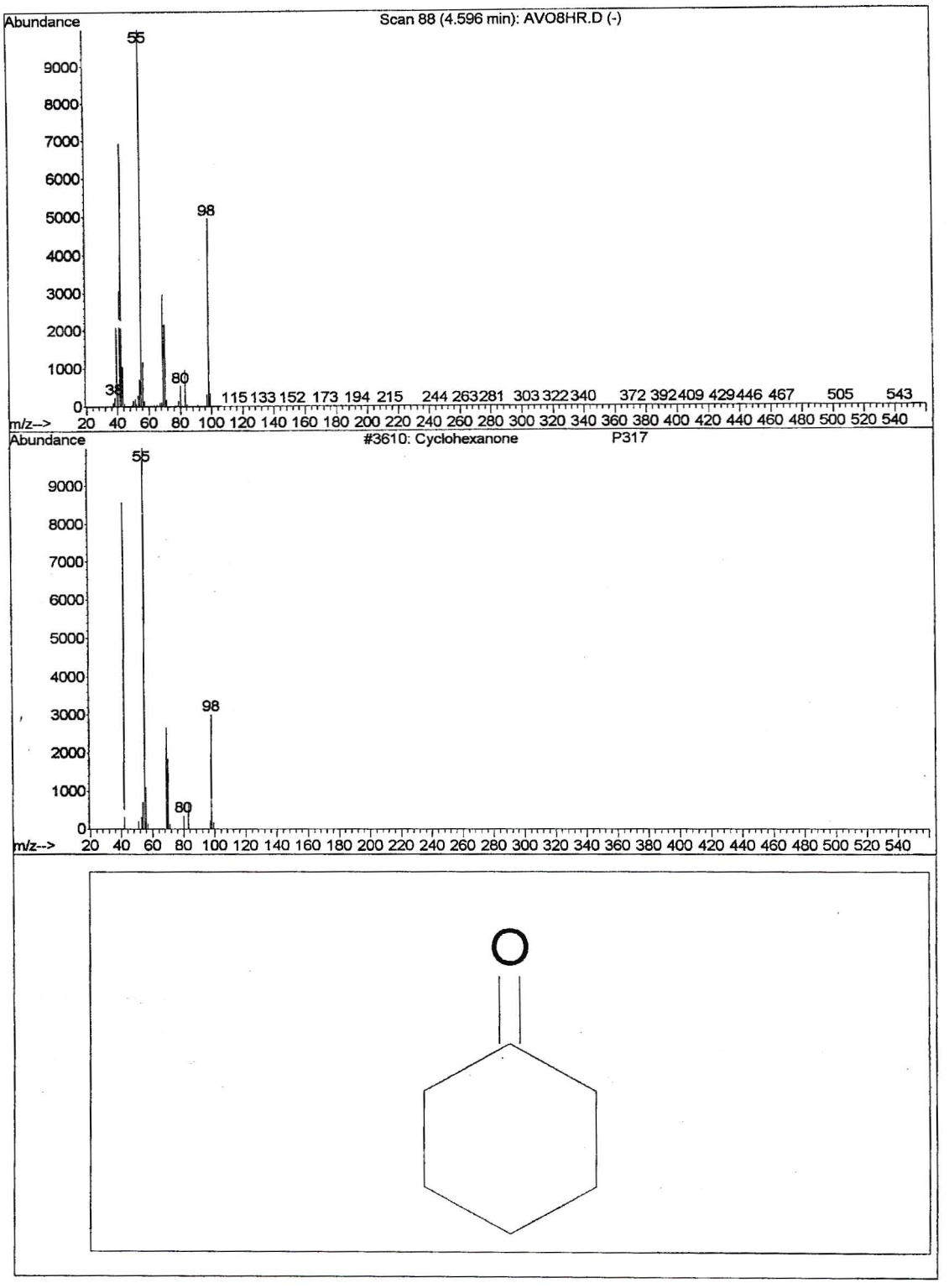

Figure 3.61: Above is the mass spectrum of cyclohexanone which eluted at 4.60 minutes and below is the match made by the library.

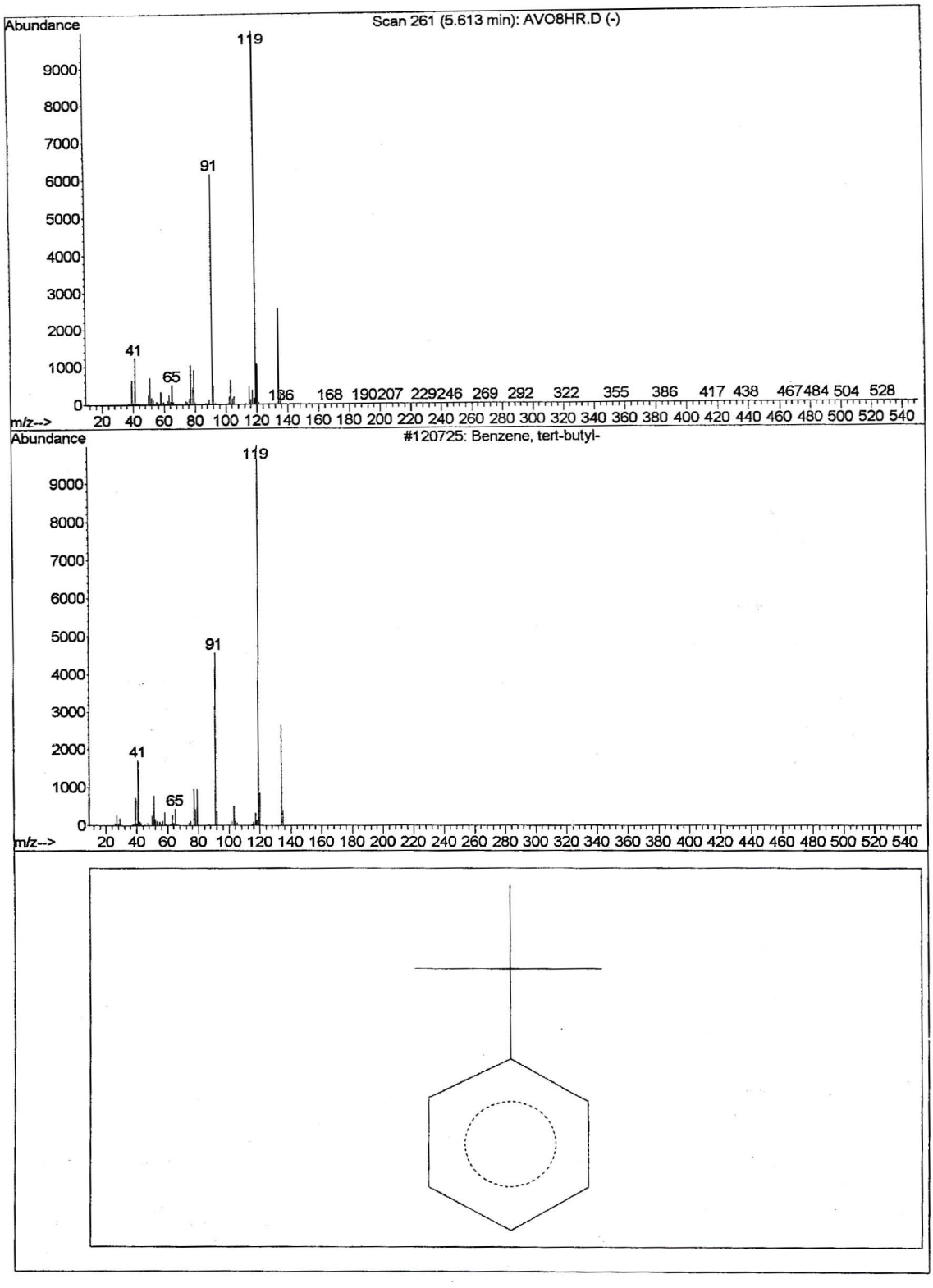

Figure 3.62: Above is the mass spectrum of *tert*-butylbenzene which eluted at 5.61 minutes and below is the match made by the library.

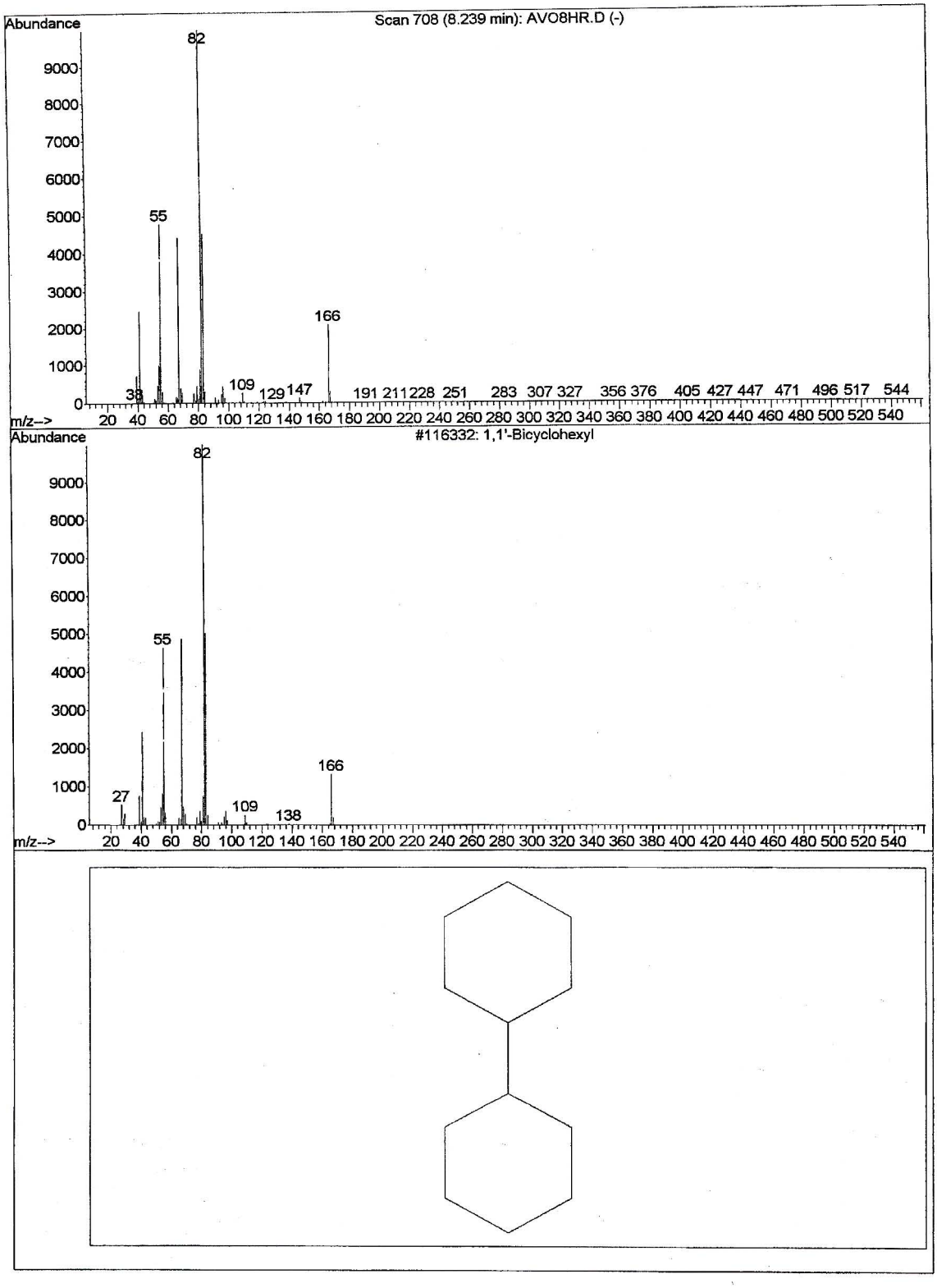

Figure 3.63: Above is the mass spectrum of bicyclohexyl which eluted at 8.24 minutes and below is the match made by the library.

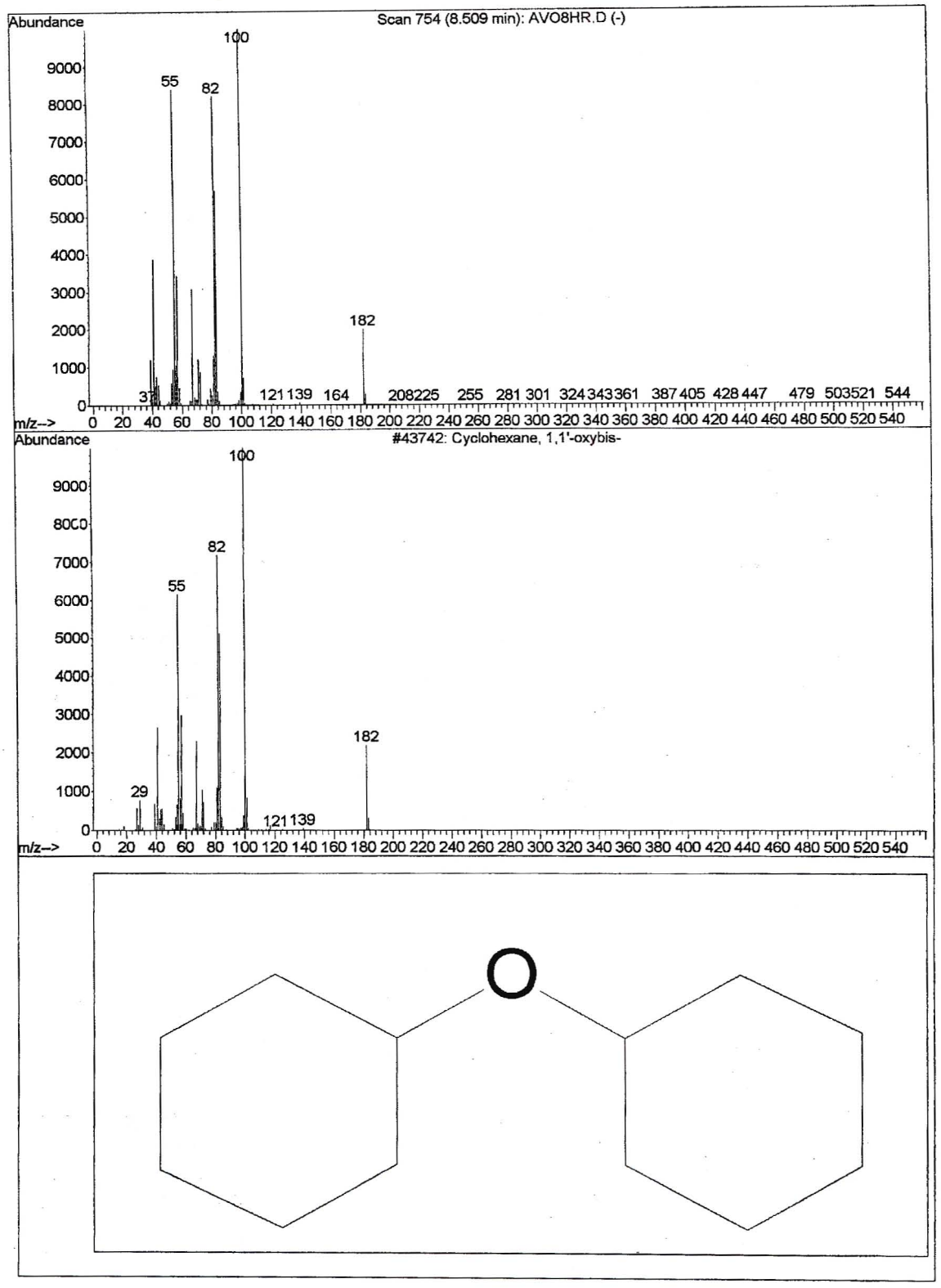

Figure 3.64: Above is the mass spectrum of dicyclohexyl ether which eluted at 8.51 minutes and below is the match made by the library.

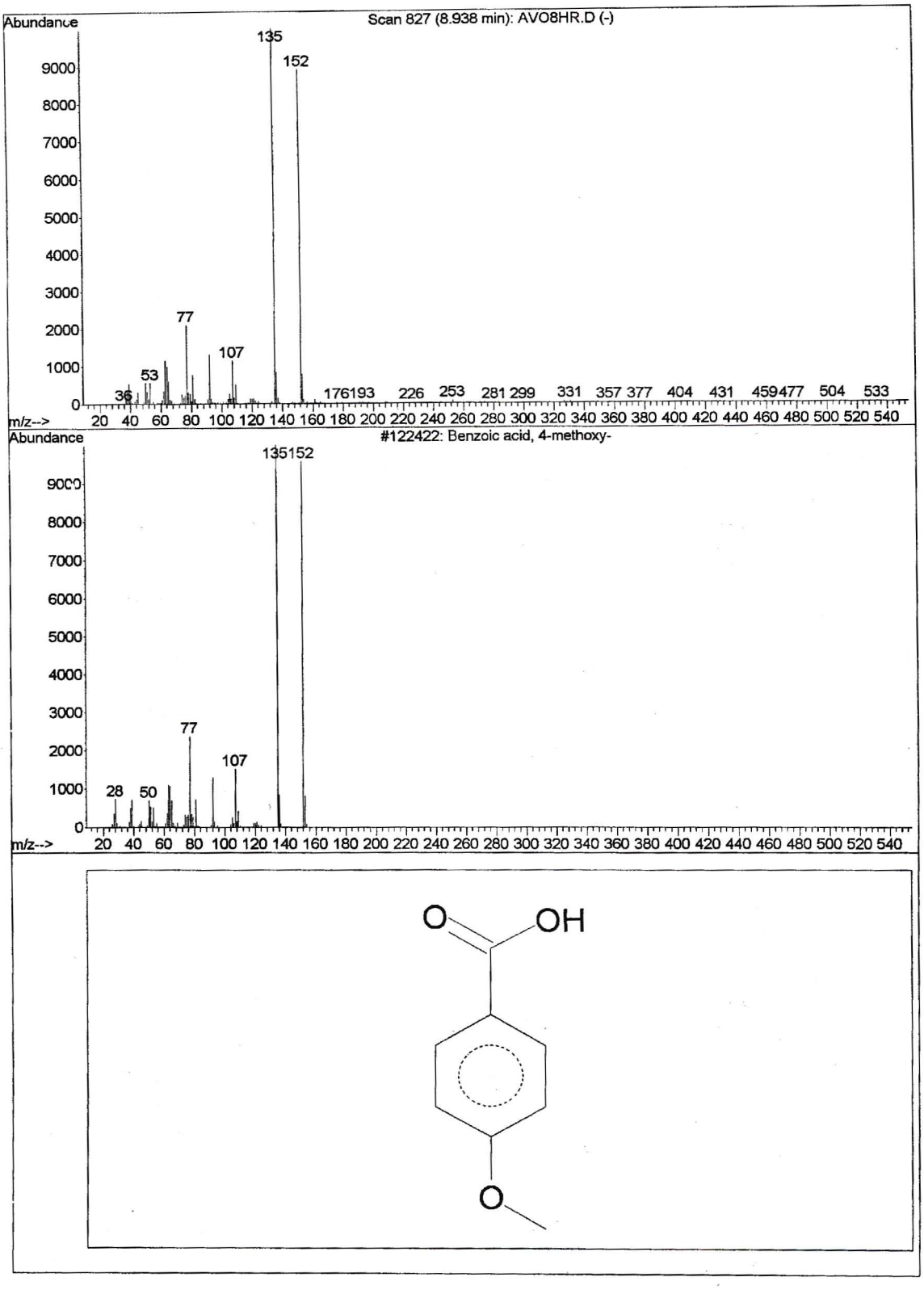

Figure 3.65: Above is the mass spectrum of *p*-methoxybenzoic acid which eluted at 8.94 minutes and below is the match made by the library.

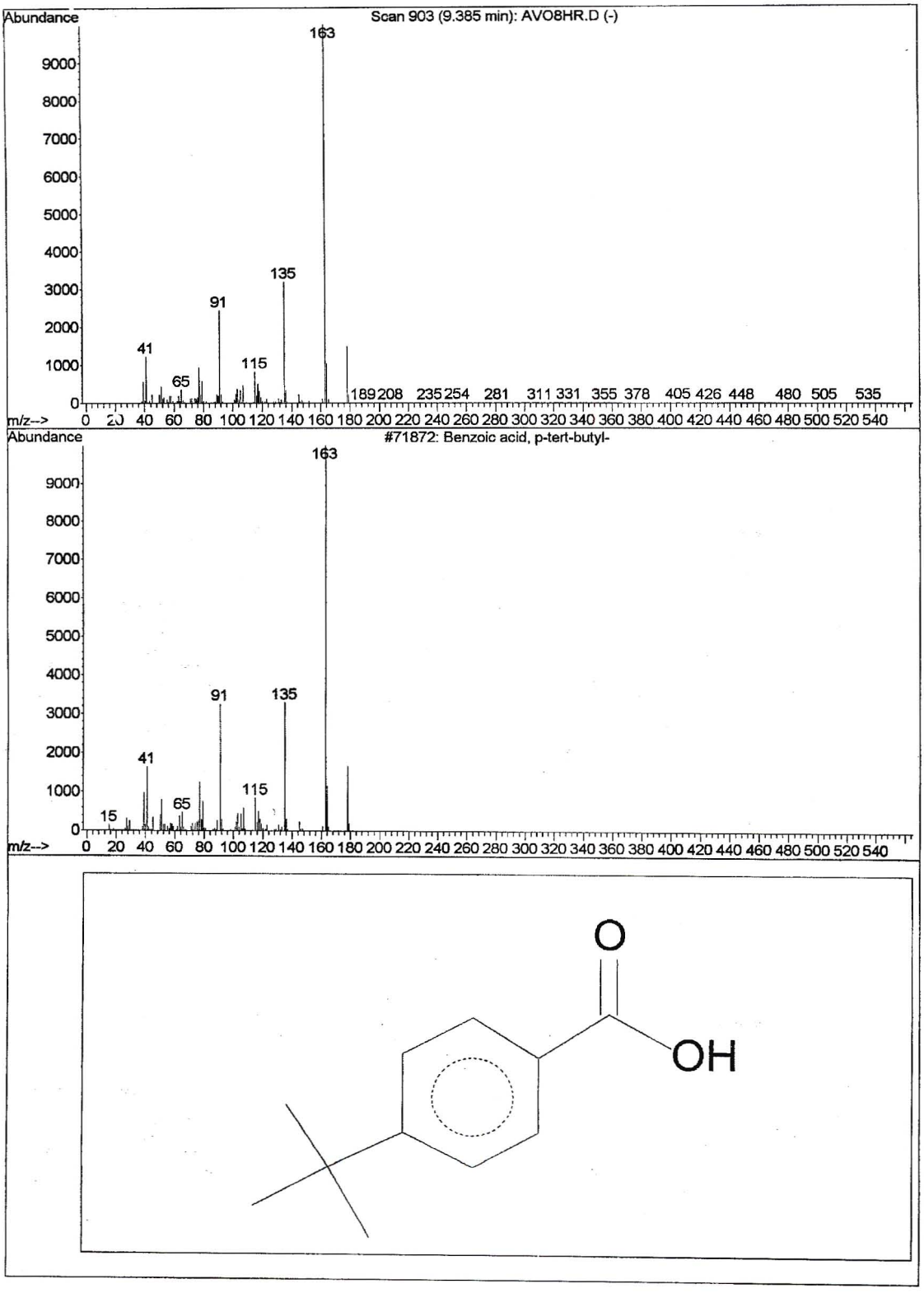

Figure 3.66: Above is the mass spectrum of *p-tert*-butylbenzoic acid which eluted at 9.39 minutes and below is the match made by the library.

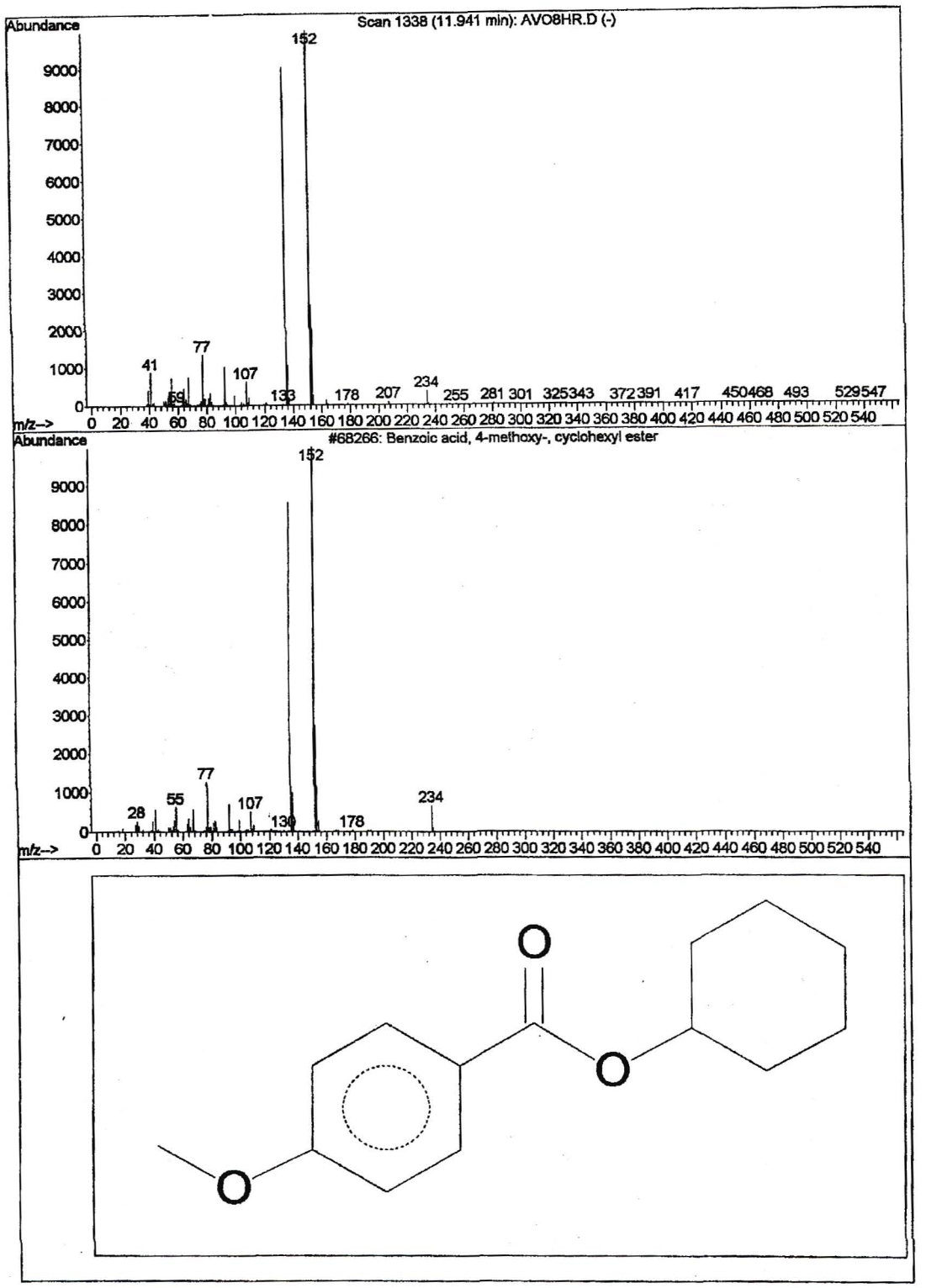

Figure 3.67: Above is the mass spectrum of the cyclohexyl ester of *p*-methoxybenzoic acid which eluted at 11.94 minutes and below is the match made by the library.

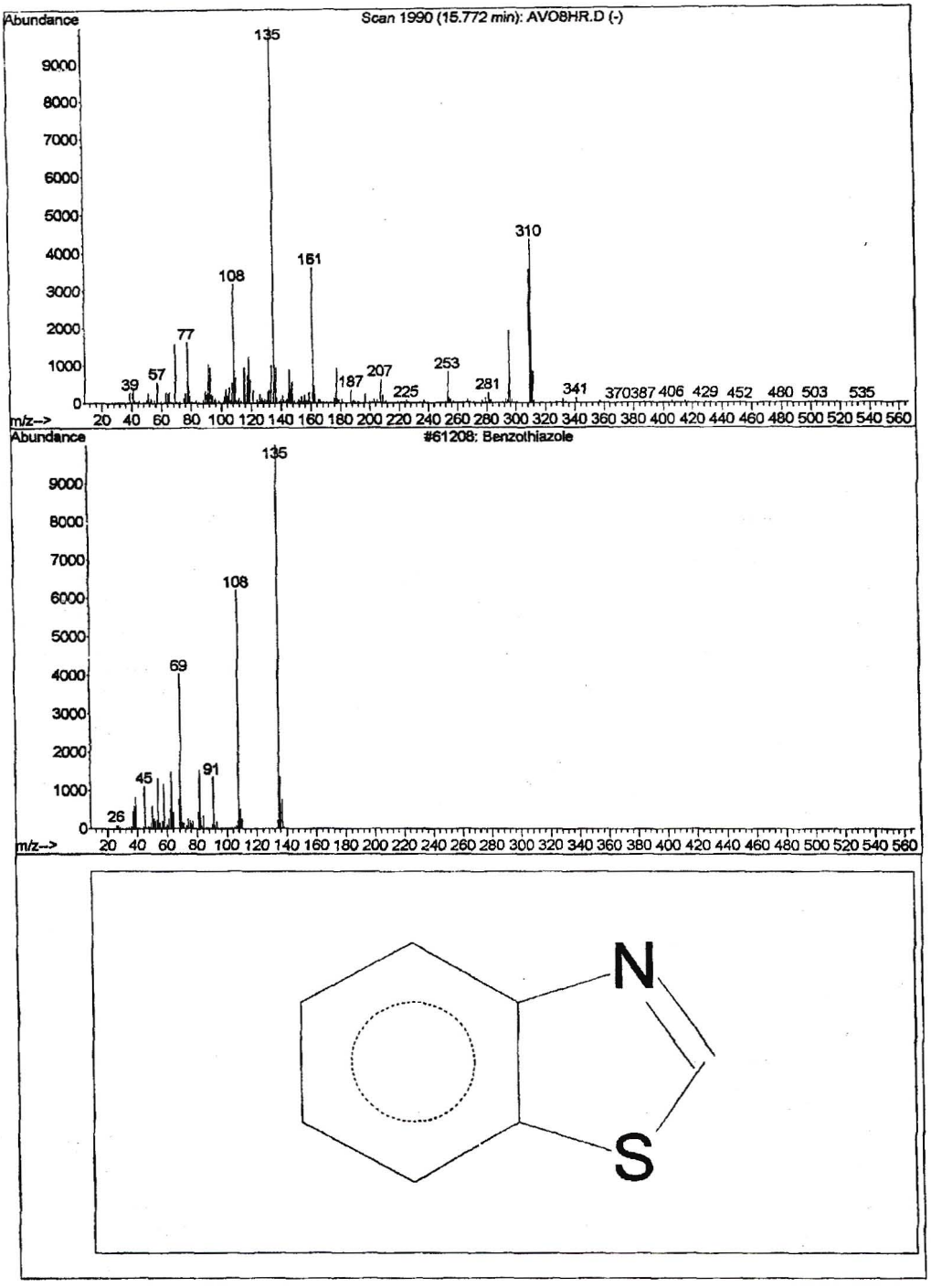

Figure 3.68: Above is the mass spectrum of AVO which eluted at 15.77 minutes which was confirmed from the retention time of standards and also the molecular mass of AVO. Below, is the incorrect match made by the library.

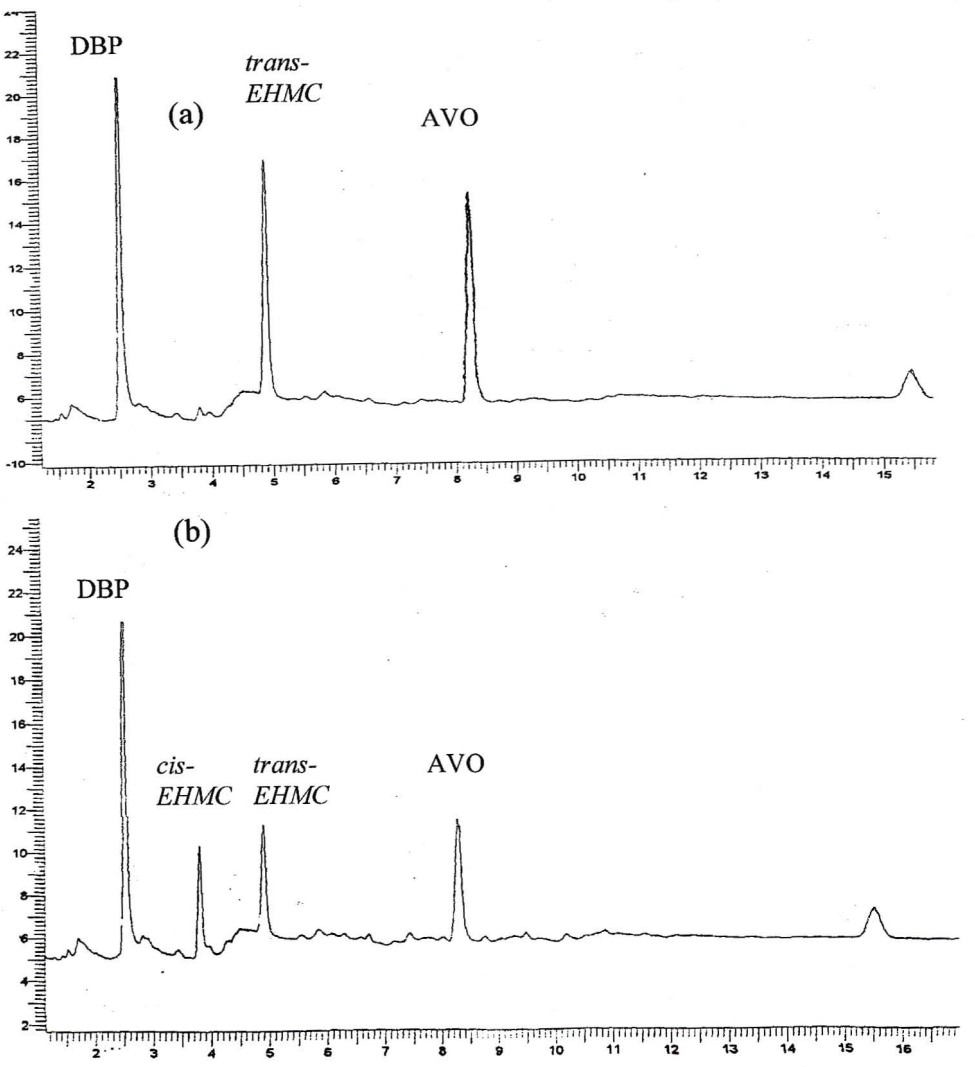

Figure 3.69: Chromatograms showing the effect of irradiating a mixture of EHMC and AVO in cyclohexane. DBP elutes at 2.5 minutes, *cis*-EHMC at 3.8 minutes, *trans*-EHMC at 4.9 minutes and AVO at 8.3 minutes. A Supelco 25 m x 250 μm PET-S fused silica capillary column was used. The conditions used are described in Section 2.7.2.2. (a) mixture unirradiated and (b) mixture upon 3 hours of irradiation. N.B.: the y-axis scale used in each chromatogram is different.

3.4.3 The use of GC-MS to show the formation of UVB-absorbing photoproducts

A mixture of EHMC and AVO dissolved in cyclohexane was irradiated for 8 hours and was then analysed using GC-MS. The instrument and the conditions used here (see Section 2.7.2.3) were different to those used for the analysis of AVO upon 8 hours of irradiation.

The total ion chromatogram (see Figure 3.70) shows the elution of several compounds. Most of the compounds were due to previous analyses of wax samples and also column breakdown due to the high temperature programme. The compounds of interest in this work are labelled according to their retention times: cyclohexanol (3.61 minutes), cyclohexanone (3.71 minutes), tert-butylbenzene (4.68 minutes), *p*-methoxybenzaldehyde (6.97 minutes), bicyclohexyl (7.43 minutes), bicyclohexyl ether (7.68 minutes), *p-tert*-butylbenzoic acid (8.18 minutes), *cis*-EHMC (12.62 minutes), *trans*-EHMC (13.41 minutes) and AVO (17.16 minutes). In Figures 3.71 to 3.80 the EI mass spectra of all photoproducts formed are shown at the top of the figure while the different library matches are shown at the bottom. The wavelength of maximum absorbance of the photoproducts are: cyclohexanone (280 nm in methanol), *tert*-butlybenzene (267 and 257 nm in cyclohexane), *p-tert*-butylbenzoic acid (237 nm in methanol) and *p*-methoxybenzaldehyde (273 nm). The formation of these products therefore explains the inconsistency in absorbance values observed in the region where EHMC absorbs when EHMC was irradiated in cyclohexane since some of these compounds absorb close to the wavelength of maximum absorbance of EHMC.

The formation of these photoproducts also explains the strong UVB absorption, experienced by Tarras-Wahlberg [21], when AVO photodegraded. The increase in absorbance in the UVB region therefore makes the calculation method developed to determine the concentrations of EHMC and AVO in a mixture dissolved in cyclohexane upon irradiation rather impractical.

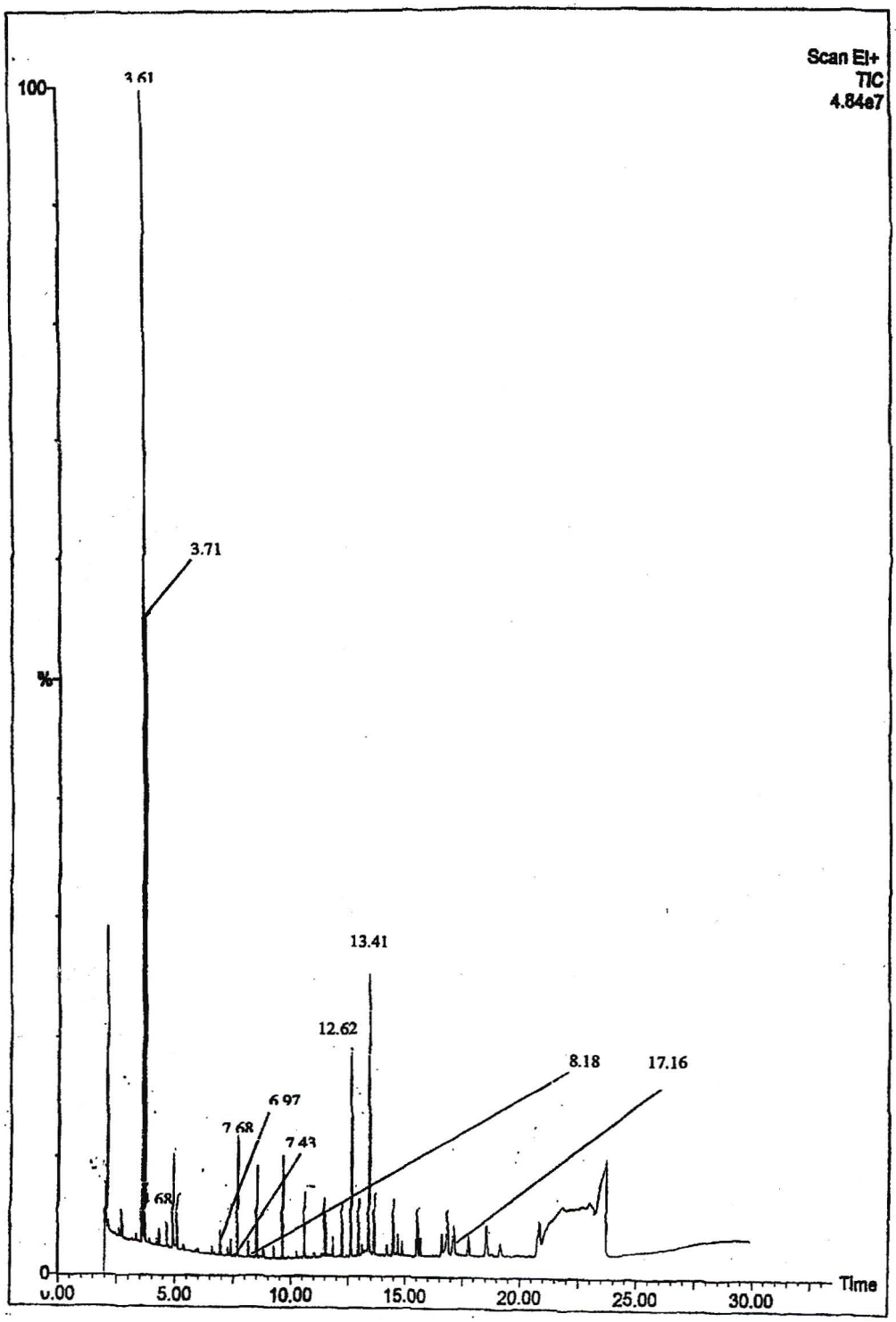

Figure 3.70: Total ion chromatogram of a mixture of EHMC and AVO upon 8 hours of irradiation. The column used was a BP-5 methyl silicon 30 m x 320 μm. The conditions used are described in Section 2.7.2.3.

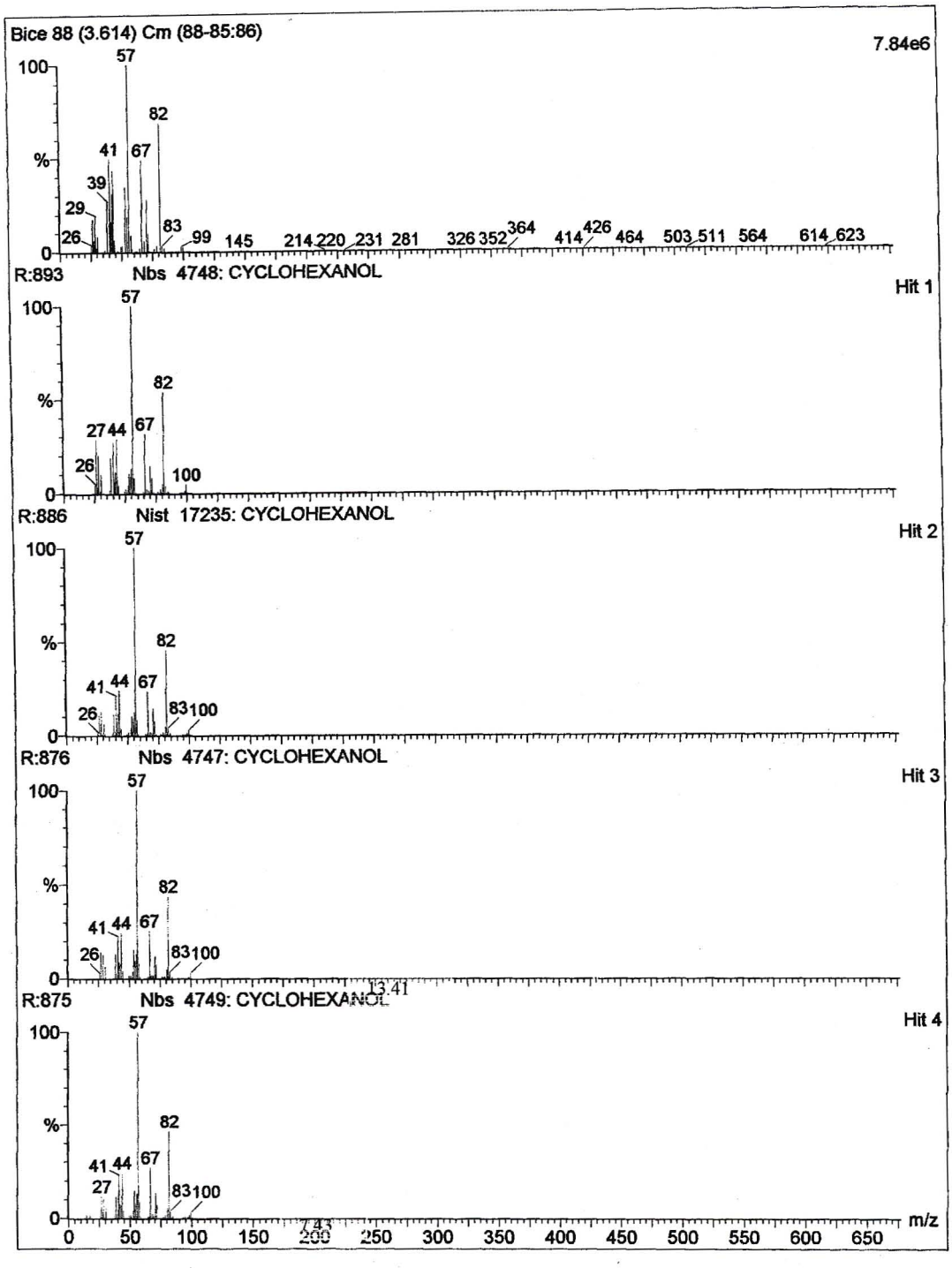

Figure 3.71: Mass spectrum of cyclohexanol which eluted at 3.61 minutes.

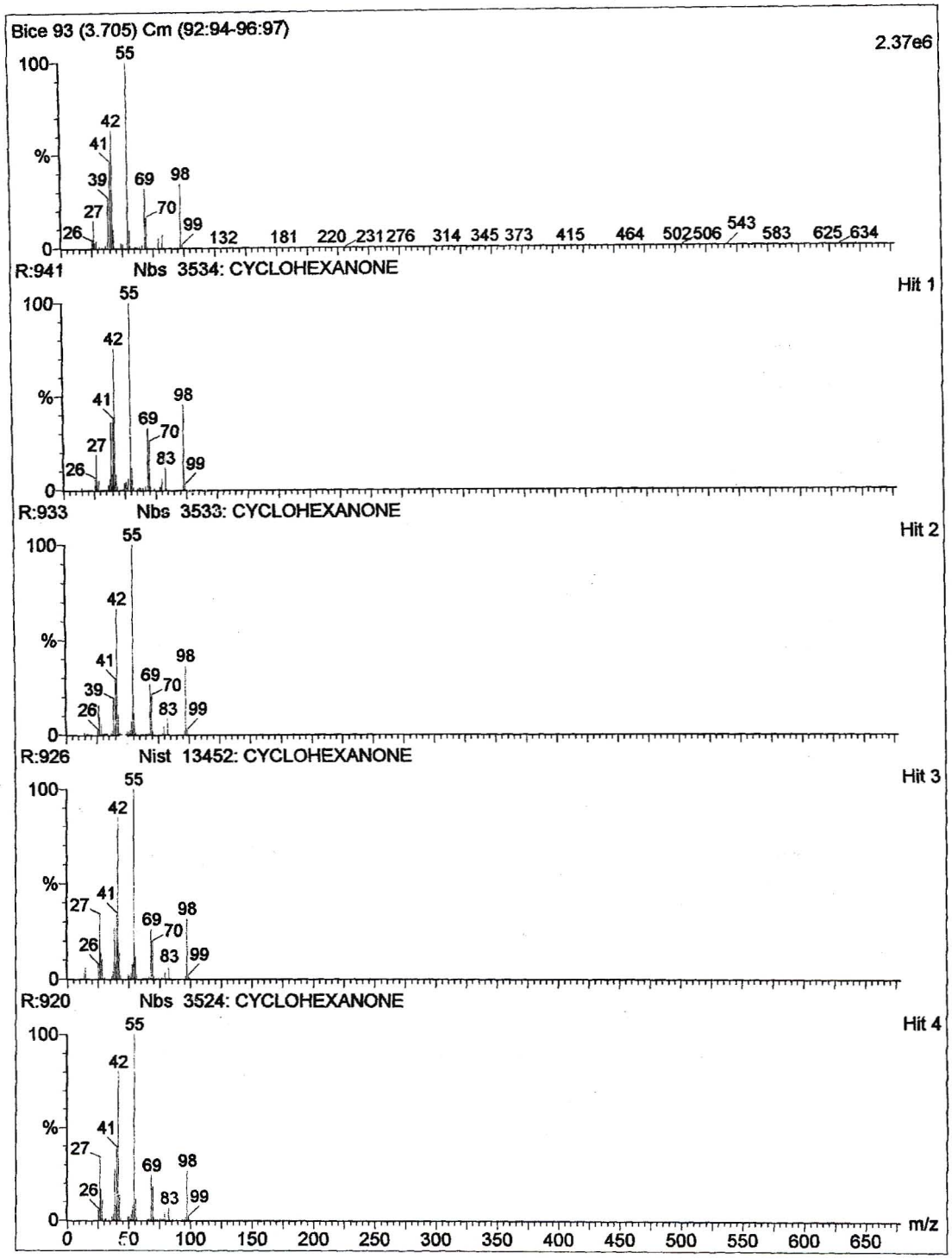

Figure 3.72: Mass-spectrum of cyclohexanone which eluted at 3.71 minutes.

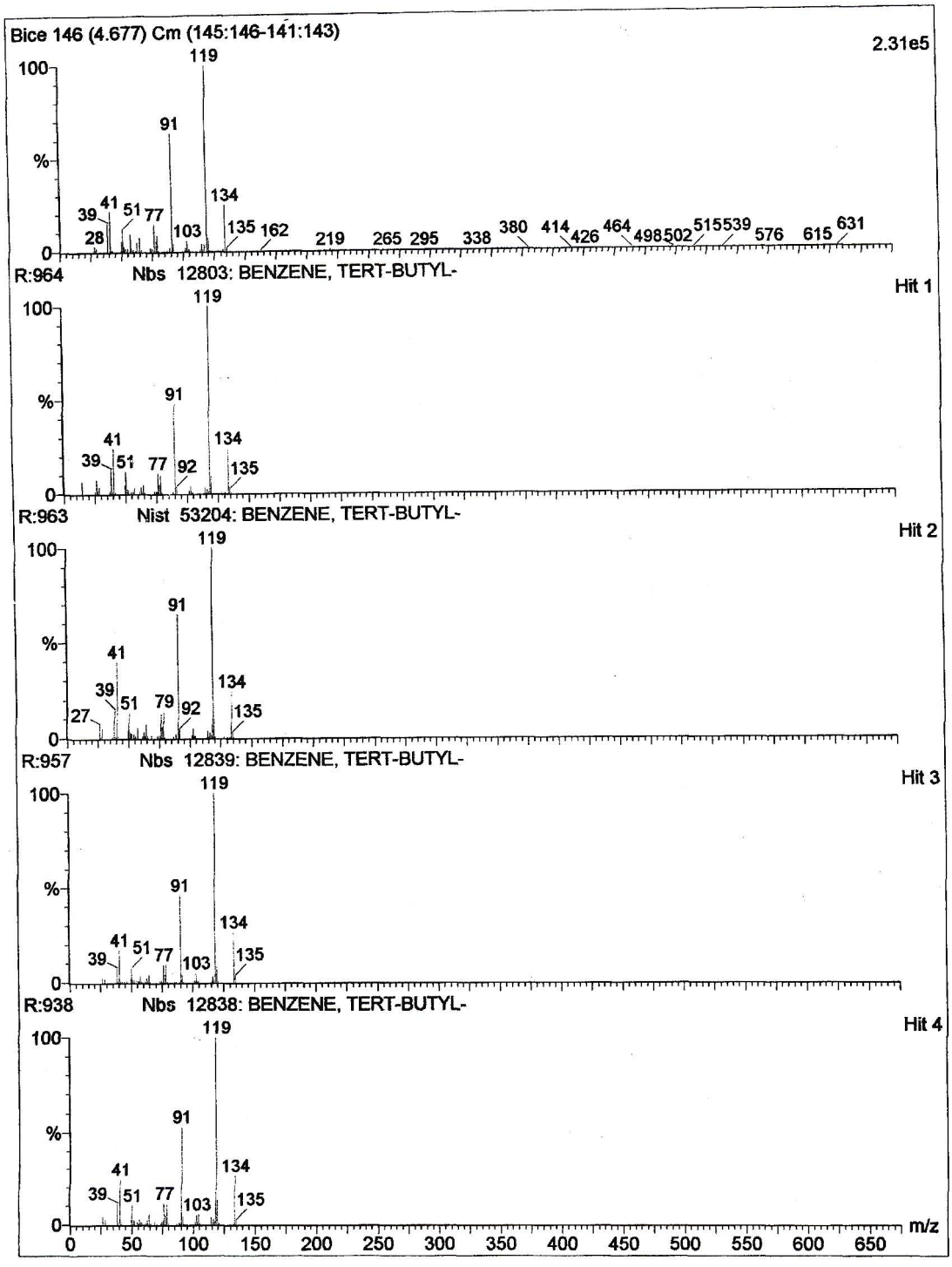

Figure 3.73: Mass-spectrum of *tert*-butylbenzene which eluted at 4.68 minutes.

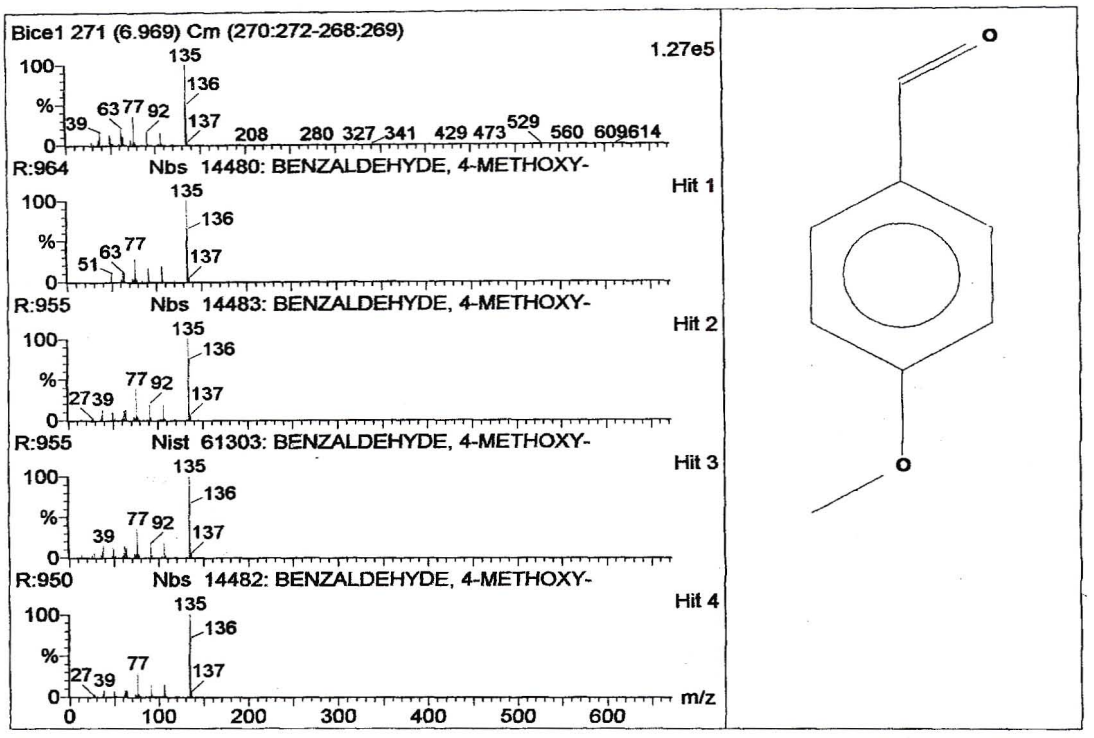

Figure 3.74: Mass-spectra of *p*-methoxybenzaldehyde which eluted at 6.67 minutes.

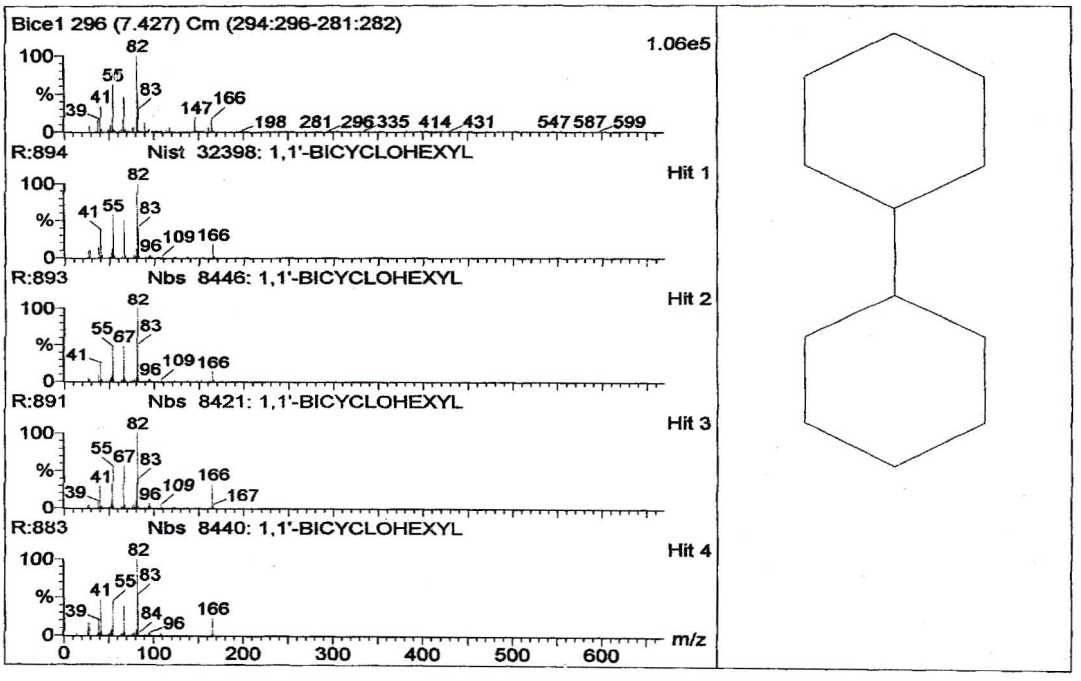

Figure 3.75: Mass-spectra of bicyclohexyl which eluted at 7.43 minutes.

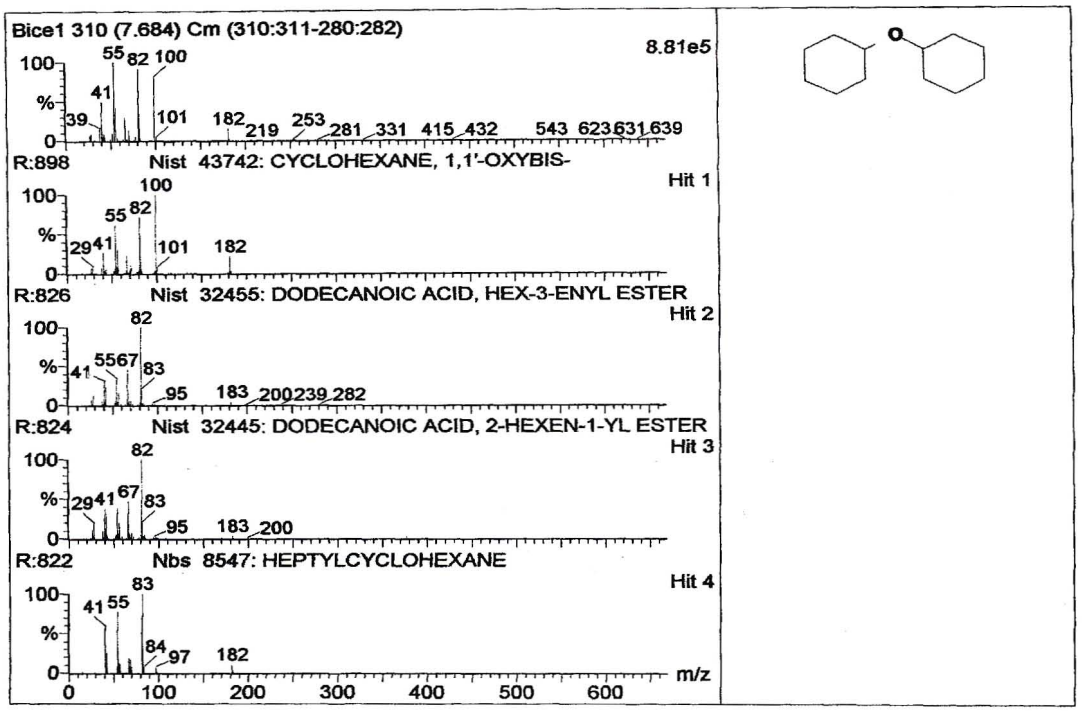

Figure 3.76: Mass-spectra of bicyclohexyl ether which eluted at 7.68 minutes.

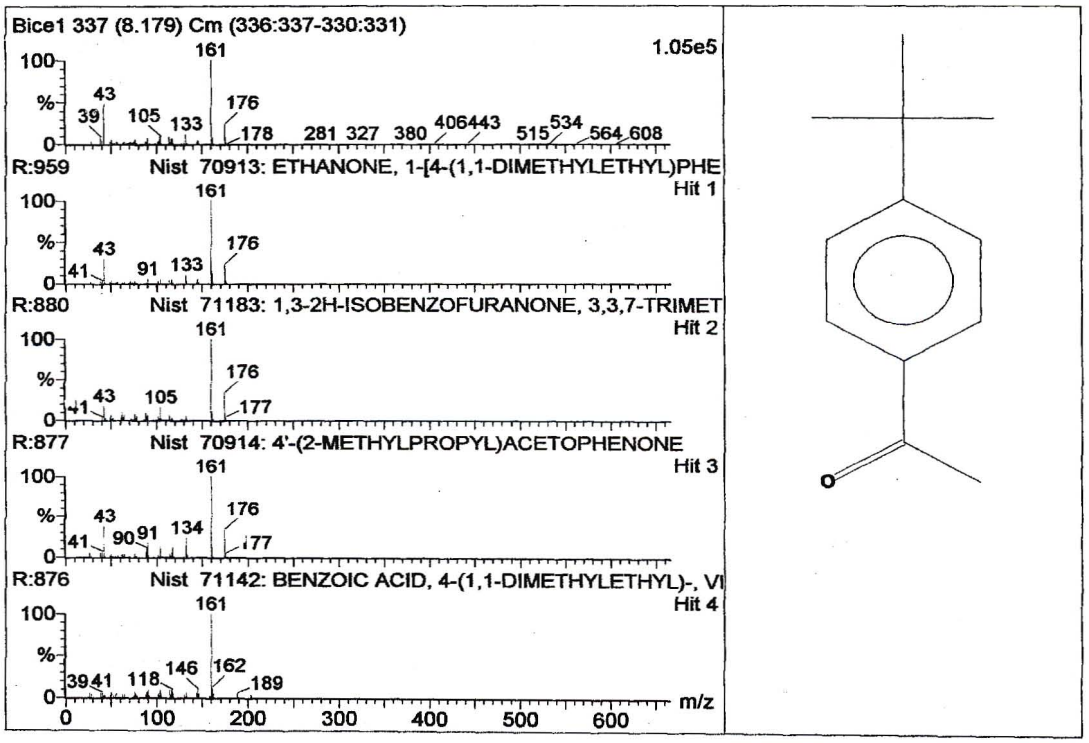

Figure 3.77: Mass-spectra of *p-tert*-butylbenzoic acid which eluted at 8.18 minutes.

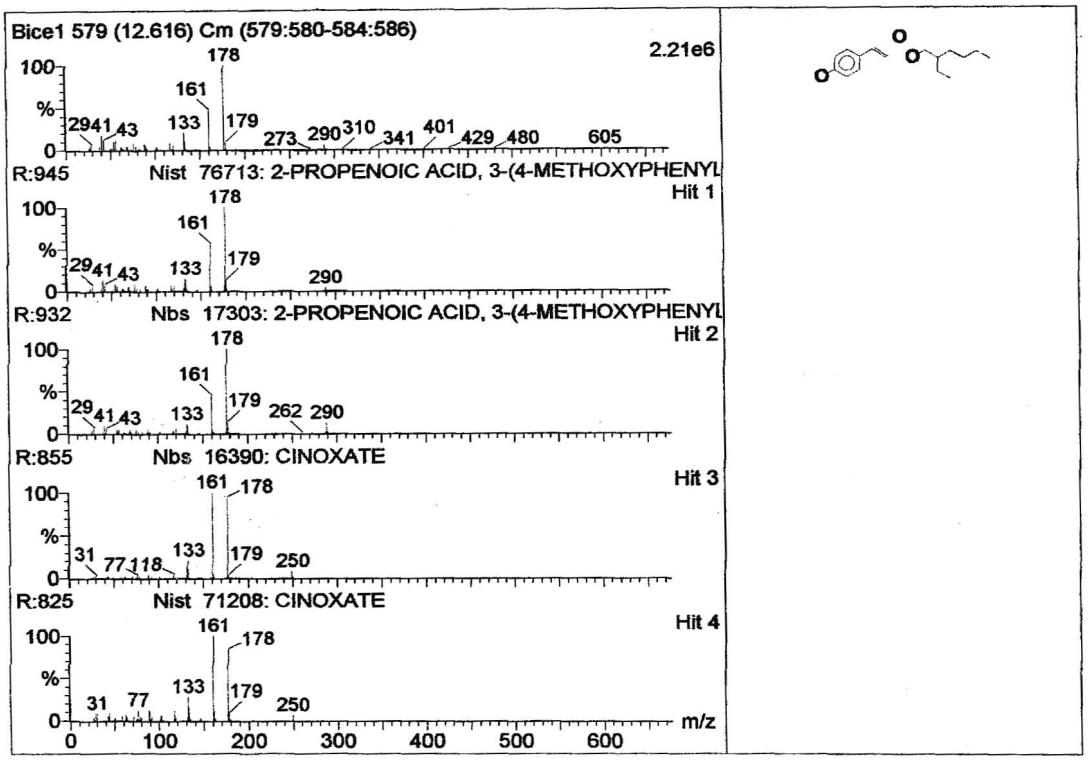

Figure 3.78: Mass-spectrum of *cis*-EHMC which eluted at 12.62 minutes and confirmed by the molar mass.

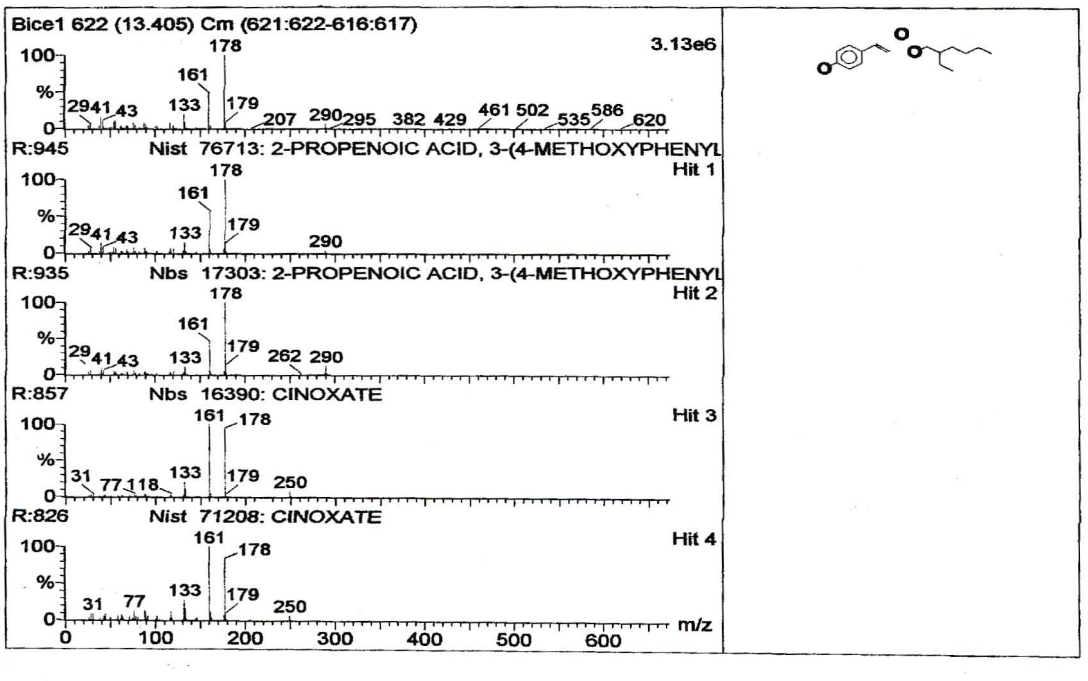

Figure 3.79: Mass-spectrum of *trans*-EHMC which eluted at 13.41 minutes and confirmed by the molar mass.

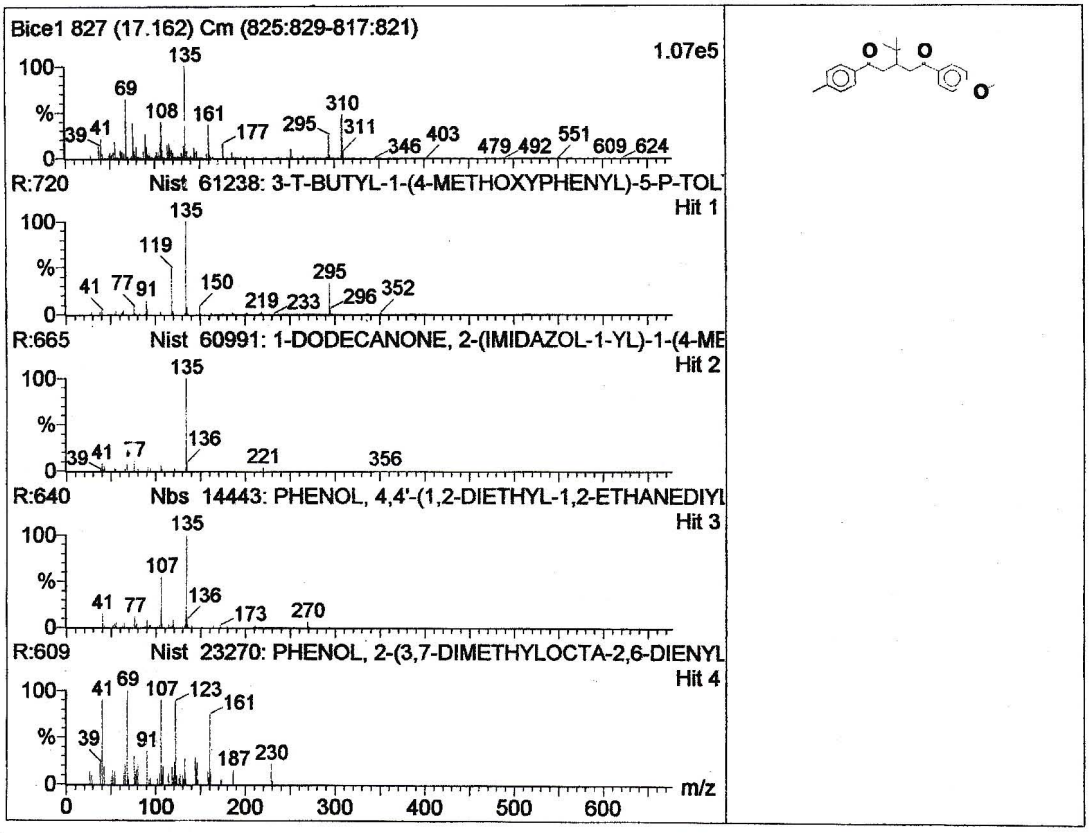

Figure 3.80: Mass-spectrum of AVO which eluted at 17.16 minutes and confirmed by the molar mass.

3.4.4 The use of GC-MS to show that AVO acts as a photosensitiser

On checking the effect of 313 nm and 365 nm irradiation on EHMC and AVO in both solvents we noticed that when a mixture of AVO and EHMC in cyclohexane was irradiated with the 365 nm filter EHMC degraded to a certain extent whereas when EHMC alone was irradiated with this filter no degradation occurred as expected since EHMC does not absorb at this wavelength. We therefore thought that AVO could possibly photosensitise the isomerisation of EHMC since AVO has a higher triplet-state energy than EHMC.

This was confirmed by irradiating a sample of *trans*-EHMC in cyclohexane and a mixture of *trans*-EHMC and AVO in cyclohexane for 1 hour with the 365 nm filter and then subjecting the samples to GC-MS analysis. *Cis*-EHMC is produced in the mixture and not in the individual EHMC sample which means that AVO photosensitizes the isomerisation *trans*-EHMC.

From the total ion chromatogram of the irradiated solution of *trans*-EHMC in cyclohexane (see Figure 3.81) the following photoproducts could be identified: bicyclohexyl (a product of cyclohexane irradiation) eluted at 8.16 minutes, *trans*-EHMC eluted at 13.61 minutes and the compounds that eluted at 14.34, 14.52 and 14.61 minutes are solvent impurities. The mass spectra of bicyclohexyl and *trans*-EHMC are shown in Figures 3.82 and 3.83 respectively and they were confirmed by their molar masses.

From the total ion chromatogram of the irradiated solution of a mixture of *trans*-EHMC and AVO in cyclohexane (see Figure 3.84) the following photoproducts could be identified: bicyclohexyl eluted at 8.16 minutes, *cis*-EHMC eluted at 12.93 minutes, *trans*-EHMC eluted at 13.61 minutes, AVO eluted at 15.67 minutes and the compounds that eluted at 13.88, 14.34, 14.52, 14.61 and 19.82 minutes were all solvent impurities. The mass spectra of the photoproducts are shown in Figures 3.85 to 3.88. From these results we can certainly say that AVO photosensitises the isomerisation of *trans*-EHMC.

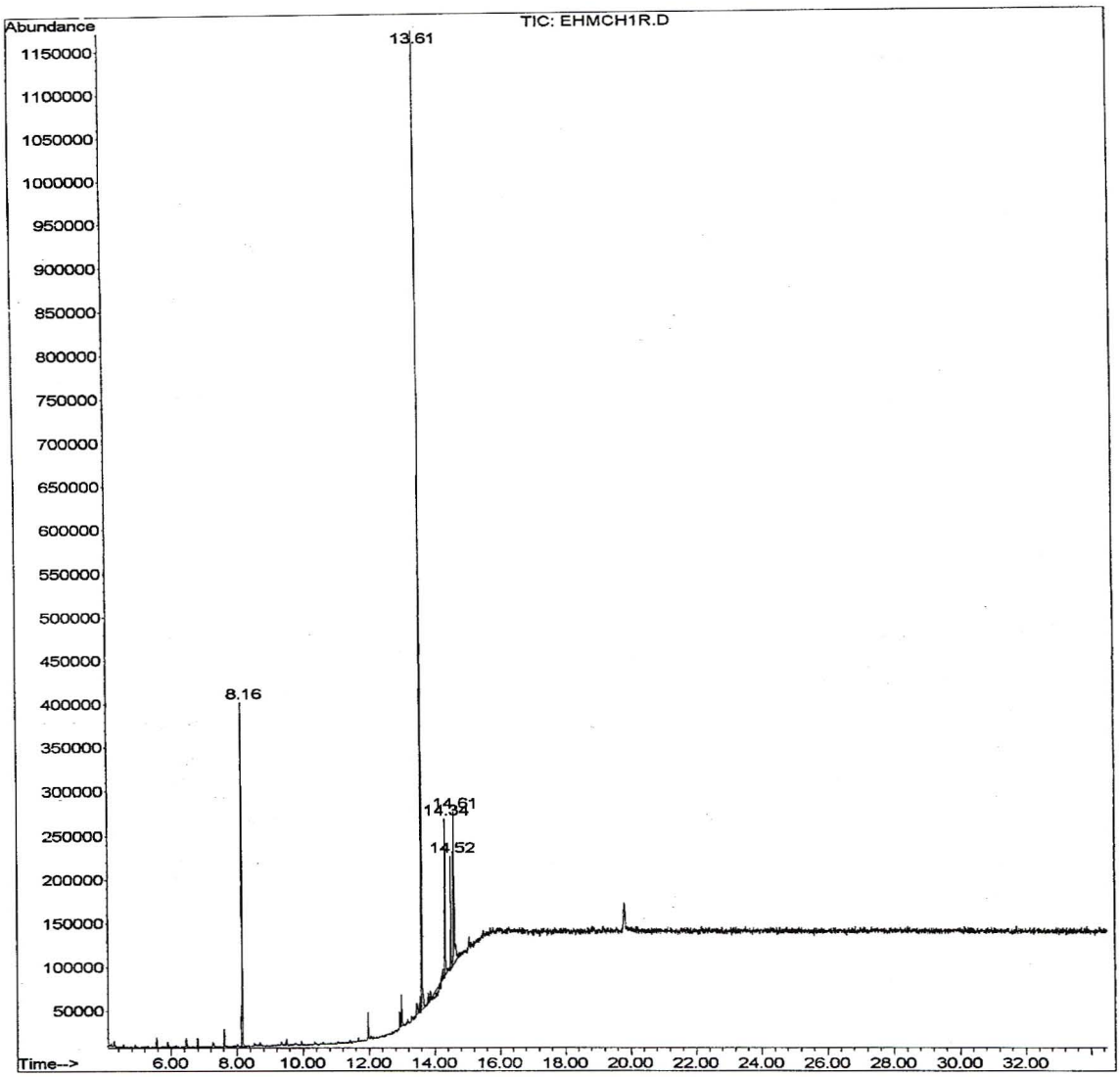

Figure 3.81: Total ion chromatogram of EHMC in cyclohexane upon 1 hour of irradiation using the 365 nm filter. EHMC elutes at 13.61 minutes. The column used was a HP-5 methyl silicon 25 m x 250 μm capillary column and the conditions used are described in Section 2.7.2.3.

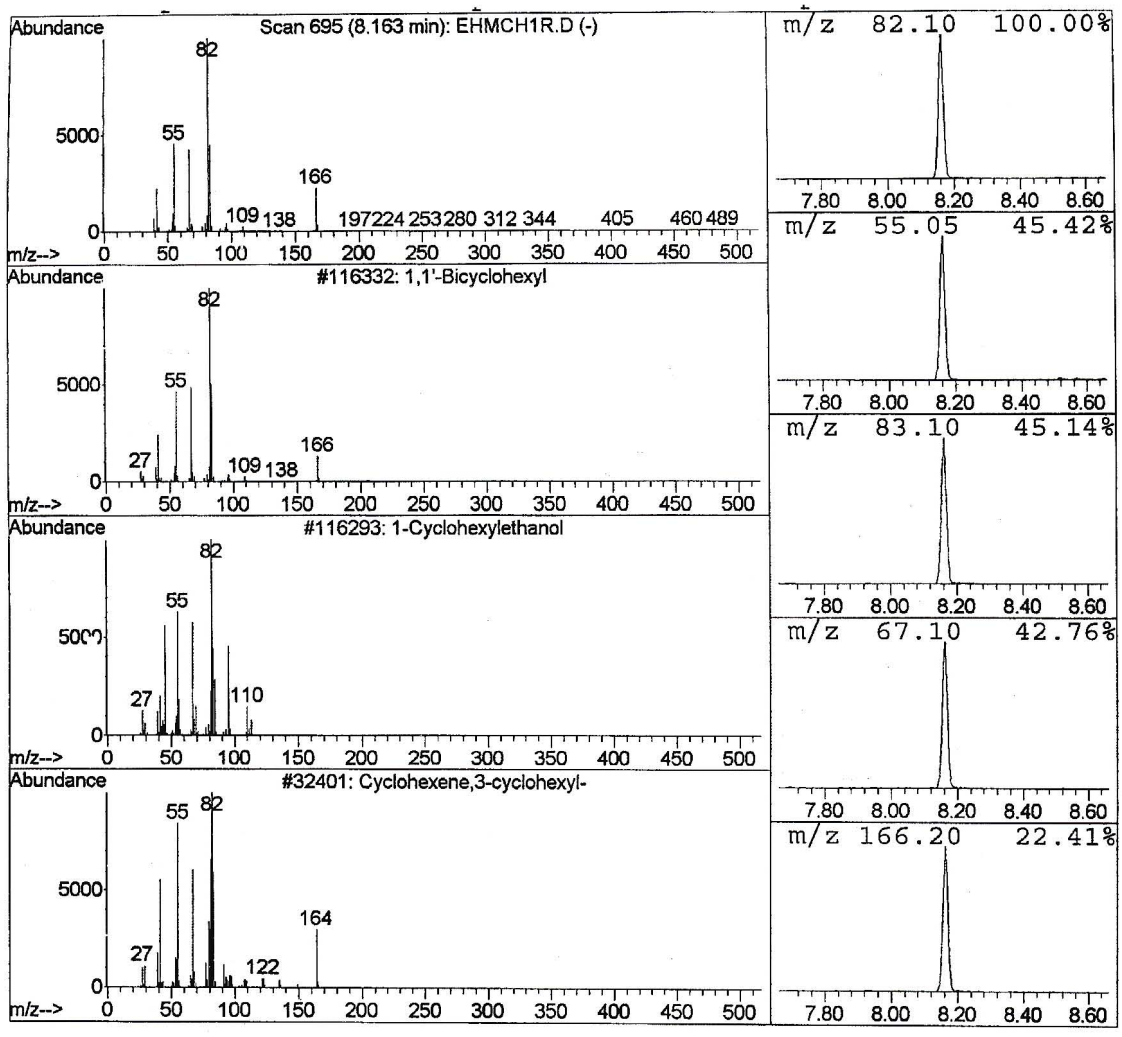

Figure 3.82: Mass spectrum of bicyclohexyl which eluted at 8.16 minutes. This was confirmed by the mass spectrum in Figure 3.63.

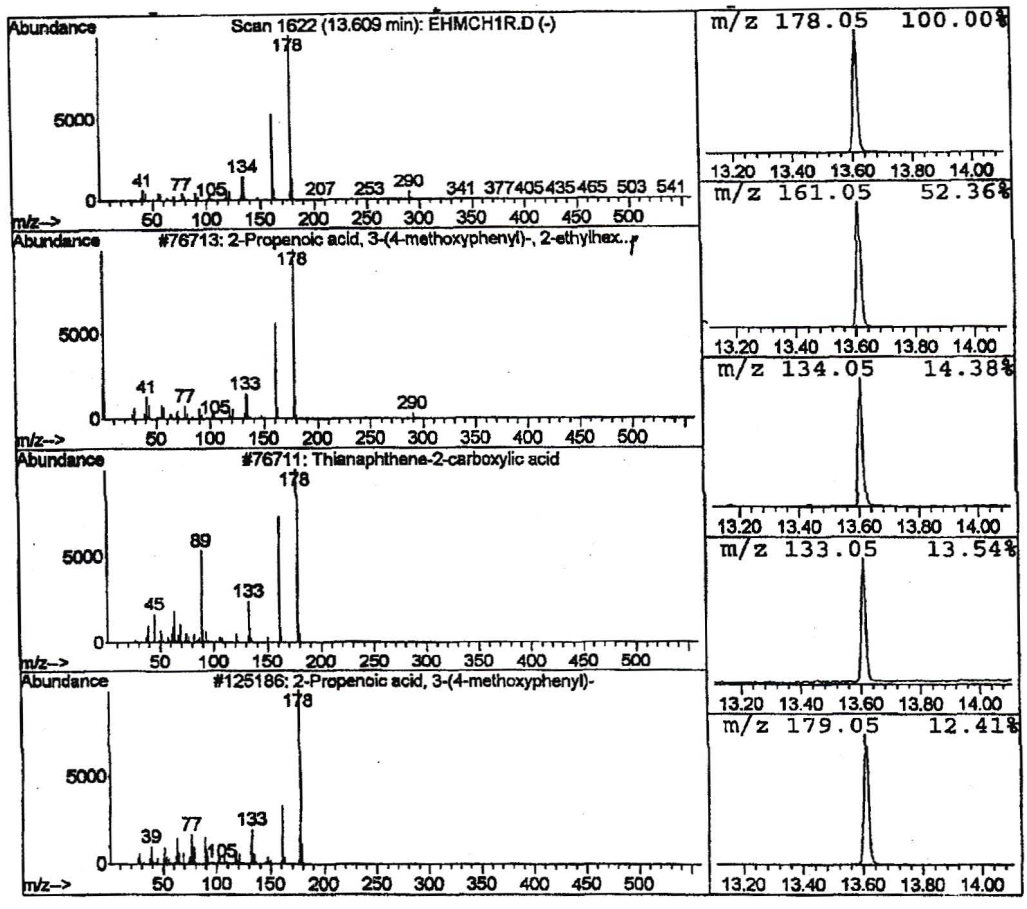

Figure 3.83: Mass spectrum of EHMC which eluted at 13.61 minutes and was confirmed by its molecular mass.

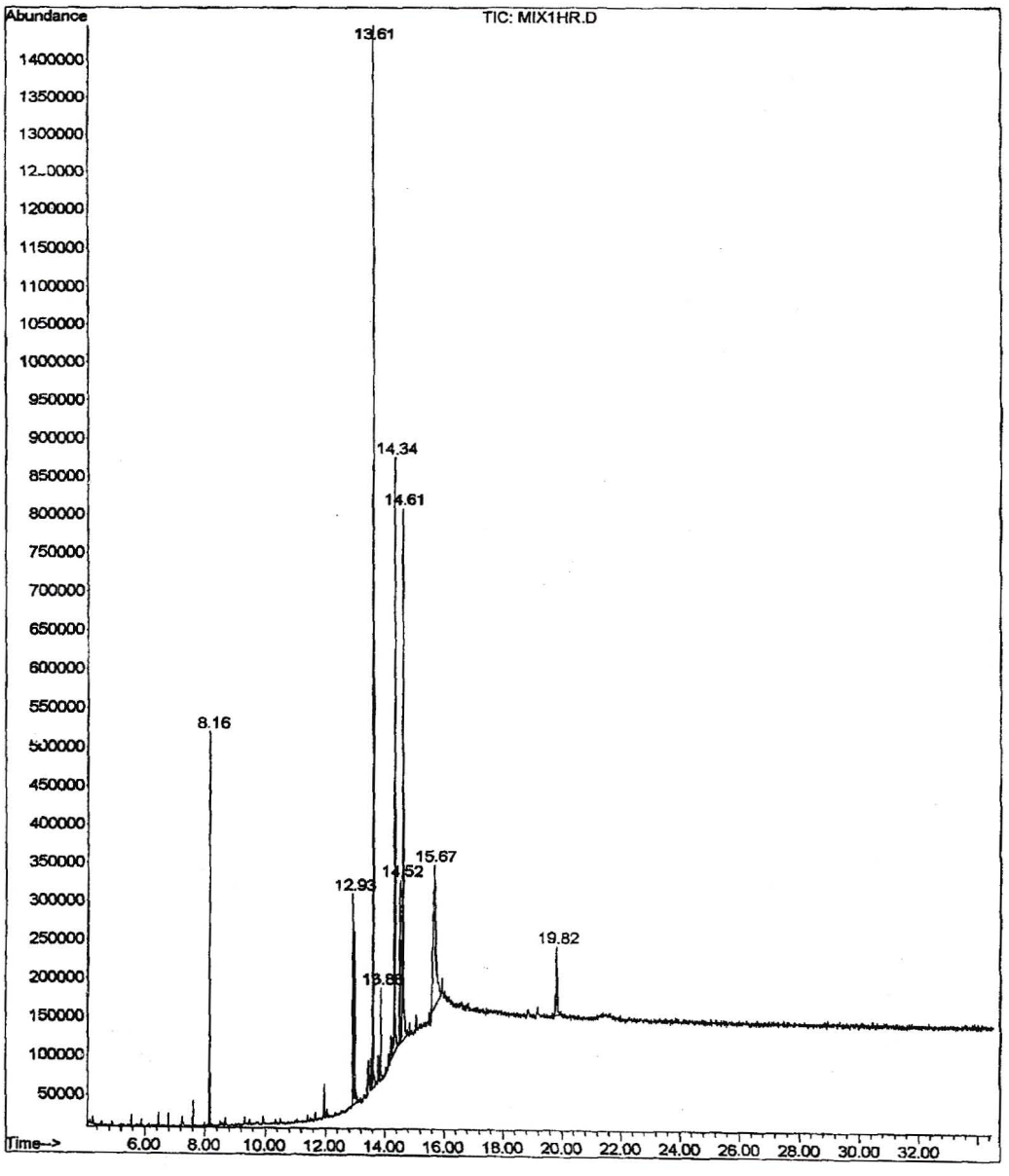

Figure 3.84: Total ion chromatogram of a mixture of EHMC and AVO in cyclohexane upon 1 hour of irradiation using the 365 nm filter. The column used was a HP-5 methyl silicon 25 m x 250 μm capillary column and the conditions used are described in Section 2.7.2.3.

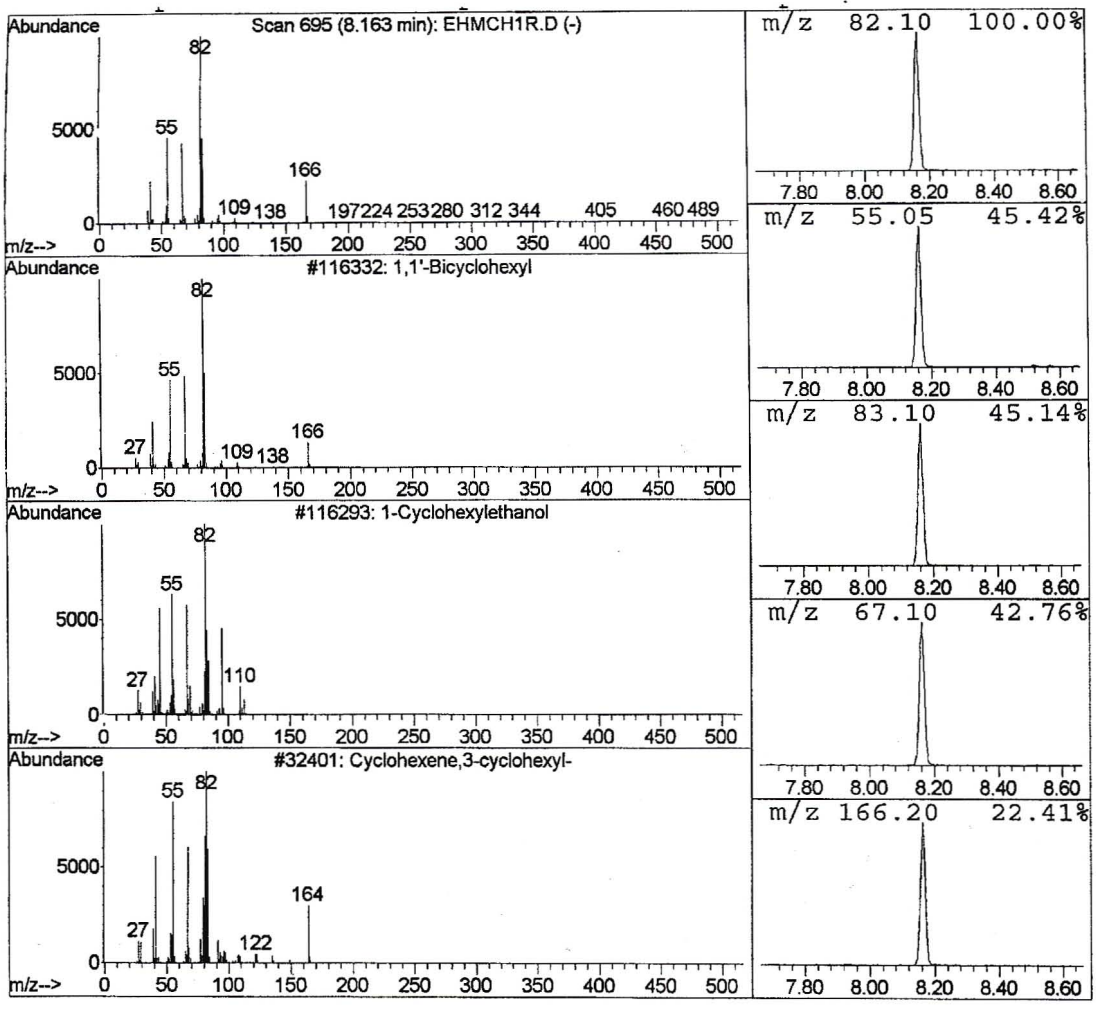

Figure 3.85: Mass spectrum of bicyclohexyl which eluted at 8.16 minutes and confirmed by the mass spectrum in Figure 3.63.

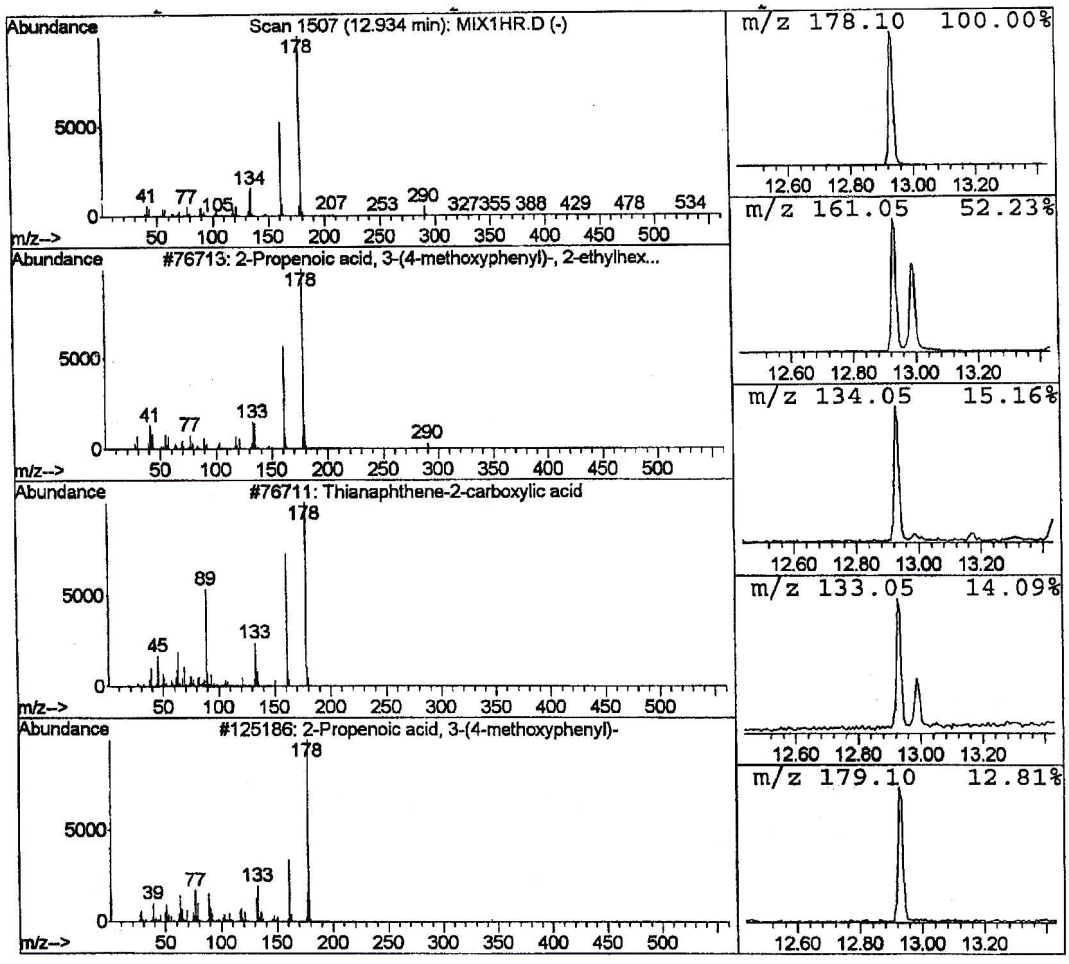

Figure 3.86: Mass spectrum of *cis*-EHMC that eluted at 12.93 minutes. This has the same molecular mass as *trans*-EHMC but different retention time.

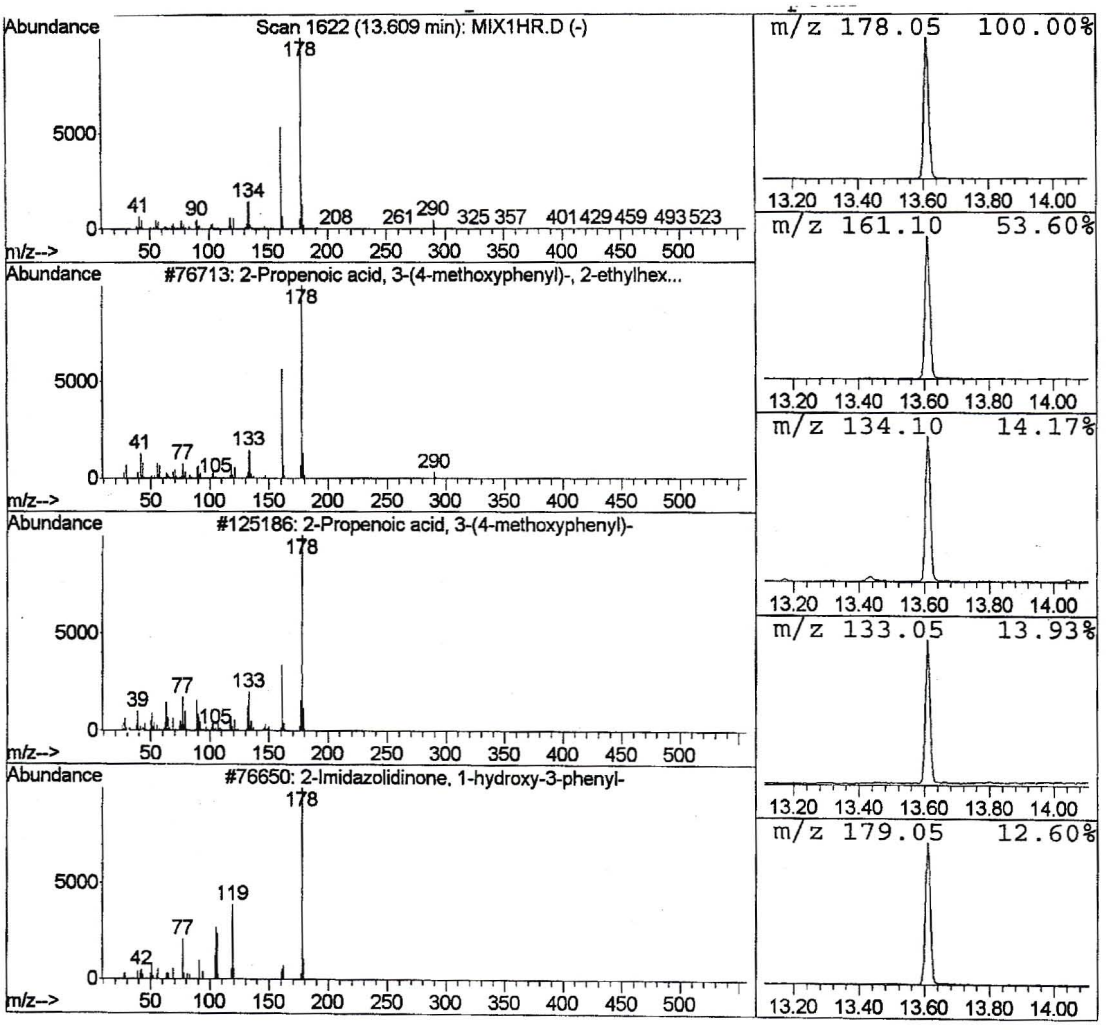

Figure 3.87: Mass spectrum of *trans*-EHMC that eluted at 13.61 minutes and was confirmed by its molecular mass.

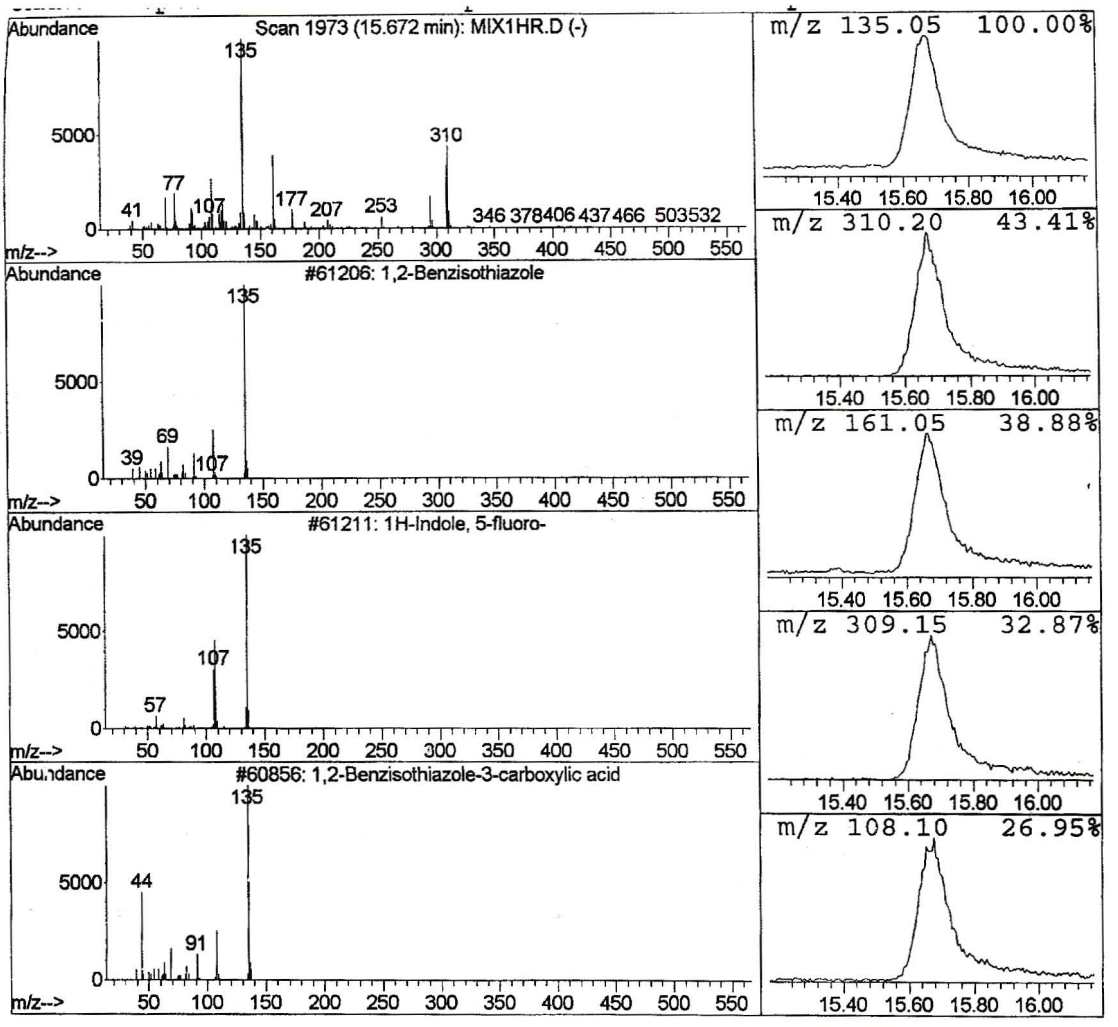

Figure 3.88: Mass spectrum of AVO that eluted at 15.67 minutes. This was confirmed from the mass spectrum in Figure 3.68.

3.5 Determination of light intensity absorbed by EHMC and AVO by chemical actinometry

The rate at which chemical absorbers degrade upon irradiation with UV-light is dependent on the number of photons absorbed. Since EHMC degrades in both methanol and cyclohexane, and AVO degrades only in cyclohexane we set out to determine the number of photons absorbed using the Hatchard and Parker method of chemical actinometry [45,46].

3.5.1 Determination of light intensity absorbed by EHMC and AVO in methanol

EHMC undergoes photodegradation in methanol while AVO is photostable. We therefore determined the number of photons absorbed by EHMC with and without the presence of AVO and also showed that AVO was fairly stable. The concentration of the sunscreen agents in methanol after irradiation was determined from the calculation method developed in Section 2.6.2.1. The number of Fe^{2+} ions formed (nFe^{2+}) was determined using equation 2.3 in Section 2.8.3, the intensity of light absorbed by the ferrioxalate solution (I_o) was determined using equation 2.4 in Section 2.8.3 as well. To determine the intensity of light absorbed by the sunscreen agent (I_a), we take the difference between the light transmitted through the photolysis solution containing water in place of the sunscreen agent and that containing the sunscreen agent. The number of photons absorbed by the sunscreen solution was determined by mutiplying the intensity of light absorbed by the sunscreen solution by the irradiation time in seconds.

Different concentrations of EHMC were used in order to determine the intensity of light absorbed within a 45 s irradiation time. The concentrations of EHMC before and after irradiation were determined from the EHMC in methanol calibration curve (see Figure 2.12). The number of Fe^{2+} ions formed (nFe^{2+}), the intensity of light absorbed by the ferrioxalate solution and the intensity of light absorbed by EHMC in methanol are shown in Table 3.29. A graph of the number of photons absorbed by EHMC in methanol was plotted against the initial concentration of EHMC (see Figure 3.89).

Table 3.29: Determination of the intensity of light absorbed by EHMC dissolved in methanol. The absorbance of the iron-phenanthroline complex was measured at 510 nm and the number of Fe^{2+} ions produced and intensity of light absorbed was then determined.

EHMC]/10^{-5} M (before irradiation)	[EHMC]/10^{-5} M (after irradiation)	$A_{510\ nm}$	$nFe^{2+}/10^{18}$ no. of ions	$I_o/10^{16}$ photons s^{-1}	$I_a/10^{16}$ photons s^{-1}	no. of photons absorbed in 45 s /10^{16}
0	-	0.777	2.953	5.286	-	-
6.3	3.5	0.658	2.500	4.475	0.811	36.50
4.6	2.5	0.703	2.671	4.781	0.505	22.73
3.0	1.7	0.727	2.763	4.946	0.340	15.30
2.0	0.7	0.753	2.861	5.121	0.165	7.43

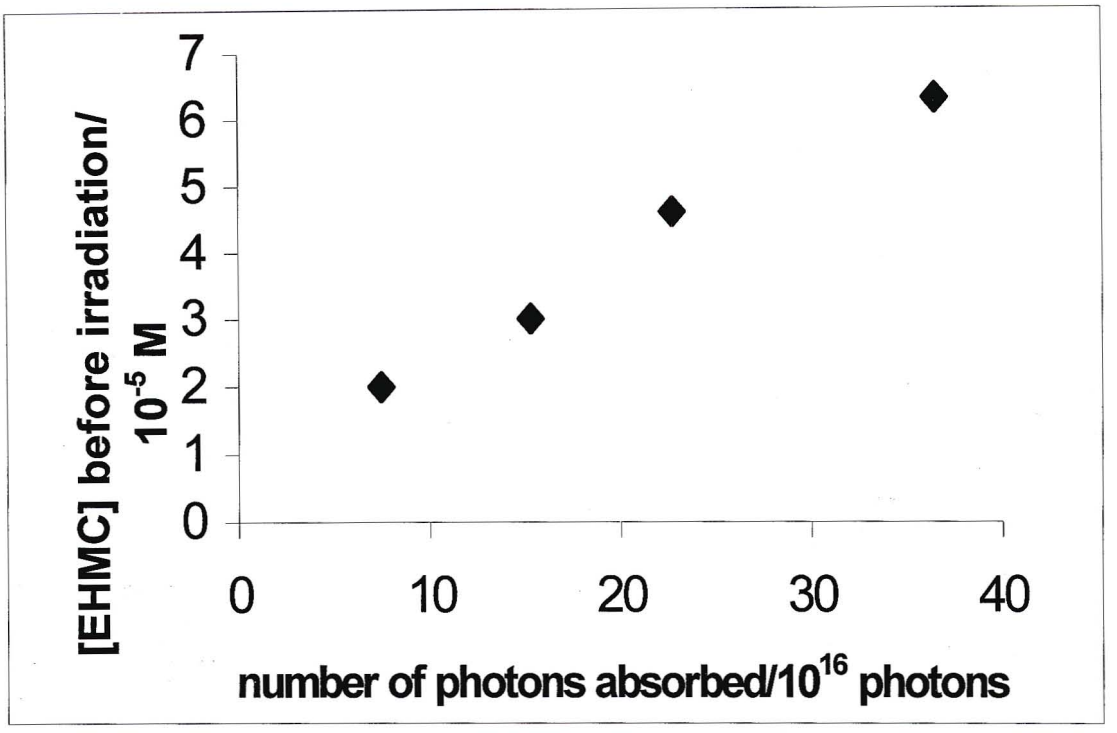

Figure 3.89: Graph showing the concentration of EHMC dissolved in methanol before irradiation against the amount of photons absorbed in 45 s.

AVO dissolved in methanol showed little or no photodegradation upon irradiation, therefore the concentrations before and after irradiation are the same (see Table 3.30). The number of photons absorbed by AVO should therefore be proportional to the concentration of AVO. By irradiating different concentrations of AVO we found that the number of photons absorbed are relatively constant (see Table 3.30).

Table 3.30: Determination of the intensity of light absorbed by AVO dissolved in methanol in 45 s of irradiation. The absorbance of the iron-phenanthroline complex was measured at 510 nm and the number of Fe^{2+} ions produced and intensity of light absorbed was then determined.

[AVO]/10^{-5} M (before irradiation)	**[AVO]/10^{-5} M (after irradiation)**	**$A_{510\ nm}$**	**$nFe^{2+}/10^{18}$ no. of ions**	**$I_o/10^{16}$ photons s^{-1}**	**$I_a/10^{16}$ photons s^{-1}**	**No. of photons absorbed in 45 s/ 10^{16}**
0	-	0.636	2.42	4.33	-	-
2.8	2.8	0.622	2.36	4.22	0.11	4.95
2.3	2.3	0.626	2.38	4.26	0.07	3.15
1.7	1.7	0.622	2.36	4.22	0.11	4.95
1.4	1.4	0.626	2.38	4.26	0.07	3.15
1.2	1.2	0.625	2.38	4.26	0.07	3.15

We looked at the intensity of light absorbed by a mixture of EHMC and AVO in methanol. Once the concentration of AVO at 356 nm was determined the concentration of *trans*-EHMC before and after irradiation in the mixture was determined by the calculation method developed in Section 2.6.2.1 (see Table 3.31). The concentration of *cis*-EHMC was determined by taking the difference of *trans*-EHMC before and after irradiation, since it is the only photoproduct formed upon *trans*-EHMC irradiation. From Figure 3.90 it is clear that the concentration of *trans*-EHMC before irradiation is proportional to the number of photons absorbed considering that EHMC photoisomerises in methanol. From Figure 3.91 it is evident that the *cis*-EHMC formed in the presence of AVO is also proportional to the number of photons absorbed.

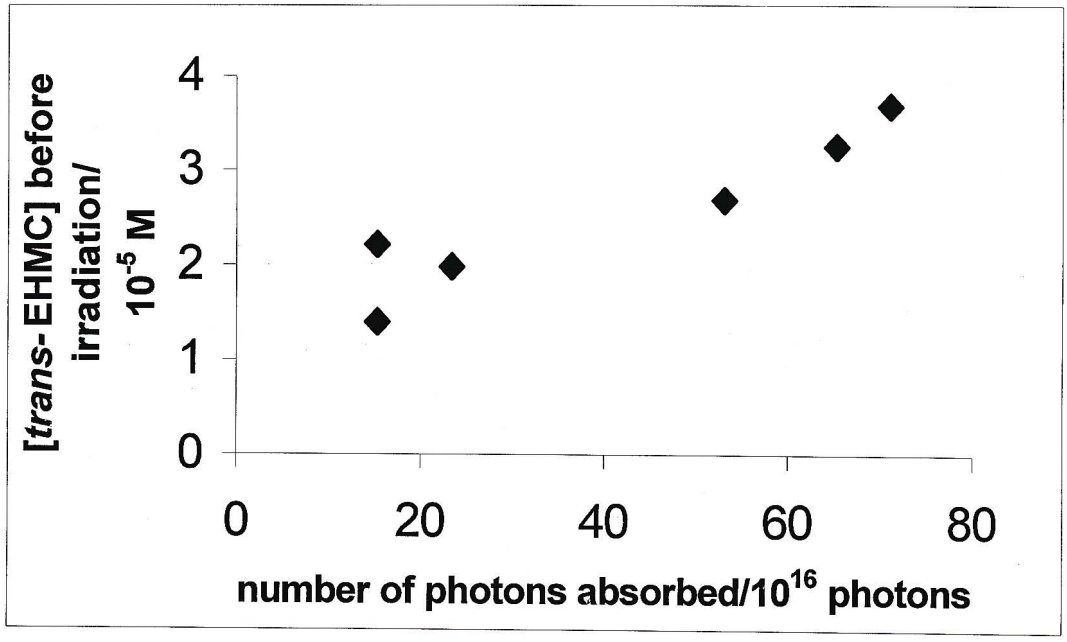

Figure 3.90: Graph showing the concentration of *trans*-EHMC dissolved in methanol before irradiation in the presence of AVO and *cis*-EHMC upon absorption of UV photons.

Table 3.31: Data for intensity of light absorbed by EHMC and AVO in methanol in the presence of AVO.

[AVO]/ 10^{-5} M	[*trans*-EHMC]/ 10^{-5} M (before irradiation)	[*trans*-EHMC]/ 10^{-5} M (after irradiation)	[*cis*-EHMC]/ 10^{-5} M	$A_{510\ nm}$	$nFe^{2+}/10^{18}$ no. of ions	$I_o / 10^{16}$ photons s^{-1}	$I_a / 10^{16}$ photons s^{-1}	no. of photons absorbed in 45 s/ 10^{16}
0	0	-	-	0.992	3.77	6.75	-	-
1.20	3.68	2.59	1.09	0.760	2.89	5.17	1.58	71.1
1.02	3.25	2.16	1.09	0.778	2.96	5.30	1.45	65.3
0.803	2.68	1.77	0.91	0.818	3.11	5.57	1.18	53.1
0.750	2.21	1.49	0.72	0.942	3.58	6.41	0.34	15.3
0.643	1.98	1.31	0.67	0.915	3.48	6.23	0.52	23.4
0.455	1.40	0.92	0.48	0.941	3.58	6.41	0.34	15.3

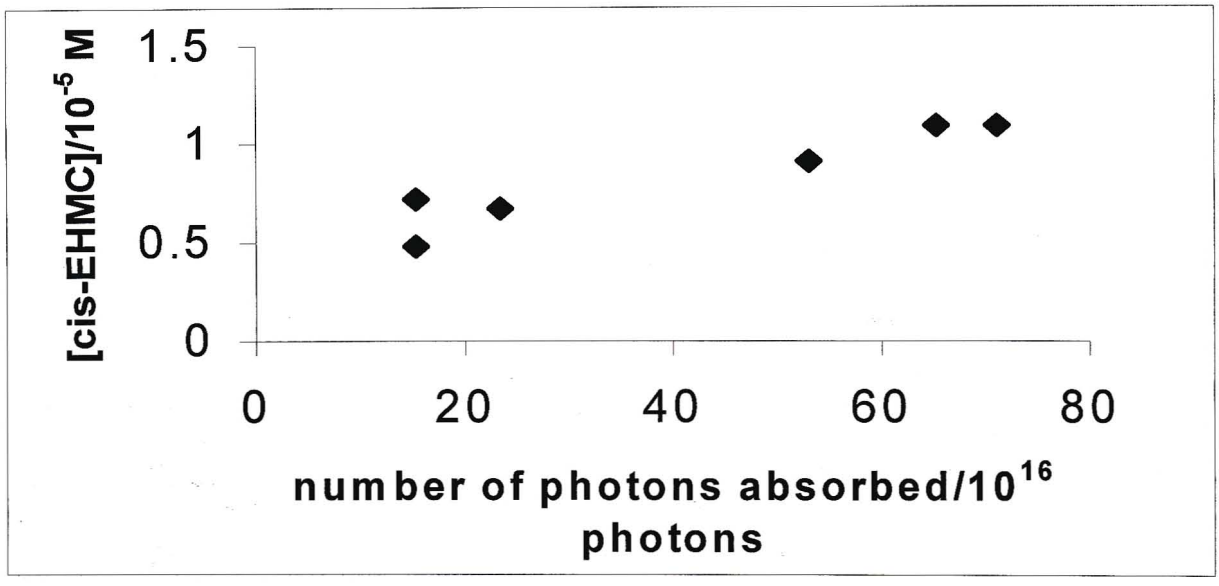

Figure 3.91: Comparison of the number of photons absorbed by the mixture and the concentration of *cis*-EHMC formed by the isomerisation of *trans*-EHMC dissolved in methanol in the presence of AVO.

3.5.2 Determination of light intensity absorbed by EHMC and AVO in cyclohexane

Both EHMC and AVO undergo photodegradation in cyclohexane. We therefore showed the number of photons absorbed by EHMC, AVO and a mixture of the two in cyclohexane. The concentration of the sunscreen agents in cyclohexane after irradiation was determined by using the calculation method developed in Section 2.6.2.2.

Different concentrations of EHMC dissolved in cyclohexane were irradiated for a 45 s duration and the absorbance of EHMC was measured at 290 nm before and after irradiation. The concentration of EHMC was then determined from the calibration curve of EHMC in cyclohexane at 290 nm (see Figure 2.15). The concentration of EHMC before and after irradiation, the absorbance of the ferrioxalate solution, the number of Fe^{2+} calculated, I_o and I_a are all shown in Table 3.32. A graph of the number of photons absorbed was plotted against the concentration of EHMC before irradiation (see Figure 3.92) and from this graph we can say that the intensity of light absorbed by EHMC in cyclohexane is not dependent on the concentration of EHMC.

The intensity of light absorbed by AVO was measured after 600 s of irradiation since AVO takes much longer to degrade in cyclohexane. The concentration of AVO was measured using the calibration curve (see Figure 2.13). The concentration of AVO before and after irradiation and the intensity of light absorbed are shown in Table 3.33. From Figure 3.93 it can be seen that the number of photons absorbed by AVO in cyclohexane is dependent on the initial concentration of AVO.

Table 3.32: Determination of the intensity of light absorbed by EHMC dissolved in cyclohexane in 45 s of irradiation. The absorbance of the iron-phenanthroline complex was used to measure the number of Fe^{2+} ions produced and the intensity of light absorbed was then determined.

[EHMC]/ 10^{-5} M (before irradiation)	[EHMC]/ 10^{-5} M (after irradiation)	$A_{510\ nm}$	$nFe^{2+}/10^{18}$ no. of ions	$I_0/10^{16}$ photons s^{-1}	$I_a/10^{16}$ photons s^{-1}	no. of photons absorbed in 45 s/ 10^{16}
0	-	0.892	3.39	6.07	-	-
3.51	2.81	0.763	2.90	5.19	0.88	39.6
2.69	2.20	0.632	2.40	4.30	1.77	79.7
1.84	1.42	0.664	2.52	4.51	1.56	70.2
1.55	1.26	0.724	2.75	4.92	1.15	51.8
1.39	1.14	0.676	2.57	4.60	1.47	66.2

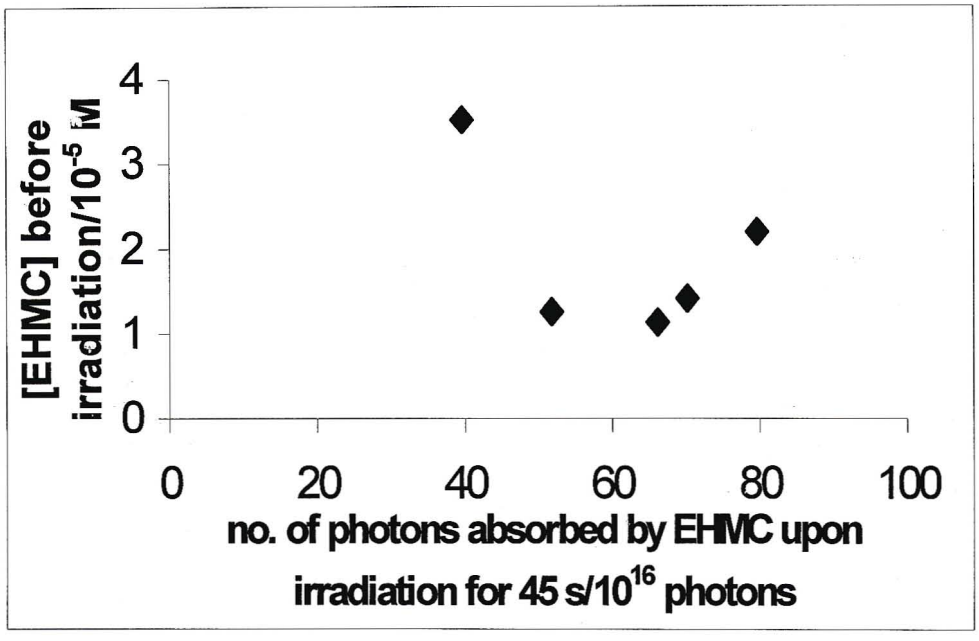

Figure 3.92: The number of photons absorbed by EHMC dissolved in cyclohexane.

Table 3.33: Determination of the intensity of light absorbed by AVO in cyclohexane in 600 s of irradiation. The absorbance of the iron-phenanthroline complex was used to measure the number of Fe^{2+} ions produced and the intensity of light absorbed was then determined.

AVO]/ 10^{-5} M (before irradiation)	AVO]/ 10^{-5} M (after irradiation)	$A_{510\ nm}$	$nFe^{2+}/10^{18}$ no. of ions	$I_o/10^{15}$ photons s^{-1}	$I_a/10^{15}$ photons s^{-1}	no. of photons absorbed in 600 $s/10^{17}$
0	-	0.952	3.62	4.85	-	-
3.26	2.84	0.876	3.33	4.46	0.39	2.34
2.69	2.34	0.890	3.38	4.53	0.32	1.86
1.67	1.61	0.915	3.48	4.66	0.19	1.14
1.46	1.35	0.928	3.53	4.73	0.12	0.72
0.59	0.23	0.950	3.61	4.84	0.01	0.12

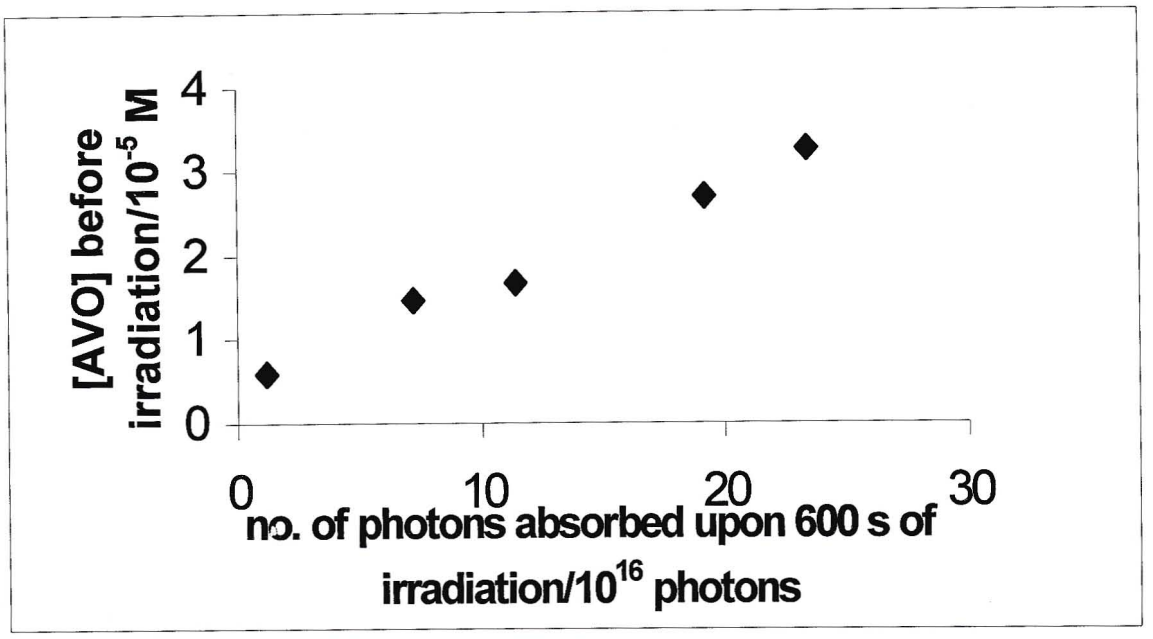

Figure 3.93: The number of photons absorbed by AVO dissolved in cyclohexane.

We determined the intensity of light absorbed by a mixture of EHMC and AVO dissolved in cyclohexane. Both EHMC and AVO photodegrade in cyclohexane. Over the wavelength range of irradiation both sunscreens absorb. Considering the fact that AVO undergoes photodegradation upon irradiation, then after 600 s of irradiation you would expect the number of photons absorbed by AVO to diminish. The concentration of AVO in the mixture of EHMC and AVO dissolved in cyclohexane before and after irradiation was determined using the method developed in Section 2.6.2.2 (see Table 3.34). From Figure 3.94 we can say that there is a direct relationship between the number of photons absorbed by the mixture and the concentration of AVO before irradiation. The concentrations of EHMC in the mixture of EHMC and AVO dissolved in cyclohexane before and after irradiation was determined using the method developed in Section 2.6.2.2 (see Table 3.35). The concentrations of EHMC after irradiation in Table 3.35 are inconsistent due to photoproducts of AVO absorbing close to the wavelength of maximum absorbance of EHMC. From Figure 3.95 we can see the relationship between the number of photons absorbed by EHMC in the presence of AVO and the concentration of EHMC before irradiation. From this plot we can certainly say that the number of photons absorbed rapidly increases as the concentration of EHMC before irradiation increases.

Table 3.34: Determination of the intensity of light absorbed by AVO dissolved in cyclohexane in the presence of EHMC. The absorbance of the iron-phenanthroline complex was used to measure the number of Fe^{2+} ions produced and the intensity of light absorbed was then determined.

[AVO]/ 10^{-5} M (before irradiation)	[AVO]/ 10^{-5} M (after irradiation)	$A_{510\ nm}$	$nFe^{2+}/ 10^{18}$ no. of ions	$I_o/10^{15}$ photons s^{-1}	$I_a/10^{15}$ photons s^{-1}	no. of photons absorbed in 600 s/ 10^{17}
0	-	0.939	3.57	4.78	-	-
3.66	3.40	0.698	2.65	3.55	1.23	7.38
2.78	2.75	0.732	2.78	3.73	1.05	6.30
2.37	2.34	0.806	3.06	4.10	0.68	4.08
1.99	1.84	0.811	3.08	4.13	0.65	3.90
1.32	1.26	0.845	3.21	4.30	0.48	2.88

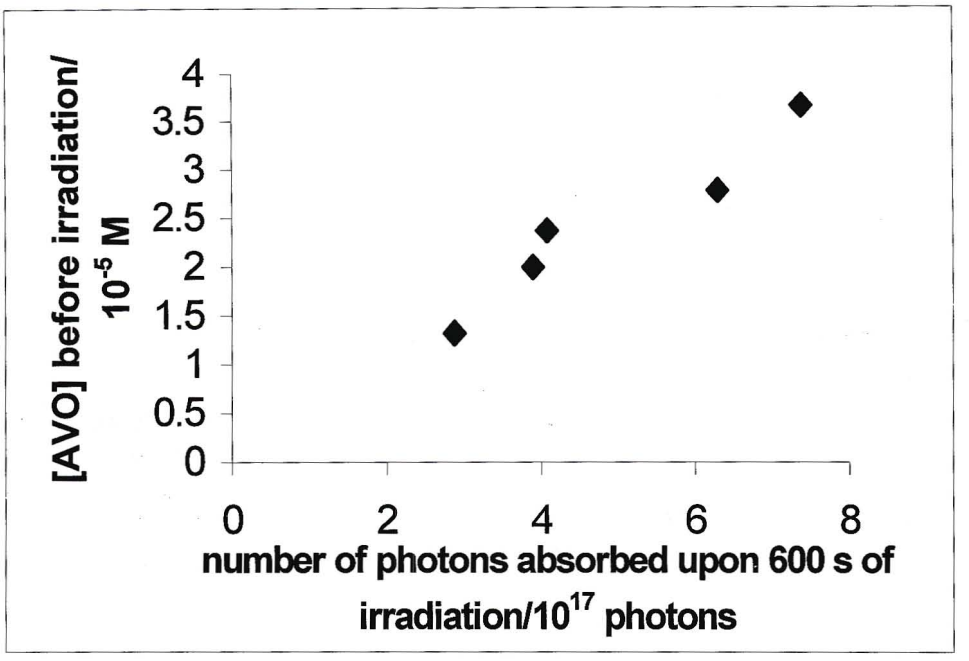

Figure 3.94: Relationship between the number of photons absorbed by AVO in the presence of EHMC and the concentration of AVO dissolved in cyclohexane before irradiation.

Table 3.35: Determination of the intensity of light absorbed by EHMC dissolved in cyclohexane in the presence of AVO. The absorbance of the iron-phenanthroline complex was used to measure the number of Fe^{2+} ions produced and the intensity of light absorbed was then determined.

[EHMC]/ 10^{-5} M (before irradiation)	[EHMC]/ 10^{-5} M (after irradiation)	$A_{510\ nm}$	$nFe^{2+}/10^{18}$ no. of ions	$I_o/10^{16}$ photons s^{-1}	$I_a/10^{16}$ photons s^{-1}	no. of photons absorbed in 45 s/ 10^{18}
0	-	0.763	2.90	5.19	-	-
4.36	4.67	0.309	1.17	2.09	3.10	1.38
4.08	3.64	0.554	2.10	3.76	1.43	0.64
3.49	3.17	0.603	2.29	4.10	1.09	0.49
2.66	2.39	0.744	2.83	5.07	0.12	0.05
0.96	1.74	0.753	2.86	5.12	0.07	0.03

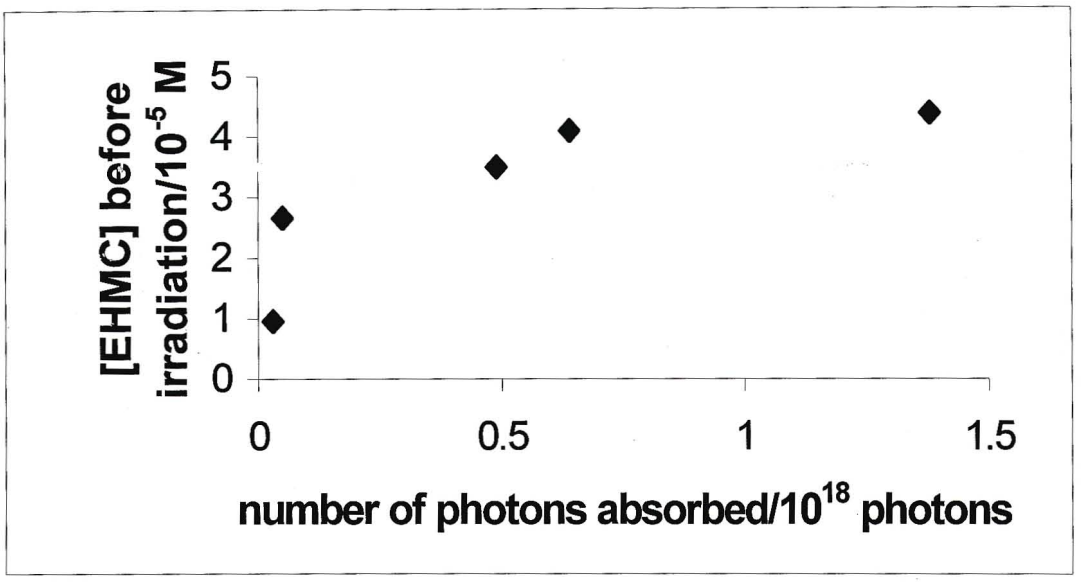

Figure 3.95: Relationship between the number of photons absorbed by EHMC in the presence of AVO and the concentration of EHMC dissolved in cyclohexane before irradiation.

3.5.3 Calculation of the quantum yield for the photodegradation of AVO

The quantum yield can be defined as the rate at which molecules undergo a given event per photon absorbed per unit time. Since the rate of a photochemical reaction is dependent on the intensity of the irradiation source this intensity must be known. The intensity of light was therefore determined using chemical actinometry (see Section 3.5.2). The quantum yield for the photodegradation of AVO (Φ) can therefore be expressed as:

$$\Phi = \frac{[AVO] \times N_A \times V}{I_a \times t} \qquad 3.1$$

where $[AVO]$ is the concentration of AVO degraded (measured by taking the difference between the initial and final concentration of AVO), N_A is Avogadro's constant (6.023×10^{23} mol^{-1}), V (4×10^{-3} dm^3) is the volume of AVO irradiated, I_a is the intensity of light absorbed by AVO which was determined by chemical actinometry and t (1800 s) is the irradiation time.

To determine the quantum yield for the photodegradation of AVO in cyclohexane we used the values of light intensity absorbed by different concentrations of AVO which were measured by chemical actinometry (see Table 3.36) and plotted a calibration curve of light intensity against different concentrations of AVO (see Figure 3.96). We then used this curve to determine the intensity of light absorbed by the concentrations of AVO in cyclohexane that were measured using UV-spectrophotometry in Section 3.3.3 (see Table 3.4) and the values obtained are shown in Table 3.37. We then determined the concentration of AVO that degraded at each data point and the respective quantum yields were calculated using equation 3.1. The average value of the quantum yield for the degradation of AVO was 1.29×10^{-2} molecules degraded per photon of light absorbed.

Table 3.36: The intensity of light absorbed by AVO in cyclohexane as determined by potassium ferrioxalate actinometry.

$[AVO]/10^{-5}$ M	$I_a/10^{15}$ photon s^{-1}
3.26	0.39
2.69	0.32
1.67	0.19
1.46	0.12
0.59	0.010

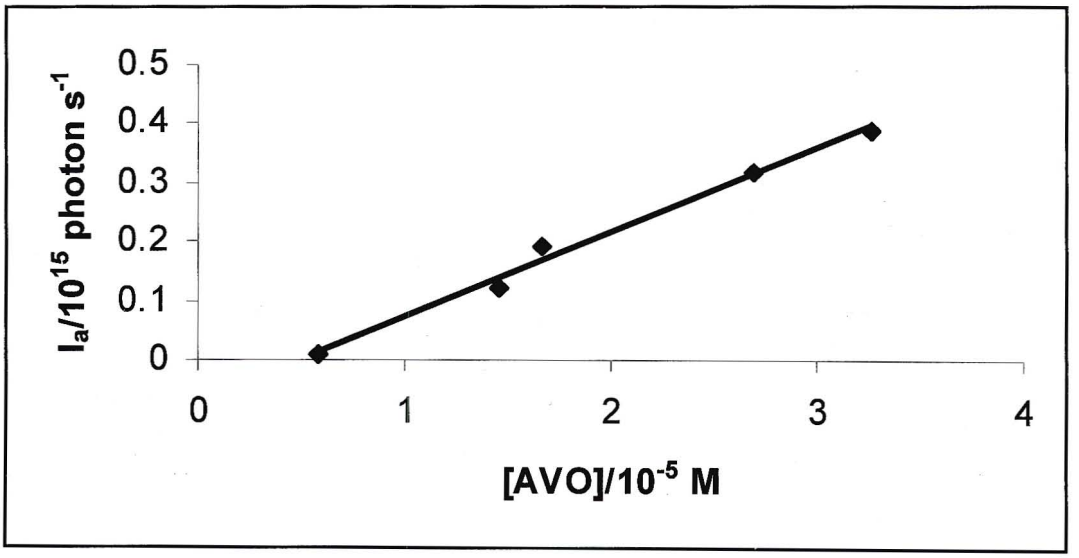

Figure 3.96: Calibration curve of light intensity against concentration of AVO used to calculate the intensity of light absorbed by different concentrations of AVO.

Table 3.37: The intensity of light absorbed by AVO which was determined from the calibration curve (see Figure 3.96) and the values of the quantum yield calculated by using Equation 3.1.

Irradiation time/minutes	**[AVO]/10^{-5} M**	**$([A]_o - [A]_t)$/ 10^{-5} M**	**$I_a/10^{15}$ photon s^{-1}**	**$\Phi/10^{-2}$ molecules degraded photon^{-1}**
0	2.5	-	0	-
30	2.3	0.2	0.260	1.03
60	2.1	0.2	0.225	1.19
90	1.8	0.3	0.185	2.17
120	1.7	0.1	0.175	0.765
				Av =1.29

3.6 Determination of rates of reaction

We have shown that EHMC and AVO undergo photochemical reactions in both methanol and cyclohexane upon exposure to UV-radiation. We therefore determined the rate constants for the photoisomerisation of EHMC and for the photodegradation of AVO.

3.6.1 The rate of EHMC photoisomerisation

In order to determine the rate of EHMC photoisomerisation the concentration of the isomers need to be determined as a function of irradiation time. From this data a kinetic relationship can be used in order to determine the rate constants for the forward and reverse reactions. The concentrations of EHMC were taken from HPLC analysis of irradiated samples of EHMC dissolved in methanol (see Table 3.26).

Assuming that the forward and reverse reactions for the photoisomerisation of EHMC are both first-order and are close to equilibrium then:

$$\textit{trans}\text{-EHMC} \underset{k'}{\overset{k}{\rightleftharpoons}} \textit{cis}\text{-EHMC}$$

Let A be the concentration of *trans*-EHMC and B the concentration of *cis*-EHMC. The rate of change of A is therefore:

$$d[A]/dt = -k[A] + k'[B]$$

If the initial concentration of A is $[A]_0$, and no B is present initially, then at all times $[A] + [B] = [A]_0$. Therefore :

$$\begin{aligned} d[A]/dt &= -k[A] + k'([A]_0 - [A]) \\ &= -(k + k')[A] + k'[A]_0 \end{aligned}$$

Upon intergration of this equation we have:

$$[A] = \frac{k' + ke^{-(k+k')t}}{k + k'}[A]_0$$

The Solver option of Microsoft Excel was used to perform non-linear least-squares curve fitting in order to determine the rate constants in the integrated rate equation. The value of k was determined to be 1.43 s^{-1} and that of k' as 0.0513 s^{-1}. The sum of the squared residuals as seen in Table 3.38 is 14.0 x 10^{-9} which is close to zero implying that the rate constants calculated are fairly acceptable. From Figure 3.97 we can say that the measured and calculated values of $[A]/[A]_0$ are more or less the same therefore the rate constants measured are valid.

Table 3.38: Concentrations of EHMC in methanolic solution as determined by HPLC analysis, where A is the concentration of *trans*-EHMC at time t and A_0 is the initial concentration of *trans*-EHMC. The calculated $[A]/[A]_0$ was determined using the Solver option of Microsoft Excel. The sum of the squared residuals (Σ) was also determined.

Irradiation time/minutes	**$[A]/10^{-5}$ M**	**measured $[A]/[A]_0$**	**calculated $[A]/[A]_0$**	**(calculated $[A]/[A]_0$ - measured $[A]/[A]_0)^2/10^{-9}$**
0	44.0	-	-	-
5	1.55	0.0352	0.0353	9.35
15	1.53	0.0347	0.0347	2.31
120	1.53	0.0347	0.0347	2.31
				$\Sigma = 14.0$

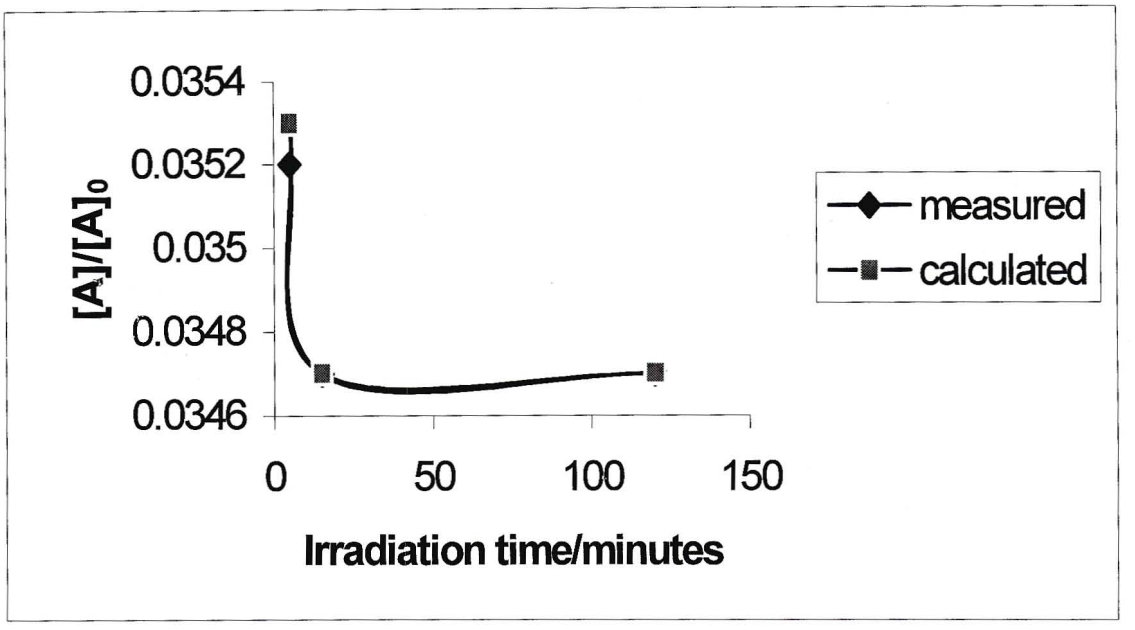

Figure 3.97: A comparison of the measured and calculated values of the concentration of *trans*-EHMC at time t divided by the initial concentration of *trans*-EHMC, i.e. $[A]/[A]_0$, against irradiation time.

The rate constants for the photoisomerisation of EHMC dissolved in cyclohexane could not be determined since the photostationary equilibrium between the *cis*- and the *trans*-isomers of EHMC was not attained (see Figure 3.57).

3.6.2 Determination of the rate constant for the photodegradation of AVO

When AVO was irradiated in cyclohexane it photodegraded to several photoproducts. The rate of photodegradation is dependent on the intensity of the light absorbed. In order to study the rate of this reaction the rate constant had to be determined. We therefore express this photochemical reaction as:

$$AVO \xrightarrow{h\nu} photoproducts$$

Assuming that the photodegradation of AVO follows first order kinetics, the rate of change of AVO can therefore be expressed as:

$$\frac{d[AVO]}{dt} = -k[AVO]$$

Upon integration of this equation we have:

$$\log \frac{[AVO]_t}{[AVO]_0} = -kt / 2.303$$

where $[AVO]_t$ is the concentration of AVO upon t seconds of irradiation, $[AVO]_0$ is the initial concentration of AVO, k is the rate constant and t is the irradiation time in seconds.

The concentrations of AVO were taken from Table 3.4. The values of log $[AVO]_t/[AVO]_o$ are shown in Table 3.39. From a plot of log $[AVO]_t/[AVO]_0$ against t (see Figure 3.98) we determined the slope of the curve to be 2.2×10^{-5} s^{-1}. By multiplying this value by a factor of 2.303 we obtain the rate constant k and hence $k = 5.1 \times 10^{-5}$ s^{-1}. The correlation coefficient of this curve is equivalent to 0.9987 which implies a good straight line. The photodegradation of AVO therefore follows first-order kinetics.

Table 3.39: The concentrations of AVO at various irradiation times in cyclohexane were taken from Table 3.4. The log $[AVO]_t/[AVO]_o$ was then calculated.

Irradiation time/minutes	$[AVO]/10^{-5}$ M	log $[AVO]_t/[AVO]_o$
0	2.5	-
30	2.3	-0.0362
60	2.1	-0.0757
90	1.8	-0.143
120	1.7	-0.167

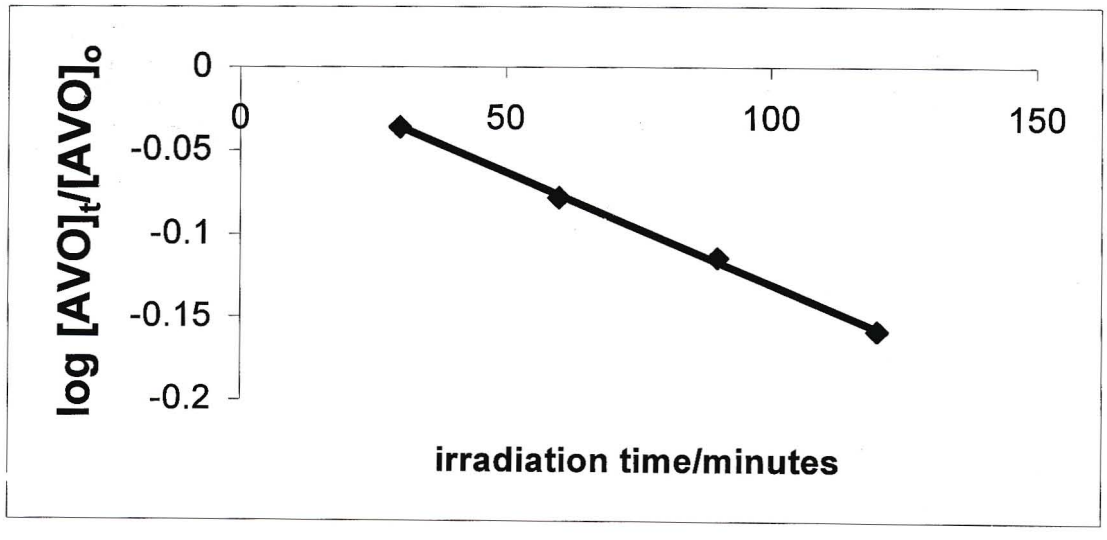

Figure 3.98: First-order plot for the photodegradation of AVO in cyclohexane. The slope of the curve is equivalent to 2.2×10^{-5} s^{-1}.

On determining the rate constant k for the photodegradation of AVO as 5.1 x 10^{-5} s^{-1} we can use the equation below to determine the intensity of light absorbed by AVO:

$$I_a = \frac{k[AVO] \times V \times N_A}{\Phi} \qquad 3.2$$

where I_a is the intensity of light absorbed, k (5.1 x 10^{-5} s^{-1}) is the rate constant, V (4 x 10^{-3} dm^3) is the volume of solution irradiated, N_A (6.023 x 10^{23} mol^{-1}) is Avogadro's constant and Φ (1.29 x 10^{-2}) is the quantum yield determined in Section 3.5.3.

The intensity of light absorbed for various concentrations of AVO calculated are shown in Table 3.40 and these values are close to those in Table 3.37.

Table 3.40: The intensity of light absorbed by AVO using equation 3.2.

[AVO]/10^{-5} M	**I_a/10^{15} photon s^{-1}**
2.5	0.238
2.3	0.219
2.1	0.200
1.8	0.171
1.7	0.162

3.7 The effect of sunlight on commercial sunscreen formulations

We have shown that *trans*-EHMC isomerises to its *cis*-conformation upon irradiation with an Osram HBO 500 W/2 high pressure mercury lamp in combination with a 10 mm Pyrex filter that allows wavelengths greater than 300 nm to be transmitted. We have also observed that AVO photodegrades in solutions of cyclohexane but not in solutions of methanol. We therefore thought it would be useful to check if these isomerisation and photodegradation reactions actually occur in a sunscreen formulation containing EHMC and AVO.

Ambre Solaire with SPF 25 (2.5% EHMC, 2.5% AVO, 5% benzophenone and 4% TiO_2) and Lubriderm with SPF 15 (4.0% EHMC and 0.8% AVO) were selected. These were accurately weighed on microscope slides and exposed to 6 hours of sunlight. Analysis and quantitation of the methanolic sunscreen formulations was carried out with the HPLC conditions described in Section 2.7.1.2 and for the sunscreen formulations dissolved in cyclohexane the GC-FID conditions described in Section 2.7.2.2 was used. The chromatograms obtained can be seen in Figures 3.99 to 3.106. The isomerisation of *trans*-EHMC to its *cis*-isomer was unambiguously evident.

From the GC-FID analysis of Lubriderm and Ambre Solaire it is evident (see Figures 3.103 to 3.106) that AVO it not present since AVO was expected to elute at 8.3 minutes. This could be due to AVO remaining in the emulsion and not being extracted into the cyclohexane solution. The analysis technique used was therefore not suitable to assess the photodegradation of AVO. Studies carried out by Maier *et al.* [1] have shown that the behaviour of sunscreen formulations cannot be predicted from their individual ingredients and also that combining complex organic filters and inorganic filters does not prevent photodegradation.

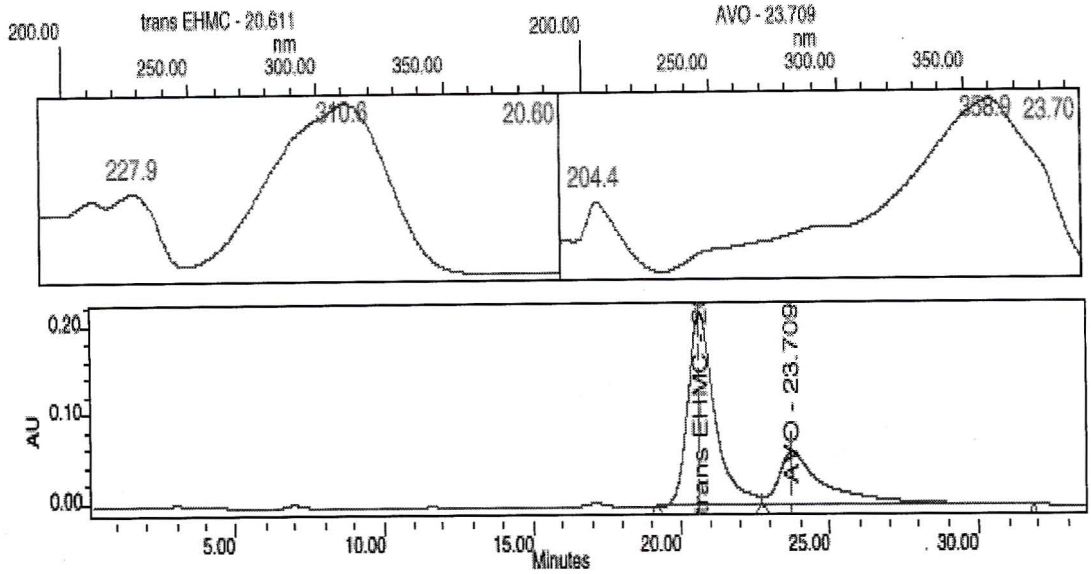

Figure 3.99: Chromatogram of Lubriderm unexposed to sunlight showing the separation of *trans*-EHMC and AVO, on a Nucleosil 100 C_{18} column using 85% (v/v) MeOH/H_2O as the mobile phase at a flow rate of 1 ml/min. The detection wavelength was set at 335 nm.

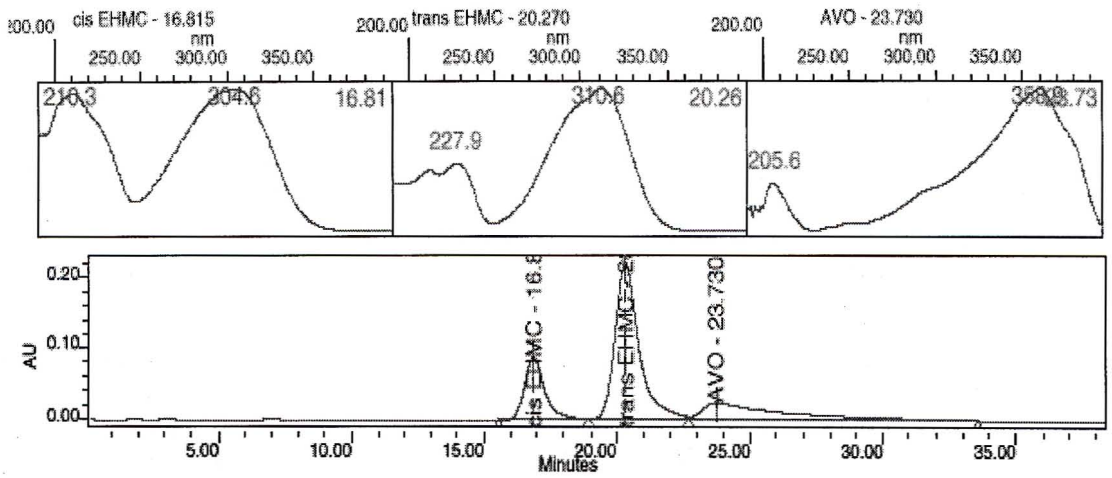

Figure 3.100: Chromatogram showing Lubriderm after a 6 hour exposure to sunlight. Separation was carried out on a Nucleosil 100 C_{18} column using 85% (v/v) MeOH/H_2O as the mobile phase at a flow rate of 1 ml/min. The detection wavelength was set at 335 nm.

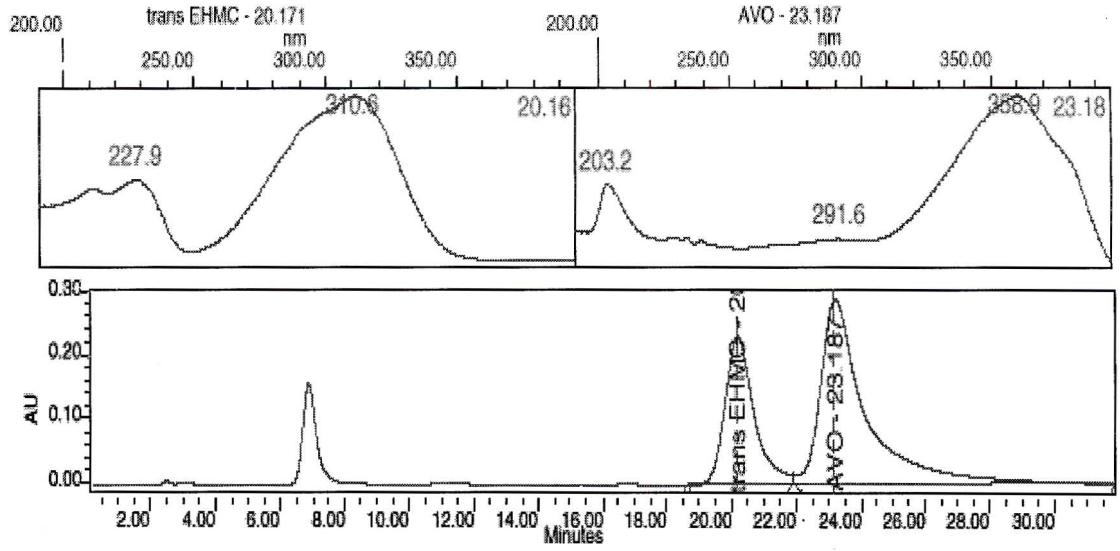

Figure 3.101: Chromatogram of Ambre Solaire unexposed to sunlight. Separation of the sunscreen absorbers was carried out on a Nucleosil 100 C_{18} column using 85% (v/v) MeOH/H_2O as the mobile phase at a flow rate of 1 ml/min. The detection wavelength was set at 335 nm. The peak at 6.8 minutes is due to benzophenone-3.

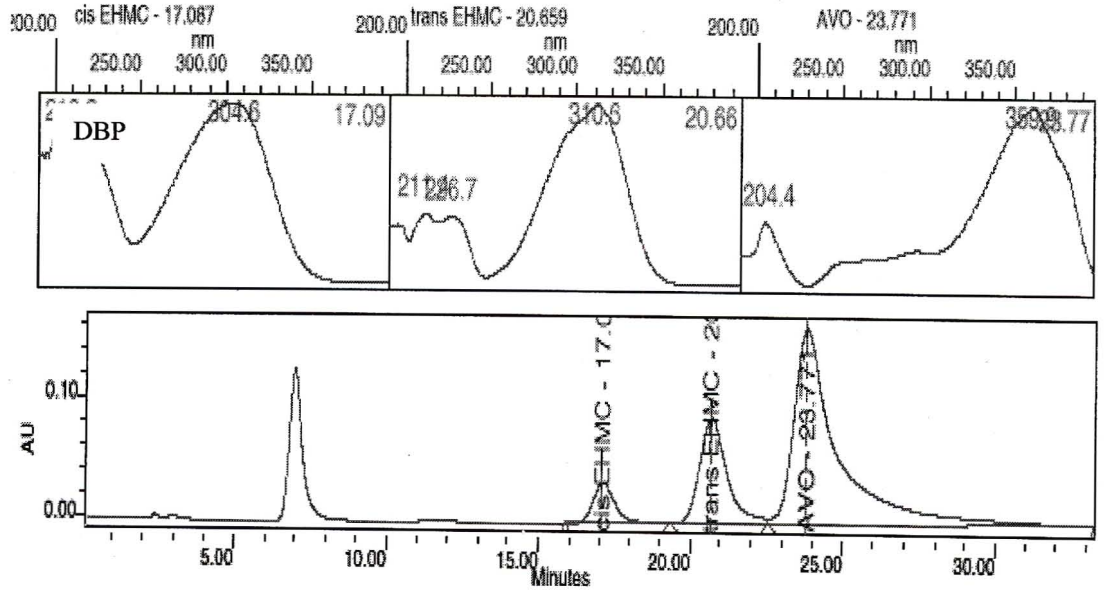

Figure 3.102: Chromatogram of Ambre Solaire exposed to 6 hours of sunlight. Separation was carried out on a Nucleosil 100 C_{18} column using 85% (v/v) MeOH/H_2O as the mobile phase at a flow rate of 1 ml/min. The detection wavelength was set at 335 nm. The peak at 7.0 minutes is due to Benzophenone-3.

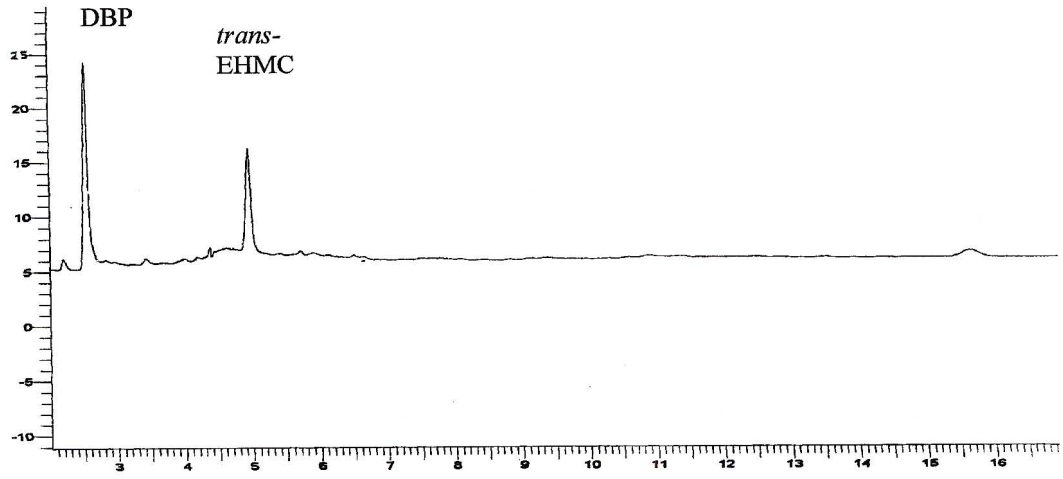

Figure 3.103: Chromatogram of the GC-FID analysis of 5 µl of Lubriderm, unexposed to sunlight, dissolved in cyclohexane. Separation was carried out on a Supelco 25 m x 250 µm PET-S fused silica capillary column. The DBP internal standard elutes at 2.5 minutes and *trans*-EHMC at 4.9 minutes.

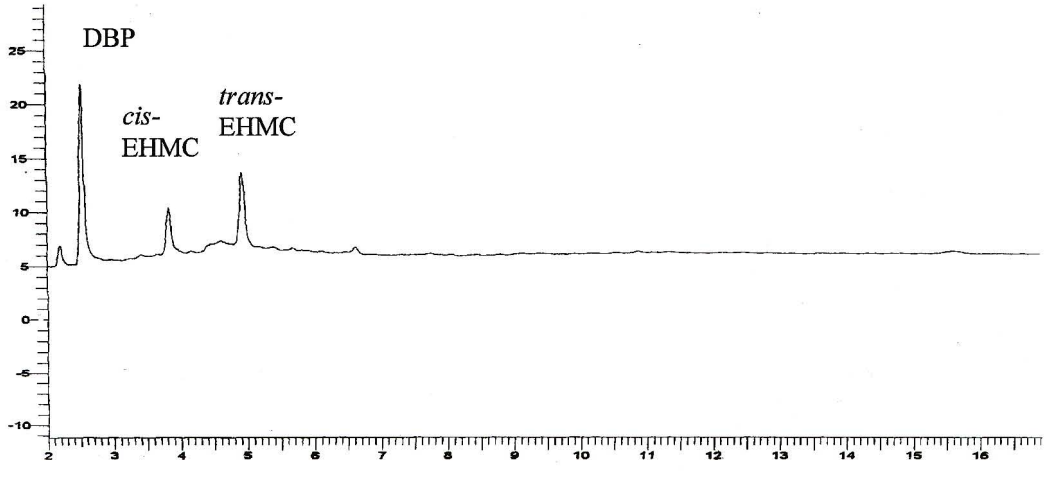

Figure 3.104: Chromatogram showing the GC-FID analysis of 5 µl of Lubriderm, exposed to 6 hours of sunlight, dissolved in cyclohexane. Separation was carried out on a Supelco 25 m x 250 µm PET-S fused silica capillary column. The DBP internal standard elutes at 2.5 minutes, *cis*-EHMC at 3.8 minutes and *trans*-EHMC 4.9 minutes.

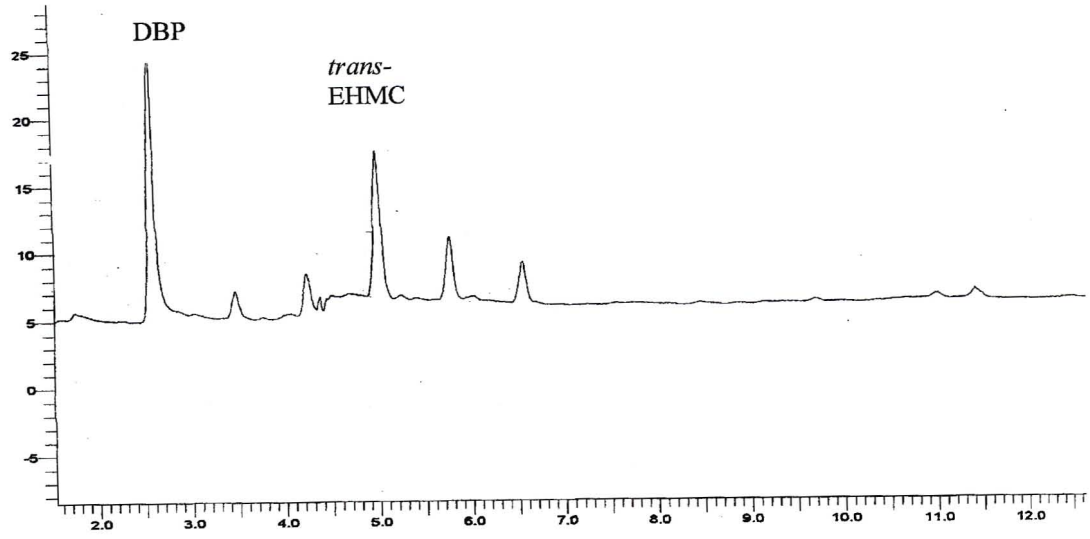

Figure 3.105: Chromatogram of the GC-FID analysis of 5 µl of Ambre Solaire, unexposed to sunlight, dissolved in cyclohexane. Separation was carried out on a Supelco 25 m x 250 µm PET-S fused silica capillary column. The DBP internal standard elutes at 2.5 minutes, *trans*-EHMC at 4.9 minutes and the rest of the peaks are unknown.

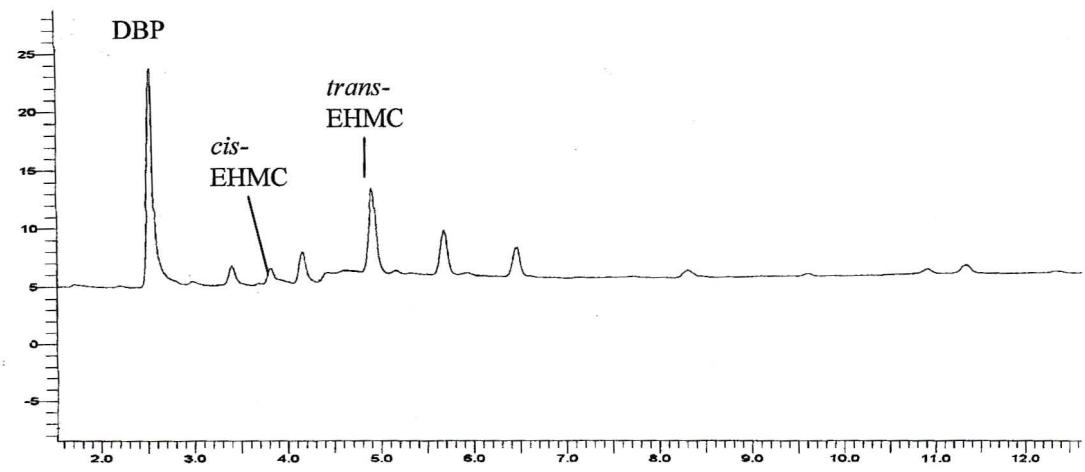

Figure 3.106: Chromatogram of the GC-FID analysis of 5 µl of Ambre Solaire, exposed to 6 hours of sunlight, dissolved in cyclohexane. Separation was carried out on a Supelco 25 m x 250 µm PET-S fused silica capillary column. The DBP internal standard elutes at 2.5 minutes, *cis*-EHMC at 3.8 minutes, *trans*-EHMC at 4.9 minutes and the rest are unknown.

It was then thought to monitor the isomerisation reaction at different time intervals. Ambre Solaire was chosen and accurately weighed out onto 6 microscope slides and placed out in the sun. The slides were removed at 1 hour intervals from 9:00 to 15:00 hours. They were analysed using the HPLC conditions described in Section 2.7.1.2. The results of the quantitation of the isomers are shown in Table 3.41. A graph representing the concentration of *trans*- and *cis*-EHMC is shown in Figure 3.107.

Table 3.41: Isomerisation of *trans*-EHMC in Ambre Solaire at different times of exposure to sunlight.

Time of sun exposure/hours	**[*trans*-EHMC]/10^{-4} M**	**[*cis*-EHMC]/10^{-4} M**
0	2.37	0
1	2.20	0.17
2	1.98	0.39
3	1.89	0.48
4	1.83	0.54
5	1.78	0.59
6	1.77	0.60

From Figure 3.107 it can be seen that the concentration of *trans*-EHMC decreases rapidly within the first 3 hours of exposure to sunlight. As the concentration of *trans*-EHMC decreases the concentration of *cis*-EHMC increases until equilibrium is attained. The photostationary state lies towards *trans*-EHMC. We have therefore shown that the photoisomerisation of EHMC does indeed occur in sunscreen formulations.

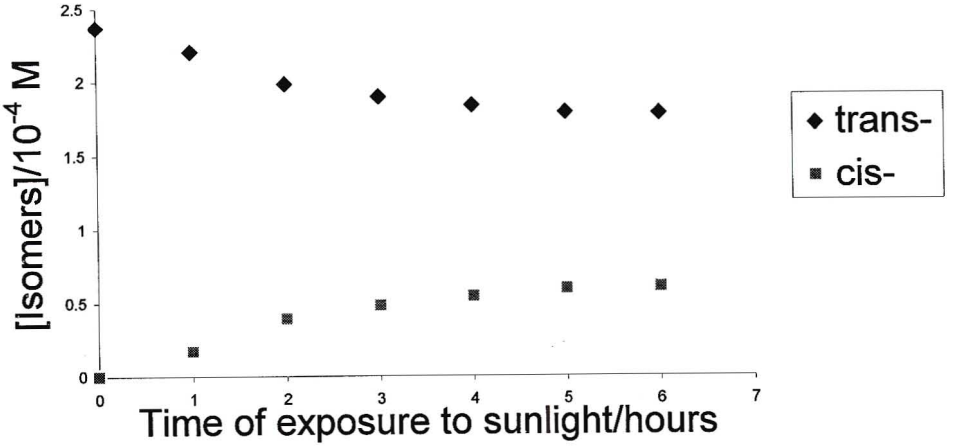

Figure 3.107: The concentration of *cis*- and *trans*-EHMC in Ambre Solaire against exposure time.

The UVB irradiance values from 9:00 to 15:00 for 8 June 2001 measured with the YES UVB pyranometer, were summed and multiplied by 600 to obtain the incident UVB irradiance (in J m^{-2}) (see Table 3.42). This specific 6 hour period was chosen since the flux of UVB radiation is maximal in a two hour period around solar noon (11 am - 1 pm). Up to 60% of the total UV radiation can be received between 11 am and 3 pm. Solar radiation incident at various localities on the earth's surface varies significantly with latitude, altitude, season, time of day, cloudiness, atmospheric aerosols, thickness of ozone layer, etc. UVB accounts for less than 1% of solar radiation and UVA accounts for about 6% of total solar radiation.

Figures 3.108 and 3.109 show that with increasing UVB irradiance and erythemal UVB the concentration of *cis* and *trans*-EHMC changes. When exposed to sunlight or UV irradiation faint reddening of the skin develops and this is termed erythema. Erythemal UVB irradiance values indicate the amount of UV that causes erythema, and increasing UVB irradiance increases the chance of erythema formation. The erythemal UVB values are obtained by multiplying the UVB irradiance by the action spectrum for erythema induction. Due to this photoisomerisation reaction sunscreen formulations that contain EHMC as a filter lose their efficiency on exposure to sunlight therefore for maximum protection sunscreen formulations need to be constantly reapplied.

Table 3.42: UVB irradiance as measured by the YES UVB pyranometer on 8 June 2001.

Exposure Time/hours	UVB Irradiance/ J m^{-2}	Erythemal UVB/ J m^{-2}
9:00 - 10:00	2150.02	103.18
10:00 - 11:00	5923.42	308.48
11:00 - 12:00	10279.0	563.05
12:00 - 13:00	15078.7	845.60
13:00 - 14:00	18863.2	1057.1
14:00 - 15:00	21137.8	1170.6

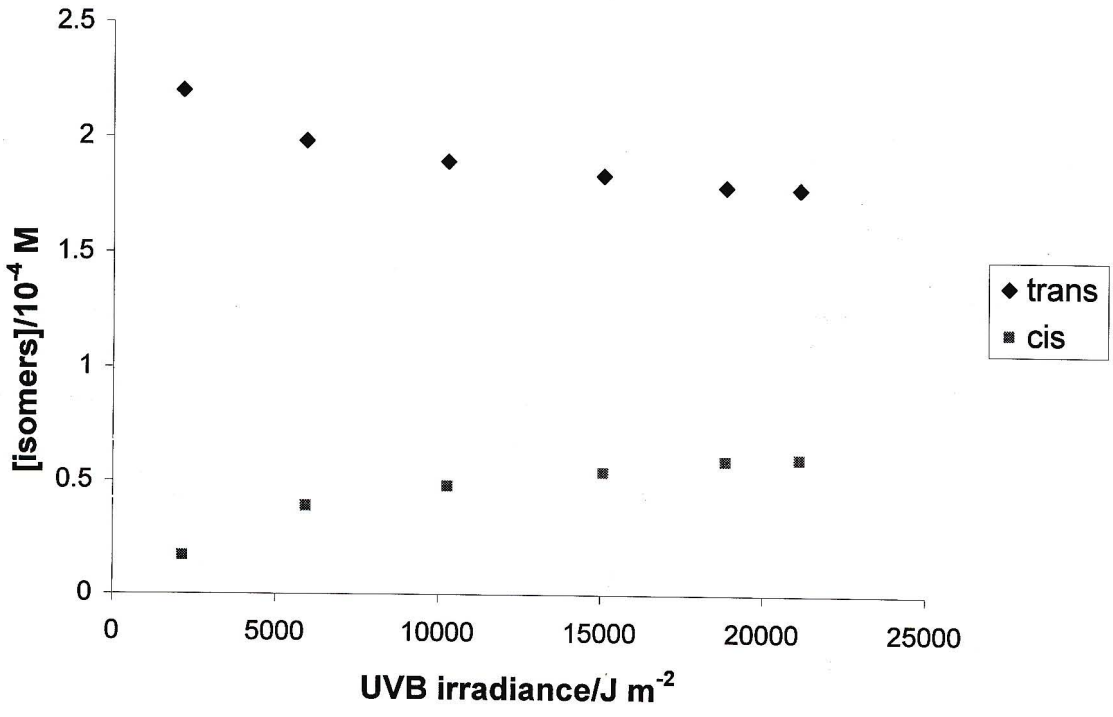

Figure 3.108: The concentrations of *trans*- and *cis*-EHMC *versus* UVB irradiance in a commercial sunscreen formulation exposed to sunlight from the period 9:00 – 15:00 hours.

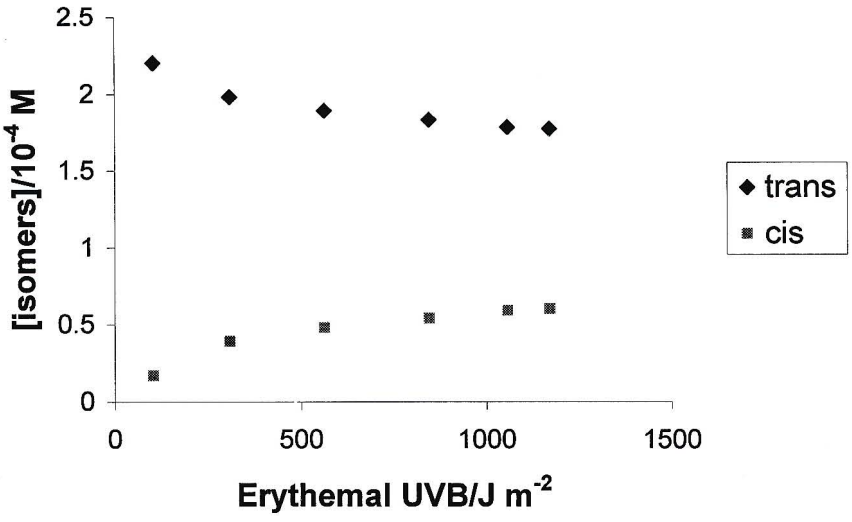

Figure 3.109: The concentrations of *trans*- and *cis*-EHMC *versus* erythemal UVB irradiance in a commercial sunscreen formulation exposed to sunlight during 9:00 –15:00 hours.

CHAPTER 4

Conclusion

EHMC and AVO are the two most common chemical absorbers used in sunscreen formulations and since the polarity of the solvent in which they are dissolved influences their photochemical behaviour the work presented in this thesis is directed toward understanding their behaviour in methanol and cyclohexane. We initially determined the isomeric forms in which they are supplied and the form in which they exist in solution. We then used UV-spectroscopy to develop a method to quantify a solution containing a mixture of EHMC and AVO. We looked at the effect of direct UVA and UVB light, quenchers and photosensitisers on irradiated sunscreen solutions. We used chromatographic techniques in photoproduct analysis of irradiated sunscreen solutions. Chemical actinometry was used in the determination of the irradiance absorbed by sunscreen solutions and finally we analysed commercial sunscreen formulations containing these two sunscreen absorbers.

The FTIR-spectrum of EHMC confirmed that it is supplied as the *trans*-isomer and the FTIR-spectum of AVO showed that it is supplied as the diketo form. The ^{1}H NMR spectra of EHMC and AVO in deuterated methanol and deuterated cyclohexane showed that EHMC exists as its *trans*-isomer in solution while AVO exists in its *cis*-enol form.

The wavelength of maximum absorbance (λ_{max}) of EHMC and AVO in methanol was found to be 308 nm and 356 nm respectively and in cyclohexane EHMC had a λ_{max} of 290 nm while AVO had a λ_{max} of 350 nm. The molar absorption coefficient of AVO at 356 nm (methanol) and 350 nm (cyclohexane) was found to be 3.86 x 10^4 dm^3 mol^{-1} cm^{-1} and 3.38 x 10^4 dm^3 mol^{-1} cm^{-1} respectively. The molar absorption coefficient of EHMC at 308 nm (methanol) and 290 nm (cyclohexane) was found to be 2.65 x 10^4 dm^3 mol^{-1} cm^{-1} and 2.53 x 10^4 dm^3 mol^{-1} cm^{-1} respectively. These trends in λ_{max} and ε values with change in solvent polarity are consistent with the behaviour of sunscreen absorbers in different solutions previously reported [3].

Upon irradiating a 4 x 10^{-5} M *trans*-EHMC solution at 1 minute intervals up to 5 minutes with an Osram HBO 500 W/2 high pressure mercury lamp in combination with a 10 mm thick Pyrex filter we observed that it photoisomerises to its *cis*-isomer. A photostationary equilibrium is reached within the first 5 minutes. When 3 x 10^{-5} M AVO dissolved in methanol was irradiated at 30 minute intervals no loss in absorbance was observed. AVO therefore does not photodegrade in methanol. We then irradiated a mixture of 3.1 x 10^{-5} M EHMC and 1.9 x 10^{-5} M AVO and noticed that only EHMC photodegraded. EHMC in the presence of AVO reaches its photostationary equilibrium at almost the same rate as when irradiated alone.

Upon irradiating 2.5 x 10^{-5} M AVO dissolved in cyclohexane at 30 minute intervals AVO showed loss in absorbance and this loss is attributed to AVO photodegrading to several photoproducts which was confirmed by GC-MS analysis (see Section 3.4.2). When EHMC was irradiated in cyclohexane the photostationary equilibrium between the *cis*- and *trans*-isomer was not attained. This is due to the initial formation of the *cis*-isomer which re-equilibrates to the *trans*-isomer which was shown in Section 3.4.2. We irradiated a mixture of 2.5 x 10^{-5} M AVO and 2.3 x 10^{-5} M EHMC dissolved in cyclohexane. The photostationary equilibrium of the isomers was not attained in the mixture as well and this was attributed to one of the photoproducts of AVO absorbing at the λ_{max} of EHMC and thereby masking changes in the EHMC concentration. We also noticed that the rate of photodegradation of AVO is enhanced in the presence of EHMC.

We looked at the direct irradiation of EHMC, AVO and a mixture of the two in methanol and cyclohexane with UVB and UVA radiation. A 313 nm narrow bandpass filter was used to provide UVB radiation while a 365 nm filter was used to provide UVA radiation. The UV-spectra obtained of the samples irradiated with these filters were compared with those obtained with the 10 mm thick Pyrex filter. EHMC when irradiated at 1 minute intervals in methanol with the 313 nm filter, reached its photostationary equilibrium at a faster rate than with the 10 mm thick Pyrex filter. When EHMC was irradiated in cyclohexane a photostationary equilibrium was attained unlike when irradiated with the 10 mm thick Pyrex filter. AVO, as in the case of irradiating with the Pyrex filter, showed no degradation when irradiated with a

313 nm filter in methanol and did not degrade in cyclohexane as well since it does not absorb much light at 313 nm. Irradiation of a mixture of EHMC and AVO in both solvents with the 313 nm filter did not have much of an effect on the photodegradation of the sunscreen absorbers.

EHMC when dissolved in either methanol or cyclohexane and irradiated using the 365 nm filter did not photodegrade since it does not absorb at 365 nm. AVO showed photostability when irradiated in methanol using the 365 nm filter and the rate of photodegradation of AVO was enhanced when irradiated in cyclohexane compared to when irradiated with the 10 mm thick Pyrex filter. We can therefore say that monochromatic light induces faster photodegradation of AVO than polychromatic light, similarly faster photoisomerisation of EHMC. Irradiating a mixture of EHMC and AVO in methanol with the 365 nm filter had no effect on the sunscreen absorbers but in cyclohexane AVO photodegraded while EHMC photodegraded slightly. This was due to AVO photosensitising the isomerisation of EHMC as proved later by GC-MS.

We then tried to determine the nature of the excited state from which photoisomerisation and photodegradation occur. We first looked at the effect of O_2 as a triplet quencher. We showed that O_2 has no quenching effect on irradiating EHMC, AVO and a mixture of the two dissolved in methanol but showed definite quenching effects on the sunscreens dissolved in cyclohexane. It is therefore possible that upon irradiating *trans*-EHMC, AVO and a mixture of the two in cyclohexane, product formation occurs from the triplet excited state.

The quenching effects of O_2 are not a conclusive test to determine whether photoproduct formation occurs from the triplet state since O_2 readily exists in the atmosphere and to remove it totally from solution is almost impossible. We therefore looked at the quenching effects of *cis*-piperylene, a well-known triplet-state quencher. We found that *cis*-piperylene had no quenching effect on irradiated solutions of AVO, EHMC and a mixture of the two in both methanol and cyclohexane. Therefore the evidence obtained with O_2 was not confirmed by these experiments.

To further investigate the nature of the excited state involved we looked at the effect of benzophenone as a photosensitiser by irradiating EHMC, AVO and a mixture of the two in methanol and cyclohexane using a 254 nm narrow bandpass filter, since EHMC and AVO hardly absorb at this wavelength and benzophenone absorbs maximally at 250 nm. We found that benzophenone only had a slight photosensitising effect on irradiated solutions of EHMC dissolved in cyclohexane. This was not conclusive evidence to state the nature of the excited state involved in photoproduct formation.

Chromatographic techniques were used in the analysis of photoproduct formation upon irradiation of EHMC, AVO and a mixture of the two in methanol and cyclohexane. HPLC with UV detection was used for analysing photoproduct formation in irradiated solutions of the sunscreen absorbers in methanol. AVO is photostable in methanol whereas *trans*-EHMC photoisomerises to its *cis*-isomer. An isocratic mobile phase of 85% (v/v) MeOH/H_2O was used for the separation of the two isomeric forms of EHMC and also AVO. Upon irradiation of EHMC and a mixture of EHMC and AVO in methanol we found the the photostationary equilibrium of the isomers lies towards to the formation of *cis*-EHMC and we later showed that when EHMC was irradiated in cyclohexane no photostationary equilibrium was achieved but the concentration of the *trans*-EHMC was greater than *cis*-EHMC.

Gas chromatography was used in the analysis of EHMC, AVO and a mixture of the two irradiated in cyclohexane. On GC-FID analysis of EHMC irradiated in cyclohexane we found that formation of *cis*-EHMC occurs initially which re-equilibrates to the *trans*-isomer (refer to Figure 3.57) hence accounting for the inconsistency in the concentration of EHMC upon irradiation. GC-FID analysis of AVO showed that AVO degrades to several photoproducts. GC-MS analysis was used to identify these products. The products formed due to the cyclohexane degrading were cyclohexanol, cyclohexanone, bicyclohexyl and dicyclohexyl ether. The products formed due to AVO degrading were *tert*-butylbenzene, *p*-methoxybenzoic acid, *p-tert*-butylbenzoic acid and cyclohexyl ester of *p*-methoxybenzoic acid. GC-FID analysis of the mixture of EHMC and AVO dissolved in cyclohexane, irradiated for 3 hours with an Osram HBO 500 W/2 high pressure

mercury lamp in combination with a 10 mm Pyrex filter, showed EHMC photoisomerising but no photoproducts of AVO were observed due to some error in sample analysis since we did see photoproduct formation from GC-MS analysis of a similar sample (see Figure 3.70).

GC-MS was also used to investigate the formation of photoproducts that absorb close to the wavelength of maximum absorbance of EHMC when a mixture of EHMC and AVO dissolved in cyclohexane was irradiated. The photoproducts identified for their absorbance close to the wavelength of maximum absorbance of EHMC were cyclohexanone, *tert*-butylbenzene and *p*-methoxybenzaldehyde. The formation of these photoproducts explains the inconsistent absorbance values observed when EHMC was irradiated in the presence of AVO in cyclohexane.

The rate at which sunscreen absorbers degrade upon irradiation with UV-light is dependent on the number of photons absorbed. Chemical actinometry using potassium ferrioxalate was employed to determine the number of photons absorbed by EHMC, AVO and a mixture of the two dissolved in methanol and cyclohexane. The photoisomerisation of EHMC when dissolved in methanol was found to be enhanced in the presence of AVO. The degradation of AVO when dissolved in cyclohexane was found to be enhanced in the presence of EHMC. We determined the quantum yield for the photodegradation of AVO to be 1.29×10^{-2} molecules per photon of light absorbed. We then determined the rate constants for the photoisomerisation of EHMC and photodegradation of AVO. The rate constants for the forward and reverse reactions for the photoisomerisation of EHMC were found to be 1.43 s^{-1} and 0.0513 s^{-1} respectively. The rate constant for the photodegradation of AVO was found to be 5.1×10^{-5} s^{-1}.

Finally we examined the effect of sunlight on commercial sunscreen formulations. Lubriderm (0.8% AVO and 4% EHMC) and Ambre Solaire (2.5% AVO, 2.5% EHMC, 5% Benzophenone and 4% TiO_2) were chosen since they contained both EHMC and AVO. Upon exposing these two sunscreen formulations to 6 hours of sunlight *trans*- to *cis*- isomerisation of EHMC was observed in both methanolic and cyclohexane solutions but AVO showed no photodegradation. We then looked at the isomerisation reaction in Ambre Solaire following solar irradiation from 9:00 to 15:00

hours. The isomers were then quantified using HPLC in an isocratic mobile phase of 85% (v/v) MeOH/H_2O. The concentration of *trans*-EHMC decreased significantly in the first three hours and then stabilised for the next three. The photostationary equilibrium was on the side of the *trans*-isomer. AVO in both formulations was not extracted into solution and therefore was not detected by HPLC analysis. The SPF values of sunscreen formulations containing EHMC would therefore be reduced due to this isomerisation reaction, since *cis*-EHMC is a less efficient UVB absorber, thus not being as effective as expected.

We have therefore shown that *trans*-EHMC photoisomerises to its *cis*-isomer in isolation and in the presence of AVO in both methanol and cyclohexane and in a commercial sunscreen formulation. Quenching experiments with O_2 indicate that in cyclohexane the nature of the excited state for photoisomerisation could be the triplet state.

In the presence of AVO, EHMC photoisomerises at a faster rate. It was proved conclusively through the use of monochromatic light and GC-MS that AVO photosensitises this isomerisation reaction, which explains the increase in the rate of this reaction and would therefore affect the rate constants k and k' for the photoisomerisation of EHMC.

AVO is photostable in methanol but photodegrades in isolation or in the presence of EHMC in cyclohexane *via* first-order reaction kinetics. In this case as well quenching experiments with O_2 indicate that the excited triplet-state could be involved but the evidence was not conclusive. AVO degrades giving rise to a number of photoproducts, which absorb in the UVB region, thereby masking the loss in absorbance due to the photoisomerisation reaction of EHMC which was assumed to occur *via* first-order reaction kinetics. By using the chromatographic technique developed it was not possible to assess the photostability of AVO in a commercial sunscreen formulation since the method used to extract AVO was inefficient, therefore an alternate method for the extraction of AVO has to be implemented.

This work has therefore shown that the polarity of the solvent influences the photochemical behaviour of EHMC and AVO. This is an important aspect as Maier

et al. [1] have shown that commercial sunscreen formulations containing the same active ingredients can show differing degrees of photostability and this can only be attributed to the nature of the medium. A consumer on buying a sunscreen formulation is unaware of these effects and could therefore not be afforded the protection expected from the SPF value quoted on the product.

REFERENCES

[1] H. Maier, G. Schauberger, K. Brunnhofer and H. Hönigsmann, *The Journal of Investigative Dermatology*, **117** (2001) 256-262.

[2] E. Chatelain and B. Gabard, *Photochemistry and Photobiology*, **74** (2001) 401-406.

[3] L.E. Agrapidis-Paloympis and R.A. Nash, *Journal of the Society of Cosmetic Chemists*, **38** (1987) 209-221.

[4] B.S. Martincigh, J.M. Allen and S.K. Allen, *Sunscreen Photobiology: Molecular, Cellular and Physiological Aspects*, F.P. Gasparro (editor), Springer-Verlag and Landes Bioscience, Berlin (1997) pp. 11-45.

[5] N.A. Shaath, P.M. Griffen, G.I. Andemichael and L.E. Agrapidis-Paloympis, *Sunscreens: Development, Evaluation and Regulatory Aspects, Cosmetic Science and Technology Series*, Volume 10, N.J. Lowe and N.A. Shaath (editor), Marcel Dekker, New York, USA (1990) pp. 505-536.

[6] G. Eggset, G. Kavli, H. Krokan and G. Volden, *Photobiochemistry and Photobiophysics*, **8** (1984) 163-167.

[7] J.S. Taylor, *Journal of Chemical Education*, **67** (1990) 835-841.

[8] N.A. Campbell, *Biology*, Benjamin/Cummings Publishing Company, Inc., California, (1990) pp. 98-125.

[9] E.J. Wood and W.R. Pickering, *Introducing Biochemistry*, John Murray (Publishers) Ltd, London, (1982) pp. 76-78.

[10] B.Alberts, D. Bray, J. Lewis, M. Raff, K. Roberts and J.D. Watson, *Molecular Biology of the Cell*, Second Edition, Garland Publishing Inc., New York (1989) pp. 235-248.

[11] J.E. Coggle, *The Molecular Basis of Cancer*, P.B. Farmer and J.M. Walker (editor), Croon Helm Ltd, London (1985) pp. 101-131.

[12] S.R. Aliwell, M.Sc. Thesis, University of Natal, Durban, South Africa (1991).

[13] G. Raghunathan, T. Kieber-Emmons, R. Rein and J. Alderfer, *Journal of Molecular Structure*, **7** (1990) 899-904.

[14] J.M. Allen, C.J. Gossett and S.K. Allen, *Journal of Photochemistry and Photobiology, B: Biology* **32** (1996) 33-37.

[15] S.R. Aliwell, B.S. Martincigh and L.F. Salter, *Journal of Photochemistry and Photobiology, A: Chemistry*, **71** (1993) 147-153.

[16] W. Schwack and T. Rudolph, *Journal of Photochemistry and Photobiology B: Biology*, **28** (1995) 229-234.

[17] G. Marginean, A.E. Fructus, J.P. Marty and J. Arnaud-Battandier, *International Journal of Cosmetic Science*, **17** (1995) 233-243.

[18] N.A. Shaath, *Cosmetics and Toiletries*, **105** (1990) 41-44.

[19] R.M. Sayre, J.C. Dowdy, A.J. Gerwig and W.J. Shields, *Photochemisty and Photobiology,* **69** (1999) 58S.

[20] D.J. Carrey, *Cosmetic Chemicals,* **91** (1991) 176-181.

[21] N. Tarras-Wahlberg, G. Stenhagen, O. Larko, A. Rosén, A. Wennberg, and O. Wennerström, *The Journal of Investigative Dermatology*, **113** (1999) 547-553.

[22] J. K. Broadbent, M.Sc. Thesis, University of Natal, Durban, South Africa (1994).

[23] K. Kowlaser, M.Sc. Thesis, University of Natal, Durban, South Africa (1998).

[24] J.K. Broadbent, B.S. Martincigh, M.W. Raynor, L.F. Salter, R Moulder, P. Sjörberg and K.E. Markides, *Journal of Chromatography A*, **732** (1996) 101-110.

[25] D. Decuyper-Debergh, J. Piette, C. Laurent and A. van de Vorst, *Mutation Research,* **22** (1989) 11-14.

[26] J.M. Allen, C.J. Gossett and S.K. Allen, *Chemical Research in Toxicology*, **9** (1996) 605-609.

[27] C.R. Taylor, R.S. Stern, J.D. Leyden and B. Gilchrest, *Journal of the American Academy of Dermatology*, **22** (1990) 1.

[28] S.T. Butt and T. Christensen, *Radiation Protection Dosimetry*, **91** (2000) 283-286.

[29] M. Dubois, P. Gilard, P. Tiercet, A. Deflandre and M.A. Lefebvre, *Journal de Chimie Physique*, **95** (1998) 388-394.

[30] I. Andrae, F. Bohm, A.O. Bringhen, H. Gozenbach, T. Hill, L. Mulroy and T.G. Truscott, *Journal of Photochemistry and Photobiology B: Biology*, **37** (1997) 147-150.

[31] N.M. Roscher, M.K.O. Lindermann, S.B. Kong, C.G. Cho and P. Jiang, *Journal of Photochemistry and Photobiology A*: *Chemistry,* **80** (1994) 417-421.

[32] E. Damiani, L. Greci, R. Parsons and J. Knowland, *Free Radical Biology and Medicine*, **26** (1999) 809-816.

[33] R. M. Sayre and J.C. Dowdy, *Cosmetics and Toiletries*, **114** (1999) 85-91.

[34] P.R. Griffiths, *Chemical Infrared Fourier Transform Spectroscopy*, John Wiley and Sons, New York (1942) pp. 7-9.

[35] R.S. Fessenden and J.S. Fessenden, *Organic Chemistry,* Second Edition, PWS Publishers, Boston (1982) pp. 1-8.

[36] R.M. Silverstein, *Spectrometric Identification of Organic Compounds*, Third Edition, J. Wiley and Sons, New York (1974) pp. 159-196.

[37] J.D. Roberts, *Nuclear Magnetic Resonance*, McGraw-Hill Book Company, New York (1959) pp. 1-18.

[38] S.L. Murov, I. Carmichael and G.L. Hug, *Handbook of Photochemistry*, Second Edition (1993) pp. 234-236.

[39] H. Gozenbach, T.J. Hill and T.G. Truscott, *Journal of Photochemistry and Photobiology B: Biology*, **16** (1992) 377-379.

[40] C.F. Poole and S.K. Poole, *Chromatography Today*, Elsevier Science Publishers, New York (1991) pp. 545-595.

[41] S. Lindsay, *High Performance Liquid Chromatography*, John Wiley and Sons, London (1987) pp. 1-122.

[42] J.E. Willet, *Gas Chromatography*, John Wiley and Sons, London (1987) pp. 1-4.

[43] A.B. Littlewood, *Gas Chromatography*, Third Edition, Academic Press, New York (1970) pp. 1-32.

[44] N.A. Ingouville, M.Sc. Thesis, University of Natal, Durban, South Africa (1998).

[45] C.A. Parker, *Proc. Roy. Soc. London*, **A220** (1953) 104-109.

[46] C.G. Hatchard and C.A. Parker, *Roy. Soc. London*, **A235** (1956) 518-525.

[47] J.G. Calvert and J.N. Pitts, *Photochemistry*, John Wiley and Sons, New York (1966) pp. 780-786.

APPENDIX A

The materials used are listed in this section.

A1 Chemicals for spectroscopic studies

Methanol (HPLC grade)	BDH	99.8%
Cyclohexane (AR)	ACE	99%
2-Ethylhexyl-*p*-methoxycinnamate	BASF	
Avobenzone	BASF	
cis-Piperylene	Aldrich	90%
N_2	Fedgas	
Benzophenone	BDH	
Deuterated methanol	Acros	99%
Deuterated chloroform	Acros	99%
Methyl ethyl ketone		
Potassium bromide (IR)	Merck	
Milli-Q-Water*		

A2 Chemicals for Actinometry

Ammonium Ferrous Sulphate Hexahydrate (AR)	BDH	
n-Phenanthranillic acid (AR)	BDH	
1,10-Phenanthroline (AR)	BDH	
Potassium Dichromate (AR)	BDH	
Potassium Oxalate Monohydrate (AR)	BDH	
Sodium Acetate (AR)	SAARCHEM	
Sodium Hydroxide (AR)	SAARCHEM	
Sulphuric Acid (AR)	SAARCHEM	98%
Ferric Chloride (AR)	BDH	

A3 Chemicals for HPLC

Milli-Q Water*		
Acetonitrile (HPLC grade)	Lab-scan	99.9%
Methanol (HPLC grade)	BDH	99.9%
Tetrahydrofuran (HPLC grade)	Riedel de Haën	99.9%
High purity helium	Fedgas	

A4 Chemicals for GC

Air	Fedgas	99.9%
Hydrogen	Fedgas	99.9%
Nitrogen	Fedgas	99.9%

A5 Commercial Sunscreens

Lubriderm

Ambre Solaire

*Milli-Q Water refers to water that has been passed through the Millipore Milli-Q apparatus which consists of a series of ion-exchange and organic removal resins.

APPENDIX B

The equipment used is listed in this section.

B1 Irradiation Equipment

Osram HBO 500 W/2 high pressure mercury lamp
Schrieber powerpack for HBO lamp
Blak-Ray J-221 longwave UV intensity meter
A 313 nm and a 365 nm narrow bandpass interference filter from Andover Corporation
A 254 nm narrow bandpass interference filter from Acton Research Laboratory
A 10 mm pyrex filter

B2 UV-spectroscopic equipment

Varian DMS 300 UV/Vis Spectrophotometer
LKB Ultrospec IIE Single Beam Spectrophotometer

B3 FTIR Equipment

Specac 15.011 ton manual hydraulic press
Nicolet Impact 400D spectometer
Hewlett Packard 7440 Color Pro plotter

B4 NMR Equipment

Varian Gemini 300 MHz NMR Spectrophotometer

B5 HPLC Equipment

Waters 600 Multisolvent Delivery System

Waters U6K Variable Injector

Waters 996 Photodiode Array Detector

De` Mark Pentium II computer

Hewlett Packard Deskjet Color Printer

Hamilton Microliter Gastight Syringe (10-100 μl)

Nucleosil 100 C_{18} reverse phase column from Anatech Instuments (4.6 mm x 250 mm and 5 μm particle size)

A Waters Guard-Pak μ-Bondapak C_{18} precolumn insert

B6 GC-FID Equipment

Perkin Elmer Autosystem Gas Chromatograph

Hamilton high pressure 10 μl syringe

Supelco 25 m x 250 μm x 0.25 μm PET-S fused silica capillary column

B7 GC-MS

Agilent 6890 gas chromatograph

Agilent 5973 series mass selective detector (electron impact)

Hewlet Packard Pentium III 600 computer

HP-5 methyl silicon 25 m x 250 μm x 0.25 μm capillary column

Agilent P/N: 23-265/42/HP syringe

Perkin Elmer Turbomas gas chromatograph with a mass selective detector (electron impact)

Dell Pentium III computer

BP-5 methyl silicon 30 m x 320 μm x 0.25 μm capillary column

B8 UVB Irradiance Measurements

UVB irradiance values and Erythemal UVB was measured using an Ultraviolet Pyranometer from Yankee Enviromental Systems (YES).

APPENDIX C

Poster presented on this work:

R. Panday and B.S. Martincigh, A photochemical investigation of two common sunscreen agents in polar and non-polar media, European Society for Photobiology Symposium on Photoprotection, Kraków, Poland, 19-22 May 2001.